

Ultrahigh Energy Cosmic Rays: The state of the art before the Auger Observatory

Luis Anchordoqui, Thomas Paul, Stephen Reucroft, and John Swain

*Department of Physics, Northeastern University
Boston, MA 02115, USA*

l.anchordoqui@neu.edu, tom.paul@cern.ch,
stephen.reucroft@cern.ch, john.swain@cern.ch

Abstract

In this review we discuss the important progress made in recent years towards understanding the experimental data on cosmic rays with energies $\gtrsim 10^{19}$ eV. We begin with a brief survey of the available data, including a description of the energy spectrum, mass composition, and arrival directions. At this point we also give a short overview of experimental techniques. After that, we introduce the fundamentals of acceleration and propagation in order to discuss the conjectured nearby cosmic ray sources. We then turn to theoretical notions of physics beyond the Standard Model where we consider both exotic primaries and exotic physical laws. Particular attention is given to the role that TeV-scale gravity could play in addressing the origin of the highest energy cosmic rays. In the final part of the review we discuss the potential of future cosmic ray experiments for the discovery of tiny black holes that should be produced in the Earth's atmosphere if TeV-scale gravity is realized in Nature.

Contents

I. Appetizer	4
II. Observation of the highest energy cosmic rays	5
A. The energy spectrum	5
B. Properties of extensive air showers and mass composition	8
C. The arrival direction distribution	13
D. Measurement techniques	17
1. Surface arrays	17
2. Fluorescence eyes	21
3. Radio detection techniques	22
E. CR-observatories: past and present	24
F. The potential of the Pierre Auger Observatory	26
G. The Telescope Array Project	28
H. 200?: A space odyssey	28
I. Ultrahigh energy neutrino experiments	29
III. Cosmic ray acceleration	30
A. The Fermi mechanism	31
B. Desperately seeking Zevatrons	35
1. Plausible sources	35
2. Radiogalaxies	38
3. γ -ray burst fireballs	40
IV. Interactions <i>en route</i> to Earth	43
A. The GZK cutoff	43
B. Photonuclear interactions	48
C. Relativistic specks of dust	52
D. Electromagnetic cascades	55
E. Deflection and delay due to magnetic fields	59
V. Our cosmic backyard	63
A. Galactic sources	64
B. Centaurus A	66
C. M87	72
D. Starbursts	76

VI. GZK–evading messengers	81
A. Super-GZK CRs from the edge of the Universe	82
B. Z -burst	82
C. SUSY U	87
D. Lorentz symmetry violations with anomalous kinematics	88
VII. Spacetime’s unseen dimensions	91
A. Influence of KK-modes on the development of extensive air showers	94
B. Gravi-burst	97
VIII. Exotica	98
A. Top-down origin	99
B. Monopoles and other topological defects as primaries	106
IX. The atmosphere as a black hole factory	109
A. Black hole production in particle collisions	109
B. Probes of TeV scale gravity in CR experiments	113
C. Prospects for distinguishing BH production in neutrino showers	116
D. p -branes from Heaven	120
X. Looking forward	123
Acknowledgments	126
A. Hadronic interaction models in the <i>terra incognita</i>	126
B. Redshifting	128
C. Kinematics of photomeson production	129
D. Iron photodisintegration	130
E. The neutron channel	132
F. Recipes for a dark matter halo	133
G. Tubular black holes	134
References	135

I. APPETIZER

Cosmic ray (CR) and accelerator based particle physics share common roots, and in fact many of the key discoveries early in the history of particle physics came from the study of CRs. After a period of divergence between the two fields, both in methodology and in the key areas of interest, a confluence is now underway, driven in no small part by the mystery of the highest energy CRs. Much of the interest in these CRs is rooted in recent developments in both experiment and theory. The most recent data reported at the 27th International Cosmic Ray Conference (ICRC) suggest that some CRs arrive at the outer limits of the Earth's atmosphere with energies above 10^{20} eV. This is in itself remarkable, as it seems difficult to explain how such high energies can be attained without invoking new physics. Moreover, the center-of-mass (c.m.) energies achieved when these CRs impinge on a stationary nucleon of the air molecules are higher than any that can be reached in present-day terrestrial experiments, or indeed any experiment in the foreseeable future. Adding to the puzzle, the HiRes and AGASA experiments continue to revise their estimates of the fluxes and energies, making the subject more confusing.

Although current theoretical and experimental uncertainties make it impossible to determine the origin and nature of the highest energy events with any certainty, the mere presence of such events suggests the exciting possibility that CRs will, once again, provide us with glimpses of physics beyond our present theories. Speculations ranging from supersymmetry to magnetic monopoles, large extra dimensions, and captivating tiny black holes produced in CR collisions fill the Los Alamos preprint archives at an ever-increasing rate. There is clearly great hope that we are at the verge of learning something revolutionary.

In this spirit then, it seems opportune to review our present understanding of the highest energy CRs: what has been measured and with what confidence, what do we know about the composition and possible acceleration mechanisms for these particles, and how much do our measurements depend on uncertainties in Standard Model calculations? Throughout the first part of this review we focus tightly on the interplay between experiment and phenomenology assuming no physics beyond the Standard Model. This provides something of a sanity check on where we are now and where we think we are going. Afterwards, we relax our grip on sanity and summarize some of the new, and sometimes fantastic, ideas that may be probed by the next generation of experiments. To paraphrase Neils Bohr, the hope is that none of these ideas is crazy enough, and that in a few years we can look forward to genuine surprises.

II. OBSERVATION OF THE HIGHEST ENERGY COSMIC RAYS

A. The energy spectrum

In 1912 Victor Hess carried out a series of pioneering balloon flights during which he measured the levels of ionizing radiation as high as 5 km above the Earth's surface [1]. His discovery of increased radiation at high altitude revealed that we are bombarded by ionizing particles from above. These CR particles are now known to consist primarily of protons, helium, carbon, nitrogen and other heavy ions up to iron.

Below 10^{14} eV the flux of particles is sufficiently large that individual nuclei can be studied by detectors carried aloft in balloons or satellites. From such direct experiments we know the relative abundances and the energy spectra of a variety of atomic nuclei, protons, electrons and positrons as well as the intensity, energy and spatial distribution of X-rays and γ -rays. Measurements of energy and isotropy showed conclusively that one obvious source, the Sun, is not the main source. Only below 100 MeV kinetic energy or so, where the solar wind shields protons coming from outside the solar system, does the Sun dominate the observed proton flux. Spacecraft missions far out into the solar system, well away from the confusing effects of the Earth's atmosphere and magnetosphere, confirm that the abundances around 1 GeV are strikingly similar to those found in the ordinary material of the solar system. Exceptions are the overabundance of elements like lithium, beryllium, and boron, originating from the spallation of heavier nuclei in the interstellar medium.

Above 10^{14} eV, the flux becomes so low that only ground-based experiments with large apertures and long exposure times can hope to acquire a significant number of events. Such experiments exploit the atmosphere as a giant calorimeter. The incident cosmic radiation interacts with the atomic nuclei of air molecules and produces extensive air showers (EASs) which spread out over large areas. Already in 1938, Pierre Auger concluded from the size of EASs that the spectrum extends up to and perhaps beyond 10^{15} eV [2, 3]. Nowadays substantial progress has been made in measuring the extraordinarily low flux (~ 1 event $\text{km}^{-2} \text{yr}^{-1}$) above 10^{19} eV. Continuously running experiments using both arrays of particle detectors on the ground and fluorescence detectors which track the cascade through the atmosphere, have detected events with primary particle energies higher than 10^{20} eV [4, 5, 6, 7, 8, 9, 10, 11, 12, 13, 14, 15, 16, 17], with no evidence that the highest energy recorded thus far is Nature's upper limit.

In contrast to the irregular shape of the isotropic electromagnetic background spectrum from, say, $10^8 - 10^{20}$ Hz, the CR energy spectrum above 10^9 eV can be described by a series of power laws, with the flux falling about 3 orders of magnitude for each decade increase in energy (see Fig. 1). In the decade centered at $\sim 10^{15.5}$ eV (the knee) the spectrum steepens from $E^{-2.7}$ to $E^{-3.0}$. This feature, discovered around 40

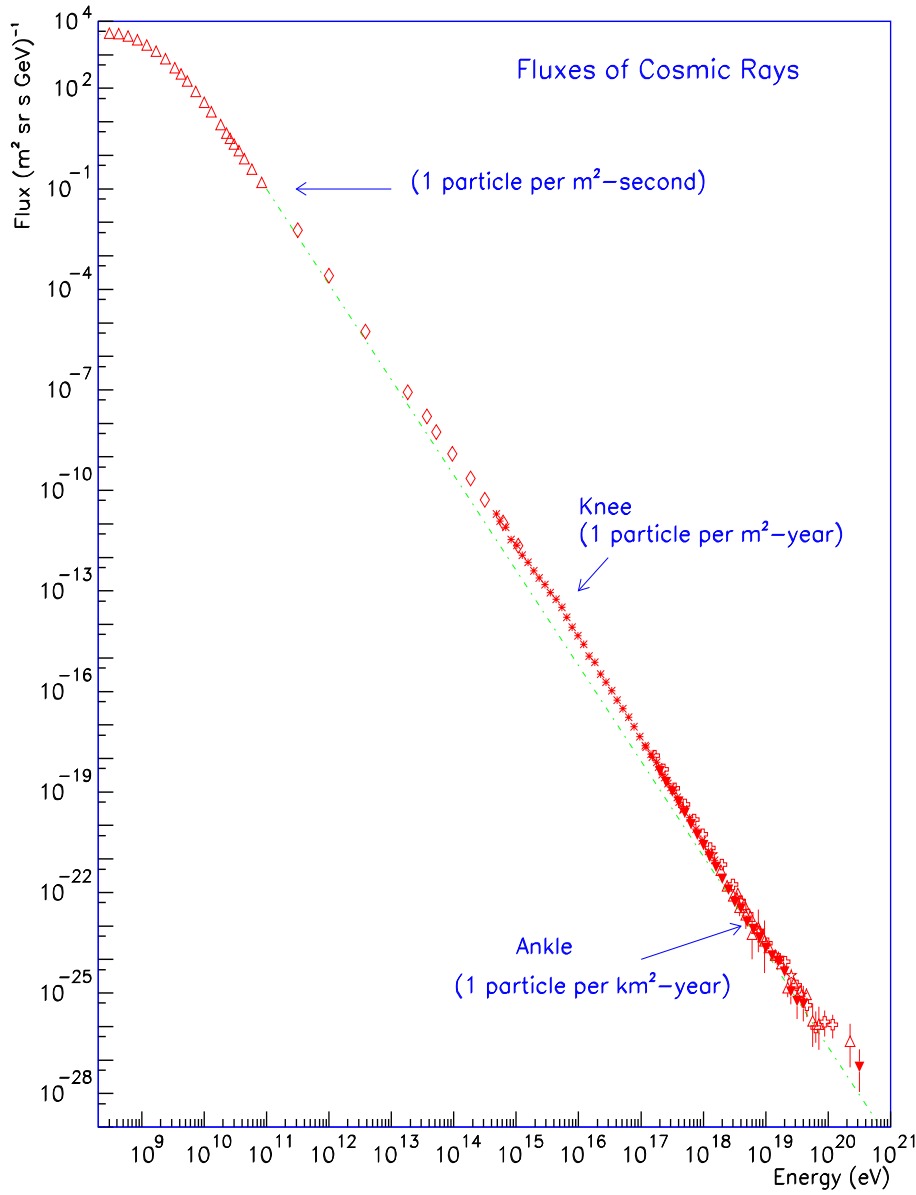


FIG. 1: Compilation of measurements of the differential energy spectrum of CRs. The dotted line shows an E^{-3} power-law for comparison. Approximate integral fluxes (per steradian) are also shown [18].

years ago [19], is still not consistently explained. The spectrum steepens further to $E^{-3.3}$ above $\sim 10^{17.7}$ eV (the dip) and then flattens to $E^{-2.7}$ at $\sim 10^{18.5}$ eV (the ankle). Within the statistical uncertainty of the data collected by AGASA [20], which is large above 10^{20} eV, the tail of the spectrum is consistent with a simple extrapolation at

that slope to the highest energies, possibly with a hint of a slight accumulation around $10^{19.5}$ eV. A very widely held interpretation of the ankle is that above $10^{18.5}$ eV a new population of CRs with extragalactic origin begins to dominate the more steeply falling Galactic population [21]. This hypothesis is supported by the data recorded at AGASA, which shows that around 10^{18} eV the angular distribution correlates with the Galactic center (anisotropy $\sim 4\%$) and is consistent with a Galactic origin, whereas at higher energy the anisotropy disappears [22, 23].

At the very high end of the spectrum the flux now appears more uncertain than was thought as recently as a year ago. At that time the event rate at 10^{19} eV reported by different experiments was in agreement at the 10 - 15% level. In particular, preliminary data reported by the HiRes group [16] showed 7 events above 10^{20} eV, in good accord with the number anticipated from the flux observed by the AGASA experiment [20]. Very recently, the AGASA Collaboration reported a total of 17 events above 10^{20} eV [17], quite consistent with their previous work [20]. However, one of the HiRes cameras, which has an exposure slightly greater than that of the AGASA experiment, recorded only 2 events above 10^{20} eV compared to the 20 expected for a spectrum similar to that reported earlier by AGASA [24]. The HiRes group also reported data from their stereo system, which has 20% of the monocular exposure. They observed one event with an energy estimated to be close to $10^{20.5}$ eV. These unexpected discrepancies are not yet understood. The “disappearance” of the events reported as being above 10^{20} eV in 1999 [16] is attributed to a better understanding of the atmosphere, which is now claimed to be clearer than had been previously supposed. Adding to the puzzle, the Haverah Park energy estimates have been re-assessed [25], resulting in a steeper reconstructed spectrum which shows differences of up to 30% compared to the one derived by fitting Akeno, AGASA and the “old” Haverah Park data [26].¹ The average energy of the 4 events observed by the Haverah Park experiment that were previously above 10^{20} eV is shifted 30% downwards to energies below 10^{20} eV. The energy weighted cosmic ray flux corresponding to these 4 events is $JE^3 = 8.3_{-4.0}^{+6.5} \times 10^{24}$ eV² sr⁻¹ m⁻² s⁻¹ at an energy of 7.62×10^{19} eV (see Fig. 113). The highest energy Haverah Park event is now estimated to have an energy of 8.3×10^{19} eV. In the “old” Haverah Park data sample, this event had a reported energy of 1.2×10^{20} eV. In Fig. 2 we show a compilation of the updated data from Haverah Park [25], AGASA [20], monocular HiRes (HiRes 1 and HiRes 2) [24], HiRes-MIA [28] and Fly’s Eye stereo [11]. For comparison, the figure also shows 4 recent parameterizations of the energy spectrum

¹ It is noteworthy that AGASA energies have been estimated under the assumption that the primaries are protons above 10^{18} eV. Though there is no evidence as to what mass species is dominant at the highest energies, the results from AGASA decrease by only about 20% when the hypothesized chemical composition is changed.

including the fit to the Akeno, AGASA and Haverah Park data sets by Nagano and Watson [26], the one obtained by Szabelski, Wibig and Wolfendale [29], the parameterization given by the HiRes Collaboration [24] and a parameterization based on a recent analysis of Haverah Park data [25]. The recalibrated Haverah Park spectrum is in very good agreement with that obtained by the fluorescence detectors of Fly’s Eye and HiRes. Reconciling the observations of the various experiments depends on a detailed understanding of detector behavior and atmospheric properties as well as reliable models to predict the evolution of cosmic air showers. These issues are discussed in the following sections.

B. Properties of extensive air showers and mass composition

We begin this section with a brief discussion of the principal observables characterizing an EAS. Next, we discuss how the shower development differs for different primary species and how these differences are manifest in the shower observables.

The incidence of a single high energy particle on the upper atmosphere gives rise to a roughly conical cascade of particles which reaches the Earth in the form of a giant “saucer” traveling at nearly the speed of light. As the cascade develops in the atmosphere, the number of particles in the shower increases until the energy of the secondary particles is degraded to the level where ionization losses dominate. At this point the density of particles starts to decline. The number of particles as a function of the amount of atmosphere penetrated by the cascade (in g cm^{-2}) is known as the “longitudinal profile” shown schematically in Fig. 3. The atmospheric depth at which the number of particles in the showers reaches its maximum, X_{max} , is often regarded as the most useful observable of the shower, as it strongly depends on the primary energy and composition. For example, X_{max} increases with primary energy since more cascade generations are required in the cooling of secondary products. The way the average depth of maximum $\langle X_{\text{max}} \rangle$ changes with energy depends on the primary composition and particle interactions according to

$$\langle X_{\text{max}} \rangle = D_e \ln \left(\frac{E}{E_0} \right), \quad (1)$$

where D_e is the so-called “elongation rate” and E_0 is a characteristic energy that depends on the primary composition [30]. Therefore, since $\langle X_{\text{max}} \rangle$ and D_e can be determined directly from the longitudinal shower profile measured with a fluorescence detector, E_0 and thus the composition, can be extracted after estimating E from the total fluorescence yield. Indeed, the parameter often measured is D_{10} , the rate of change of $\langle X_{\text{max}} \rangle$ per *decade* of energy. We note that one can discern changes in the primary composition from breaks in the elongation rate, and such breaks are relatively

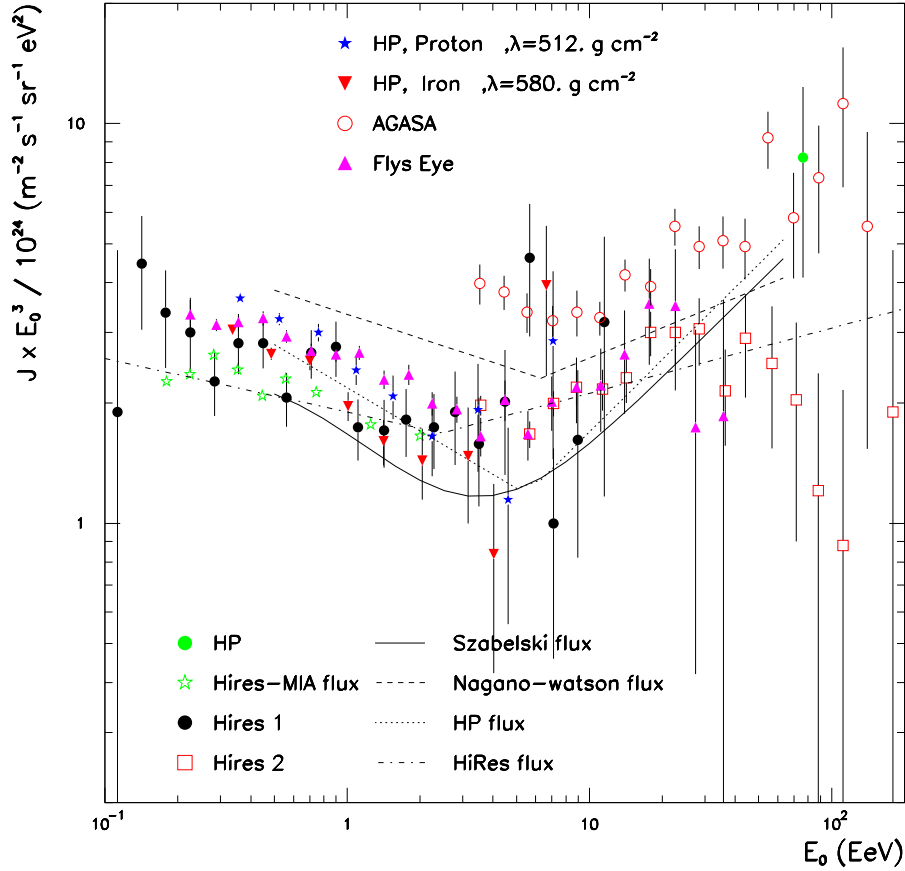


FIG. 2: A composite energy spectrum including recently reanalysed Haverah Park data assuming proton and iron primaries (the parameter λ measures the attenuation length of the density of charged particles at 600 m from the shower core), stereo Fly’s Eye data, monocular HiRes data from both eyes up to 60° , and hybrid HiRes–MIA data. The measurements are compared to spectrum parameterizations given by different authors as described in the text. Published in Ref. [27].

insensitive to certain systematic uncertainties.

If the primary particle is a nucleon or a nucleus the shower begins with a hadronic interaction. The number of hadrons increases through subsequent generations of particle interactions. However, in each generation about 30% of the energy is transferred to an electromagnetic cascade by the prompt decay of neutral pions. Ultimately, the electromagnetic cascade dissipates around 90% of the primary particle’s energy, and hence the total number of electromagnetic particles is very nearly proportional to the shower energy. The remaining energy is carried by muons and neutrinos from π^\pm decays. The

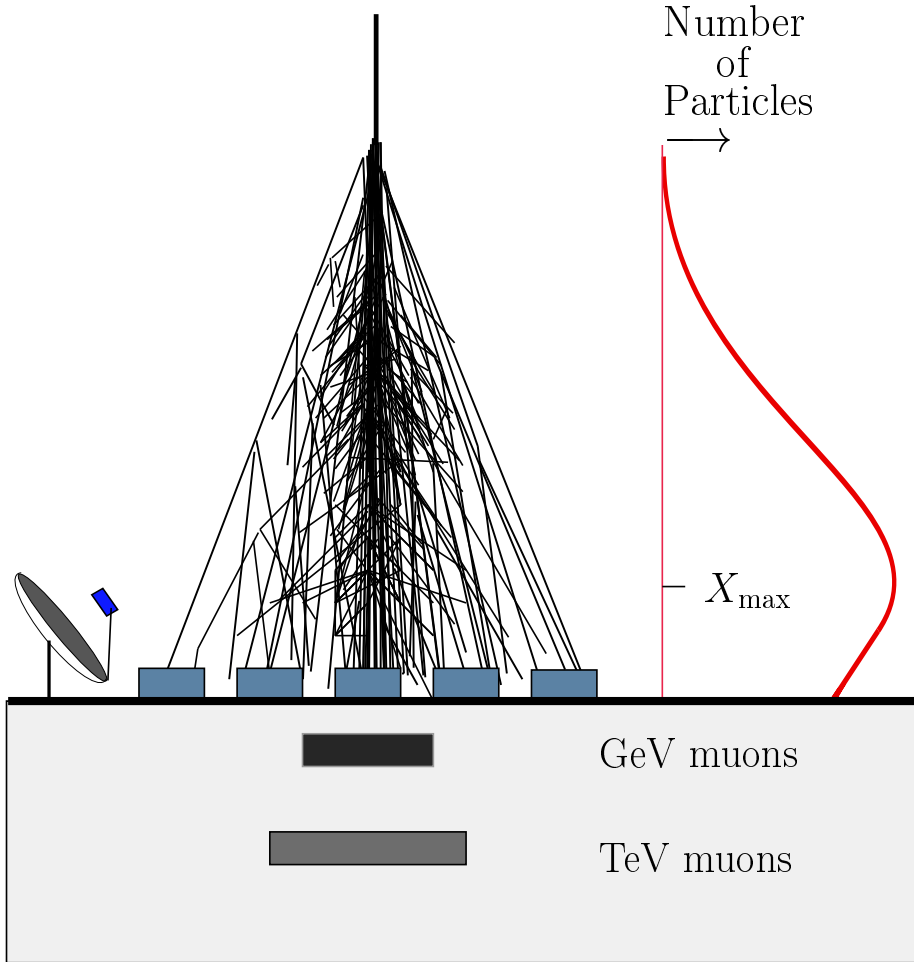


FIG. 3: Particles interacting near the top of the atmosphere initiate an electromagnetic and hadronic cascade. Its profile is shown on the right. The different detection methods are illustrated. Mirrors collect the Čerenkov and nitrogen fluorescent light, arrays of detectors sample the shower reaching the ground, and underground detectors identify the muon component of the shower.

number of muons does not increase linearly with energy, since at higher energy more generations are required to cool the pions to the point where they are likely to decay before interaction. Production of extra generations results in a larger fraction of the energy being lost to the electromagnetic cascade, and hence a smaller fraction of the original energy being delivered to the π^\pm . With this in mind, one can evaluate the

muon production in a heavy nucleus shower relative to that in a proton shower by viewing a nucleus with atomic number A and energy E as a collection of individual nucleons each with energy E/A . The muon production in a proton shower increases with energy as $E^{0.85}$ [31], and thus the total number of muons produced by a nucleus of mass A is $N_\mu^A \propto A(E/A)^{0.85}$, or, comparing to proton showers, $N_\mu^A = A^{0.15} N_\mu^p$. Therefore, an iron nucleus produces a shower with around 80% more muons than a proton shower of the same energy. Around 10^{20} eV, the hadronic mean free path is roughly 40 g/cm^2 .

On the other hand, if the primary particle is a γ -ray the basic interactions that cool the cascade development are pair production, Bremsstrahlung, ionization losses, and Compton scattering. Above 10^{19} eV the Landau-Pomeranchuk-Migdal (LPM) effect leads to significant suppression of the Bethe-Heitler cross section for pair production and Bremsstrahlung, and so the growth of N_μ with energy gradually disappears [32]. However, the muon suppression in electromagnetic showers caused by the LPM effect become largely compensated by the interactions of γ -rays with the geomagnetic field [33]. Above the ankle ($\sim 10^{18.5}$ eV), a γ -shower produces less than 20% as many muons as a proton shower of the same energy. The energy dependence of this effect has a rather complicated (non power-law) form [34]. Gamma-rays of energy $\sim 3 \times 10^{20}$ eV have interaction lengths of approximately 60 g/cm^2 with a standard deviation of 80 g/cm^2 if the LPM effect is taken into account, but these figures reduce to 46 g/cm^2 and 45 g/cm^2 , respectively, if the LPM effect is ignored [32].

The experimental observables for inclined showers (incident zenith angle $\theta > 60^\circ$) are complimentary to those for vertical showers, since inclined showers are mostly comprised of muons which were produced far from the detection zone [35]. In contrast to vertical showers the shower front is extremely flat (radius of curvature $> 100 \text{ km}$) and the particle time spread is very narrow ($\Delta t < 50 \text{ ns}$). For $\theta > 70^\circ$ the electromagnetic component arising from the hadronic channel through π^0 decays is totally extinguished, as more than 3 equivalent vertical atmospheres are traversed. There remains only a residual electromagnetic component in the shower front which is produced by the muons themselves, mostly through muon decay.

Extracting information on the nature of the primaries from D_e and $\langle X_{\text{max}} \rangle$, or from the variation of the muon content has proved to be exceedingly difficult for a number of reasons. The most fundamental drawback is that the first few cascade steps are subject to large inherent fluctuations and consequently this limits the event-by-event mass resolution of the experiments. In addition, the c.m. energy of the first interactions is well beyond any reached in collider experiments. Thus, one needs to rely on hadronic interaction models that attempt to extrapolate, using different mixtures of theory and

phenomenology, our understanding of particle physics.²

The analysis of the elongation rate and the spread in X_{\max} at a given energy reported by the Fly’s Eye Collaboration suggests a change from an iron dominated composition at $10^{17.5}$ eV to a proton dominated composition near 10^{19} eV [10]. Such behavior of D_e is in agreement with an earlier analysis from Haverah Park [36]. However, the variation of the density of muons with energy reported by the Akeno Collaboration favours a composition that remains mixed over the $10^{18} - 10^{19}$ eV decade [37]. At this stage, it is worthwhile to recall that any inferred mass composition would be model-dependent (see Appendix A). Recently, Wibig and Wolfendale [38] reanalyzed the Fly’s Eye data considering not only proton and iron components (as in [10]) but a larger number of atomic mass hypotheses. Additionally, they adopted a different hadronic model that shifts the prediction of X_{\max} for primary protons of 10^{18} eV from 730 g cm^{-2} [10] to 751 g cm^{-2} . The difference, although apparently small, has a significant effect on the mass composition inferred from the data. The study indicates that at the highest energies ($10^{18.5} - 10^{19}$ eV and somewhat above) there is a significant fraction of nuclei with charge greater than unity. This result is more in accord with the conclusions of the Akeno group than those of the Fly’s Eye group. Deepening the problem, there is a difference between the conclusion reached from data on X_{\max} from the Fly’s Eye experiment [10] and those reached from the HiRes prototype, operated with the MIA detector in the range 10^{17} to 10^{18} eV [39].

Nowadays, the most powerful tool for extracting the primary mass spectrum relies on comparing the flux of vertical showers to that of inclined showers. For example, if all primaries were photons, one would expect to observe a great asymmetry in the number of vertical and inclined events. Ave *et al.* [40, 41] have used the observed Fly’s Eye spectrum to predict the rate of inclined events. Comparing the predicted rate to the rate observed by Haverah Park for showers in the range $60^\circ < \theta < 80^\circ$, they conclude that above 10^{19} eV, less than 48% of the primary cosmic rays can be photons and above 4×10^{19} eV less than 50% can be photons. Both of these statements are made at the 95% CL. This analysis is consistent with the search for showers which have significantly fewer muons than normal as reported by the AGASA Collaboration [42]. In addition, according to the predictions of QGSJET for high energy interactions (see Appendix A), the difference in abundance of muons with respect to photons and electrons in the Haverah Park inclined shower measurements seems to favour a light composition above 10^{19} eV [43]. A more robust statement awaits a better understanding of the sensitivity of this kind of analysis to different models of particle interactions.

Finally, if the primary is a neutrino the first interaction occurs deep in the atmosphere, triggering showers in the volume of air immediately above the detector. The

² A brief summary of the current status of hadronic models is provided in Appendix A.

shower would thus present a very curved front (radius of curvature of a few km), with particles arriving over $\mathcal{O}(\mu\text{s})$. If the primaries are ν_e and ν_μ , as expected from π^\pm decays, one expects a different type of shower for each neutrino species: “mixed” (with full energy) for ν_e or “pure hadronic” (with reduced energy) for ν_μ . In the charged current interaction of a ν_e , an ultrahigh energy electron is produced which initiates a large electromagnetic cascade parallel to the hadronic cascade. In contrast, the charged current interaction of a ν_μ produces an ultrarelativistic muon that is not detectable by the experiments. In the presence of maximal ν_μ/ν_τ mixing, ν_τ showers must also be considered. However, since the τ mean flight distance is $\sim 50E$ km/EeV, only τ 's with energy $\lesssim 8 \times 10^{17}$ eV will decay. Thus, ν_τ showers above this energy will be indistinguishable from ν_μ showers. The characteristics of these anomalous showers can be easily identified by fluorescence eyes and surface arrays.

C. The arrival direction distribution

The investigation of anisotropy, when taken together with analyses of the spectral shape and particle species, can yield very important clues to reveal the CR origin. For example, if CRs mostly come from the direction of the Galactic plane and are largely protonic in composition, one expects to see a dipole anisotropy favoring the direction of the Galactic center. Moreover, since magnetic rigidity increases with energy, the angular width of the Galactic plane as seen in CRs would shrink slowly with rising energy. Of course, a heavy composition dominated by iron nuclei would show much smaller anisotropy at any given energy because of the smaller Larmor radius. The deviation from isotropy in galactic latitude is generally expressed in terms of the Wdowczyk-Wolfendale [44] plane enhancement function,

$$\frac{I_{\text{obs}}(b)}{I_{\text{exp}}(b)} = (1 - f_E) + 1.437 f_E \exp[-b^2], \quad (2)$$

where b is the galactic latitude in radians, I_{obs} and I_{exp} are observed and expected (for isotropy) intensities at latitude b , and f_E is an energy dependent galactic latitude enhancement factor. A galactic origin for most of the particles would be expected to result in a positive value of f_E that increases steadily with energy. A negative f_E shows depression around the plane and $f_E = 0$ indicates the arrival direction distribution is isotropic. Much of the data suggests that the magnitude of the Galactic plane enhancement increases systematically with energy until a little more than 10^{19} eV, above which it disappears and, indeed, there is evidence for a deficit in the direction of the Galactic plane above this energy [45]. The most significant Galactic plane enhancement factor reported by Fly’s Eye, $f_E = 0.104 \pm 0.036$, is in the energy range $(0.4 - 1.0) \times 10^{18}$ eV [46]. In a similar energy range, the AGASA Collaboration reported

a strong anisotropy with first harmonic amplitude of $\sim 4\%$, corresponding to a chance probability of 0.2% after taking the number of independent trials into account [22]. A recent analysis of SUGAR data confirms the existence of an excess flux of CRs from a direction near the Galactic center [47]. The signal is consistent with that from a point source [48].

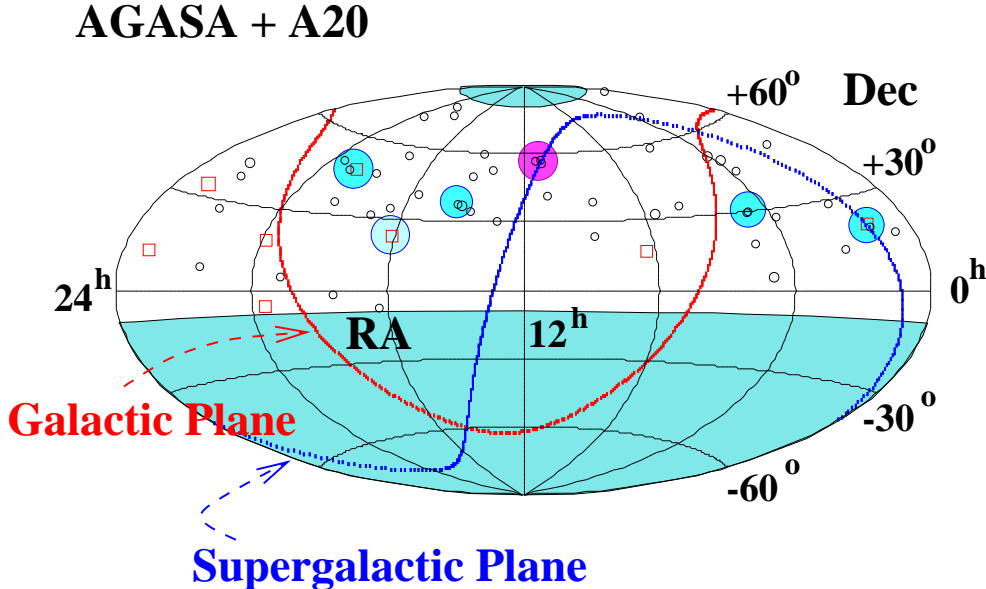


FIG. 4: Arrival directions of cosmic rays detected by the AGASA and Akeno (A20) experiments in equatorial coordinates. Open circles and open squares represent cosmic rays with energies $(4 - 10) \times 10^{19}$ eV, and $\geq 10^{20}$ eV, respectively. The Galactic and super-Galactic planes are shown. Large shaded circles indicate event clusters within 2.5° . The shaded regions indicate the celestial regions excluded by a zenith angle cut of $\leq 45^\circ$. Published in Ref. [20].

In a much higher energy range, the analysis of Haverah Park data seems to indicate that events with primary energy $> 4 \times 10^{19}$ eV reach the Earth preferentially from the direction of the super-Galactic plane, a swath in the sky along which radio galaxies are clustered [49]. The magnitude of the observed excess is found to be 2.5 - 2.8 σ in terms of Gaussian probabilities. However, such large-scale correlation with the super-Galactic plane was not observed in the data sets of the AGASA [50], SUGAR [51, 52] and Fly's Eye [46] experiments.

The arrival direction of the events with energy $> 4 \times 10^{19}$ eV registered by the AGASA experiment is shown in Fig. 4. The data show no significant super-Galactic plane enhancement. However, some excess of particles from the general direction of

the super-Galactic plane is observed in the energy bin $\log(E[\text{eV}]) = [19.1, 19.2]$, with $f_E^{\text{SG}} = 0.36 \pm 0.15$ [53].³ The highest energy events are distributed widely over the sky, without any apparent counterparts, such as sources in the Galactic plane or in the local supercluster. Moreover, the data are consistent with an isotropic distribution of sources, in sharp contrast to the anisotropic distribution of light in the local supercluster [54].

Adding to the puzzle, the AGASA experiment draws attention to the fact that the pairing of events on the celestial sky could be occurring at higher than chance coincidence [20]. Specifically, when showers with separation angle less than the angular resolution $\theta_{\text{min}} = 2.5^\circ$ are paired up, AGASA finds five doublets and one triplet among the 58 events reported with mean energy above 4×10^{19} eV (see Fig. 4). The chance probability of observing such topology in an isotropic distribution can be estimated by means of the Goldberg-Weiler formalism [55]. To do so, consider the solid angle $\Omega \sim 4.8$ sr on the celestial sphere covered by AGASA to be divided into N equal angular bins, each with solid angle $\omega \simeq \pi\theta^2$. Then, by tossing n events randomly into

$$N \simeq \frac{\Omega}{\pi\theta^2} = 1045 \frac{\Omega}{1 \text{ sr}} \left(\frac{\theta}{1^\circ}\right)^{-2} \quad (3)$$

bins, one is left with a random distribution. Now, identify each event distribution by specifying the partition of the total sample of AGASA into a number m_0 of empty bins, a number m_1 of single hits, a number m_2 of double hits, etc., among the N angular bins that constitute the whole exposure. The probability to obtain a given event topology is [55]

$$P = \frac{N!}{N^N} \frac{n!}{n^n} \prod_{j=0}^{\infty} \frac{(\overline{m}_j)^{m_j}}{m_j!}, \quad (4)$$

where

$$\overline{m}_j \equiv N \left(\frac{n}{N}\right)^j \frac{1}{j!}. \quad (5)$$

Using Stirling's approximation for the factorials with the further assumption $N \gg n \gg 1$, Eq. (4) can be re-written in a quasi-Poisson form

$$P \approx \mathcal{P} \left[\prod_{j=2}^{\infty} \frac{(\overline{m}_j)^{m_j}}{m_j!} e^{-\overline{m}_j r^j (j-2)!} \right], \quad (6)$$

³ The super-Galactic plane enhancement factor is given by $I_{\text{obs}}(b)/I_{\text{exp}}(b) = (1 - f_E^{\text{SG}}) + 1.402 f_E^{\text{SG}} \exp[-b^2]$. Compare this with the Fly's Eye parameterization for the Galactic plane given in Eq. (2).

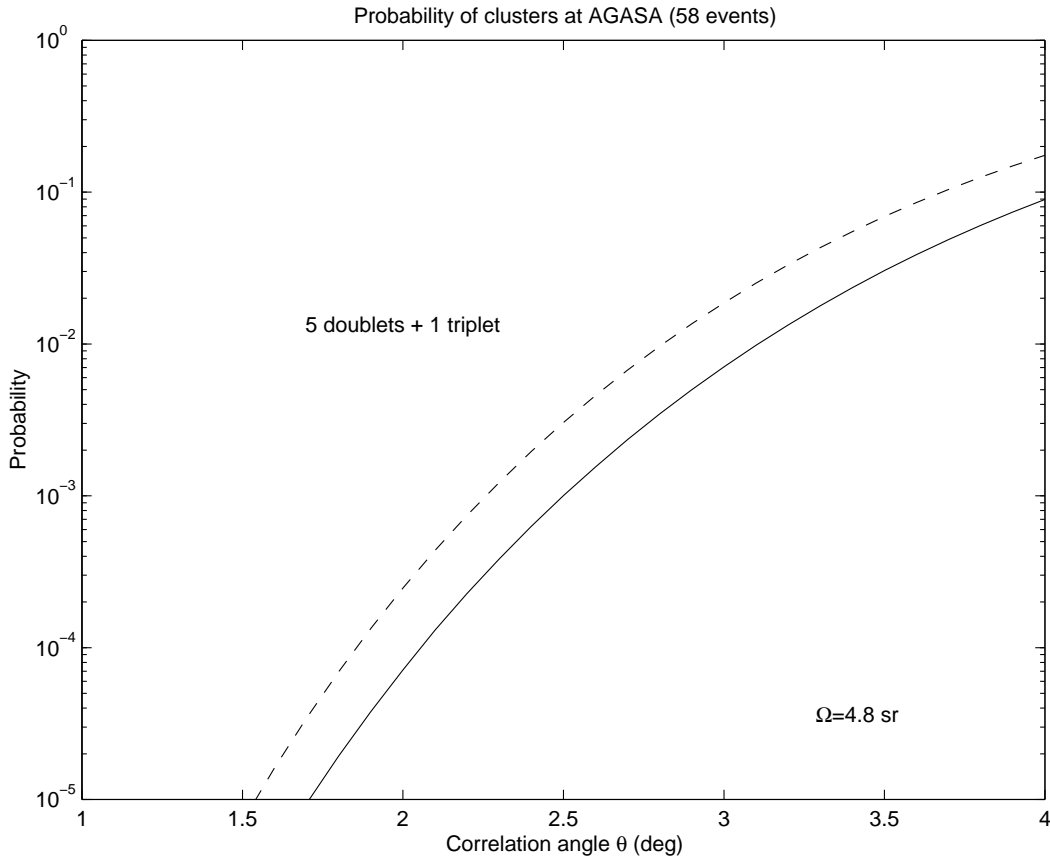


FIG. 5: Inclusive probabilities for five doublets and one triplet in a 58-event sample at AGASA. Solid (exact), dashed (Poisson). From Ref. [56].

where $r \equiv (N - m_0)/n \approx 1$, and the prefactor \mathcal{P} is given by

$$\mathcal{P} = e^{-(n-m_1)} \left(\frac{n}{m_1} \right)^{m_1 + \frac{1}{2}}. \quad (7)$$

For “sparse events”, where $N \gg n$, one expects the number of singlets m_1 to approximate the number of events n . In such a case the prefactor is near unity. Figure 5 shows the inclusive probabilities for observing 5 doublets and one triplet given 58 events at AGASA as a function of the angular resolution.⁴ The inclusive probability is extremely sensitive to the angular binning. The chance probability within the experimental angular resolution of AGASA is less than 10^{-3} , in agreement with the estimates of the AGASA Collaboration [53].

The “world” data set has also been studied [58]. Six doublets and two triplets out

⁴ The specified number of j -plets plus any other cluster, counts as all the j -plets + extra-clusters.

of 92 events with energies $> 4 \times 10^{19}$ eV were found, with the chance probability being less than 1% in the restricted region within $\pm 10^\circ$ of the super-Galactic plane. Very recently, the angular two-point correlation function of a combined data sample of AGASA ($E > 4.8 \times 10^{19}$ eV) and Yakutsk ($E > 2.4 \times 10^{19}$ eV) was analyzed [57]. For a uniform distribution of sources, the probability of chance clustering is reported to be as small as 4×10^{-6} . The implication of such clusters would be profound, but the case for them is not yet proven. To calculate a meaningful statistical significance in such an analysis, it is important to define the search procedure *a priori* in order to ensure it is not (inadvertently) devised especially to suite the particular data set after having studied it [59]. In the above mentioned analysis, for instance, the angular bin size was not defined ahead of time.

D. Measurement techniques

There are several techniques which can be employed in detecting ultrahigh energy CRs, ranging from direct sampling of particles in the shower to measurements of associated fluorescence, Čerenkov or radio emissions, or possibly even radar detection of the air shower. Direct detection of shower particles is the most commonly used method, and involves constructing an array of sensors spread over a large area to sample particle densities as the shower arrives at the Earth's surface. Another well-established method involves measurement of the longitudinal development of the EAS by sensing the fluorescence light produced via interactions of the charged particles in the atmosphere. A more recently proposed technique uses radar echos from the column of ionized air produced by the shower. In the rest of this section, we give an overview of the main features of these experimental techniques, and afterwards outline the status of existing and pending ultrahigh energy CR experiments. More detailed and rigorous treatments of the current experimental situation of ultrahigh energy CRs are given in several review articles [26, 60, 61, 62, 63].

1. Surface arrays

A surface array is comprised of particle detectors, such as plastic scintillators or Čerenkov radiators, distributed with approximately regular spacing. Such detectors measure the energy deposited by particles in the EAS as a function of time, and from energy density measured at the ground and the relative timing of hits in the different

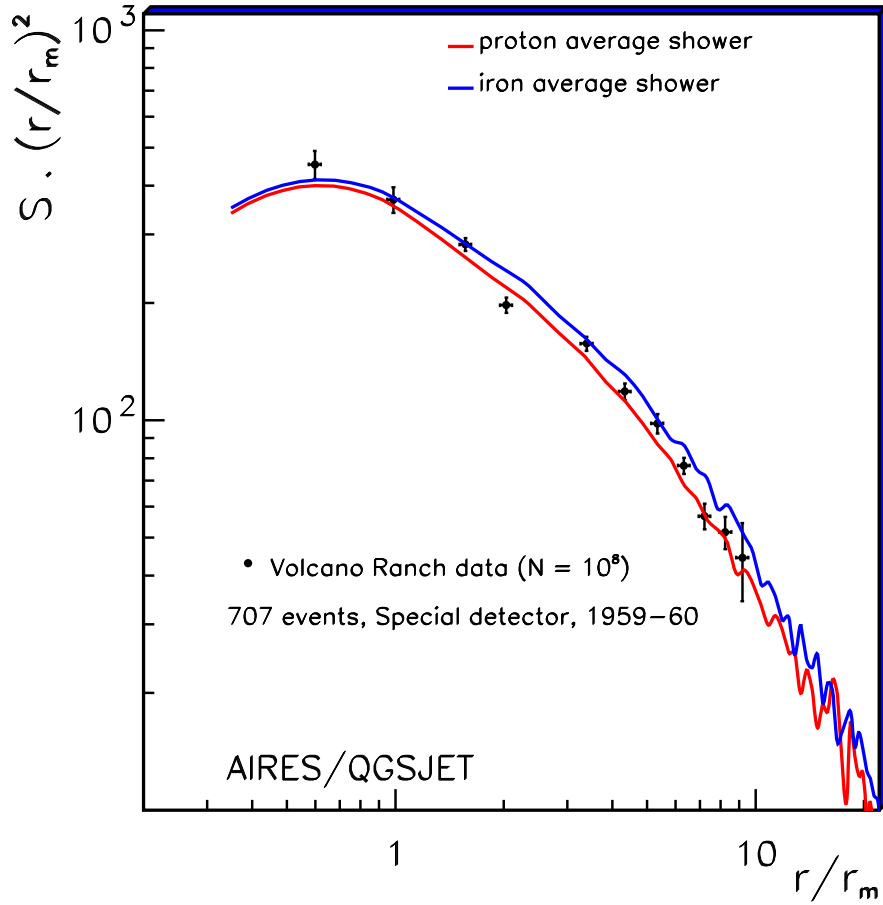


FIG. 6: Average lateral distribution of simulated showers (with the program AIRES/QGSJET [64]) compared to average measurements from Volcano Ranch [65]. Here r/r_M is the distance to the shower axis in units of the Moliere radius (at the Volcano Ranch elevation $r_M \approx 100$ m) and S is the lateral distribution of particles at ground in units of minimum ionizing particles per square meter (mips/m²). The estimated size of the showers is 10^8 particles, which corresponds to an energy of about 10^{18} eV. Taken from Ref. [66].

detectors one can estimate the energy and direction of the primary CR.⁵

Reconstruction of air showers involves fitting the lateral distribution (LD) function of particle densities at the ground (see for example Fig. 6). The exact form of the LD depends on how the experimental apparatus responds to the shower particles. The AGASA experiment, for example, employs 5 cm thick plastic scintillators. For energies which are typical of particles at about 1 km from the shower axis (usually

⁵ An assumption of axial symmetry is generally made; this assumption is only valid for zenith angles $\theta < 60^\circ$, because at larger angles the low energy secondaries are deflected by geomagnetic fields.

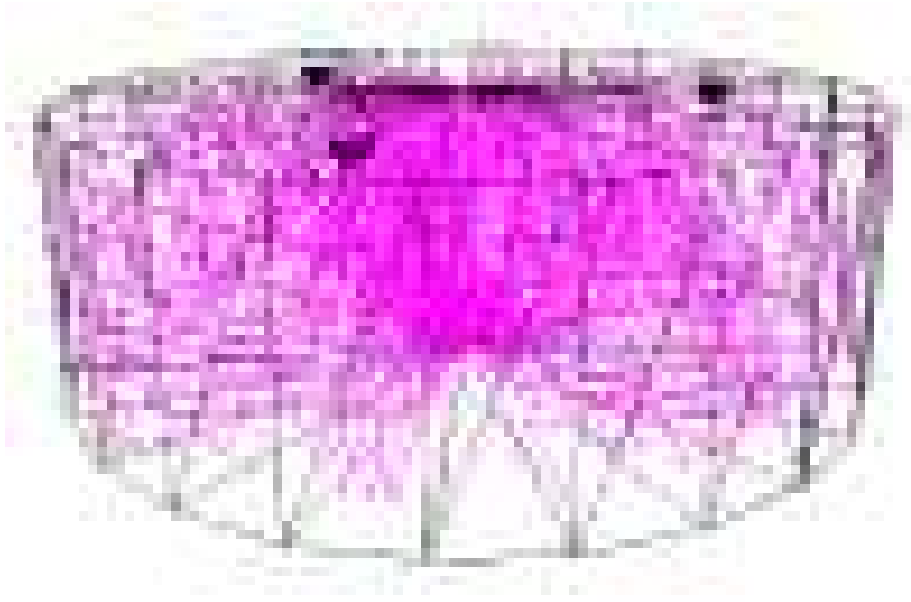


FIG. 7: Simulation of a muon entering a tank of water from above and radiating Čerenkov light. Housings for three photomultiplier tubes are visible at the top of the tank. This is a simulation of a Pierre Auger Observatory water tank [67].

called the “core”) these scintillators generate similar signals for the electron and muon components of the shower, while producing much smaller signals for the photons. The Haverah Park and Auger experiments, on the other hand, employ tanks of water about a meter deep and a meter and a half in radius, as illustrated in Fig. 7. In this case, Čerenkov radiation produced by charged particles passing through the water bounces off the reflective tank walls and is picked up by photomultiplier tubes mounted inside. The signal size is thus proportional to the track length of the charged particle in the water. For energies typical of particles about 1 km from the core, muons tend to penetrate the full depth of the tank and thus produce large signals, whereas electrons and photons are quickly absorbed and produce signals an order of magnitude smaller.

Furthermore, the fraction of the energy deposited by the muon and electromagnetic components changes with distance from the core and has been determined experimentally. For the Haverah Park experiment, for instance, the lateral density distribution of the water Čerenkov signal in units of fully penetrating vertical equivalent muons per m^2 , can be fitted with a modified power-law [68]

$$\rho(r) = k r^{-(\eta+r/4000)+\beta} \left(\frac{r}{800} \right)^\beta, \quad (8)$$

where the distance to the shower core, r , is in meters, k is a normalization parameter,

$\beta = 1.03 \pm 0.05$, and η is given by

$$\eta = 3.49 - 1.29 \sec \theta + 0.165 \log \left(\frac{E}{10^{17} \text{ eV}} \right), \quad (9)$$

with θ the shower zenith angle, and $E \gtrsim 10^{19}$ eV the shower energy.

Since the response of plastic scintillator slabs to electrons, muons and photons is somewhat different from that of deep water Čerenkov radiators, a different form of the LD function is appropriate. For instance, in the case of AGASA, the empirical formula for the LD of charged particles with $\sec \theta \leq 1.7$ reads [69]

$$S(r) = C \left(\frac{r}{r_M} \right)^{-\alpha} \left(1 + \frac{r}{r_M} \right)^{-\eta+\alpha} \left[1 + \left(\frac{r}{1 \text{ km}} \right)^2 \right]^{-\delta}, \quad (10)$$

where r is the distance in meters from the core, r_M is the Moliere radius at two radiation lengths above the observation level (91.6 m at Akeno), C is a normalization factor, α and δ are 1.2 and 0.6, respectively. η is the parameter which indicates the slope of the LD⁶ for $r \geq r_M$ as a function of the zenith angle of the arrival direction, and is given by

$$\eta = 3.97 - 1.79 (\sec \theta - 1.0). \quad (11)$$

The primary CR energy is determined using a formula derived from simulations,

$$E = 2.0 \times 10^{17} S_0(600) \text{ eV}, \quad (12)$$

where $S_0(600)$ is the charged particle density in $1/\text{m}^2$ at 600 m from the core for a vertical equivalent shower. $S_0(600)$ is evaluated from the observed local density at 600 m,

$$S_0(600) = S(600) \exp \left[-\frac{X_0}{\Lambda_1} (\sec \theta - 1) - \frac{X_0}{\Lambda_2} (\sec \theta - 1)^2 \right], \quad (13)$$

where $X_0 = 920 \text{ g/cm}^2$, $\Lambda_1 = 500 \text{ g/cm}^2$, and $\Lambda_2 = 594_{-120}^{+268} \text{ g/cm}^2$. The first order approximation agrees with measurements for $\sec \theta < 1.4$. The error quoted in the second term is at the 68% CL.

As discussed previously, the muon content of the EAS at ground level depends on the composition of the primary CR. Thus, surface arrays with some ability to distinguish muons from electrons and photons can determine something about the primary CR species. Water Čerenkov detectors and scintillator-absorber combinations have such distinguishing power, for example. It is also possible to gauge the muon content of an EAS from the signal rise time, as the muonic component tends to be compressed

⁶ The selection criterion of deeply developing showers is η of 4 to 6, which indicates a steeper lateral distribution than that of the average EAS (more on this below) [70].

in time compared to the electromagnetic component. Typically experiments measure something like the time interval between the arrival of the 10% and 50% points of the integrated signal (t_{10}/t_{50}).

2. *Fluorescence eyes*

As an EAS develops in the atmosphere it dissipates much of its energy by exciting and ionizing air molecules along its path. Excited nitrogen molecules fluoresce producing ultraviolet radiation. The shower development appears as a rapidly moving spot of light describing a great circle path across a night-sky background of starlight, atmospheric airglow, and man-made light pollution. The angular motion of the spot depends on both the distance and the orientation of the shower axis. The apparent brightness of the spot depends on the instantaneous number of charged particles present in the shower, but it is also affected by Čerenkov contamination and atmospheric scattering.

The fluorescence trail is emitted isotropically with an intensity that is proportional to the number of charged particles in the shower, N_e .⁷ The ratio of the energy emitted as fluorescence light to the total energy deposited is less than 1%, hence low energy ($< 10^{17}$ eV) showers can hardly be observed. Furthermore, observations can only be done on clear moon-less nights, resulting in an average 10% duty cycle. The emitted light is typically in the 300 - 400 nm ultraviolet range to which the atmosphere is quite transparent. Under favorable atmospheric conditions EASs can be detected at distances as large as 20 km, about 2 attenuation lengths in a standard desert atmosphere at ground level.

A fluorescence eye consists of several large light collectors (or telescopes) which image regions of the sky onto clusters of light sensing and amplification devices. The basic elements of a telescope are the diaphragm, which defines the telescope aperture, the spherical mirror that must be dimensioned to collect all the light entering the diaphragm in the acceptance angular range, and the camera which consists of an array of photomultiplier tubes (PMTs) positioned approximately on the mirror focal surface [71].⁸ The PMTs effectively pixelize the region of the sky covered by the telescope. The shower development is detected as a long, rather narrow sequence of hit PMTs. As the point-like image of the shower proceeds through an individual PMT, the signal rises, levels off, and falls again. The collection of vectors pointing from the

⁷ We stress that N_e denotes the charged multiplicity, but in practice it is often used to express the number of electrons and positrons since they completely dominate the total number of charged particles.

⁸ A potential future development could involve the use of avalanche photodiodes (APDs) instead of PMTs. APDs have several advantages [72].

hit PMTs defines the shower detector plane (SDP).

The sensitivity of the detector depends primarily on the signal (S) to noise (N) ratio. The signal is proportional to the diaphragm area, whereas the background (B) is proportional to the pixel (the area read out by a single PMT) solid angle times the diaphragm area, thus

$$\frac{S}{N} = \frac{S}{\sqrt{B}} \propto \frac{d_{\text{dph}}}{\alpha_{\text{pix}}} \quad (14)$$

where d_{dph} is the diaphragm diameter, and α_{pix} is the angular diameter of a pixel.

Shower reconstruction involves first determining the geometry of the shower, and then reconstructing the shower's longitudinal profile. The first step of the geometrical reconstruction is the SDP determination from the PMT hit pattern. Next, the tube hit times are used to find the shower impact parameter and incident angle in the SDP; the resolution obtained for these parameters depends on the length of the observed track [73]. Once the geometry is known, the track can be chopped into angular bins and the longitudinal profile can be determined. Extracting the profile usually involves 3-parameter fits to the Gaisser-Hillas function [74],

$$N_e(X) = N_{e,\text{max}} \left(\frac{X - X_0}{X_{\text{max}} - X_0} \right)^{[(X_{\text{max}} - X_0)/\lambda]} \exp \left\{ \frac{X_{\text{max}} - X}{\lambda} \right\}, \quad X \geq X_0, \quad (15)$$

where $N_{e,\text{max}}$ is the size at the maximum, X_0 is the depth of the first observed interaction, and $\lambda = 70 \text{ g/cm}^2$. The integral of the longitudinal profile is a calorimetric measure of the total electromagnetic shower energy. A charged particle in the cascade deposits an average of 2.2 MeV into the atmosphere in each depth interval of 1 g/cm^2 [75], so the total electromagnetic energy (in MeV) is given by

$$E_{\text{em}} = 2.2 \int N_e(X) dX . \quad (16)$$

The largest cosmic ray air shower ever recorded has an estimated energy of $(3.2 \pm 0.9) \times 10^{20} \text{ eV}$, reaching the maximum size near a depth of 815 g/cm^2 [12]. The longitudinal development is shown in Fig. 8. The size at maximum is greater than 200 billion particles!

3. Radio detection techniques

In addition to the ultraviolet emission exploited by fluorescence eyes, it may also be possible to call into service the radio frequency (RF) energy generated by air-showers. CR showers may induce radio pulses through several mechanisms, though it is thought that from about 20-100 MHz, the dominant process can be described as coherent

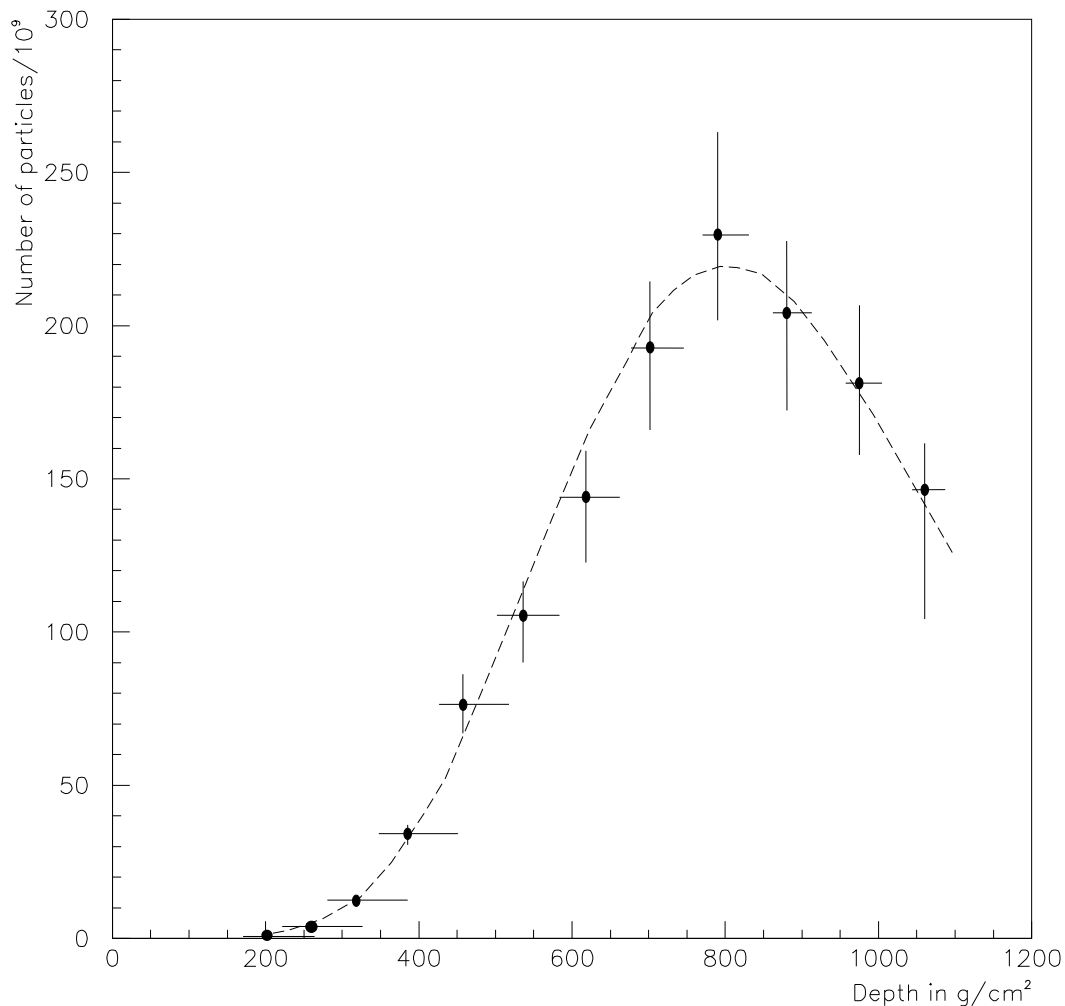


FIG. 8: The 3-parameter best fit shower profile for the highest energy event observed by the Fly’s Eye experiment. Published in [12].

synchrotron emission by the electron and positron pairs propagating in the Earth’s magnetic field [76, 77].

RF pulses coincident with EASs were first measured in the 1960’s [78], and these early results were followed up with additional work over another decade or so. Subsequently the technique was mostly abandoned in light of the promising results from surface arrays and fluorescence eyes, though quite recently a few groups have undertaken a new examination of the method. For example, a prototype RF detection system using a single antenna in conjunction with the buried muon detectors of the CASA-MIA array has recently been evaluated, with the goal of demonstrating the feasibility of incorporating such an RF receiver into an existing experiment like the Pierre Auger

Observatory [79]. Though no significant EAS-induced pulses were observed, a number of technical issues relevant to future development were uncovered.

More ambitious possibilities have been recently described [80] in the context of next-generation digital telescopes. In particular, the planned Low-Frequency Array (LOFAR)⁹, which could begin construction as early as 2004, would be well-suited to study RF emissions from EASs. This device will comprise around 100 stations of 100 dipoles distributed over a region some 400 km in radius. A cluster of computers will correlate data from the antennae to synthesize “virtual telescopes” which look in any desired direction. The CR energy range for which one achieves both a reasonable signal-to-noise ratio and a reasonable event rate depends on the number of dipoles actually employed. A single LOFAR-type station of about 100 dipoles, for example, would be useful for measurements in the range 10^{15} – 10^{17} eV; indeed just such a prototype station, known as LOPES [81], is scheduled to be operational in 2003 at the KASCADE experiment. Falcke and Gorham [80] estimate that LOFAR should be able to observe events up to 10^{20} eV at a rate of order 1 per year.

In addition to such passive radio techniques, it may also be possible to detect radar reflections off the ionization columns produced by EASs. This idea was suggested already in 1940 [82], and recently the issue has been re-explored [83, 84] as either an independent method to study air showers, or as a compliment to existing fluorescence and surface detectors. For example, one could use a fluorescence detector to trigger a radar system to interrogate in the approximate direction of the shower. It has been estimated that showers from primaries of order 10^{18} eV should be detectable [83], and that range estimates with precision around 20 m may be possible. The technique would work best for distant or horizontal showers, the latter being of particular interest in searches for deeply penetrating showers induced by neutrino primaries. One important uncertainty is the lifetime of the ionization trail, which decays away due to electron recombination and attachment and can thus limit the time available for radar interrogation; these effects depend on altitude and atmospheric conditions. A proposal has recently been put forth to evaluate the method using the Jicamarca radar system near Lima, Peru [85].

E. CR-observatories: past and present

The first measurements of ultrahigh energy CRs were carried out by Linsley at Volcano Ranch ($35^{\circ}09'N$, $106^{\circ}47'W$) in the late 1950's [86, 87]. The detector comprised an array of 19 scintillation counters each of 3.3 m^2 , spaced on a 884 m hexagonal grid.

⁹ <http://www.lofar.org>

More recently, experiments have been performed at Haverah Park in England (53°58'N, 1°38'W), Yakutsk in Russia (62°N, 130°E), Sydney in Australia (30°32'S, 149°43'E), Dugway in the Utah desert (40°N, 112°W), and near the village of Akeno, about 100 km west of Tokyo (38°47'N, 138°30'E).

The Haverah Park detector [8] ceased operation in July 1987 after a life of 19 years. The detector array consisted of deep (1.2 m) water Čerenkov detectors with stations ranging in area from 1 to 54 m² (typically 34 m²) distributed over an area of approximately 12 km². Restrictions on land access made it impossible to position the detectors on a uniform grid. Therefore, a 4 detector array with 500 m spacing was deployed at the center and 6 sub-arrays of 50 m and 150 m spacing were located at about 2 km from the center. In the ongoing analyses of the data, primary energies are derived from the water Čerenkov detector density at 600 m from the shower axis, $\rho(600)$. Random errors in the determination of $\rho(600)$ are less than 30% [88]. The energy threshold was approximately 6×10^{16} eV. The angular resolution of the array was measured to be: for zenith angle (θ), $2.5^\circ \times \sec \theta$ with $\theta \in (0^\circ, 75^\circ)$, whereas for azimuth angle (ϕ), $2.5 \times \operatorname{cosec} \theta$ with $\theta \in (15^\circ, 90^\circ)$ [89].

The Yakutsk array, in operation since 1972, was expanded in 1974 for sensitivity to ultrahigh energy CRs, and spread over a ground area of approximately 18 km². Most of the detectors are plastic scintillators arranged on a triangular grid. The spacing of the detectors was around 1 km, with the center of the array filled with 7 detectors on a 500 m triangular grid [90]. Underground stations measured the muon flux, with an energy threshold of 1 GeV. The primary energy is estimated from the particle density at 600 m from the shower core. In 1995, the array was re-arranged into a smaller area (~ 10 km²) in order to investigate in detail the spectrum around 10^{19} eV [91].

The Sydney University Giant Air-shower Recorder (SUGAR) [7] operated between 1968 and 1979, and is the largest array to date in the Southern hemisphere. 47 detector stations were arranged to cover an area of approximately 70 km². Each of these stations consisted of two 6 m² conical liquid scintillator tanks separated by 50 m. The angular resolution of the array is quoted [7] to be $3^\circ \times \sec \theta$ for showers detected by more than three stations. However, most of the events were only viewed by 3 stations, and consequently the resolution is closer to 6° for vertical showers [92].

The Akeno Giant Air Shower Array (AGASA) [93, 94] consists of 111 scintillation detectors each of area 2.2 m², spread over an area of 100 km² with 1 km spacing. This gives an acceptance of 125 km² sr for CRs above 10^{19} eV.¹⁰ The array detectors are

¹⁰ The array has been divided into 4 branches for the purpose of trigger and data acquisition. These branches are called the “Akeno Branch”, the “Sudama Branch”, the “Takane Branch”, and the “Nagasaka Branch”. The 20 km² array [95], operational since the end of 1984, forms a part of the “Akeno Branch”.

connected and controlled through a sophisticated optical fiber network. The array also contains a number of shielded scintillation detectors which provide information about the muon content of the showers. The full AGASA experiment has been running since 1992.

The fluorescence technique has so far been implemented only in the Dugway desert by the Fly’s Eye group from the University of Utah. Following a successful trial at Volcano Ranch [96] the Utah group built a device containing two separated Fly’s Eyes made up of 880 and 460 PMTs, 3.3 km apart [97, 98]. The two-eye configuration monitored the sky from 1986 until 1993. The first detector, Fly’s Eye I, had full operation since 1981. It was made of 67 telescopes of $d_{\text{dph}} = 1.5$ m and spherical curvature, each with 12 or 14 PMTs at the focus. The mirrors were arranged so that the entire night sky was imaged, with each PMT viewing a hexagonal region of the sky with $\alpha_{\text{pix}} = 5^\circ$. Fly’s Eye II was made of of 36 mirrors of the same design. This detector viewed only half of the night sky.

As an up-scaled version of Fly’s Eye, the High Resolution (HiRes) Fly’s Eye detector has recently begun operations [99]. It uses 14 spherical telescopes of $d_{\text{dph}} = 2.0$ m to collect the light from a 0.95 sr portion of the sky. The image plane of each telescope is populated with an array of 256 hexagonal PMTs, yielding $\alpha_{\text{pix}} = 1^\circ$. In monocular mode, the effective acceptance of this instrument is $\sim 350(1000)$ km² sr at 10^{19} (10^{20}) eV, on average about 6 times the Fly’s Eye acceptance, and the threshold energy is 10^{17} eV. This takes into account a duty cycle of about 10% typical of the fluorescence technique. The field of view of the telescopes is centered on the Chicago Air Shower Array (CASA) and the Michigan Muon Array (MIA) [100], situated 3.3 km to the northeast. The combination of these instruments has been used as a prototype hybrid detector in which HiRes records the development profile, CASA records the ground particle density and MIA detects the muonic component of a common shower.

F. The potential of the Pierre Auger Observatory

The Pierre Auger Observatory (PAO) [101, 102] is designed to work in a hybrid mode, employing fluorescence detectors overlooking a ground array of deep water Čerenkov radiators. During clear, dark nights, events will be simultaneously observed by fluorescence light and particle detectors at ground level. The PAO is expected to measure the energy, arrival direction and primary species with unprecedented statistical precision. It will eventually consist of two sites, one in the Northern hemisphere and one in the Southern, each covering an area of 3000 km² and consisting of 1600 particle detectors overlooked by 4 fluorescence detectors. The overall acceptance (2 sites) is 14000 km² sr. A prototype engineering array, 1/40th-scale, is (at the time of writing) already taking data in Malargüe, Argentina ($35^\circ 12'S$, $69^\circ 12'W$) [103].

The surface array stations are cylindrical water Čerenkov detectors with area 10 m^2 , spaced 1.5 km from each other in a hexagonal grid. Čerenkov radiation emitted by charged particles penetrating the detector is read out by 3 PMTs. The output signal is digitised by flash ADCs, with the aim of separating the electromagnetic signal (low energy electrons and photons) from the muons crossing the tank. Event timing is made possible via global positioning system (GPS) satellites with a precision of a few tens of ns. Communication between the stations is achieved using radio signals by methods similar to cellular telephone techniques. The stations are powered by solar panels and batteries which allow autonomous operation.

The configuration of the fluorescence detectors is arranged to optimize the hybrid detector performance. The number of eyes and their location on the site are chosen so that all showers of energy $> 10^{19} \text{ eV}$ that hit the surface array are seen by at least one eye. A further constraint comes from the need to limit the systematic error in the measurements deriving from uncertainty in the attenuation length of the atmosphere traversed by the light in its path from shower to detector. The optimal configuration was determined by Monte Carlo simulation, guided by the orographic constraints on the site. The base-line design of the detector includes 4 fluorescence eyes, each comprised of six telescopes with $d_{\text{dph}} = 1.7 \text{ m}$ and $\alpha_{\text{pix}} = 1.5^\circ$ [104].

The angular and energy resolution of the ground array (without coincident fluorescence data) are typically less than 1.5° and less than 20%, respectively. “Golden events,” events detected by both methods simultaneously, will have a directional reconstruction resolution of about 0.3° for energies near 10^{20} eV . If an event trigger is assumed to require 5 detectors above threshold, the array is fully efficient at 10^{19} eV . In three years of running, the surface arrays in both hemispheres, operating 24 hours per day, will collect more than 1000 showers above $4 \times 10^{19} \text{ eV}$ with approximately uniform sky exposure. This will enable a straightforward search for correlations with discrete sources and also a sensitive large scale anisotropy analysis.

In addition, PAO offers a window for neutrino astronomy above 10^{17} eV . For standard neutrino interactions in the atmosphere, each site of PAO reaches $\sim 15 \text{ km}^3$ w.e. sr of target mass around 10^{19} eV [105], which is comparable to other neutrino detectors being planned.¹¹ An even greater acceptance [106] should be achievable for the case of Earth-skimming neutrinos which produce a τ , as we discuss in Sec.II-I.

¹¹ w.e. \equiv water equivalent.

G. The Telescope Array Project

The Telescope Array will comprise a collection of fluorescence detectors dispersed over a large area near Salt Lake City, Utah [107]. Ten observational stations separated from each other by 30 – 40 km are planned, each station containing 40 telescopes of $d_{\text{dph}} = 3$ m. An imaging camera with 256 PMTs ($\alpha_{\text{pix}} = 1^\circ$) will be installed on the focal plane of each telescope. The effective aperture of the array will be approximately $5000 \text{ km}^2 \text{ sr}$ for 10^{20} eV particles assuming a 10% observation duty factor. This aperture is around 30 times larger than the existing AGASA ground array. The energy, arrival direction, and shower maximum will be determined with an accuracy of 6%, 0.6° , and 20 g/cm^2 , respectively. In addition, the Telescope Array will observe high energy gamma rays from point sources in the sub-TeV energy region. Gamma rays will be distinguished from the large hadronic background using the imaging patterns observed with many telescopes.

H. 200?: A space odyssey

Recently, NASA initiated a concept study for space-based detectors which will stereoscopically image, from equatorial orbit, the nitrogen fluorescence light generated by EASs induced by ultrahigh energy ($> \text{few} \times 10^{19}$ eV) CRs. The Orbiting Wide-angle Light-collectors (OWL) [108] mission will involve photodetectors mounted on 2 satellites orbiting at 640 km above the Earth's surface. The eyes of the OWL will monitor a large atmospheric volume and record the ultraviolet fluorescent trails with a time resolution of $\sim 1 \mu\text{s}$ or less in segmented focal plane arrays. The segmentation of the arrays will be such as to sample the atmosphere near the Earth's surface in $\sim 1 \text{ km}^2$ pixels. The use of a space-based platform enables an extremely large event acceptance, allowing a high statistics measurement. OWL is set for possible implementation after 2007.

Two different baseline instruments have been proposed to achieve wide-field of views. The first is a refractive design using two Fresnel lenses which focus onto a large focal plane array [109]. The second design uses Fresnel correcting optics which focus onto a spherical reflector in a Maksutov design that in turn focuses the light onto a focal plane array [110, 111]. For a satellite separation of 500 (2000) km, the instantaneous acceptance is 1.5×10^6 (3.75×10^6) $\text{km}^2 \text{ sr}$. Using a 10% duty factor, the 500 (2000) km configuration leads to an effective acceptance of 1.5×10^5 (3.75×10^5) $\text{km}^2 \text{ sr}$. Therefore, assuming a continuation of the CR-spectrum $\propto E^{-2.75}$, one expects rates of 1500 events/yr (500 km) and 3750 events/yr (2000 km) for $E \gtrsim 10^{20}$ eV [112]. The effective acceptance for the Maksutov baseline assuming 1000 km orbits and 500 (2000) km is 2.0×10^5 (4.0×10^5) $\text{km}^2 \text{ sr}$ which leads to an event rate of 2000 (4000) events per year

for $E \gtrsim 10^{20}$, again assuming an $E^{-2.75}$ spectrum continuation [112].

For the near future (≈ 2006), the European Space Agency is studying the feasibility of placing a single eye on the International Space Station, which will serve as a pathfinder mission to develop the required technology to observe the fluorescent trails of EASs. The smaller viewing volume of the Extreme Universe Space Observatory (EUSO) [113] will result in a smaller event rate by a factor of ~ 5 compared to OWL.

I. Ultrahigh energy neutrino experiments

Up to now, we have discussed experiments designed primarily to study air showers initiated by hadrons or photons. As pointed out in Sec.II-B, however, neutrinos may also induce extensive air showers, so current and future air shower experiments might also function as neutrino detectors. In this section, we briefly review dedicated neutrino detectors as well as neutrino searches carried out by existing air shower experiments.

The traditional technique to observe high energy neutrinos involves detecting the optical Čerenkov light emitted by muons produced in charged current interactions of neutrinos with nucleons either in ice or water. The largest pilot experiments (~ 0.1 km in size) are: the now defunct DUMAND (Deep Underwater Muon and Neutrino Detector) experiment [114] in the deep sea near Hawaii, the underwater experiment in Lake Baikal [115], and AMANDA (Antarctic Muon And Neutrino Detector Array) [116] in the South Pole ice. Next generation neutrino telescopes aim towards an active volume in the range of 1 km^3 of water. Projects under construction or in the proposal stage are: two deep sea experiments in the Mediterranean, the French ANTARES (Astronomy with a Neutrino telescope Abyss environment REsearch) [117] and NESTOR (Neutrino Experiment SouthwesT Of GReece [118]), and ICECUBE [119], a scaled up version of the AMANDA detector.

Above 10^{17} eV the neutrino interaction length is below 2000 km w.e. in rock, and so upward going neutrinos are typically blocked by the Earth. This shadowing severely restricts the high energy event rates in underground detectors. Current limits on high energy ($10^{15} - 10^{17}$ eV) neutrino fluxes come from measurements of the Extensive Air Shower array on the TOP of the underground Gran Sasso Laboratory in central Italy (EAS-TOP) [120, 121], and the Fréjus detector [122, 123], located in an underground laboratory near the middle of the road tunnel connecting Modane (France) and Bardonecchia (Italy) in the Alps.

Large ground arrays or fluorescence eyes, for which the interaction medium is not the Earth but the atmosphere, are complementary to neutrino telescopes in the analysis of the energy spectrum. Specifically, the neutrino cross section at ultrahigh energies is non-negligible (about 10^{-32} cm^2 at 10^{18} eV [124]), and so quasi-horizontal ($\theta >$

75°) neutrinos that traverse an atmospheric depth of up to 360 m w.e. can initiate a shower. As discussed earlier, hadronic showers at large zenith angles have their electromagnetic component extinguished, and only high energy muons created in the first stages of the shower development survive. Therefore, the shape of the shower front is relatively flat. The Fly’s Eye Collaboration searched for deeply developing air showers (DDASs) and upward-moving showers above 10^{17} eV and no unusual events were found in 10^6 s of running time [125]. Additionally, the AGASA group searched for giant deeply developing air showers [70]. During the observation live time of 9.7×10^7 s no candidate DDAS was found. From this, the AGASA Collaboration concluded that the 90% CL upper limit on the flux of DDASs with energy $\gtrsim 10^{19.5}$ eV is $1.9 \times 10^{-16} \text{ m}^{-2} \text{ s}^{-1} \text{ sr}^{-1}$, a factor of 10 lower than the flux of cosmic rays above $10^{19.5}$ eV. The current upper bound ($E_\nu \sim 10^{19.5}$ eV) on the total cosmic neutrino flux, obtained by combining the exposures of the AGASA and Fly’s Eye experiments (the latter integrated over all its operating epochs), is found to be $5.1 \times 10^{-12} \text{ m}^{-2} \text{ s}^{-1} \text{ sr}^{-1}$, at the 95% CL [126]. The sensitivity of surface arrays and fluorescence eyes could be significantly enhanced by triggering on neutrinos that skim the Earth, traveling at low angles along chords with lengths of order their interaction length [127, 128, 129, 130, 131, 132, 133]. Some of these Earth-skimming neutrinos may be converted into tau leptons in the Earth’s crust. Unlike electrons, which do not escape from rocks, or muons, that do not produce any visible signal in the atmosphere, taus can escape even from inside the rock and produce a clear signal if they decay above the detector, increasing the ν -event rate.

The study of radio pulses from electromagnetic showers created by neutrino interactions in ice would provide an increase in the effective area up to 10^4 km^2 . A prototype of this technique is the Radio Ice Čerenkov Experiment (RICE) [134]. Similar concepts are used by the Goldstone Lunar ultrahigh energy neutrino Experiment (GLUE) to set an upper bound on the ultrahigh energy neutrino flux [135, 136]. In this experiment, the non-observation of microwave Čerenkov pulses from electromagnetic showers induced by neutrinos interacting in the moon’s rim leads to flux upper limits: $\log(E^2 J) = -3.03, -2.66, \text{ and } -2.30 \text{ GeV cm}^{-2} \text{ s}^{-1} \text{ sr}^{-1}$, for $1.0 \times 10^{22}, 3.0 \times 10^{22}$, and 1.0×10^{23} eV, respectively.

For a more extensive discussion on the status of ultrahigh energy neutrino experiments the reader is referred to [137].

III. COSMIC RAY ACCELERATION

It is most likely that the bulk of the cosmic radiation is a result of some very general magneto-hydrodynamic (MHD) phenomenon in space which transfers kinetic or magnetic energy into cosmic ray energy. The details of the acceleration process and the maximum attainable energy depend on the particular physical situation under consider-

ation. There are basically two types of mechanism that one might invoke for bottom-up CR production.¹² The first type assumes the particles are accelerated directly to high energy by an extended electric field [138]. This idea can be traced back to the early 1930’s when Swann [139] pointed out that betatron acceleration may take place in the increasing magnetic field of a sunspot. These so-called “one-shot” mechanisms have been worked out in greatest detail, and the electric field in question is now generally associated with the rapid rotation of small, highly magnetized objects such as neutron stars (pulsars) or active galactic nuclei (AGN). Electric field acceleration has the advantage of being fast, but suffers from the circumstance that the acceleration occurs in astrophysical sites of very high energy density, where new opportunities for energy loss exist. Moreover, it is usually not obvious how to obtain the observed power law spectrum in a natural way, and so this kind of mechanism is not widely favored these days. The second type of process is often referred to as statistical acceleration, because particles gain energy gradually by numerous encounters with moving magnetized plasmas. These kinds of models were mostly pioneered by Fermi [140]. In this case the E^{-2} spectrum very convincingly emerges.¹³ However, the process of acceleration is slow, and it is hard to keep the particles confined within the Fermi engine. In this section we first provide a summary of statistical acceleration based on the simplified version given in Ref [31] (See also [142]). For a more detailed and rigorous discussion the reader is referred to [143]. After reviewing statistical acceleration, we turn to the issue of the maximum achievable energy within diffuse shock acceleration and explore the viability of some proposed ultrahigh energy CR-sources.

A. The Fermi mechanism

In his original analysis, Fermi [140] considered the scattering of CRs on moving magnetized clouds. In this case, a CR entering into a single cloud with energy E_i and incident angle θ_i with the cloud’s direction undergoes diffuse scattering on the irregularities in the magnetic field. After diffusing inside the cloud, the particle’s average motion coincides with that of the gas cloud. The energy gain by the particle, which emerges at an angle θ_f with energy E_f , can be obtained by applying Lorentz transformations between the laboratory frame (unprimed) and the cloud frame (primed). In

¹² In bottom-up models the CR particles start with low energy and are accelerated, as opposed to top-down models where usually exotic particles start initially with very high energy and cascade decay to the CR particles.

¹³ A point worth noting at this juncture: A power law spectrum does not necessarily point to the Fermi mechanism [141].

the rest frame of the moving cloud, the CR particle has a total initial energy

$$E'_i = \Gamma E_i (1 - \beta \cos \theta_i), \quad (17)$$

where Γ and $\beta = V/c$ are the Lorentz factor and velocity of the cloud in units of the speed of light, respectively. In the frame of the cloud we expect no change in energy ($E'_i = E'_f$), because all the scatterings inside the cloud are due only to motion in the magnetic field (so-called collisionless scattering). There is elastic scattering between the CR and the cloud as a whole, which is much more massive than the CR. Transforming to the laboratory frame we find that the energy of the particle after its encounter with the cloud is

$$E_f = \Gamma E'_f (1 + \beta \cos \theta_f). \quad (18)$$

The fractional energy change in the laboratory frame is then

$$\frac{\Delta E}{E} = \frac{E_f - E_i}{E_i} = \frac{1 - \beta \cos \theta_i + \beta \cos \theta'_f - \beta^2 \cos \theta_i \cos \theta'_f}{1 - \beta^2} - 1. \quad (19)$$

Inside the cloud the CR direction becomes randomized and so $\langle \cos \theta'_f \rangle = 0$. The average value of $\cos \theta_i$ depends on the relative velocity between the cloud and the particle. The probability P per unit solid angle Ω of having a collision at angle θ_i is proportional to $(v - V \cos \theta_i)$, where v is the CR speed. In the ultrarelativistic limit, i.e., $v \sim c$ (as seen in the laboratory frame),

$$\frac{dP}{d\Omega_i} \propto (1 - \beta \cos \theta_i), \quad (20)$$

so

$$\langle \cos \theta_i \rangle = -\frac{\beta}{3}. \quad (21)$$

Now, inserting Eq. (21) into Eq.(19) one obtains for $\beta \ll 1$,

$$\frac{\langle \Delta E \rangle}{E} = \frac{1 + \beta^2/3}{1 - \beta^2} - 1 \approx \frac{4}{3} \beta^2. \quad (22)$$

Note that $\langle \Delta E \rangle / E \propto \beta^2$, so even though the average magnetic field may vanish, there can still be a net transfer of the macroscopic kinetic energy from the moving cloud to the particle. However, the average energy gain is very small, because $\beta^2 \ll 1$.

A version of Fermi's mechanism which is first order in β , and thus a more efficient accelerator, is realized for CR encounters with plane shock fronts [144]. In this case, a large shock wave propagates with velocity $-\vec{u}_1$, as depicted in Fig. 9. Relative to the shock front, the downstream shocked gas is receding with velocity \vec{u}_2 , where $|u_2| < |u_1|$, and thus in the laboratory frame it is moving in the direction of the front with velocity $\vec{V} = -\vec{u}_1 + \vec{u}_2$. In order to find the energy gain per shock crossing, we identify the

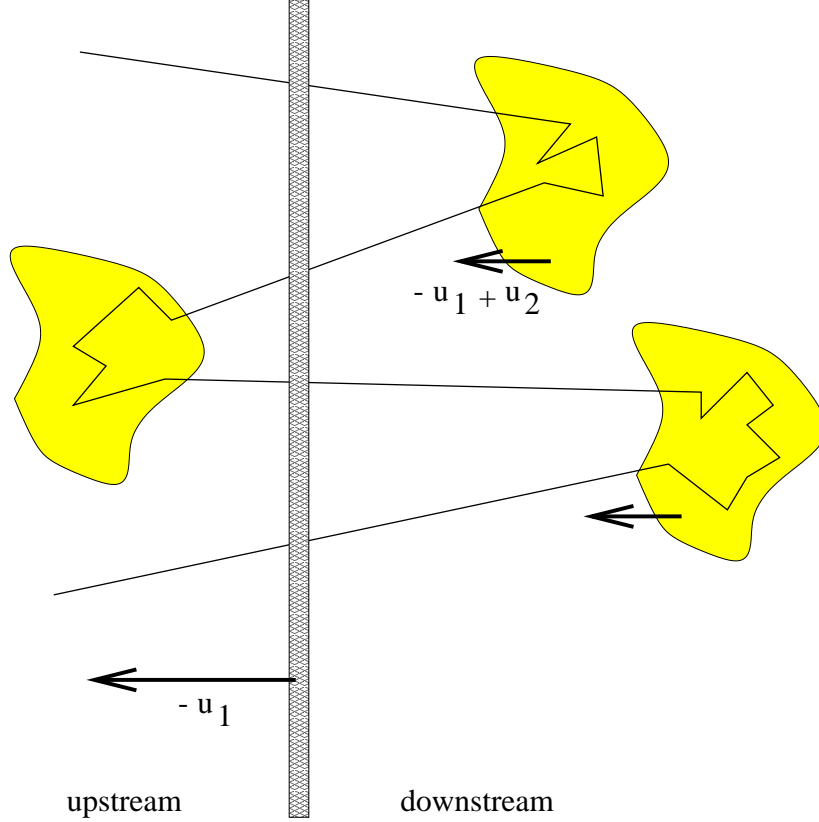


FIG. 9: CR acceleration at a shock front. A planar shock wave is moving with velocity $-u_1$. A CR particle is repeatedly crossing the front and scattering in magnetic irregularities.

magnetic irregularities on either side of the shock as the clouds of magnetized plasma in the Fermi mechanism we discussed previously. By considering the rate at which CRs cross the shock from downstream to upstream, and upstream to downstream, one finds $\langle \cos \theta_i \rangle = -2/3$ and $\langle \cos \theta'_f \rangle = 2/3$. Hence, Eq. (19) can be re-written as

$$\frac{\langle \Delta E \rangle}{E} \simeq \frac{4}{3} \beta = \frac{4}{3} \frac{u_1 - u_2}{c}. \quad (23)$$

Note this is first order in $\beta = V/c$, and is therefore more efficient than Fermi's original mechanism. This is because of the converging flow – whichever side of the shock you are on, if you are moving with the plasma, the plasma on the other side of the shock is approaching you.

The rate at which CRs cross from upstream to downstream is given by the projection of the isotropic CR flux onto the plane shock front

$$r_{\text{cross}} = \int_0^1 d(\cos \theta) \int_0^{2\pi} d\phi \frac{n_{\text{CR}} v}{4\pi} \cos \theta \sim \frac{n_{\text{CR}} v}{4}, \quad (24)$$

where n_{CR} is the number density of particles undergoing acceleration. On the other hand, the rate of convection downstream away from the shock front is

$$r_{\text{loss}} = n_{\text{CR}} u_2, \quad (25)$$

so the probability of crossing the shock once and then escaping from the shock (being lost downstream) is given by

$$\text{Prob.}(\text{escape}) = \frac{r_{\text{loss}}}{r_{\text{cross}}} \sim 4 \frac{u_2}{v}. \quad (26)$$

The probability of returning to the shock after crossing from upstream to downstream is

$$\text{Prob.}(\text{return}) = 1 - \text{Prob.}(\text{escape}), \quad (27)$$

and so the probability of returning to the shock n times and also of crossing the shock at least n times is

$$\text{Prob.}(\text{cross} \geq n) = [1 - \text{Prob.}(\text{escape})]^n. \quad (28)$$

Therefore, the energy after n shock crossings is

$$E = E_0 \left(1 + \frac{\langle \Delta E \rangle}{E} \right)^n \quad (29)$$

where E_0 is the overall initial energy. With this in mind, the number of encounters needed to reach an energy E reads

$$n = \frac{\ln(E/E_0)}{\ln(1 + \langle \Delta E \rangle / E)}, \quad (30)$$

and the number of particles accelerated to energies greater than E is

$$Q(> E) \propto \sum_{m=n}^{\infty} [1 - \text{Prob.}(\text{escape})]^m = \frac{[1 - \text{Prob.}(\text{escape})]^n}{\text{Prob.}(\text{escape})}. \quad (31)$$

Substitution of Eq. (30) into Eq. (31) leads to

$$Q(> E) \propto \frac{1}{\text{Prob.}(\text{escape})} \left(\frac{E}{E_0} \right)^{-\gamma} \quad (32)$$

with

$$\gamma = \frac{\ln[1 - \text{Prob.}(\text{escape})]^{-1}}{\ln(1 + \langle \Delta E \rangle / E)}. \quad (33)$$

All in all, Fermi's mechanism yields the desired power law spectrum for CR acceleration. Note that in the first order mechanism the spectral index, γ , is independent of the absolute magnitude of the velocity of the plasma, and depends only on the ratio of the upstream and downstream velocities.

B. Desperately seeking Zevatrons

1. *Plausible sources*

Now we focus attention on the direct identification of candidate CR-sources. For well-researched reviews on this topic see [145, 146]. A variety of astrophysical objects have been proposed to account for the origin of high energy CRs. The options include:

- Supernovae explosions [147, 148].
- Large scale Galactic wind termination shocks [149].
- Pulsars (neutron stars) [150].
- Active galactic nuclei (AGNs) [151].
- BL Lacertae (BL Lac) – a sub-class of AGN [152, 153].
- Spinning supermassive black holes associated with presently inactive quasar remnants [154, 155].¹⁴
- Large scale motions and the related shock waves resulting from structure formation in the Universe [157] such as accretion flow onto galaxy clusters and cluster mergers [158, 159].¹⁵
- Relativistic jets and “hot-spots” produced by powerful radiogalaxies. Relativistic jets occurring in very powerful radiogalaxies carry large amounts of energy up to the radio hot-spots situated far (~ 100 kpc) from the central engine. These hot-spots are believed to harbor strong, mildly relativistic shocks dissipating the jet bulk kinetic energy into heating plasma, thus generating magnetic fields which efficiently accelerate CRs to ultrahigh energies [161, 162, 163]. Additionally, a velocity shear layer at the relativistic jet side boundary can play an active role in the acceleration process [164, 165].
- The electrostatic polarization fields that arise in plasmoids produced in planetoid impacts onto neutron star magnetospheres [166].
- Magnetars – pulsars with dipole magnetic fields approaching $\sim 10^{15}$ G [167, 168, 169]– appear also as serious candidates [170, 171].

¹⁴ An unexpected apparent correlation between the highest energy events reported by the AGASA Collaboration and dead quasars was recently reported [156].

¹⁵ The famous AGASA triplet points towards the merger galaxies Arp 299 (NGC 3690 + IC 694), at a distance of 70 Mpc [160].

- Starburst galaxies [172, 173, 174].
- Magnetohydrodynamic (MHD) winds of newly formed strongly magnetized neutron stars [175].
- Gamma ray burst (GRB) fireballs [176, 177, 178, 179].
- Strangelets, stable lumps of quark matter, accelerated in astrophysical environments [180].
- Hostile aliens with a big CR gun [181].

In general, the maximum attainable energy of Fermi's mechanism is determined by the time scale over which particles are able to interact with the plasma. Sometimes the acceleration region itself only exists for a limited period of time; for example, supernovae shock waves dissipate after about 10^4 yr [182]. In such a case, Eq. (32) would have to be modified accordingly. Otherwise, if the plasma disturbances persist for much longer periods, the maximum energy may be limited by an increased likelihood of escape from the region. The latter case is relevant to ultrahigh energies, because when the Larmor radius of the particle (of charge Ze),

$$r_L \sim 110 \frac{E_{20}}{Z B_{\mu\text{G}}} \text{ kpc}, \quad (34)$$

approaches the accelerator size it becomes very difficult to confine the CR magnetically to the acceleration region. Here, $B_{\mu\text{G}}$ is the magnetic field in units of μG , and $E_{20} \equiv E/10^{20}$ eV. If one includes the effect of the characteristic velocity βc of the magnetic scattering centers, the above argument leads to the general condition [138],

$$E_{\text{max}} \sim 2\beta c Ze B r_L, \quad (35)$$

for the maximum energy acquired by a particle traveling in a medium with magnetic field B . This is sometimes called the ‘‘Hillas criterion.’’ The upper limit on the energy of one-shot acceleration scenarii turns out to be quite similar to the shock acceleration case of Eq. (35). For instance, a dimensional analysis suggests that the maximum energy that can be obtained from a pulsar is [138]

$$E_{\text{max}} = \frac{\omega}{c} Ze B_s r_{\text{ns}}^2, \quad (36)$$

where ω is the pulsar angular velocity, B_s the surface magnetic field and r_{ns} the neutron star radius. Therefore, if $B_s \sim 10^{12}$ G, $r_{\text{ns}} \sim 10$ km, and $\omega \sim 60\pi \text{ s}^{-1}$ (as for the Crab pulsar), a circuit connected between pole and equator would see an emf $\sim 10^{18}$ V for an aligned or oblique dipole. When realistic models of acceleration are constructed,

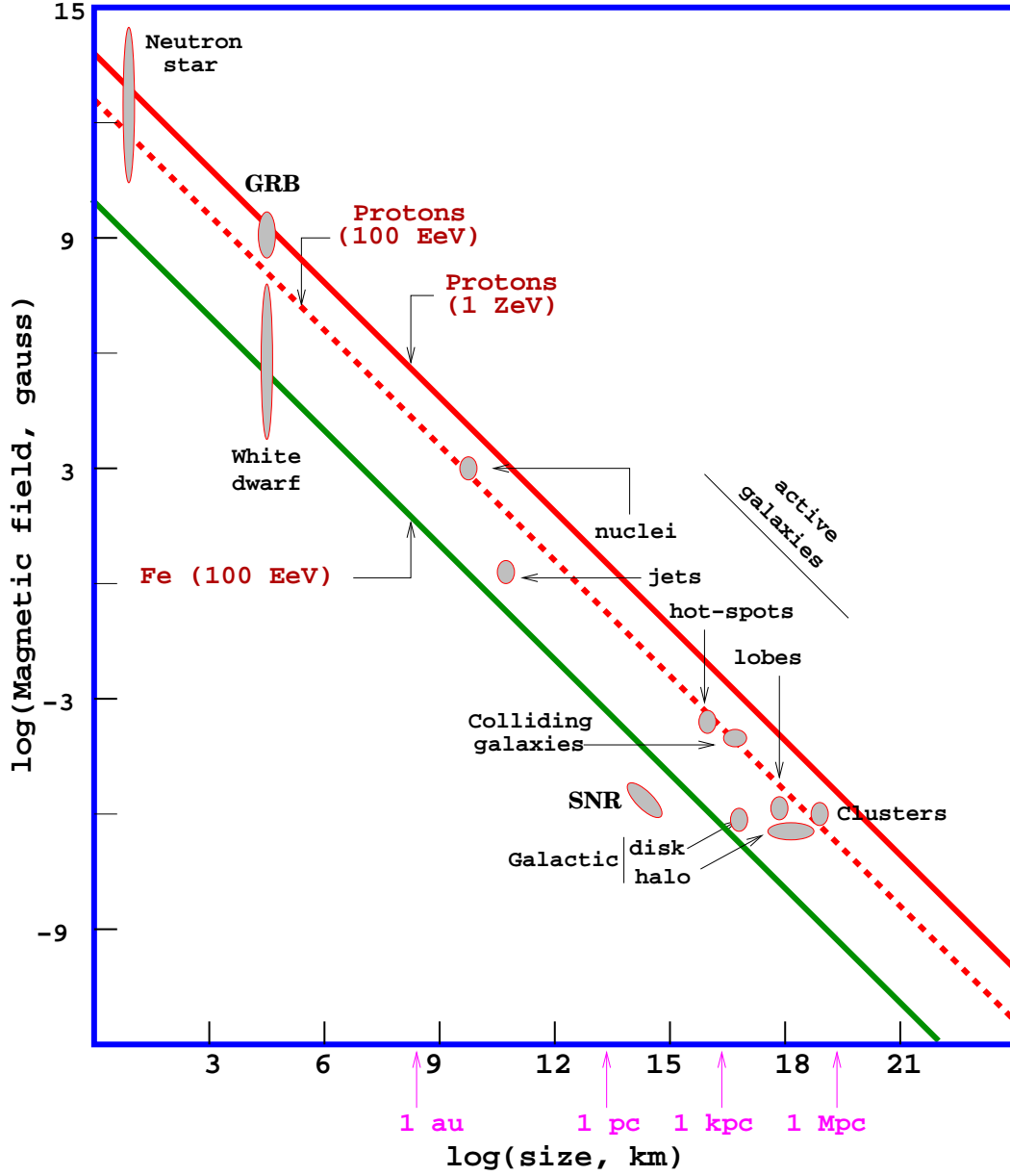


FIG. 10: The Hillas diagram showing size and magnetic field strengths of possible sites of particle acceleration. Objects below the diagonal lines (from top to bottom), derived from Eq. (35) assuming the extreme value $\beta = 1$, cannot accelerate protons above 10^{21} eV, above 10^{20} eV and iron nuclei above 10^{20} eV, respectively. (This version of the picture is courtesy of Murat Boratav).

however, this ideal dimensional limit is not realized, because the large potential drop along the magnetic field lines is significantly short-circuited by electron and positrons moving in the opposite directions along the field lines [150].

The dimensional arguments of Eqs. (35) and (36) are usually summarized in the form of the popular “Hillas diagram” [138] shown in Fig. 10. Clearly, very few sites appear able to generate particle energies $> 10^{20}$ eV; either this occurs on highly condensed objects with huge B or enormously extended objects.¹⁶ From a glance at Fig. 10 it seems that the structures associated with active galaxies, neutron stars and GRBs have sufficient size and field strength to be considered as potential sources. In subsequent sections we discuss these potential sources in more detail.

2. Radiogalaxies

Fanaroff-Riley II (FRII) galaxies [184] are the largest known dissipative objects (non-thermal sources) in the Universe. Localized regions of intense synchrotron emission, known as “hot spots”, are observed within their lobes. These regions are presumably produced when the bulk kinetic energy of the jets ejected by a central active nucleus (supermassive black hole + accretion disk) is reconverted into relativistic particles and turbulent fields at a “working surface” in the head of the jets [185]. Specifically, the speed v_h with which the head of a jet advances into the intergalactic medium of particle density n_e can be obtained by balancing the momentum flux in the jet against the momentum flux of the surrounding medium. Measured in the frame comoving with the advancing head, $v_h \approx v_j [1 + (n_e/n_j)^{1/2}]^{-1}$, where n_j and v_j are the particle density and the velocity of the jet flow, respectively. Clearly, $v_j > v_h$ for $n_e \geq n_j$, in such a way that the jet will decelerate. The result is the formation of a strong collisionless shock, which is responsible for particle reacceleration and magnetic field amplification [186]. The acceleration of particles up to ultrarelativistic energies in the hot spots is the result of repeated scattering back and forth across the shock front, similar to that discussed in Sec.III-A. The particle deflection in this mechanism is produced by Alfvén waves in the turbulent magnetic field. This process has been studied in detail by Biermann and Strittmatter [187]. Dimensional arguments suggest that the energy density per unit of wave number of MHD turbulence is of the Kolmogorov type [188], and so for strong shocks the acceleration time for protons is [189]

$$\tau_{\text{acc}} \simeq \frac{40}{\pi} \frac{1}{c \beta_{\text{jet}}^2} \frac{1}{u} \left(\frac{E}{eB} \right)^{1/3} R^{-2/3} \quad (37)$$

¹⁶ For a comprehensive discussion on the electrodynamic limitations of CR sources the reader is referred to the recent study in Ref. [183].

where β_{jet} is the jet velocity in units of c , u is the ratio of turbulent to ambient magnetic energy density in the region of the shock (of radius R), and B is the total magnetic field strength. The acceleration process will be efficient as long as the energy losses by synchrotron radiation and photon–proton interactions do not become dominant. The subtleties surrounding the conversion of a particle kinetic energy into radiation provide ample material for discussion [187, 190, 191, 192, 193, 194]. The most popular mechanism to date relates γ -ray emission to the development of electromagnetic cascades triggered by secondary photomeson products that cool instantaneously via synchrotron radiation [187, 190, 191, 192, 193]. The synchrotron loss time for protons is given by [195]

$$\tau_{\text{syn}} \sim \frac{6 \pi m_p^3 c}{\sigma_T m_e^2 \Gamma B^2}, \quad (38)$$

where m_e , m_p , σ_T and Γ are the electron mass, proton mass, Thomson cross section, and Lorentz factor, respectively. The characteristic single photon energy in synchrotron radiation emitted by an electron is

$$E_\gamma = \left(\frac{3}{2}\right)^{1/2} \frac{h e E^2 B}{2 \pi m_e^3 c^5} \sim 5.4 \times 10^{-2} B_{\mu\text{G}} E_{20}^2 \text{ TeV} . \quad (39)$$

For a proton this number is $(m_p/m_e)^3 \sim 6 \times 10^9$ times smaller. Thus, it is evident that high energy gamma ray production through proton synchrotron radiation requires very large ($\mathcal{O}(100 \text{ G})$) magnetic fields. Considering an average cross section $\bar{\sigma}_{\gamma p}$ for the three dominant pion–producing interactions [196],

$$\gamma p \rightarrow p \pi^0, \quad (40)$$

$$\gamma p \rightarrow n \pi^+, \quad (41)$$

$$\gamma p \rightarrow p \pi^+ \pi^-, \quad (42)$$

the time scale of the energy losses, including synchrotron and photon interaction losses, reads [187]

$$\tau_{\text{loss}} \simeq \frac{6 \pi m_p^4 c^3}{\sigma_T m_e^2 B^2 (1 + Aa)} E^{-1} = \frac{\tau_{\text{syn}}}{1 + Aa}, \quad (43)$$

where a stands for the ratio of photon to magnetic energy densities and A gives a measure of the relative strength of γp interactions versus the synchrotron emission. Note that channel (41) involves the creation of ultrarelativistic neutrons (but $\Gamma_n \lesssim \Gamma_p$) with mean free path in the observer rest frame given by $\lambda_n = \Gamma_n c \tau_n$, where $\tau_n \sim 900 \text{ s}$, is the neutron lifetime. Since $\lambda_n > \lambda_p$ for $\Gamma_n \lesssim \Gamma_{p \text{ max}}$, such neutrons can readily escape the system, thereby modifying the high end of the proton spectrum. Biermann and Strittmatter [187] have estimated that $A \approx 200$, almost independently of the source

parameters. The most energetic protons injected in the intergalactic medium will have an energy that can be obtained by balancing the energy gains and losses [197]

$$E_{20} = 1.4 \times 10^5 B_{\mu\text{G}}^{-5/4} \beta_{\text{jet}}^{3/2} u^{3/4} R_{\text{kpc}}^{-1/2} (1 + Aa)^{-3/4}, \quad (44)$$

where $R_{\text{kpc}} \equiv R/1 \text{ kpc}$.

As noted in the previous section, the canonical theory of diffuse shock acceleration not only assumes an infinite time, but also an infinite space for the particles to diffuse in the medium around the shock front. Therefore, in order to ascertain the capability of FR II to accelerate particles to ultrahigh energies, one also has to apply the Hillas criterion [138] for localizing the Fermi engine in space, namely that the Larmor radius be less than the size of the magnetic region. For typical hot-spot conditions ($B \sim 300 \mu\text{G}$, $u \sim 0.5$, and $\beta_{\text{jet}} \sim 0.3$) and assuming that the magnetic field of the hot spot is limited to the observable region, one obtains $E < 5 \times 10^{20} \text{ eV}$ for $a < 0.1$ [161]. Therefore, one concludes that protons can be accelerated to the highest observed energies in typical FR II hot spots. Moreover, the shock structure in hot spots is likely to be much more extended than the visible region in the nonthermal radioemission, as suggested by magnetohydrodynamical modeling [161].

Particles can also attain ultrahigh energies ($E \gtrsim 10^{20} \text{ eV}$) within the jets or the AGNs themselves. For instance, the knot A in the M87 jet, with a length scale $l_{87} \sim 2 \times 10^{20} \text{ cm}$, has a magnetic field strength $B_{87} \sim 300 \mu\text{G}$ [198]. Typical AGN sizes are $l_{\text{AGN}} \sim 10^{15} \text{ cm}$, and $B_{\text{AGN}} \sim 1 \text{ G}$ [199]. Observational evidence suggests that in the jets $a \ll 1$, whereas $a \sim 1$ for AGNs [187].

In Sec.V the ideas developed in this section will be applied to specific models.

3. γ -ray burst fireballs

Gamma ray bursts (GRBs) are flashes of high energy radiation that can be brighter, during their brief existence, than any other gamma ray source in the sky. The bursts present an amazing variety of temporal profiles, spectra, and timescales that have puzzled astrophysicists for almost three decades [200]. In recent years, our observational insight of this phenomenon has been dramatically increased by the huge amount of data collected by the Burst and Transient Source Experiment (BATSE) on board the Compton Gamma Ray Observatory (CGRO), a satellite launched by NASA in 1991. In 9 years of operation, BATSE has accumulated a database of more than 2000 observations.

The temporal distribution of the bursts is one of the most striking signatures of the GRB phenomenon. There are at least four classes of distributions, from single-peaked bursts, including the fast rise and exponential decaying (FREDs) and their inverse

(anti-FREDS), to chaotic structures [201, 202]. There are well separated episodes of emission, as well as bursts with extremely complex profiles. Most of the bursts are time asymmetric but some are symmetric. Burst timescales go through the 30 ms scale to hundreds of seconds. The measurement of these timescales is a rather complicated task, since it may depend on the intensity of both the background and the source. At high energies (> 100 MeV), some extremely long bursts have been detected. The angular distribution of these bursts is isotropic within the statistical limits, and the paucity of comparatively faint bursts implies that we are seeing to near the edge of the source population [203]. Both effects, isotropy and non-homogeneity in the distribution, strongly suggest a cosmological origin of the phenomenon. Moreover, the recent detection of “afterglows”, delayed low energy (X -ray to radio) emission of GRBs, has confirmed the cosmological origin of the burst via a redshift determination of several GRB host-galaxies [204, 205].

If the sources are so distant, the energy necessary to produce the observed events by an intrinsic mechanism is astonishing: about 10^{51} erg of gamma rays must be released in less than 1 second. The most popular interpretation of the GRB-phenomenology is that the observable effects are due to the dissipation of the kinetic energy of a relativistic expanding plasma wind, a “fireball”, whose primal cause is not yet known [206, 207, 208, 209, 210, 211, 212]. The very short timescale observed in the time profiles indicate an extreme compactness that implies a source initially opaque (because of $\gamma\gamma$ pair creation) to γ -rays. The radiation pressure on the optically thick source drives relativistic expansion, converting internal energy into the kinetic energy of the inflating shell. Baryonic pollution in this expanding flow can trap the radiation until most of the initial energy has gone into bulk motion with Lorentz factors of $\Gamma \geq 10^2 - 10^3$ [213]. The kinetic energy, however, can be partially converted into heat when the shell collides with the interstellar medium or when shocks within the expanding source collide with one another. The randomized energy can then be radiated by synchrotron radiation and inverse Compton scattering yielding non-thermal bursts with timescales of seconds.

We now consider Fermi acceleration in the fireball internal shocks. As usual, r_L should be smaller than the largest scale l_{GRB} over which the magnetic field fluctuates, since otherwise Fermi acceleration may not be efficient. One may estimate l_{GRB} as follows. The comoving time, i.e., the time measured in the fireball rest frame, is $t = r/\Gamma c$. Hence, the plasma wind properties fluctuate over comoving scale length up to $l_{\text{GRB}} \sim r/\Gamma$, because regions separated by a comoving distance larger than r/Γ are causally disconnected. Moreover, the internal energy is decreasing because of the expansion and thus it is available for proton acceleration (as well as for γ -ray production) only over a comoving time t . The typical acceleration time scale is

then [176]

$$\tau_{\text{acc}}^{\text{GRB}} \sim \frac{r_{\text{L}}}{c\beta^2}, \quad (45)$$

where βc is the Alfvén velocity. In the GRB scenario $\beta \sim 1$, so Eq. (45) sets a lower limit on the required comoving magnetic field strength, and the Larmor radius $r_{\text{L}} = E'/eB = E/\Gamma eB$, where $E' = E/\Gamma$ is the proton energy measured in the fireball frame. The dominant energy loss process in this case is synchrotron cooling. Therefore, the condition that the synchrotron loss time of Eq. (38) be smaller than the acceleration time sets the upper limit on the magnetic field strength. A dissipative ultra-relativistic wind, with luminosity and variability time implied by GRB observations, satisfies the constraints necessary to accelerate protons to energy $> 10^{20}$ eV, provided that $\Gamma > 100$, and the magnetic field is close to equipartition with electrons. We stress that the latter must be satisfied to account for both γ -ray emission and afterglow observations [213]. At this stage, it is worthwhile to point out that for the acceleration process at shocks with large Γ the particle distributions are extremely anisotropic in shock, with the particle angular distribution opening angles $\sim \Gamma^{-1}$ in the upstream plasma rest frame. Therefore, when transmitted downstream the shock particles have a limited chance to be scattered efficiently to re-enter the shock [214]. However, in this particular case, the energy gain by any “successful” CR can be comparable to its original energy, i.e., $\langle \Delta E \rangle / E \sim 1$.

Now we comment on the data. It was pointed out that two of the highest energy CRs come from directions that are within the error boxes of two remarkable GRBs detected by BATSE with a delay of $\mathcal{O}(10)$ months after the bursts [215]. However, a rigorous analysis shows no correlation between the arrival direction of ultrahigh energy CRs and GRBs from the third BATSE catalog [216]. Moreover, no correlations were found between a pre-CGRO burst catalog and the Haverah Park shower set that covered approximately the same period of time. These analyses, however, could have been distorted by the angular resolution ($\Delta\theta \sim 3^\circ$) of the GRB measurements. A sensitive anisotropy analysis between ultrahigh energy CRs and GRBs will be possible in the near future with the facilities of PAO and the High Energy Transient Explorer (HETE).¹⁷

Finally, it is also interesting to note that if the GRBs are uniformly distributed (independent of redshift), and if in the past they emitted the same amount of energy in ultrahigh energy ($\sim 10^{14}$ MeV) CRs as in \sim MeV photons, the energy input of these particles into the extragalactic space would be enough to account for the observed CR

¹⁷ This satellite, designed to localize GRBs, is expected to detect around 50 events per year with a 10 arc-minute accuracy in the medium energy X-ray band, and around 10 events per year with 10 arc-second accuracy in the soft X-ray band. <http://space.mit.edu/HETE/Welcome.html>.

flux [176]. However, recent afterglow studies indicate that their redshift distribution likely follows the average star formation rate of the Universe and that GRBs are more numerous at high redshift. If this is the case, ultrahigh energy CRs coming from GRBs would produce too sharp a spectral energy cutoff to be consistent with the AGASA data, because of energy degradation *en route* to Earth [217, 218].¹⁸

IV. INTERACTIONS *EN ROUTE* TO EARTH

In this section we review the propagation of cosmic rays. We start with the hadronic component, continue with a discussion of electromagnetic cascades initiated by ultrahigh energy photons in extragalactic space, and then discuss how propagation can be influenced by cosmic magnetic fields. For alternative discussions see, for instance, Refs. [170, 221].

A. The GZK cutoff

Shortly after the discovery of the microwave echo of the big bang [222], Greisen [223] and independently Zatsepin and Kuzmin [224] (GZK) pointed out that this radiation would make the Universe opaque to protons of sufficiently high energy. At energies above a few 10^{19} eV, the thermal photons are seen highly blue-shifted by the protons in their rest frames. The energy of the relic photons is sufficient to excite baryon resonances thus draining the energy of the proton via pion production and, coincidentally, producing a source of ultrahigh energy gamma rays and neutrinos. Since the implications of this process have been revisited in many forms [225, 226, 227, 228, 229, 230, 231, 232, 233, 234, 235, 236, 237, 238, 239, 240, 241], the concept of GZK sphere is by now a somewhat fuzzy notion. Naïvely, it is the radius of the sphere within which a source has to lie in order to provide us with protons of 10^{20} eV. In what follows we extensively discuss the phenomenology of proton-photon interactions and discuss in some detail the GZK radius.

There are three sources of energy loss of ultrahigh energy protons. These are the adiabatic fractional energy loss due to the expansion of the Universe, pair production ($p\gamma \rightarrow pe^+e^-$) and photopion production ($p\gamma \rightarrow \pi N$), each successively dominating as the proton energy increases. The adiabatic fractional energy loss at the present

¹⁸ It has been noted by Bahcall and Waxman [219] that if one excludes the AGASA results, the remaining data from Fly’s Eye, HiRes, and Yakutsk CR experiments show evidence for a cutoff in the CR energy spectrum below 10^{20} eV with 7σ significance. In such a case, the door is open for a common origin between GRBs and ultrahigh energy CRs [220].

cosmological epoch is given by

$$-\frac{1}{E} \left(\frac{dE}{dt} \right)_{\text{adiabatic}} = H_0, \quad (46)$$

where $H_0 \sim 100 h \text{ km s}^{-1} \text{ Mpc}^{-1}$ is the Hubble constant, with $h \sim (0.71 \pm 0.07) \times_{0.95}^{1.15}$ the normalized Hubble expansion rate [242] (see Appendix B). The fractional energy loss due to interactions with the cosmic background radiation at a redshift $z = 0$ is determined by the integral of the nucleon energy loss per collision multiplied by the probability per unit time for a nucleon collision in an isotropic gas of photons [225]. This integral can be explicitly written as follows,

$$-\frac{1}{E} \frac{dE}{dt} = \frac{c}{2\Gamma^2} \sum_j \int_0^{w_m} dw_r K_j \sigma_j(w_r) w_r \int_{w_r/2\Gamma}^{w_m} dw \frac{n(w)}{w^2} \quad (47)$$

where w_r is the photon energy in the rest frame of the nucleon, and K_j is the inelasticity, i.e., the average fraction of the energy lost by the photon to the nucleon in the laboratory frame for the j th reaction channel.¹⁹ The sum is carried out over all channels, $n(w)dw$ stands for the number density of photons with energy between w and dw , $\sigma_j(w_r)$ is the total cross section of the j th interaction channel, Γ is the usual Lorentz factor of the nucleon, and w_m is the maximum energy of the photon in the photon gas.

Pair production and photopion production processes are only of importance for interactions with the 2.7 K blackbody background radiation. Collisions with optical and infrared photons give a negligible contribution. Therefore, for interactions with a blackbody field of temperature T , the photon density is that of a Planck spectrum [243], so the fractional energy loss is given by

$$-\frac{1}{E} \frac{dE}{dt} = -\frac{ckT}{2\pi^2\Gamma^2(c\hbar)^3} \sum_j \int_{w_{0j}}^{\infty} dw_r \sigma_j(w_r) K_j w_r \ln(1 - e^{-w_r/2\Gamma kT}) \quad (48)$$

where k and \hbar are Boltzmann's and Planck's constants respectively, and w_{0j} is the threshold energy for the j th reaction in the rest frame of the nucleon.

Berezinsky and Grigor'eva have examined in detail the pair production process [227]. At energies $E \ll m_e m_p/kT = 2.1 \times 10^{18} \text{ eV}$ (i.e., $w_r/m_e - 2 \ll 1$), when the reaction takes place on the photons from the high energy tail of the Planck distribution, the fraction of energy lost in one collision and the cross section can be approximated by the threshold values

$$K_{e^+e^-} = 2 \frac{m_e}{m_p}, \quad (49)$$

¹⁹ Here the laboratory frame is the one in which the cosmic microwave background is at a temperature $\approx 2.7 \text{ K}$.

and

$$\sigma_{e^+e^-}(w_r) = \frac{\pi}{12} \alpha r_0^2 \left(\frac{w_r}{m_e} - 2 \right)^3, \quad (50)$$

where α is the fine structure constant and r_0 is the classical radius of the electron. The fractional energy loss due to pair production for $E \lesssim 10^{18}$ eV is then,

$$-\frac{1}{E} \left(\frac{dE}{dt} \right)_{e^+e^-} = \frac{16c}{\pi} \frac{m_e}{m_p} \alpha r_0^2 \left(\frac{kT}{hc} \right)^3 \left(\frac{\Gamma kT}{m_e} \right)^2 \exp\left(-\frac{m_e}{\Gamma kT}\right). \quad (51)$$

At higher energies ($E > 10^{19}$ eV) the characteristic time for the energy loss due to pair production is $t \approx 5 \times 10^9$ yr [244]. In this energy regime, the photopion reactions $p\gamma \rightarrow p\pi^0$ and $p\gamma \rightarrow \pi^+n$ on the tail of the Planck distribution give the main contribution to proton energy loss. The cross sections of these reactions are well known and the kinematics is simple.

Photopion production turns on at a photon energy in the proton rest frame of 145 MeV with a strongly increasing cross section at the $\Delta(1232)$ resonance, which decays into the one pion channels π^+n and π^0p . With increasing energy, heavier baryon resonances occur and the proton might reappear only after successive decays of resonances. The most important channel of this kind is $p\gamma \rightarrow \Delta^{++}\pi^-$ with intermediate Δ^{++} states leading finally to $\Delta^{++} \rightarrow p\pi^+$. Δ^{++} examples in this category are the $\Delta(1620)$ and $\Delta(1700)$ resonances. The cross section in this region can be described by either a sum or a product of Breit-Wigner distributions over the main resonances produced in $N\gamma$ collisions considering πN , $\pi\pi N$ and $K\Lambda$ ($\Lambda \rightarrow N\pi$) final states [245]. At high energies, $3.0 \text{ GeV} < w_r < 183 \text{ GeV}$, the CERN-HERA and COMPAS Groups have made a fit to the $p\gamma$ cross section [246]. The parameterization is

$$\sigma_\pi(w_r) = A + B \ln^2\left(\frac{w_r}{\text{GeV}}\right) + C \ln\left(\frac{w_r}{\text{GeV}}\right) \text{ mb}, \quad (52)$$

where $A = 0.147 \pm 0.001$, $B = 0.0022 \pm 0.0001$, and $C = -0.0170 \pm 0.0007$. In this energy range, the $\sigma_{\text{total}}(n\gamma)$ is to a good approximation identical to $\sigma_{\text{total}}(p\gamma)$.

We turn now to the kinematics of photon-nucleon interactions. Assuming that reactions mediated by baryon resonances have spherically symmetric decay angular distributions, the average energy loss of the nucleon after n resonant decays is given by

$$K_\pi(m_{R_0}) = 1 - \frac{1}{2^n} \prod_{i=1}^n \left(1 + \frac{m_{R_i}^2 - m_M^2}{m_{R_{i-1}}^2} \right), \quad (53)$$

where m_{R_i} denotes the mass of the i^{th} resonant system of the decay chain, m_M the mass of the associated meson, $m_{R_0} = \sqrt{s}$ is the total energy of the reaction in the c.m., and m_{R_n} the mass of the nucleon. See Appendix C for details. For multi-pion production the case is much more complicated because of the non-trivial final state kinematics.

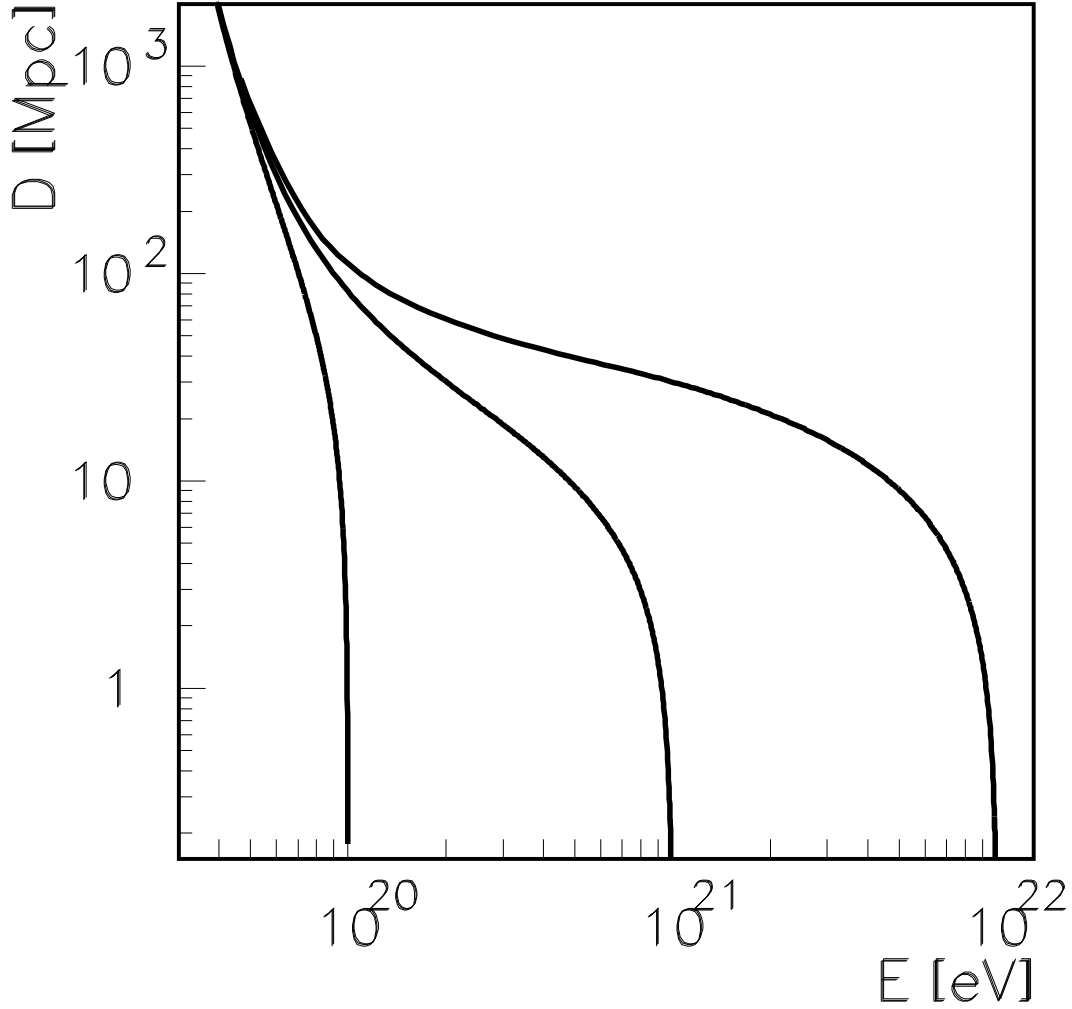


FIG. 11: Energy attenuation length of nucleons in the intergalactic medium. Note that after a distance of ~ 100 Mpc, or propagation time $\sim 3 \times 10^8$ yr, the mean energy is essentially independent of the initial energy of the protons, with a critical energy around 10^{20} eV. Published in Ref. [234].

However, it is well established experimentally [247] that, at very high energies ($\sqrt{s} \gtrsim 3$ GeV), the incoming particles lose only one-half their energy via pion photoproduction independently of the number of pions produced. This is the “leading particle effect”.

For $\sqrt{s} < 2$ GeV, the best maximum likelihood fit to Eq. (48) with the exponential behavior

$$-\frac{1}{E} \left(\frac{dE}{dt} \right)_{\pi} = A \exp[-B/E], \quad (54)$$

derived from the values of cross section and fractional energy loss at threshold, gives [234]

$$A = (3.66 \pm 0.08) \times 10^{-8} \text{ yr}^{-1}, \quad B = (2.87 \pm 0.03) \times 10^{20} \text{ eV}. \quad (55)$$

The fractional energy loss due to production of multipion final states at higher c.m. energies ($\sqrt{s} \gtrsim 3 \text{ GeV}$) is roughly a constant,

$$-\frac{1}{E} \left(\frac{dE}{dt} \right)_{\pi} = C = (2.42 \pm 0.03) \times 10^{-8} \text{ yr}^{-1}. \quad (56)$$

From the values determined for the fractional energy loss, it is straightforward to compute the energy degradation of ultrahigh energy cosmic rays in terms of their flight time. This is given by,

$$A t - \text{Ei}(B/E) + \text{Ei}(B/E_0) = 0, \quad \text{for } 10^{19} \text{ eV} \lesssim E \lesssim 10^{21} \text{ eV}, \quad (57)$$

and

$$E(t) = E_0 \exp[-C t], \quad \text{for } E \gtrsim 10^{21} \text{ eV}, \quad (58)$$

where Ei is the exponential integral [248]. Figure 11 shows the proton energy degradation as a function of the mean flight distance. Notice that, independent of the initial energy of the nucleon, the mean energy values approach 10^{20} eV after a distance of $\approx 100 \text{ Mpc}$.

Nevertheless, the definition of the GZK radius is subject to possible magnetic field deflections. To obtain quantitative estimates, one generally defines the 50% horizon R_{50} as the light propagation distance from the source at which $1/e$ of all injected protons have retained 50% or more of their energy, i.e., R_{50} is achieved when

$$\int_{E_0/2}^{E_0} \frac{dN}{dE} dE = N_0 \exp(-1), \quad (59)$$

where N_0 is the number of particles injected with energy E_0 [237]. For injection energies $> 10^{20} \text{ eV}$ the protons are not affected much by magnetic field strengths in the range $1-10 \text{ nG}$ (more on this below) since their scattering angles are small, and so the horizon energy dependence is similar to that of the energy loss distance. At $E = 10^{20} \text{ eV}$ R_{50} is about 100 Mpc , whereas at $2 \times 10^{20} \text{ eV}$ it decreases to 20 Mpc and becomes smaller than 10 Mpc for energies above $3 \times 10^{20} \text{ eV}$ [237]. Below 10^{20} eV the scattering in the magnetic field increases the propagation time and thus causes additional energy loss and an increase of the ratio between the mean energy loss length and R_{50} . In summary, the GZK-cutoff implies that if the primary ultrahigh energy CRs are protons energetic sources should be very close to the Earth, say within about 20 Mpc .

On a different track, the GZK-cutoff guarantees a cosmogenic flux of neutrinos, caused by the decay of charged pions produced in the photon-nucleon interactions [249, 250]. The resulting neutrino flux depends critically on the cosmological evolution of the cosmic ray sources and on their proton injection spectra [230, 232, 252]. Of course, the neutrino intensity will also depend on the homogeneity of sources. For example, semi-local objects, such as the Virgo cluster [226], could contribute to the high energy tail of the neutrino spectrum. Additionally, there is a weak dependence on the details of the cosmological expansion of the Universe. For example, a small cosmological constant tends to increase the contribution to neutrino fluxes from higher redshifts [252].

In Fig. 12 we show the cosmogenic neutrino flux obtained by Protheroe and Johnson [232] using Monte Carlo simulation techniques for a proton injection spectrum with $E_{\text{cutoff}} = 3 \times 10^{21}$ eV. This study incorporates the cosmological evolution of the sources from estimates [161] of the power per comoving volume emitted as protons by powerful radiogalaxies, taking into account the radio luminosity functions given in Ref. [254]. The flux peaks around $E \approx 2 \times 10^{17}$ eV, which is roughly the same energy suggested by other analyses following a source evolution scaling like $(1+z)^4$ [230, 252]. The figure also shows the flux-estimates by Hill and Schramm [226] considering contributions from semi-local nucleon sources, and an earlier estimate by Stecker which does not take into account the source evolution [250].

In summary, cosmic microwave background (CMB) renders the Universe opaque to protons above about 5×10^{19} eV. If proton sources are at cosmological distances ($\gtrsim 100$ Mpc), the observed proton spectrum should display the GZK cutoff.

B. Photonuclear interactions

The relevant mechanisms for the energy loss that extremely high energy nuclei suffer during their trip to Earth are: Compton interactions, pair production in the field of the nucleus, photodisintegration, and hadron photoproduction. The Compton interactions have no threshold energy. In the nucleus rest-frame, pair production has a threshold at ~ 1 MeV, photodisintegration is particularly important at the peak of the giant dipole resonance (15 to 25 MeV), and photomeson production has a threshold energy of ~ 145 MeV.

Compton interactions result in only a negligibly small energy loss for the nucleus given by [255]

$$-\frac{dE}{dt} = \frac{Z^4}{A^2} \rho_\gamma \left(\frac{E}{Am_p c^2} \right)^2 \text{ eV s}^{-1} \quad (60)$$

where ρ_γ is the energy density of the ambient photon field in eV cm^{-3} , E is the total energy of the nucleus in eV, and Z and A are the atomic number and weight of the

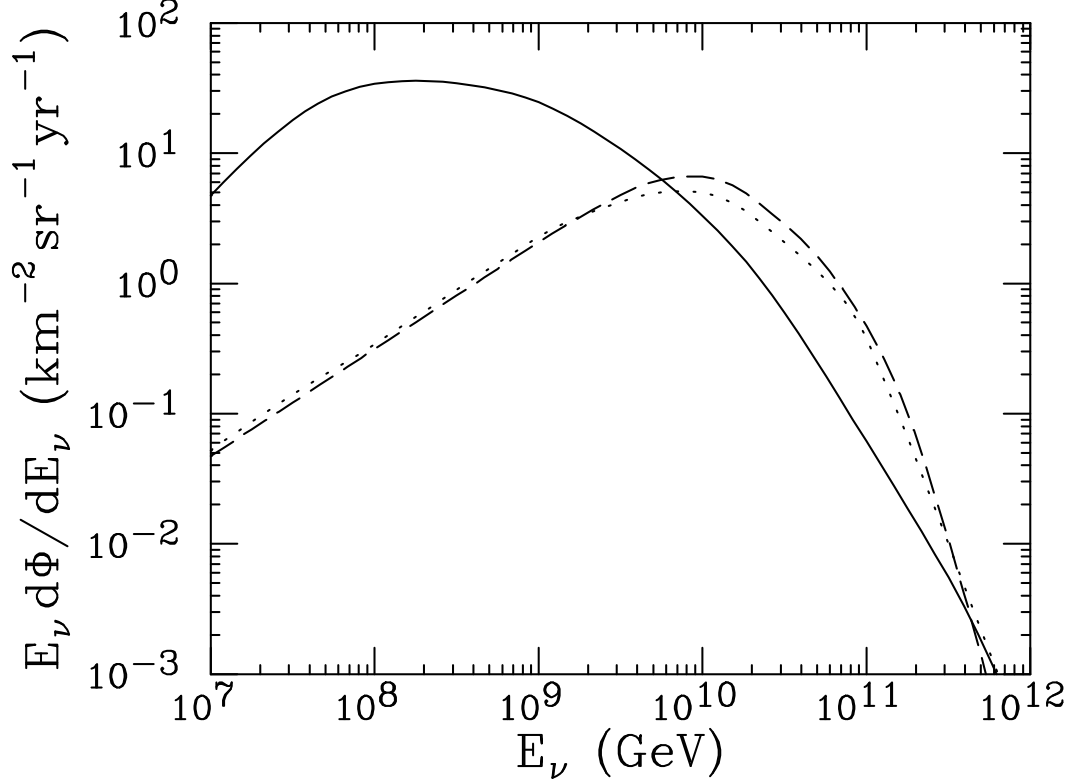


FIG. 12: Cosmogenic $\nu_\mu + \bar{\nu}_\mu + \nu_e$ fluxes from Protheroe and Johnson with energy cutoff of 3×10^{21} eV (solid) [251], Hill and Schramm (dashed) [226], and previous estimate by Stecker without source evolution (dotted) [250]. Published in Ref. [253].

nucleus. The energy loss rate due to photopair production is Z^2/A times higher than for a proton of the same Lorentz factor [256], whereas the energy loss rate due to photomeson production remains roughly the same. The latter is true because the cross section for photomeson production by nuclei is proportional to the mass number A [257], while the inelasticity is proportional to $1/A$. However, it is photodisintegration rather than photopair and photomeson production that determines the energetics of ultrahigh energy cosmic ray nuclei. During this process some fragments of the nuclei are released, mostly single neutrons and protons. Experimental data of photonuclear interactions are consistent with a two-step process: photoabsorption by the nucleus to form a compound state, followed by a statistical decay process involving the emission of one or more nucleons.

Following the conventions of Eq. (47), the disintegration rate with production of i nucleons is given by [258]

$$R_{Ai} = \frac{1}{2\Gamma^2} \int_0^\infty dw \frac{n(w)}{w^2} \int_0^{2\Gamma w} dw_r w_r \sigma_{Ai}(w_r) \quad (61)$$

with σ_{Ai} the cross section for the interaction. Using the expressions for the cross section fitted by Puget, Stecker and Bredekamp [255], it is possible to work out an analytical solution for the nuclear disintegration rates (see Appendix D). Summing over all the possible channels for a given number of nucleons, one obtains the effective nucleon loss rate $R = \sum_i iR_{Ai}$. The effective nucleon loss rate for light elements, as well as for those in the carbon, silicon and iron groups can be scaled as [255]

$$\left. \frac{dA}{dt} \right|_A \sim \left. \frac{dA}{dt} \right|_{\text{Fe}} \left(\frac{A}{56} \right) = R|_{\text{Fe}} \left(\frac{A}{56} \right), \quad (62)$$

with the photodisintegration rate parametrized by [259]

$$R(\Gamma)|_{\text{Fe}} = 3.25 \times 10^{-6} \Gamma^{-0.643} \exp(-2.15 \times 10^{10}/\Gamma) \text{ s}^{-1} \quad (63)$$

for $\Gamma \in [1.0 \times 10^9, 36.8 \times 10^9]$, and

$$R(\Gamma)|_{\text{Fe}} = 1.59 \times 10^{-12} \Gamma^{-0.0698} \text{ s}^{-1} \quad (64)$$

for $\Gamma \in [3.68 \times 10^{10}, 10.0 \times 10^{10}]$.

For photodisintegration, the averaged fractional energy loss results equal the fractional loss in mass number of the nucleus, because the nucleon emission is isotropic in the rest frame of the nucleus. During the photodisintegration process the Lorentz factor of the nucleus is conserved, unlike the cases of pair production and photomeson production processes which involve the creation of new particles that carry off energy. The total fractional energy loss is then

$$-\frac{1}{E} \frac{dE}{dt} = \frac{1}{\Gamma} \frac{d\Gamma}{dt} + \frac{R}{A}. \quad (65)$$

For $w_r \lesssim 145$ MeV the reduction in Γ comes from the nuclear energy loss due to pair production. The γ -ray momentum absorbed by the nucleus during the formation of the excited compound nuclear state that precedes nucleon emission is $\mathcal{O}(10^{-2})$ times the energy loss by nucleon emission [260]. For $\Gamma > 10^{10}$ the energy loss due to photopair production is negligible, and thus

$$E(t) \sim 938 A(t) \Gamma \text{ MeV} \sim E_0 \exp \left[\frac{-R(\Gamma)|_{\text{Fe}} t}{56} \right]. \quad (66)$$

Figure 13 shows the energy of the heaviest surviving nuclear fragment as a function of the propagation time, for initial iron nuclei. The solid curves are obtained using Eq. (66), whereas the dashed and dotted-dashed curves are obtained by means of Monte Carlo simulations [262]. One can see that nuclei with Lorentz factors above 10^{10} cannot survive for more than 10 Mpc. For these distances, the approximation given in Eq. (66)

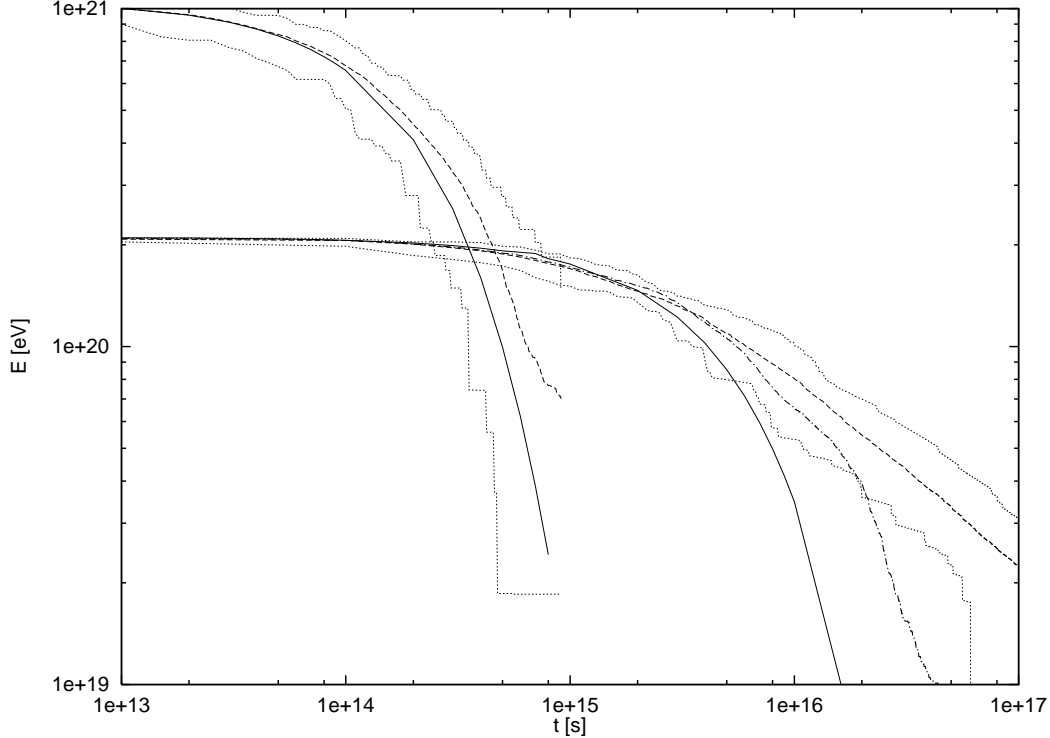


FIG. 13: The energy of the surviving fragment ($\Gamma_0 = 4 \times 10^9$, $\Gamma_0 = 2 \times 10^{10}$) vs. propagation time obtained using Eq. (66) is indicated with a solid line. Also included is the energy attenuation length obtained from Monte Carlo simulations with (dashed) and without (dotted-dashed) pair creation production, for comparison. The region between the two dotted lines includes 95% of the simulations. This gives a clear idea of the range of values which can result from fluctuations from the average behaviour. It is important to keep in mind that a light propagation distance of 1.03×10^{14} s corresponds to 1 Mpc. From Ref. [261].

always lies in the region which includes 95% of the Monte Carlo simulations. When the nucleus is emitted with a Lorentz factor $\Gamma_0 < 5 \times 10^9$, pair production losses start to be relevant, significantly reducing the value of Γ as the nucleus propagates distances of $\mathcal{O}(100 \text{ Mpc})$. The effect has a maximum for $\Gamma_0 \approx 4 \times 10^9$ but becomes small again for $\Gamma_0 \leq 10^9$, for which appreciable effects only appear for cosmological distances ($> 1000 \text{ Mpc}$), see for instance [262].

Note that Eq. (66) imposes a strong constraint on the location of nucleus-sources: less than 1% of iron nuclei (or any surviving fragment of their spallations) can survive more than 3×10^{14} s with an energy $> 10^{20.5}$ eV. For straight line propagation, this represents a maximum distance of $\sim 3 \text{ Mpc}$.

Because of the position of ^{56}Fe on the binding energy curve, it is generally considered to be a significant end product of stellar evolution, and indeed higher mass nuclei are found to be much rarer in the cosmic radiation. Specifically, the atomic abundance of

nuclei heavier than iron (in the cosmic radiation) is expected to be smaller by 3 or 5 orders of magnitude relative to the lighter ones [263]. However, for super-heavy nuclei the GZK sphere is substantially increased, because for $\Gamma \lesssim 10^9$ the nucleus interacts only with the tail of the Planck spectrum and infrared backgrounds [264, 265]. Indeed, because of the paucity of data, there is a great uncertainty in the chemical composition at the end of the spectrum, so the situation is ripe for speculation on super-heavy nuclei as primaries [266].

C. Relativistic specks of dust

Dust is a very widespread component of diffuse matter in the galaxy and, apparently, in intergalactic space. In particular, specks expelled by radiation pressure from cool stars may be injected into the interstellar medium with speeds $\sim 10^8$ cm s⁻¹ [267], generally carrying a net electric charge. Therefore, these small solid particles can be re-accelerated very effectively to ultra-high energies at shock-wave fronts [268, 269, 270]. However, the situation is unusual, because the Lorentz factors involved can be small even at very high energies.

We now discuss the survival probability of such specks of dust. The break up of dust grains is mainly due to electrical stresses induced by the accumulation of charge as a result of the photoelectric effect in the galactic optical radiation and also as a result of ionization by the hydrogen atoms of interstellar gas. The critical electric charge on the surface of a dust grain of radius R , for which repulsion forces break up the particle is given by [271]

$$q_c = \sqrt{4\pi f_0} R^2, \quad (67)$$

where f_0 denotes the breaking stress. Subrelativistic ($v \lesssim 3 \times 10^9$ cm/s) dust grains disintegrate in collisions with the nuclei and electrons of the interstellar medium. Ionization takes place along the path of the nucleus in the dust grain, heating the matter up to 10^5 K in a narrow channel of radius $\sim 10^{-7}$ cm. Close to the surface of the channel the local pressure reaches 10^4 kg mm⁻², which results in microfractures. Because of the small size of the grain, microfractures are unstable and increase until the complete break-up of the particle occurs. The charge accumulation rate on a small grain ($R < \bar{R}$) is given by [272]

$$\frac{dq}{dt} = 0.6 A^{-1} v n_{\text{H}} \pi R^2 \left(\frac{c}{v}\right)^2 (\rho R)^{0.41} \quad (68)$$

and on a large one ($R > \bar{R}$)

$$\frac{dq}{dt} = 2 A^{-1} v n_{\text{H}} \pi R^2 \sigma_T N_A \rho \left(\frac{c}{v}\right)^2 \frac{m_e c^2}{e \sqrt{4\pi f_0}}, \quad (69)$$

with

$$\overline{R} = 1.1 \times 10^2 \rho^{1.44} f_0^{-1.22} \mu\text{m}. \quad (70)$$

Here, v is the velocity of the dust grain, ρ its density, n_{H} is the density of hydrogen atoms in the surrounding medium, A is the mass number, N_A is Avogadro's number, and σ_T is the Thomson cross section. Significant accumulation of charge occurs during the trip through the galaxy, where the density of hydrogen is $n_{\text{H}} \sim 0.6$ atoms/cm³. The path length up to the first break up in the galactic gas,

$$D = vq_c \left(\frac{dq}{dt} \right)^{-1}, \quad (71)$$

turns out to be $D \lesssim 10^{15}$ cm, for graphite grains ($f_0 \sim 1$ kg mm⁻²), and $D \lesssim 10^{16}$ cm, for iron grains ($f_0 \sim 10$ kg mm⁻²) [272].

The threshold value of the Lorentz factor of a relativistic grain with energy E and density ρ (measured in g cm⁻³), under the influence of the photoelectric effect with photons of energy w , is given by [271]

$$\Gamma \sim \left(\frac{3E}{4\pi\rho} \right)^{1/4} \left(\frac{\mathcal{E}}{wc} \right)^{3/4} = 9.0 \times 10^{-2} \left(\frac{f_0^{3/2} E_{\text{GeV}}}{w_{\text{eV}}^3 \rho} \right)^{1/4}, \quad (72)$$

where $E_{\text{GeV}} \equiv E/\text{GeV}$, $w_{\text{eV}} \equiv w/\text{eV}$, and f_0 is measured in kg mm⁻². Thus, a carbon dust grain with $E \sim 10^{20}$ eV and $\Gamma > 25$ is split up by starlight photons ($w \lesssim 2$ eV). Relativistic dust grain break up is particularly effective within the solar system. The distance the grain can approach the Sun without splitting up is given by [271]

$$D \sim \frac{L(w) \chi e R^2}{4 c q_c} = 2.3 \times 10^{-25} \frac{\chi L(w)}{\sqrt{f_0}} \text{ cm}, \quad (73)$$

where $L(w)$ is the number of photons with energy above threshold emitted by the Sun measured in s⁻¹, and $\chi \sim 0.01 - 0.1$ is the number of electrons stripped from the speck of dust by one photon. For carbon dust grains with $\Gamma > 25$ ($w \lesssim 2$ eV and $L(w) \sim 3.5 \times 10^{44}$ s⁻¹), Eq. (73) leads to $D \sim 10$ pc. Figure 14 shows the path length of a typical graphite grain in the field of the galactic optical radiation.

Doubts have also been expressed about the prospects of surviving against the heating from photoionization within the solar radiation field [273]. Consider a grain moving (radially) towards the Sun with constant velocity $v \equiv \beta c$ and subtending an effective solid angle $d\Omega$, with α the angle between the position vector \hat{r} of the grain and the positive x -axis defined by a line parallel to the direction of motion. In the rest system of the grain, the average energy of the photons is blue-shifted to $\Gamma w(1 - \beta \cos \alpha)$. The Sun no longer appears to emit isotropically; namely, the number of incident photons

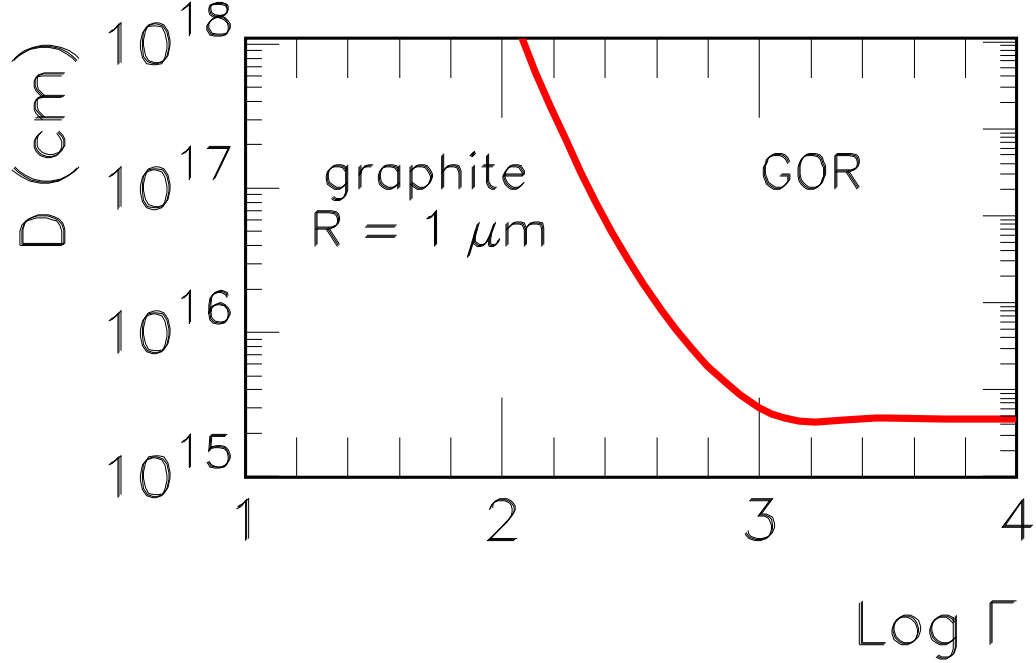


FIG. 14: The path length of a graphite grain of radius $R = 1 \mu\text{m}$ up to the first break-up, in the field of the galactic optical radiation (GOR). Adapted from Ref. [272].

per second is $\Gamma L(w) (1 - \beta \cos \alpha) d\Omega / 4\pi$. To estimate the surface temperature T of the grain we assume that it radiates as a black body,

$$\epsilon \sigma_B T^4 4\pi R^2 = \Gamma^2 L(w) w (1 - \beta \cos \alpha)^2 \frac{d\Omega}{4\pi}, \quad (74)$$

where σ_B is the Stefan-Boltzman constant and ϵ the emissivity of the grain. The solid angle is determined by the cross section for absorption by the grain. For a particle traveling in the r -direction towards the Sun,

$$d\Omega = 4 N \sigma \pi R^3 3 r^2, \quad (75)$$

where N is the volume density of grain atoms and σ the ionization cross section per atom. For iron, $\sigma \sim 3 \times 10^{-16} \Gamma^{-1} \text{ cm}^2$ [274]. Now, setting T equal to the melting point T_c of the grain, Eqs. (74) and (75) combine to yield the following expression for the position r_α at which the grain melts

$$r_\alpha = \tilde{r}_\alpha (1 - \beta \cos \alpha), \quad (76)$$

where

$$\tilde{r}_\alpha = \sqrt{\frac{\Gamma^2 R L(w) w N \sigma}{12\pi \epsilon \sigma_B T_c^4}}. \quad (77)$$

For an iron grain with $T_c \sim 1800$ K, $\epsilon \sim 0.5$ and $N \sim 8.6 \times 10^{22}$ atoms cm^{-3} , Eq. (77) leads to

$$\tilde{r}_\alpha \sim 3 \times 10^{15} \sqrt{\Gamma R} \text{ cm.} \quad (78)$$

Now, since

$$E = \frac{4}{3} \pi R^3 c^3 \Gamma \rho. \quad (79)$$

for an iron grain of $E \sim 10^{19}$ eV, $\tilde{r}_\alpha = 1.0 \times 10^{13} \Gamma^{1/3}$ cm. Hence, relativistic ($\log \Gamma < 2$) iron grains would melt before reaching the Earth's orbit around the Sun, i.e., $r_\alpha \sim 1$ au = 1.5×10^{13} cm. There is no substantial change for an iron grain traveling non-radially, it would melt before reaching the Earth [273]. However, note that dust grains composed of carbon ($T_c \sim 4000$ K) may reach the Earth's orbit with $E \sim 10^{20}$ eV if $\Gamma \sim 20$.

In summary, subrelativistic dust grains have no chance to survive the trip to Earth. However, relativistic carbon specks could survive a trip of ≈ 100 pc if one assumes the most optimistic parameters. Since the closest supernova remnant is about 200 pc away [275], astrophysical models cannot rule out relativistic dust grains as ultrahigh energy CR primaries.

D. Electromagnetic cascades

The dominant absorption process for high energy γ -rays (energy E) traversing cosmic distances is pair creation through collisions with the various radiation fields (energy w) permeating the Universe [276, 277, 278, 279, 280, 281, 282]. The fundamental process is well understood and its amplitude can be calculated accurately by general perturbation methods developed in quantum electrodynamics (QED) [283, 284, 285]. The lowest-order single pair creation cross section [276]

$$\sigma = \frac{1}{2} \pi r_0^2 (1 - \beta^2) \left[(3 - \beta^4) \ln \left(\frac{1 + \beta}{1 - \beta} \right) - 2\beta(2 - \beta^2) \right], \quad (80)$$

peaks near the threshold $E_{\text{th}} = m_e^2/w \sim 2.6 \times 10^2 (w/\text{eV})^{-1}$ GeV, and falls off asymptotically as $s \rightarrow \infty$ [285],

$$\sigma(s) \sim \frac{4\pi\alpha^2}{s} \left[\ln \left(\frac{s}{m_e^2} \right) - 1 \right]. \quad (81)$$

Here, $\beta = (1 - 1/s)^{1/2}$ is the electron (positron) velocity in the c.m. system and r_0 is the classical electron radius. Higher order QED processes with more than two final state particles become important with rising energy. For example, the fourth-order

two-pair creation cross section is a sharply rising function of s near the threshold that quickly approaches its asymptotic value [285]²⁰

$$\sigma(s) \sim \frac{\alpha^4}{36\pi m_e^2} [175\zeta(3) - 38] \sim 6.45 \mu\text{b}, \quad (82)$$

and becomes bigger than the single pair creation cross section when $s \gtrsim 1 \text{ GeV}^2$. With this in mind, the most efficient targets for γ -rays of energy E are background photons of energy $w \sim m_e^2/E$. This implies that for γ -ray energies $\gtrsim 10^{20} \text{ eV}$, interactions with the radio background ($w \lesssim 10^{-6} \text{ eV} \sim 100 \text{ MHz}$) become more important than those with the CMB.

We have no direct knowledge of the cosmic radio background, mostly because it is difficult to disentangle the galactic and extragalactic component. For a temperature of the extragalactic component of 15 K at 178 MHz one finds

$$n(w) \sim Kw^{-2}, \quad (83)$$

with $K = 1.09 \times 10^{20} \text{ erg/cm}^3$ [286]. At frequencies somewhere below 1 MHz the intensity is expected to fall off exponentially; the principal absorption process would be inverse Bremsstrahlung or “free-free” absorption by the intergalactic plasma. Observational estimates are consistent with a cutoff in the spectrum at $w \lesssim 10^{-8} \text{ eV}$ [287]. However, that part of the spectrum where the Universe is optically thick to radio emission depends on the abundance and clustering of electrons in the extragalactic medium and/or the radio source, and is uncertain between 0.1 - 2 MHz. A theoretical estimate [288] of the intensity down to kHz frequencies, based on the observed luminosity functions and radio spectra of normal galaxies and radio-galaxies, tends to give higher estimates than those of Ref. [287].

The probability per unit path length that a γ -ray is converted into e^+e^- pairs in a collision with a low-energy photon is given by [276]

$$\frac{dP}{dx} = 2 \left(\frac{m_e^2}{E} \right)^2 \int_0^\infty \frac{n(w)}{w^2} dw \int_1^{s_0} s \sigma(s) ds, \quad (84)$$

where $s_0 = Ew/m_e$. The mean interaction length of pair production, showing the contribution of the various radiation fields, is given in Fig. 15. For the radio background, we assume the conservative estimate of Ref. [287]. Using the radio spectrum derived by Protheroe and Biermann leads to a photon mean free path (at $E \sim 10^{21} \text{ eV}$) a factor of 3 - 10 smaller [288].

In the Klein-Nishina limit, $s \gg m_e^2$, one of the pair-produced particles carries most of the γ -ray energy. In the absence of magnetic fields, this leading electron (positron) can

²⁰ $\zeta(3) \approx 1.202$ is the zeta function with argument 3.

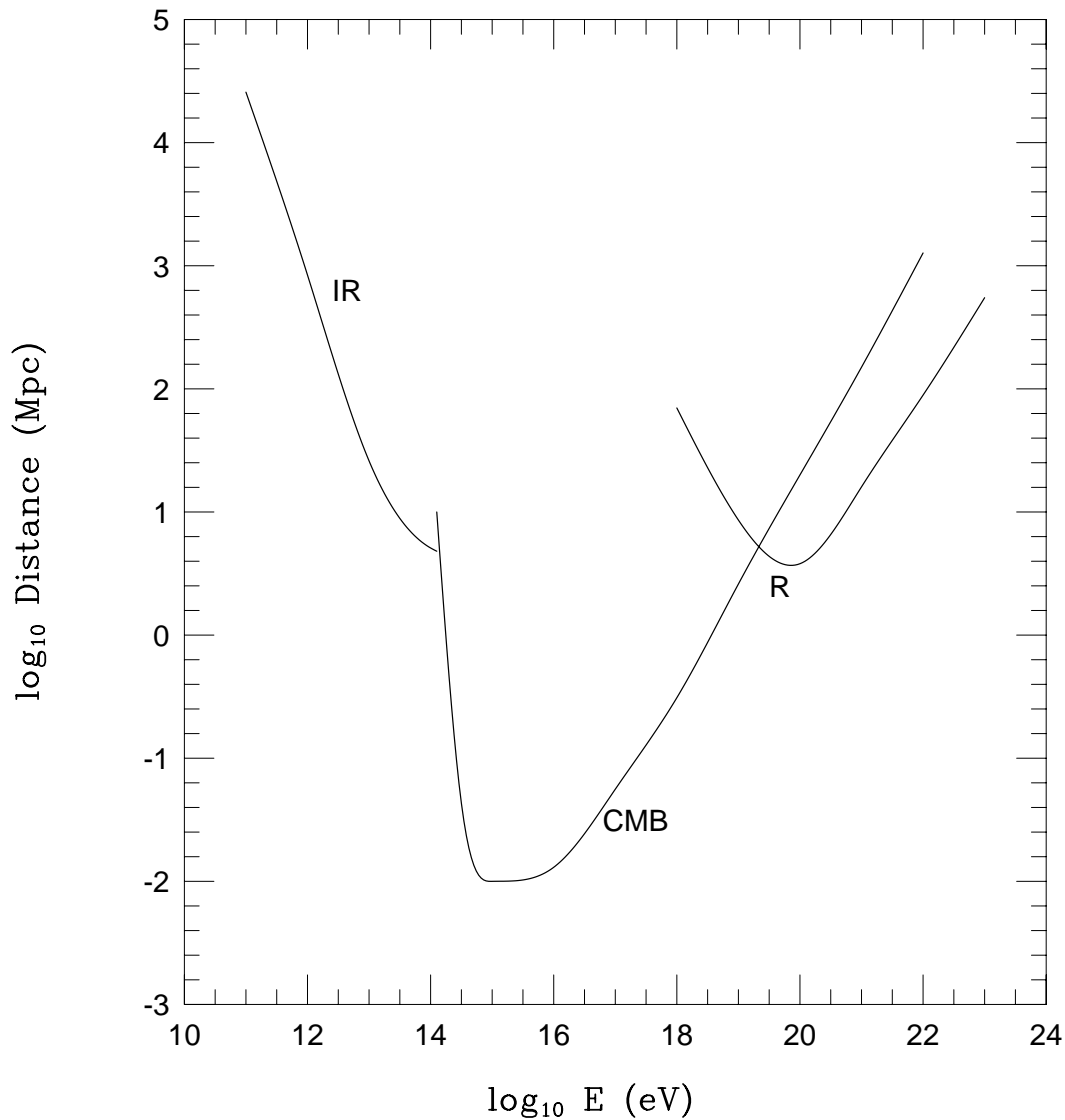


FIG. 15: Mean pair production interaction length for γ -rays in the infrared and optical backgrounds (IR), radio background (R), and relic photons (CMB). Adapted from Ref. [232].

deliver a substantial fraction of the original γ -ray's energy to a new γ -ray via inverse Compton scattering (ICS), with cross section

$$\sigma_{\text{ICS}}(s) \sim \frac{2\pi\alpha^2}{s} \left[\ln \left(\frac{s}{m_e^2} \right) - 1 \right]. \quad (85)$$

The scattered photon, which is now the leading particle, can initiate a fresh cycle of pair production and inverse Compton scattering interactions, yielding an electromagnetic cascade.

For $s \ll m_e^2$, $\sigma_{\text{ICS}} \sim \sigma_{\text{T}}$, and the fractional energy loss is given by [289]

$$-\frac{1}{E} \left(\frac{dE}{dt} \right)_{\text{ICS}} \sim \frac{4}{3} \sigma_{\text{T}} c \Gamma \frac{w n(w)}{m_e}. \quad (86)$$

Corrections to the lowest order ICS cross section from processes involving additional photons in the final state are less than 10% in the ultrahigh energy range [290]. Furthermore, various other possible processes, such as those involving production of one or more muons, taus, pion pairs, and Bethe-Heitler pairs ($\gamma X \rightarrow X e^+ e^-$, where X stands for an atom, ion or free electron), can be safely neglected [285]. For example, the total cross section for the lowest-order single muon pair production is around an order of magnitude smaller than that for electron pair production.

The development of electromagnetic cascades depends sensitively on the strength of the extragalactic magnetic field B , which is rather uncertain. For $B \gtrsim 10^{-11}$ G the electrons will lose much of their energy through synchrotron radiation before they have the opportunity to undergo ICS, and the electromagnetic cascade will be virtually terminated [291]. Specifically, an electron of energy E moving in a field having a perpendicular component of magnitude B_{\perp} radiates energy at a rate

$$-\frac{dE}{dx} = 3.3 \times 10^{-14} \left(\frac{B_{\perp}}{1 \text{ G}} \right)^2 \left(\frac{E}{m_e c^2} \right)^2 \text{ eV cm}^{-1}. \quad (87)$$

Hence, if the radiated energy is less than say 10% of the electron energy in an interaction length λ , the electron synchrotron cools before it can undergo ICS, and thus the cascade development stops. The above cooling time scale holds provided that

$$B_{\perp}^2 < 7.9 \times 10^{23} \frac{1}{E_{\text{eV}} \lambda_{\text{cm}}} \text{ G}^2, \quad (88)$$

where $E_{\text{eV}} \equiv E/1 \text{ eV}$ and $\lambda_{\text{cm}} \equiv \lambda/1 \text{ cm}$. Then, for 3×10^{-12} G, 2×10^{-11} G, and 1×10^{-10} G, the intergalactic space becomes opaque to the propagation of γ -rays of $E = 10^{21}$ eV, $E = 10^{20}$ eV, and $E = 10^{19}$ eV, respectively.

Putting all this together, the GZK radius of the photon channel strongly depends on the strength of extragalactic magnetic fields. In principle, distant sources with $z > 0.03$ can contribute to the observed rays above 5×10^{19} eV if the extragalactic magnetic field does not exceed 10^{-12} G [292]. However, comparison of the expected and observed numbers of CRs from the direction of the nearby source Centaurus A allows one to place bounds on intergalactic magnetic fields of $\gg 10^{-11}$ G [197]. In such a case, the survival probability for 3×10^{20} eV γ -rays to distance D ,

$$P(> D) = \exp[-D/6.6 \text{ Mpc}], \quad (89)$$

becomes less than 10^{-4} after traversing a distance of 50 Mpc [172].

E. Deflection and delay due to magnetic fields

Cosmic rays *en route* to Earth suffer deflection and delay in magnetic fields, effects which can camouflage their origins. In this section, we discuss bending of cosmic ray orbits in both Galactic and extragalactic fields. Various combinations of field strength and coherence length are considered, and we discuss solutions to the diffusion equations as well as results from Monte Carlo simulation.

The magnetic deflection of protons in the Galactic disk has been studied in detail by Stanev [293]. This analysis includes two extreme options for the behaviour of the field, reflecting the different symmetries with respect to field reversals in the r - and z -directions. The B -field has a $1/r$ behaviour, with deviations calculated out to 20 kpc from the Galactic center. The r.m.s. deviation averaged over arrival direction, for an energy of 2×10^{19} eV (4×10^{19} eV), varies from 17.7° to 23.7° (7.9° to 10.5°) in going between the two models. This deviation shows an approximately linear decrease with increasing energy. In the case of heavy nuclei, the arrival direction of the particles is strongly dependent on the coordinates of the source [294, 295, 296]. The Larmor radius of a nucleus with $E/Z = 10^{19}$ eV in a uniform magnetic field of strength $B \sim 3 \mu\text{G}$ is slightly larger than 3 kpc. The typical large scale field intensity of the Milky Way is a few μG , and is approximately uniform over scales of the order of a few kpc. Therefore, the propagation in the Galactic magnetic field of a nucleus with $E/Z > 10^{19}$ eV should in general be not very different from a quasi-rectilinear trajectory, with deflections away from the straight path becoming smaller with increasing energy. However, for 10^{18} eV $< E/Z < 10^{19}$ eV, the deflection may be high enough ($> 20^\circ$) to make any identification of the sources extremely difficult.²¹ Moreover, lensing effects yield (de)magnification of the CR-fluxes, and not every incoming particle direction is allowed between a given source and the detector. This generates sky patches which are virtually unobservable from Earth [294, 295]. On the other hand, the enhancement of the probability to detect events from a given source in a narrow energy range near the caustic implies a concentration of events around the location where the new pair of images forms. Therefore, magnetic lensing around caustics becomes a potential source of clustering in the angular distribution of arrival directions [296]. Precise predictions depend upon the detailed structure of the magnetic field configuration, which is not so well known. However, new experiments such as PAO may make it possible to use CRs as probes of the magnetic field structure [298, 299].

At present, surprisingly little is known about extragalactic magnetic fields (EGMFs). There are some measurements of diffuse radio emission from the bridge area between the Coma and Abell superclusters [300], which, under assumptions of equipartition allows

²¹ At smaller energies the drift and diffusive regimes dominate [297].

an estimate of $\mathcal{O}(0.2 - 0.6) \mu\text{G}$ for the magnetic field in this region.²² Such a large field may possibly be understood if the bridge region lies along a filament or sheet [302]. In addition, the absence of a positive signal in Faraday rotation measurements on distant quasars [303] provides upper limits on magnetic fields of any origin as a function of reversal scale [304]. These bounds depend significantly on assumptions about the electron density profile as a function of the redshift. When electron densities follow that of the Lyman- α forest, the average magnitude of the magnetic field receives an upper limit of $B \sim 10^{-9}$ G for reversals on the scale of the horizon, and $B \sim 10^{-8}$ G for reversal scales on the order of 1 Mpc [305]. The latter upper bound is roughly coincident with the lower limit in the Galactic neighborhood [197].

If the Larmor radius of a particle is sizably larger than the coherence length ℓ of the extragalactic magnetic field, the typical deflection angle from the direction of the source, located at a distance d , can be estimated assuming that the particle makes a random walk in the magnetic field [306],

$$\theta(E) \simeq 0.54^\circ Z \left(\frac{d}{1 \text{ Mpc}} \right)^{1/2} \left(\frac{\ell}{1 \text{ Mpc}} \right)^{1/2} \frac{B_{\text{nG}}}{E_{20}}, \quad (90)$$

where $B_{\text{nG}} \equiv B/1 \text{ nG}$, and $E_{20} \equiv E/10^{20} \text{ eV}$. Note that deflection also implies an average time delay

$$\tau_{\text{delay}}(E) \approx \frac{d \theta^2}{4c} \quad (91)$$

relative to rectilinear propagation with the speed of light. With increasing magnetic field strength, the Larmor radius decreases and the hypothesis of straight line propagation between scatterings, that Eq. (90) relies upon, breaks down. A diffusive approach is more appropriate for this situation [307, 308, 309, 310, 311, 312, 313].

The Local Supercluster is a flattened overdensity of galaxies extending for $\sim 30 - 40$ Mpc with a width of ~ 10 Mpc [272]. The Virgo cluster is approximately in the center of this distribution, about 17 Mpc away from the Milky Way, which is located at the edge. This large scale distribution defines the super-Galactic plane where it intersects almost perpendicular the Galactic plane. A broad $\sim 50^\circ$ region centered at the Local Supercluster seems to be endowed with a magnetic field with a uniform component of strength $\sim 1.5 \mu\text{G}$ [314], and a random component of strength $\sim 1 \mu\text{G}$ [315]. If this is indeed the case, all CRs traveling to Earth will propagate diffusively.

The evolution of the nucleon spectrum is governed by the balance equation

$$\frac{\partial n}{\partial t} = \frac{\partial[b(E)n]}{\partial E} + D(E) \nabla^2 n + Q \quad (92)$$

²² Fields of $\mathcal{O}(\mu\text{G})$ are also indicated in a more extensive study of 16 low redshift clusters [301].

which takes into account the conservation of the total number of particles in the spectrum, i.e., $\int n d^3\vec{r} = n_0$. In the first term on the right, $b(E) \equiv dE/dt$ is the mean rate at which particles lose energy, and the last term, Q is the number of nucleons per time generated by the source(s). The second term stands for the diffusion in the extragalactic medium. Two extreme regimes can be distinguished depending on whether the particle remains trapped in magnetic subdomains or not, yielding different functional dependence on energy of the diffusion coefficient [316]

$$D(E) = \frac{1}{3} r_L c \frac{B^2}{\int_{\frac{1}{r_L}}^{\infty} dk P(k)}. \quad (93)$$

Here, $P(k)$ is the magnetic field power spectrum. As mentioned earlier, extragalactic magnetic field strengths and coherence lengths are not well established, but for $r_L \lesssim \ell$, it may be plausible to assume a Kolmogorov [188] form for the turbulent magnetic field power spectrum, $P(k) = P_0(k/k_0)^{-5/3}$, with coherent directions on scales of 0.5 - 1 Mpc. Here, $k_0 \sim 1/\ell$ is the small wavenumber limit for the magnetic field and $3 P_0 k_0/2 = B^2$. One can now easily estimate that protons with energies $E_c < 10^{21} \ell_{\text{Mpc}} B_{\mu\text{G}}$ eV remain trapped inside magnetic subdomains of size $\ell_{\text{Mpc}} = \ell/(1 \text{ Mpc})$, attaining efficient diffusion when the wave number of the associated Alfvén wave is equal to the Larmor radius of the particle [189, 316]. The replacement of the Kolmogorov spectrum into Eq. (93) leads to

$$D(E) \approx 0.048 \left(\frac{E_{20} \ell_{\text{Mpc}}^2}{B_{\mu\text{G}}} \right)^{1/3} \text{Mpc}^2/\text{Myr}. \quad (94)$$

As the particle energy increases ($E > E_c$), there is a transition to Bohm diffusion when $r_L \sim \ell$, and the diffusion coefficient is of the order of the Larmor radius times the velocity. Numerical simulations [309] show that for Bohm diffusion, $D \sim 3r_L c$, or equivalently, $D(E) \sim 0.1 E_{20}/B_{\mu\text{G}} \text{Mpc}^2/\text{Myr}$.²³

Now we consider the propagation of a burst from a single source. Idealizing the emission to be uniform with a rate $dN/dt = n_0/\tau$, we have

$$Q = \frac{n_0}{\tau} \delta^3(\vec{r}) [\Theta(t' - t_{\text{on}}) - \Theta(t' - t_{\text{off}})], \quad (95)$$

where $\int Q d^3\vec{r} dt' = N_{\text{tot}}$, and Θ is the Heaviside step function. Here t_{on} (t_{off}) is the time since the engine turned on (off) its CR production. If the energy loss term is neglected, the solution to Eq. (92) reads,

$$n(\vec{r}, t) = \int dt' \int d^3\vec{r}' G(\vec{r} - \vec{r}', t - t') Q(\vec{r}', t'), \quad (96)$$

²³ Criticisms of these assumptions have been raised in [317].

where

$$G(\vec{r} - \vec{r}', t - t') = [4\pi D(t - t')]^{-3/2} \Theta(t - t') \exp\{-(\vec{r} - \vec{r}')^2/4D(t - t')\}, \quad (97)$$

is the Green function [318]. Before integrating over the range of possible propagation times, we note that there is a negligible contribution from times prior to the arrival time of the diffusion front,

$$\tau_D = \frac{r^2}{4D}. \quad (98)$$

For a bursting source, i.e, $t_{\text{off}} - t_{\text{on}} \sim \delta t$, Eq. (96) leads to [319]

$$\begin{aligned} n(\vec{r}, t) &= \frac{n_0}{\tau} \int_{t_{\text{min}}}^{t_{\text{max}}} dt' \frac{e^{-r^2/4(t-t')}}{[4\pi D(t-t')]^{3/2}} = \frac{n_0}{\tau} \frac{1}{4\pi D r} \Phi \left[\frac{r}{\sqrt{4D(t-t')}} \right] \\ &\approx \frac{n_0}{\tau} \frac{2}{[4\pi D]^{3/2}} [t_{\text{min}}^{-1/2} - t_{\text{max}}^{-1/2} + \mathcal{O}(t^{-3/2})], \end{aligned} \quad (99)$$

where $\Phi(x)$ is the error function, and we have set present observation time at $t = 0$. Note that for Kolmogorov diffusion $D \sim E^{1/3}$. Now, shock acceleration results in a spectrum at the source $Q \propto E^{-\gamma}$ with γ slightly greater than 2. Therefore, the purely diffusive solution results in a spectrum $n(E) \propto E^{-\gamma+1/3}$, close to the observed spectrum $E^{-2.7}$ [308]. The condition of diffuse propagation is

$$\tau_D \gg \tau_s, \quad (100)$$

where $\tau_s = r/c$ is the time required for a straight line propagation.

If photopion production becomes important, one has to resort to numerical Monte Carlo simulations. Detailed studies of CR propagation in turbulent plasmas have been reported [309, 311]. In these analyses the magnetic field is characterized by a Gaussian random field with zero mean and a power spectrum with $\langle B^2(k) \rangle \propto k^{n_B}$ for $k < k_0$ and $\langle B^2(k) \rangle = 0$ otherwise, where $k_0 = 2\pi/\ell$ represents the numerical cutoff scale and the r.m.s. strength is $B^2 = \int_0^\infty dk k^2 \langle B^2(k) \rangle$. The field is then calculated on a grid in real space via Fourier transform. Figure 16 shows an example of the distribution of arrival time and energies obtained via simulation of a bursting source located at $d = 10$ Mpc and assuming $n_B = -11/3$, i.e., a turbulent Kolmogorov type spectrum [309, 311]. Note that for $B = 0.3 \mu\text{G}$, $\ell = 1$ Mpc, $r = 10$ Mpc, and $E = 10^{19}$ eV, Eq. (94) leads to $\tau_D = 750$ Myr, in the midregion of the time-delay given in Fig. 16. For $E = 10^{20}$ eV (where proton energy losses are still small), $\tau_D = 350$ Myr, not inconsistent with the results of Fig. 16, although at the margin of the distribution of time-delays for this energy. This marginal agreement is indicative of the transition to Bohm diffusion, where the validity of Eq. (94) begins to flag.

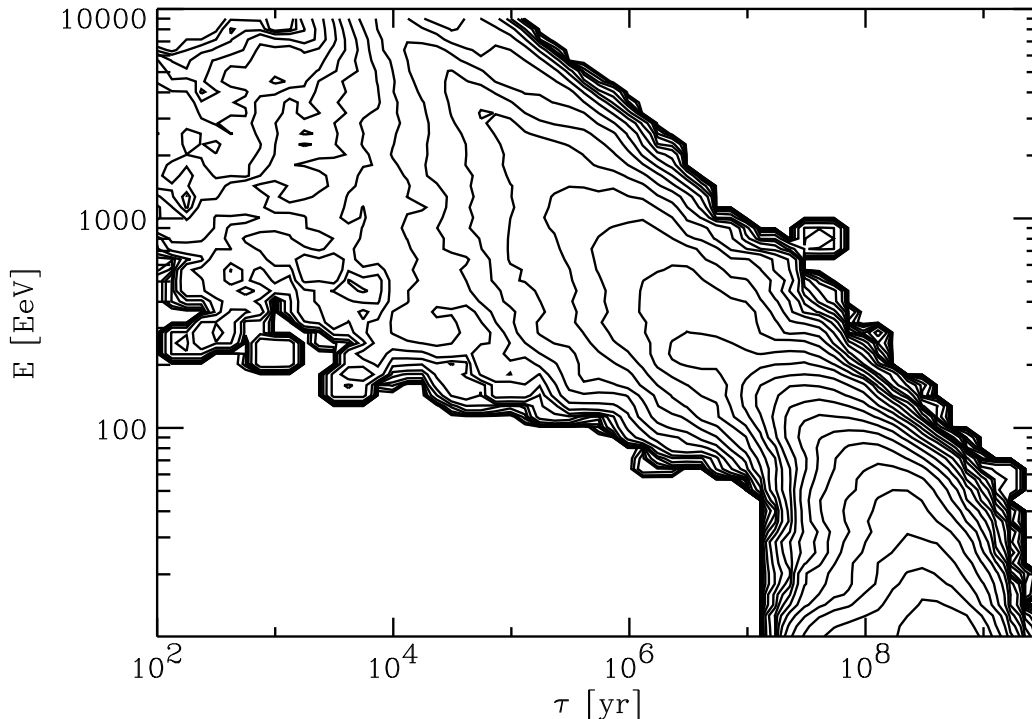


FIG. 16: The distribution of time delays $\tau(E)$ and energies E for a burst with spectral index $\gamma = 2.4$ at a distance $d = 10$ Mpc and r.m.s. strength $B = 3 \times 10^{-7}$ G. The inter-contour interval is 0.25 in the logarithm to base 10 of the distribution per logarithmic energy and time interval. Published in Ref. [309].

V. OUR COSMIC BACKYARD

In order to analyze the effect of energy losses on the observed spectrum, it is convenient to introduce the accumulation factor f_{acc} , defined as the ratio of energy-weighted fluxes for “low” ($10^{18.7}$ eV – $10^{19.5}$ eV) and high ($> 10^{20}$ eV) energy CRs above the ankle. For ordinary baryonic CRs, if the Earth is located in a typical environment and all CR-sources have smooth emission spectra, the observed spectrum above the ankle should have an offset in normalization between low and high energy given by f_{acc} . In the case where the cosmic rays are protons from a uniform distribution of sources active over cosmological times, the cutoff due to photopion processes relates the accumulation factor to a ratio of GZK distances [319] and leads to $f_{\text{acc}} \sim 100$. A similar value for f_{acc} is obtained for nuclei due to photodisintegration. The smoothness of the observed CR spectrum [20], i.e., $f_{\text{acc}} \sim 1$, suggests that the power of nearby sources must be comparable to that of all other sources (redshift $z > 0.5$) added together. Otherwise, one would have to invoke an apparently miraculous matching of spectra to account

for the smoothness of the CR energy spectrum. Of course, the GZK cutoff can be overcome if nearby sources are significantly more concentrated. However, this does not seem to be the case: if one simply assumes that the distribution of CR sources follows the distribution of galaxies, the local overdensity is only a factor of two above the mean, and thus insufficient to explain the measured flux above 10^{20} eV [320].²⁴ Several proposals with a smooth high energy spectrum due to nearby sources have been put forward. In this section we discuss these models.

A. Galactic sources

Galactic sources would satisfy the power condition trivially. However, the observed approximate isotropy would be difficult to reconcile with a galactic explanation, unless CRs diffuse in the magnetic field. Specks of dust could constitute diffuse galactic CRs, though the depth of shower maxima recorded so far are not consistent with the exact picture of showers initiated by dust grains [322, 323]. Heavy nuclei will also diffuse in the Galactic magnetic field [324]. Indeed, it was suggested by Blasi, Epstein, and Olinto [175] that iron ions from the surfaces of newly formed strongly magnetized pulsars may be accelerated to super-GZK energies through relativistic MHD winds. The iron ejected with energies $\sim 10^{20}$ eV will reach the Earth after some diffusion through the Galactic magnetic field. Note that the Larmor radius ($Z_{26} \equiv Z/26$)

$$r_L \sim 1.4 \frac{E_{20}}{Z_{26}} \left(\frac{B}{3 \mu\text{G}} \right)^{-1} \text{ kpc}, \quad (101)$$

is a few times the typical distance to a young neutron star, which is of order $d \sim 8$ kpc.

Pulsars begin their life with very fast rotation, $\omega \sim 3000 \text{ s}^{-1}$, and very large magnetic fields, $B_s \gtrsim 10^{13}$ G. Inside the light cylinder, i.e. $r \lesssim c/\omega$, a magnetosphere of density [325]

$$n_{\text{GJ}}(r) \sim \frac{B(r)\omega}{4\pi Zec} \quad (102)$$

corotates with a dipole magnetic field component that scales as $B(r) = B_s(r_{\text{ns}}/r)^3$. As the distance from the star increases, the dipole field structure cannot be maintained and beyond the light cylinder the field is mostly azimuthal. From the light cylinder a relativistic plasma with Alfvén speed close to the speed of light expands as a MHD wind.

²⁴ We note that an earlier analysis [321] overestimated the local overdensity by an order of magnitude.

This large discrepancy was caused by neglecting the necessary galaxy selection functions which account for the fact that nearby galaxies are easier to detect than far away galaxies [320].

The surface of a young neutron star is composed of elements near to the iron peak formed during the supernova event. Iron ions can be stripped off the hot surface of the neutron star by strong electric fields and can be present throughout much of the magnetosphere [326, 327]. The typical CR energy can be estimated by considering the magnetic energy per ion at the light cylinder [175]

$$E_{\text{CR}} = \frac{B_{\text{lc}}^2}{8\pi n_{\text{GJ}}}, \quad (103)$$

where $B_{\text{lc}} \sim 10^{10} B_{13} \omega_{3k}^3$ G is the magnetic field strength at the light cylinder, $n_{\text{GJ}} \sim 1.7 \times 10^{11} B_{13} \omega_{3k}^4 / Z \text{ cm}^{-3}$, $\omega_{3k} \equiv \omega / 3000 \text{ s}^{-1}$ and $B_{13} \equiv B_s / 10^{13} \text{ G}$. Replacing by fiducial values, Eq. (103) leads to [175]

$$E_{\text{CR}} = 4 \times 10^{20} Z_{26} B_{13} \omega_{3k}^2 \text{ eV}, \quad (104)$$

less than the maximum energy of particles that can be contained in the wind near the light cylinder [328, 329].

The injection spectrum is determined by the evolution of the rotational frequency. As the pulsar spin slows down because of electromagnetic and gravitational radiation [330, 331], the energy available for CR production decreases. For $B_s \gtrsim 10^{13} \text{ G}$, the rotation speed decreases mainly by magnetic dipole radiation [332],

$$\omega_{3k}^2(t) = \frac{\omega_{i3k}^2}{1 + t_8 B_{13}^2 \omega_{i3k}^2}, \quad (105)$$

where ω_{i3k} is the initial spin period and $t_8 = t / 10^8 \text{ s}$. With this in mind, the particle spectrum from each neutron star is given by [175]

$$N(E) = \epsilon \frac{5.5 \times 10^{31}}{B_{13} E_{20} Z_{26}} \text{ GeV}^{-1}, \quad (106)$$

where $\epsilon < 1$ is the efficiency for accelerating particles at the light cylinder.

Even though young neutron stars are surrounded by remnants of the presupernova star, the accelerated particles can easily escape the supernova remnant without significant degradation for a wide range of initial magnetic fields and spinning rates. Specifically, consider a supernova that imparts $E_{\text{SN}} \sim 10^{51} E_{51} \text{ erg}$ on the stellar envelope of mass $M_{\text{env}} \sim 10 M_1$ solar masses, where $E_{51} \equiv E / 10^{51} \text{ erg}$, and M_1 is the mass of the envelope in units of $10 M_\odot$. The column density of the envelope surrounding the neutron star is given by

$$\Sigma \sim \frac{M_{\text{env}}}{4\pi (r_0 + v_e t)^2} \quad (107)$$

where $v_e \sim \sqrt{2E_{\text{SN}}/M_{\text{env}}}$ is the envelope dispersion velocity, t is in seconds, and $r_0 \sim 10^{13} r_{13} \text{ cm}$. The condition for iron nuclei to traverse the supernova envelope without

significant losses is $\Sigma < 100 \text{ g cm}^{-2}$. At late times compared with $t_e = r_0/v_e$, this transparency condition gives $t > t_{\text{tr}} \sim 1.3 \times 10^7 M_1 E_{51}^{-1/2}$ s.

The evolution of the maximum energy is thus given by

$$E_{\text{CR}}(t) \sim 4 \times 10^{20} \frac{Z_{26} B_{13} \omega_{i3k}^2}{1 + t_8 B_{13}^2 \omega_{i3k}^2} \text{ eV}. \quad (108)$$

The maximum energy decreases as the source evolves, and so the condition to produce ultrahigh energy CRs is that E_{CR} exceeds the needed energy when the envelope becomes transparent [175]

$$E_{\text{CR}}(t_{\text{tr}}) > E_{20}, \quad (109)$$

or equivalently,

$$\omega_i > \frac{3000}{B_{13}^{1/2} [4Z_{26} E_{20}^{-1} - 0.13 M_1 B_{13} E_{51}^{-1/2}]^{1/2}} \text{ s}^{-1}. \quad (110)$$

Eq. (110) translates into upper bounds on the surface magnetic field strength and the star initial spin period $P_i = 2\pi/\omega_i$,

$$B_{13} < \frac{31 Z_{26} E_{51}^{1/2}}{M_1 E_{20}}, \quad (111)$$

and

$$P_i < 8\pi B_{13}^{1/2} Z_{26} E_{20}^{-1}. \quad (112)$$

For $M_1 = 2$ and $E_{20} = E_{51} = Z_{26} = 1$, Eq (111) gives $B_{13} < 15.4$, whereas Eq. (112) leads to $P_i \lesssim 10$ ms, not very restrictive values for a young neutron star. Moreover, for a reasonable pulsar production rate, the CR-flux on Earth is easily consistent with observation, i.e., $\epsilon \gtrsim 4 \times 10^{-7}$ [175].

B. Centaurus A

Centaurus A (Cen A) is the nearest active galaxy, at a distance of ~ 3.4 Mpc [333]. It is a complex FRI radio-loud source with galactic coordinates $l \approx 310^\circ$, $b \approx 20^\circ$, and identified at optical frequencies with the galaxy NGC 5128.²⁵ Different multi-wavelength studies have revealed a rather complex morphology: it comprises a compact

²⁵ Galactic longitude, l , is measured eastward along the galactic equator from 0° (in Sagittarius) to 360° . The galactic equator is defined by the central plane of the Milky Way. Galactic latitude, b , is the angular distance from the galactic equator ($b = 0^\circ$) toward either north ($b = 90^\circ$) or south ($b = -90^\circ$) galactic pole. Note that before August 1958 a different, now obsolete, system was used.

core, a jet also visible at X -ray frequencies, a weak counterjet, two inner lobes, a kpc-scale middle lobe, and two giant outer lobes. The jet would be responsible for the formation of the northern inner and middle lobes when interacting with the interstellar and intergalactic media, respectively. There appears to be a compact structure in the northern lobe, at the extrapolated end of the jet. This structure resembles the hot spots such as those existing at the extremities of FR II galaxies. However, at Cen A it lies at the side of the lobe rather than at the most distant northern edge, and the brightness contrast (hot spot to lobe) is not as extreme [334].

In order to ascertain the capability of Cen A to accelerate particles to ultrahigh energies, one first applies the Hillas criterion [138] (see Fig. 10). Low resolution polarization measurements in the region of the suspected hot spot give fields as high as $25 \mu\text{G}$ [334]. However, in certain regions where measurements at both high and low resolution are available, the B -field amplitude at high resolution can be seen to be twice that at low resolution. The higher resolution can reveal amplification in the post-shock region [335], yielding B -fields possibly as high as $50 - 60 \mu\text{G}$ [336, 337]. The radio-visible size of the hot spot can be directly measured from the large scale map [338], giving $R_{\text{HS}} \simeq 2 \text{ kpc}$. The actual size can be larger by a factor ~ 2 because of uncertainties in the angular projection of this region along the line of sight.²⁶ All in all, if the magnetic field of the hot spot is confined to the visible region, the limiting energy imposed by Eq. (34) is $\sim 2 \times 10^{20} \text{ eV}$. Estimates of the radio spectral index of synchrotron emission in the hot spot and the observed degree of linear polarization in the same region suggests that the ratio of turbulent to ambient magnetic energy density in the region of the shock is $u \sim 0.4$ [339]. The jet velocity is model dependent: possible values range from $\sim 500 \text{ km s}^{-1}$ to $0.99c$ [334]. For FRI galaxies, the ratio of photon to magnetic energy densities, a , is expected to be $\ll 1$. Figure 17 shows curves of constant ultrahigh energy in the $\beta_{\text{jet}} - a$ plane, for $B = 60 \mu\text{G}$, $R = 4 \text{ kpc}$, according to Eq. (44). Since the range of values for a , and the jet velocity in units of c conform to expected values, it is plausible that Cen A can accelerate particles to energies $\gtrsim 10^{20} \text{ eV}$.

Recent observations of the gamma ray flux for energies $> 100 \text{ MeV}$ by EGRET [340]²⁷ allow an estimate $L_{\gamma} \sim 10^{41} \text{ erg s}^{-1}$ for the source.²⁸ This value of L_{γ} is consistent with an earlier observation of photons in the TeV-range during a period of elevated

²⁶ For example, an explanation of the apparent absence of a counterjet in Cen A via relativistic beaming suggests that the angle of the visible jet axis with respect to the line of sight is at most 36° [334], which could lead to a doubling of the hot spot radius. It should be remarked that for a distance of 3.4 Mpc , the extent of the entire source has a reasonable size even with this small angle.

²⁷ The Energetic Gamma Ray Experiment Telescope (EGRET) was on board the CGRO mission.

²⁸ Note that the received radiation is negligibly affected by interactions with the various radiation backgrounds [194].

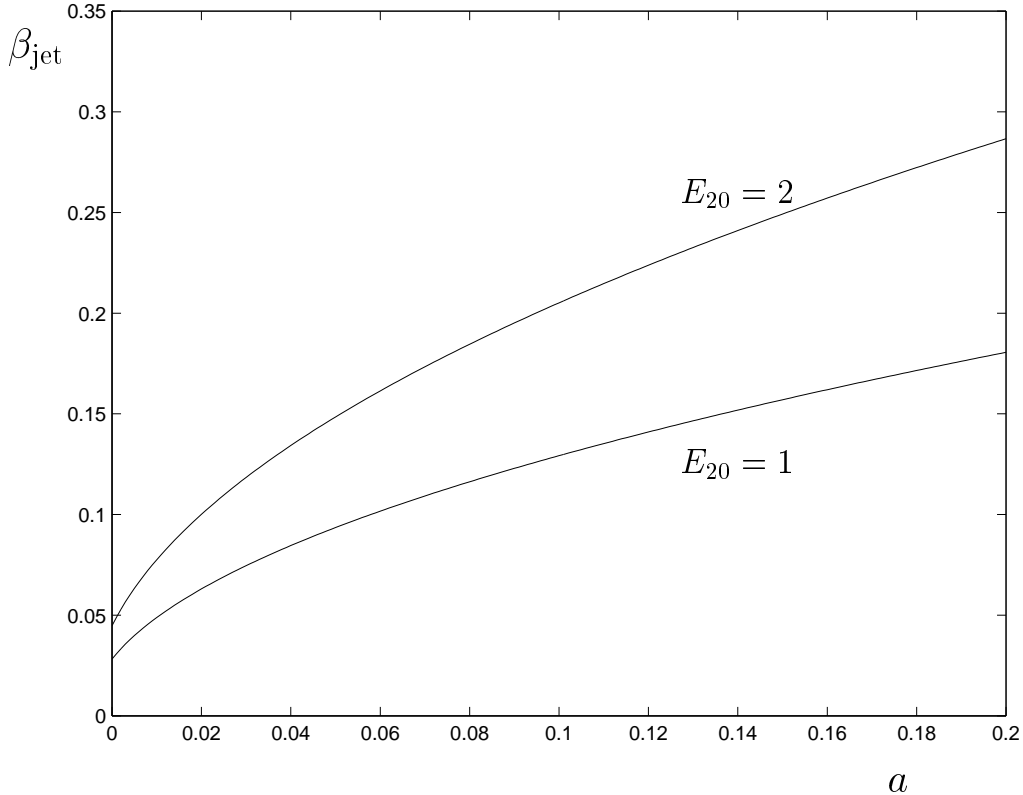


FIG. 17: Jet velocity as a function of the parameter a (defined in the text), for different proton energies. Published in Ref. [197].

activity [341], and is considerably smaller than the estimated bolometric luminosity $L_{\text{bol}} \sim 10^{43} \text{ erg s}^{-1}$ [333]. Data across the entire gamma ray bandwidth of Cen A is given in Ref. [342], reaching energies as high as 150 TeV [343], though data at this energy await confirmation. For values of B in the μG range, substantial proton synchrotron cooling is suppressed, allowing the production of high energy electrons through photomeson processes. The average energy of synchrotron photons scales as $\overline{E}_\gamma \simeq 0.29 E_\gamma$ [344]. With this in mind, it is straightforward to see that to account for TeV photons, Cen A should harbor a population of ultra-relativistic electrons with $E \sim 6 \times 10^{18} \text{ eV}$. We further note that this would require the presence of protons with energies between one and two orders of magnitude larger, since the electrons are produced as secondaries.²⁹

There are plausible physical arguments [176, 193] as well as some observational

²⁹ Consecutive factors of ~ 2 energy loss occur in the processes $p\gamma \rightarrow N\pi^0$, $\pi^0 \rightarrow \gamma\gamma$, $\gamma \rightarrow e^+e^-$. Eq.(39) then implies proton energies of $\sim 10^{20} \text{ eV}$ for 100 TeV photons.

reasons [345] to believe that when proton acceleration is being limited by energy losses, the CR luminosity $L_{\text{CR}} \approx L_\gamma$. Defining ϵ , the efficiency of ultra high energy CR production compared to high energy γ production – from the above, $\epsilon \simeq 1$ – and using equal power per decade over the interval $(E_{\text{min}}, E_{\text{max}})$, the source luminosity is found to be [319]

$$\frac{E^2 dN_0^{p+n}}{dE dt} \approx \frac{6.3 \epsilon L_{41} 10^{52} \text{eV/s}}{\ln(E_{\text{max}}/E_{\text{min}})}, \quad (113)$$

where $L_{41} \equiv$ luminosity of Cen A/ $10^{41} \text{erg s}^{-1}$ and the subscript “0” refers to quantities at the source.

It is straightforward to see, using Eqs. (94) and (98) that for $E = 10^{19}$ eV, $B = 0.5 \mu\text{G}$, $\ell = 0.5$ Mpc, the diffusive distance traveled $c\tau_D = 50$ Mpc $\gg d = 3.4$ Mpc is in very good agreement with the diffusion condition given in Eq. (100). For higher energies, the validity of the diffusive approach must be checked on a case-by case basis. For these purposes, in the case of a continuously emitting source, the definition of a diffusion time is somewhat arbitrary. In the following discussion we adopt as the diffusion time τ_D , a choice partially consistent with simulations (see Sec.IV-E). Moreover, one can easily check that for 3.4 Mpc the diffusion time of any proton with energy above the photopion production threshold is always less than the GZK-time, and consequently energy losses can be safely neglected. The density of protons at the present time t of energy E at a distance r from Cen A, which is assumed to be continuously emitting at a constant spectral rate $dN_0^{p+n}/dE dt$ from time t_{on} until the present, is [346]

$$\frac{dn(r, t)}{dE} = \frac{dN_0^{p+n}}{dE dt} \frac{1}{[4\pi D(E)]^{3/2}} \int_{t_{\text{on}}}^t dt' \frac{e^{-r^2/4D(t-t')}}{(t-t')^{3/2}} = \frac{dN_0^{p+n}}{dE dt} \frac{1}{4\pi D(E)r} I(x), \quad (114)$$

where $D(E)$ stands for the diffusion coefficient, $x = 4DT_{\text{on}}/r^2 \equiv T_{\text{on}}/\tau_D$, $T_{\text{on}} = t - t_{\text{on}}$, and

$$I(x) = \frac{1}{\sqrt{\pi}} \int_{1/x}^{\infty} \frac{du}{\sqrt{u}} e^{-u}. \quad (115)$$

For $T_{\text{on}} \rightarrow \infty$, the density approaches its time-independent equilibrium value n_{eq} , while for $T_{\text{on}} = \tau_D$, $n/n_{\text{eq}} = 0.16$.

To estimate the power of Cen A, one can evaluate the energy-weighted approximately isotropic proton flux at 1.5×10^{19} eV, which lies in the center of the flat “low” energy region of the spectrum,

$$E^3 J_p(E) = \frac{Ec}{(4\pi)^2 d D(E)} \frac{E^2 dN_0^{p+n}}{dE dt} I(t/\tau_D) \approx 7.6 \times 10^{24} \epsilon L_{41} I \text{ eV}^2 \text{ m}^{-2} \text{ s}^{-1} \text{ sr}^{-1}. \quad (116)$$

In Eq. (116) we have used the fiducial values of B and ℓ as given in the previous paragraph, and set $E_{\text{min}} = 1 \times 10^{19}$ eV, $E_{\text{max}} = 4 \times 10^{20}$ eV, assuming (as discussed

in Sec.III-B.2) that the shock structure can be more extended than the visible region in the non-thermal radioemission. As noted by Farrar and Piran [319], one can see, by stretching at most the source parameters, that the “low” energy flux from Cen A could be comparable to that of all other sources in the Universe. To this end, first fix $\epsilon L_{41} I = 0.40$, after comparing Eq. (116) to the observed CR-flux: $E^3 J_{\text{obs}}(E) = 10^{24.5} \text{ eV}^2 \text{ m}^{-2} \text{ s}^{-1} \text{ sr}^{-1}$ [20]. Next, $\epsilon L_{41} \simeq 1$, determines $I \simeq 0.40$, and consequently the required age of the source T_{on} to be about 400 Myr. There is still a great uncertainty on jet evolutionary behavior. Experimental approaches and theoretical studies suggest ages that run from a few tens of Myr, up to half the Hubble time in some extreme cases [186]. Moreover, $T_{\text{on}} \sim 400 \text{ Myr}$ is consistent with FRI lobe ages [345]. To maintain flux at the “ankle” for the same T_{on} , one requires an approximate doubling of L_{CR} at $5 \times 10^{18} \text{ eV}$. Because of the larger diffusive time delay at this energy, this translates into an increased luminosity in the early phase of Cen A. From Eq. (39), the associated synchrotron photons are emitted at energies $< 30 \text{ MeV}$. The increase in radiation luminosity in this region is not inconsistent with the flattening of the spectrum observed at lower energies[347, 348].

Let us turn now to the discussion of anisotropy. This can be found by computing the incoming current flux density $D\nabla n$ as viewed by an observer on Earth, and one finds for a continuously-emitting source a distribution $\sim (1 + \alpha \cos \theta)$ about the direction of the source, where θ is the angle to the zenith and

$$\alpha = \frac{2D(E)}{cr} \cdot \frac{I'}{I}. \quad (117)$$

Here,

$$I'(x) = \frac{1}{\sqrt{\pi}} \int_{1/x}^{\infty} du \sqrt{u} e^{-u}, \quad (118)$$

with $x = T_{\text{on}}/\tau_D$, and I as defined in Eq. (115) [346]. For our choices of B and ℓ , and $T_{\text{on}} = 400 \text{ Myr}$, we find for $E = 10^{19} \text{ eV}$ ($E = 10^{20} \text{ eV}$) that $\alpha = 0.04$ ($\alpha = 0.07$).

Neutrons at the highest energies could survive decay and produce a spike in the direction of the source (see Appendix E). However, those that are able to decay will beget secondary proton diffusion fronts with asymmetry parameters given by

$$\alpha = \frac{2D(E)}{cr} \cdot \frac{I''}{I}, \quad (119)$$

where

$$I''(x) = \frac{1}{4\sqrt{\pi\kappa}} \int_{1/x}^{\infty} \frac{du}{u^{3/2}} \left[\left((1 - \kappa)u + \frac{1}{2} \right) e^{-(1-\kappa)^2 u} - \left((1 + \kappa)u + \frac{1}{2} \right) e^{-(1+\kappa)^2 u} \right] \quad (120)$$

and $\kappa = \lambda(E)/r$, where $\lambda(E) = 0.9 E_{20} \text{ Mpc}$ is the neutron decay length. In spite of the complicated nature of Eq.(120), the results for α are very similar to the ones for the primary diffusion front given above.

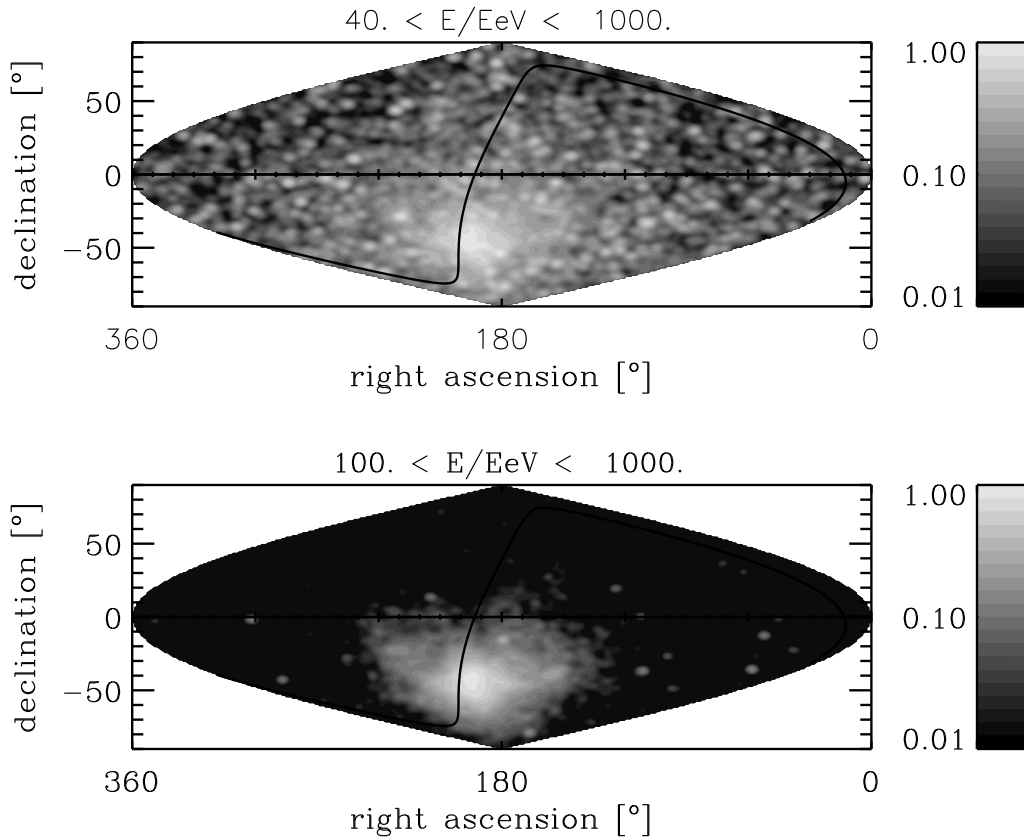


FIG. 18: The angular image in equatorial coordinates, averaged over all 20 magnetic field realizations of 5000 trajectories each, for events above 40 EeV (upper panel) and above 100 EeV (lower panel), as seen by a detector covering the whole sky, for the case suggested in Ref. [319] corresponding to $B = 0.3 \mu\text{G}$, and the source Cen A. The grey scale represents the integral flux per solid angle. The solid line marks the Super-Galactic plane. The pixel size is 1° ; the image has been convolved to an angular resolution of 2.4° corresponding to AGASA. Published in Ref. [349].

Detailed Monte Carlo simulations [349, 350], however, reveal that the predicted distributions of arrival directions are more anisotropic than current data even at 10^{19} eV (see Fig. 18.). In particular, for a spectral index $\gamma = 2.4$ and a maximum injection energy of 10^{21} eV, the angular power spectrum shows a 3σ quadrupole deviation from observation, and the auto-correlation function is not consistent with the clustering at small scale observed by AGASA [350]. The discrepancy between phenomenology and Monte Carlo simulations could arise from a number of factors. The simulations are considerably more detailed than the phenomenological arguments; for instance effects of photopion production are taken into account. Furthermore, they simulate

the subtleties in transitions from Kolmogorov to Bohm diffusion. On the other hand, the Monte Carlo simulations rely on a statistical description of the magnetic field, in which the field is arranged into domains or “cells” with a characteristic coherence length. There is some uncertainty in the sensitivity to the geometry of the cell, which is reflected in the presence or absence of resonant modes in the spectrum. For instance, if one considers coherence domains generated in some Gaussian manner (say with spatial spread R) rather than as small cubes, then $k_0 = 1/R$ instead of $k_0 = 2\pi/\ell$, and for $R \sim 0.7$ Mpc, the diffusive resonant condition is satisfied even for the highest observed energies. Whichever point of view one may find more convincing, it seems most conservative at this point to depend on experiment (if possible) to resolve the issue. In particular, PAO will be in a unique position to search the sky in the direction of Cen A.

C. M87

At a distance of ~ 20 Mpc, M87 is the dominant radio galaxy in the Virgo cluster ($l = 282^\circ$, $b = 74^\circ$) [351]. This powerful FRI has been under suspicion to be the primary source of ultrahigh energy cosmic rays for a long time [307, 352]. The emission of synchrotron radiation with a steep cutoff at frequencies about 3×10^{14} Hz from its radiojets and hot spots [353, 354] implies an initial turbulence injection scale having the Larmor radius of protons at 10^{21} eV (see Sec.III-B.2). Hence, because of its relative proximity to Earth, M87 becomes a potential candidate to account for the observed events above 10^{20} eV. The major difficulty with this idea is the observation of the nearly isotropic distribution of the CR arrival directions. One can again argue that the orbits are bent. However, the bending cannot add substantially to the travel time, otherwise the energy would be GZK-degraded. An interesting explanation to overcome this difficulty relies on a Galactic wind, akin the solar wind, that would bend all the orbits of the highest energy CRs towards M87 [355, 356]. Indeed, it has long been expected that such a kind of wind is active in our Galaxy [357, 358, 359]. In the analysis of [355], it was assumed that the magnetic field in the Galactic wind has a dominant azimuthal component, with the same sign everywhere. This is because in a spherical wind the polar component of the magnetic field becomes negligible rather quickly, decaying like $1/r^2$, and thus the azimuthal part of the magnetic field quickly becomes dominant, with $B_\phi \sim \sin\theta/r$ in polar coordinates [360]. Under these considerations one is left with two degrees of freedom: the strength of the azimuthal component at the location of the Sun, and the distance to which this wind extends. Recent estimates suggest that the magnetic field strength near the Sun is $\sim 7 \mu\text{G}$ [361]. The second parameter is more uncertain. Our Galaxy dominates its near environment well past our neighbor, M31, the Andromeda galaxy, and might well extend its sphere of influence to half way

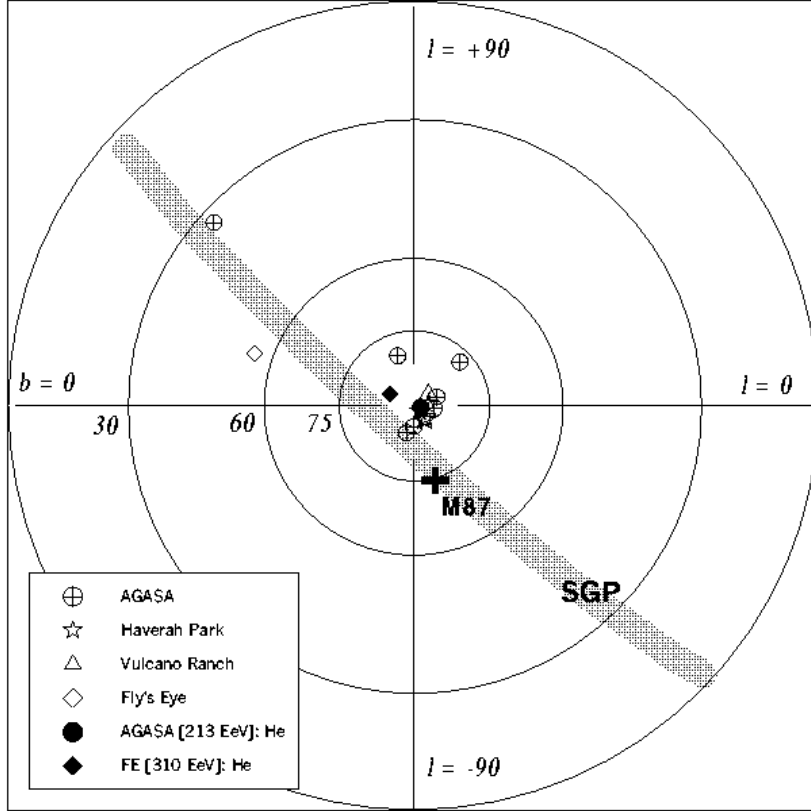


FIG. 19: Directions in polar projection of the highest energy CR events when they enter the halo of our Galaxy. The two highest energy events have two entries, under the assumptions that they are either protons or helium nuclei (filled black symbols). The cross indicates the position of M87 and the grey band stands for the super-Galactic plane. Published in Ref. [355].

to M81. This implies an outer halo wind of ~ 1.5 Mpc. With this in mind, the mean flight time of the protons in the Galaxy is $\sim 5.05 \times 10^6$ yr $\ll \tau_s$, the time for straight line propagation from M87 [362]. Figure 19 shows the directions where the 13 highest energy CR events point towards when they leave the halo wind of our Galaxy. Note that except for the two highest energy events, all other events can be traced back to within less than about 20 degrees from Virgo. If one takes into account the uncertainty of the magnetic field distribution, all events are consistent with arising originally from Virgo. Moreover, if one assumes that the two highest event are helium nuclei, all 13 events point within 20° of Virgo. Note that a bending of 20° could be easily accommodated with a fine tuning of the magnetic field strength within the super-Galactic sheet from here to Virgo (more on this below). Criticisms of this model [363] have been addressed in [364].

We now focus attention on the power of M87. To this end, we analyze another

interesting limit of Eq. (92) in which diffusion is found to be extremely small. In such a case, the second term in the r.h.s. can be neglected, and the solution for a single point source reads [228]

$$n(E, t) = \frac{1}{b(E)} \int_E^\infty Q(E_0, t') dE_0, \quad (121)$$

where

$$t' = t - \int_E^{E_0} \frac{d\tilde{E}}{b(\tilde{E})}, \quad (122)$$

and E_0 is the energy of the nucleon when emitted by the source. Using Eq. (32) we model the injection spectrum of a single source located at t_0 from the observer by

$$Q(E, t) = \kappa E^{-\gamma} \delta(t - t_0), \quad (123)$$

where κ is a normalization constant and for simplicity we consider the distance as measured from the source, i.e., $t_0 = 0$. At very high energies, the total number of particles at a given distance from the source is

$$n(E, t) \approx \frac{\kappa}{b(E)} \int_E^\infty E_0^{-\gamma} \delta\left(t - \frac{1}{C} \ln \frac{E_0}{E}\right) dE_0, \quad (124)$$

or equivalently,

$$n(E, t) \approx \kappa E^{-\gamma} e^{-(\gamma-1)Ct}, \quad (125)$$

where C is given in Eq. (56). Thus, the injection spectrum is uniformly damped by a factor that depends on the proximity of the source.

At low energies, in the region dominated by baryon resonances, the parameterization of $b(E)$ does not allow a complete analytical solution. However using the change of variables,

$$\tilde{t} = \int_E^{E_0} \frac{d\tilde{E}}{b(\tilde{E})}, \quad (126)$$

with $E_0 = \xi(E, \tilde{t})$ and $d\tilde{t} = dE_0/b(E_0)$, one easily obtains,

$$n(E, t) = \frac{\kappa}{b(E)} \int_0^\infty \xi(E, \tilde{t})^{-\gamma} \delta(\tilde{t} - t) b[\xi(E, \tilde{t})] d\tilde{t}, \quad (127)$$

and then, the compact form,

$$n(E, t) = \frac{\kappa}{b(E)} E_0^{-\gamma} b(E_0), \quad (128)$$

where the relation between E_0 and E is given in Eq. (57). Now, to take into account the extension of the cluster, we assume that the concentration of potential sources at the

center is higher than that in the periphery, and adopt a spatial gaussian distribution. With this hypothesis, the particle injection rate into the intergalactic medium is given by

$$Q(E, t) = \kappa \int_{-\infty}^{\infty} \frac{E^{-\gamma}}{\sqrt{2\pi}\sigma} \delta(t - T) \exp\left\{-\frac{(T - t_0)^2}{2\sigma^2}\right\} dT \quad (129)$$

A delta function expansion around t_0 , with derivatives denoted by lower case Roman superscripts,

$$\delta(t - T) = \delta(t - t_0) + \delta^{(i)}(t - t_0)(T - t_0) + \frac{1}{2!}\delta^{(ii)}(t - t_0)(T - t_0)^2 + \dots \quad (130)$$

leads to a convenient form for the injection spectrum, which is given by,

$$Q(E, t') = \kappa E^{-\gamma} [\delta(t' - t_0) + \frac{\sigma^2}{2!} \delta^{(ii)}(t' - t_0) + \frac{\sigma^4}{4!} \delta^{(iv)}(t' - t_0) + \dots]. \quad (131)$$

By replacing the above expression into Eq. (121) one obtains [234]

$$n = \kappa \frac{E_0^{-\gamma} b(E_0)}{b(E)} \left\{ 1 + \frac{\sigma^2 A^2 e^{-2B/E_0}}{2!} F_1(E_0) + \frac{\sigma^4 A^4 e^{-4B/E_0}}{4!} F_2(E_0) + \mathcal{O}(6) \right\}, \quad (132)$$

where

$$F_1(E_0) = 2B^2 E_0^{-2} + (2 - 3\gamma) B E_0^{-1} + (1 - \gamma)^2, \quad (133)$$

$$F_2(E_0) = 24B^4 E_0^{-4} + (4 - 50\gamma) B^3 E_0^{-3} + (35\gamma^2 - 25\gamma + 8) B^2 E_0^{-2} \\ + (-10\gamma^3 + 20\gamma^2 - 15\gamma + 4) B E_0^{-1} + (1 - \gamma)^4, \quad (134)$$

and A and B as given in Eq. (55). Figure 20 shows the evolved energy spectrum of nucleons assuming a cosmologically homogeneous population of sources (universal hypothesis) [230] together with the modified spectrum as given by Eq. (132) for an extended source modeled by a Gaussian distribution of width 2 Mpc at a distance of 18.3 Mpc. The extended source spectrum was normalized in the “low” energy region with the spectral index, $\gamma = 3.27$, obtained from a maximum likelihood fit to the Fly’s Eye data [365]. From Fig. 20 one can see that the proton component of the Virgo cluster partially reproduces AGASA data, but apparently cannot account for the super-GZK Fly’s Eye event. However, lensing effects may come to the rescue [366]. The magnetic field in the Galactic wind strongly magnifies the flux, reducing the power requirements of the source. Specifically, with fine-tuning of the source direction relative to the symmetry axis of the wind, M87 could be as high as $> 10^2$ times more powerful than if unlensed at energies below $E/Z \sim 1.3 \times 10^{20}$ eV [366]. Moreover, as noted in [367], the super-Galactic plane sheet can focus ultrahigh energy CRs along the sheet. Hence, the particles would arrive at the boundary of our Galactic wind with the arrival directions described by an elongated ellipse along the super-Galactic plane sheet. This in turn would allow magnetic lensing to produce many hot spots, just as sunlight dapples the bottom of a swimming pool, and so easily explain the apparent CR-clustering.

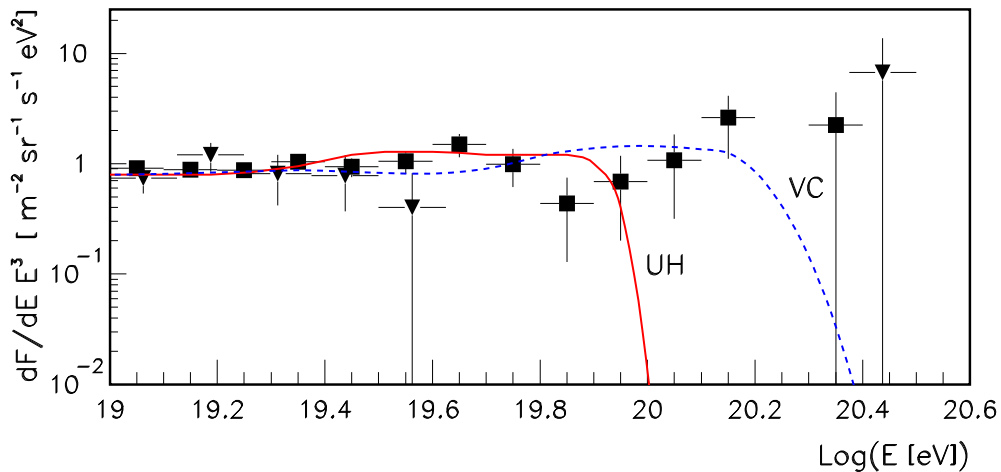


FIG. 20: The CR flux as observed by AGASA (square) and Fly’s Eye (triangle) experiments. The solid line indicates the CR spectrum assuming the universal hypothesis (UH), i.e., homogeneous source distribution, whereas the dotted line indicates the evolved spectrum from the Virgo cluster (VC). Published in Ref. [264].

D. Starbursts

If the super-GZK particles are heavy nuclei from outside our Galaxy, then the nearby (~ 3 Mpc [368]) starburst galaxies M82 ($l = 141^\circ, b = 41^\circ$) and NGC 253 ($l = 89^\circ, b = -88^\circ$) would probably be the sources of most ultrahigh energy CRs observed on Earth. Starbursts are galaxies undergoing a massive and large-scale star formation episode. Their characteristic signatures are strong infrared emission (originating in the high levels of interstellar extinction), a very strong HII-region-type emission-line spectrum (due to a large number of O and B-type stars), and considerable radio emission produced by recent supernova remnants (SNRs). Typically, the starburst region is confined to the central few hundreds of parsecs of the galaxy, a region that can be easily 10 or more times brighter than the center of normal spiral galaxies. In the light of such a concentrated activity, the existence of galactic superwinds is not surprising [368].

Galactic-scale superwinds are driven by the collective effect of supernovae and massive star winds. The high supernovae rate creates a cavity of hot gas ($\sim 10^8$ K) whose cooling time is much greater than the expansion time scale. Since the wind is sufficiently powerful, it can blow out the interstellar medium of the galaxy preventing it from remaining trapped as a hot bubble. As the cavity expands a strong shock front is formed on the contact surface with the cool interstellar medium. The shock

velocity can reach several thousands of kilometers per second and ions like iron nuclei can be efficiently accelerated in this scenario, up to ultrahigh energies, by Fermi's mechanism [173].

In a first stage, ions are diffusively accelerated at single supernova shock waves within the nuclear region of the galaxy. Energies up to $\sim 10^{15}$ eV can be achieved in this step [147]. Heavy nuclei are not photodissociated in the process despite the large photon energy densities (mostly in the far infrared) measured in the central region of the starburst. The escape of the CR outflow is convection dominated. In fact, the presence of several tens of young SNRs with very high expansion velocities and thousands of massive O stars, with stellar winds of terminal velocities up to 3000 km s^{-1} , must generate collective plasma motions of several thousands of km per second. Then, due to the coupling of the magnetic field to the hot plasma, the magnetic field is also lifted outwards and forces the CR gas to stream along from the starburst region. Most of the nuclei escape in opposite directions along the symmetry axis of the system, as the total path traveled is substantially shorter than the mean free path [173].

Once the nuclei escape from the central region of the galaxy, with energies of $\sim 10^{15}$ eV, they are injected into the galactic-scale wind and experience further acceleration at its terminal shock up to 10^{20} eV. For this second step in the acceleration process, the photon field energy density drops to values of the order of the microwave background radiation, as we are now far from the starburst region, and consequently, iron nuclei are safe from photodissociation. In terms of parameters that can be determined from observations, the nucleus maximum energy is given by [173]

$$E_{\text{max}} \approx \frac{1}{2} Ze B \frac{\dot{E}_{\text{sw}}}{\dot{M}} T_{\text{on}} , \quad (135)$$

where $\dot{E}_{\text{sw}} \sim 2.7 \times 10^{42} \text{ erg s}^{-1}$ is the superwind kinetic energy flux and $\dot{M} = 1.2 M_{\odot} \text{ yr}^{-1}$ is the mass flux generated by the starburst [368]. The age T_{on} can be estimated from numerical models that use theoretical evolutionary tracks for individual stars and make sums over the entire stellar population at each time in order to produce the galaxy luminosity as a function of time [369]. Fitting the observational data, these models provide a range of suitable ages for the starburst phase that goes from 50 Myr to 160 Myr [369]. These models must assume a given initial mass function (IMF), which usually is taken to be a power-law with a variety of slopes. Recent studies have shown that the same IMF can account for the properties of both NGC 253 and M82 [370]. Besides, a region referred to as M82 "B" near the galactic center of M82, has been under suspicion as a fossil starburst site in which an intense episode of star formation occurred over 100 Myr ago [371, 372]. The derived age distribution suggests steady, continuing cluster formation at a modest rate at early times (> 2 Gyr ago), followed by a concentrated formation episode 600 Myr ago and more recent suppression of cluster

formation. In order to get some estimates on the maximum energy, let us assume $B \sim 50 \mu\text{G}$, a choice consistent with observation [373]. Inserting all of these figures in Eq. (135), already for $T_{\text{on}} = 50 \text{ Myr}$ one obtains for iron nuclei

$$E_{\text{max}}^{\text{Fe}} > 10^{20} \text{ eV}. \quad (136)$$

Now, we can use the rates at which starbursts inject mass, metals and energy into superwinds to get an estimate on the CR-injection spectra. We once again use ϵ to denote the efficiency of ultrahigh energy CR production by the superwind kinetic energy flux. Using equal power per decade over the interval $10^{18.5} \text{ eV} < E < 10^{20.6} \text{ eV}$, we obtain a source CR-luminosity

$$\frac{E^2 dN_0}{dE dt} \approx 3.5 \epsilon 10^{53} \text{ eV/s}. \quad (137)$$

The assumption that the giant air showers with $E > 10^{20} \text{ eV}$ were triggered by heavy nuclei implies ordered extragalactic magnetic fields $B_{\text{nG}} < 15$ (at least in the outskirts of the Galaxy), or else nuclei would be captured in magnetic subdomains suffering catastrophic spallations. Moreover, even for fields $\mathcal{O}(\text{nG})$, CR nuclei with energies $E_c < 10^{18} \ell_{\text{Mpc}} Z B_{\text{nG}} \text{ eV}$ remain trapped inside cells of size ℓ_{Mpc} , attaining efficient diffusion, with

$$D(E) \approx 0.048 \left(\frac{E_{18} \ell_{\text{Mpc}}^2}{Z B_{\text{nG}}} \right)^{1/3} \text{ Mpc}^2/\text{Myr}. \quad (138)$$

The power of the starbursts can then be estimated by straightforward generalization of the procedure discussed in Sec.V-B. Specifically, first evaluate the energy-weighted approximately isotropic nucleus flux at 10^{19} eV ,

$$E^3 J(E) = \frac{E c}{(4\pi)^2 d D(E)} \frac{E^2 dN_0}{dE dt} I_{\star} \approx 2.3 \times 10^{26} \epsilon I_{\star} \text{ eV}^2 \text{ m}^{-2} \text{ s}^{-1} \text{ sr}^{-1}, \quad (139)$$

where $I_{\star} = I_{\text{M82}} + I_{\text{NGC 253}}$, $B_{\text{nG}} = 15$, $\ell_{\text{Mpc}} = 0.5$, and $\langle Z \rangle = 20$. Then, fix

$$\epsilon I_{\star} = 0.013, \quad (140)$$

after comparing Eq.(139) to the observed CR-flux. Note that the contribution of I_{M82} and $I_{\text{NGC 253}}$ to I_{\star} critically depends on the age of the starburst. Figure 21 shows the relation “starburst-age/superwind-efficiency” derived from Eq. (140), assuming that both M82 and NGC 253 were active for 115 Myr ($\epsilon \approx 10\%$). Beyond this epoch, CR-emission must be associated with M82 “B”.

Above $> 10^{20.2} \text{ eV}$ iron nuclei do not propagate diffusively. Moreover, the CR-energies get attenuated by photodisintegration on the microwave background radiation and the intergalactic infrared background photons. In the non-diffusive regime, the

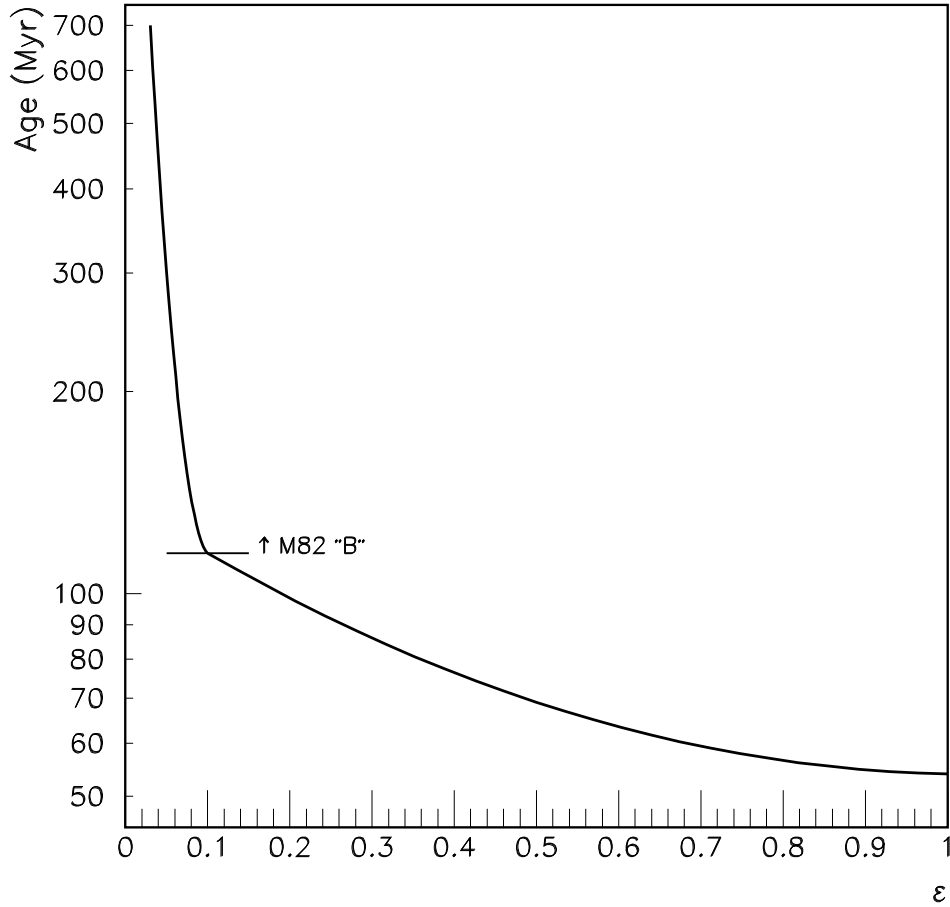


FIG. 21: Age of the starbursts as a function of the efficiency of CR-production, ϵ . Published in [174].

accumulated deflection angle $\theta(E)$ from the direction of the source can be estimated using Eq. (90). Therefore, if $B \sim 15$ nG all directionality is lost. The resulting time delay with respect to linear propagation is given by Eq. (91), and the total travel time is

$$t \approx \frac{d}{c} \left(1 + \frac{1}{4}\theta^2 \right) . \quad (141)$$

As an interesting exercise one can apply these considerations to the highest energy Fly's Eye event. Including statistical and systematic uncertainties, the energy of this event is $3.2 \pm 0.9 \times 10^{20}$ eV. Eqs. (63) and (66) relate the uncertainty in energy to the

uncertainty in the attenuation time

$$\frac{\delta t}{t} \simeq \left(\frac{11.3}{E_{20}} \right) \left(\frac{\delta E}{E} \right) . \quad (142)$$

From these considerations, we find that the upper limit on the transit time for a nuclear candidate for the highest energy Fly’s Eye event is $\sim 6 \times 10^{14}$ s. The arrival direction of the highest energy Fly’s Eye event is 37° from M82 [172]. With $d \simeq 3$ Mpc and $\theta = 37^\circ$, one finds from Eq. (141) a transit time $t \simeq 3.4 \times 10^{14}$ s, well within the stated upper limit.

For average deflections of 60° , the time of flight is $\sim 3.9 \times 10^{14}$ s, and consequently the CR-spectrum falls off sharply in the neighborhood of the GZK limit. A slight anisotropy should arise just before this cutoff. As the candidate sources in the northern and southern hemispheres are presumably at different distances,³⁰ a north-south asymmetry should also eventually emerge. It is rather difficult to assess whether events with energies $> 10^{20.5}$ eV are plausible, because the maximum energy depends strongly on τ_{delay} .

The photodisintegration process results in the production of nucleons of ultrahigh energies with the same Lorentz factor as the parent nucleus. As a consequence, the total number of particles is not conserved during propagation. However, to a very good approximation one can treat separately the evolution of the heaviest fragment and those fragments corresponding to nucleons emitted from the traveling nuclei. With this in mind, the evolution of the differential spectrum of the surviving fragments is given by Eq. (92). Now, generalizing the formalism discussed in the previous section for the case of a single source located at t_0 from the observer, one obtains a slightly modified expression for the evolution of the spectrum [259]

$$n(E, t) \sim \frac{\kappa E_0^{-\gamma+1}}{E} , \quad (143)$$

where the relation between E_0 and E is given in Eq. (66). Putting all this together, the energy-weighted flux beyond the GZK-energy due to a single M82 flare

$$E^3 J(E) = \frac{E}{(4\pi d)^2} \frac{E_0^2}{dE_0} \frac{dN_0}{dt} e^{-Rt/56} \approx 2.7 \times 10^{25} E_{20} \epsilon e^{-Rt/56} \text{ eV}^2 \text{ m}^{-2} \text{ s}^{-1} \text{ sr}^{-1} , \quad (144)$$

is easily consistent with observation [20]. It is important to stress that these phenomenological arguments are in agreement with Monte Carlo simulations [375]. In 5 years of operation PAO will provide enough statistics to test the starburst anisotropy predictions [299].

³⁰ The location of NGC 253 is still subject to large uncertainties [374].

VI. GZK-EVADING MESSENGERS

Several attempts have been made to explain the high end of the spectrum as a manifestation of some kind of physics beyond the SM. These suggestions became really interesting after Farrar and Biermann [376] reported an intriguing correlation between the arrival directions of 5 extremely high energy CRs and compact radio quasars at high redshifts ($z = 0.2 - 0.3$). However, with the present data, such “evidence” for directional correlation is still a subject of debate [377, 378, 379, 380]. The most economical proposal to sneak away the GZK-cutoff involves a familiar extension of the SM, namely, neutrino masses. As noted by Weiler [381, 382], neutrinos can travel over cosmological distances with negligible energy loss and could, in principle, produce Z bosons on resonance through annihilation on the relic neutrino background within a GZK distance of Earth. If this were the case, the highly boosted decay products of the Z could be observed as super-GZK primaries, since they do not have to travel cosmological distances to reach us, and would be pointing directly back to the source. This proposal requires very luminous sources of extremely high energy neutrinos throughout the Universe. Another possibility in which the ultrahigh energy CR should point directly to its source assumes that the CR is a new, neutral, stable or very long lived supersymmetric hadron of mass a few GeV [383]. From all the candidates *en vogue*, the light glueballino seems the most plausible, because it can be efficiently produced in pp collisions, it is not strongly absorbed by the CMB, and produces extensive air showers with longitudinal development very similar to those observed [384]. An even more radical proposal postulates a tiny violation of Lorentz invariance, such that some processes become kinematically forbidden [385, 386, 387, 388, 389]. In particular, photon-photon pair production and photopion production may be affected by Lorentz invariance violation. Hence, the absence of the GZK-cutoff would result from the fact that the threshold for photopion production “disappears” and the process becomes kinematically not allowed.

For models that rely on GZK-evading messengers, the accumulation factor f_{acc} depends on the details of the model. In the case of messengers which can induce showers across the entire energy spectrum, one expects enhancement on the low energy side only from the baryonic component, and f_{acc} depends on the interaction length in the CMB and on the energy spectra at the different sources. For messengers whose attenuation length is comparable to the horizon, and which do not shower at the lower energies, $f_{\text{acc}} \ll 1$. In what follows, we give a somewhat more detailed account of these general considerations.

A. Super-GZK CRs from the edge of the Universe

The neutrino is the only known stable particle that can propagate through the CMB essentially uninhibited even at the highest CR energies. Specifically, the corresponding $\nu\bar{\nu}$ annihilation mean free path on the cosmic neutrino background,

$$\lambda_\nu = (n_\nu \sigma_{\nu\bar{\nu}})^{-1} \approx 4 \times 10^{28} \text{ cm} , \quad (145)$$

is just above the present size of the horizon (recall that $H_0^{-1} \sim 10^{28} \text{ cm}$) [390]. One may then entertain the notion that neutrinos are indeed the super-GZK primaries. However, in the SM model a neutrino incident vertically on the atmosphere would pass through it uninhibited, never initiating an extensive air shower. Consequently one has to postulate new interactions so that these neutrinos acquire a strong cross section above 10^{20} eV .

The idea that neutrinos are the super-GZK primaries was introduced by Beresinsky and Zatsepin in 1969 [249]. Since then, explicit models have been devised in which the neutrino-nucleon cross section is enhanced by some new physics beyond the electroweak scale. One interesting proposal is that leptons are bound states of dual QCD gluons, and therefore can interact “strongly” with all partons in the nucleon attaining an effective cross section comparable to the geometric nucleon cross section [391, 392, 393, 394]. More recently, low scale gravity models have provided new impetus to the hypothesis of strongly interacting neutrinos. In particular, the neutrino nucleon cross section can be made large enough due to a quick rise of the density of states, possibly increasing exponentially, $\rho \sim e^{\sqrt{s/s_0}}$, above a characteristic energy scale s_0 [395]. A specific implementation of this idea is given in theories with n additional large compact dimensions and TeV scale quantum gravity [396]. A detailed discussion of this last proposal is left until Sec.VII-A. For now, we will focus on the Z -burst model, in which everyday weekly interacting neutrinos explain the super-GZK primaries.

B. Z -burst

To ascertain whether the Z -burst hypothesis is viable, we would like to know what neutrino energy and flux would actually be required to generate observed highest energy CRs. This in turn depends on the neutrino mass, the distribution of thermal neutrinos and the kinematics of the Z decay products. These three points are discussed in the following paragraphs. At the end of the section, we comment on the compatibility of the Z -burst hypothesis with current EAS data and plausible astrophysical sources.

In recent years, stronger and stronger experimental evidence for neutrino oscillations has been accumulating. Certainly, this evidence – which is compelling for atmospheric neutrinos [397, 398, 399, 400, 401], strong for solar neutrinos [402, 403, 404, 405, 406,

407], and so far unconfirmed for neutrinos produced in the laboratory and studied by various groups [408, 409, 410, 411, 412, 413, 414, 415, 416] – would extend the SM by requiring non-vanishing neutrino masses and mixing. A precise estimate of the ν -masses and mixing parameters would be an important clue to any physics beyond the SM. However, neutrino oscillations are sensitive to the mass (squared) splittings $\Delta m_{ij}^2 = m_{\nu_i}^2 - m_{\nu_j}^2$, and so only a lower bound on the mass of the heaviest neutrino can be obtained.³¹ Strictly speaking, using the atmospheric mass splitting in a 3 neutrino flavor scenario one obtains

$$m_{\nu_3} \geq \sqrt{\Delta m_{\text{atm}}^2} \gtrsim 0.04 \text{ eV}, \quad (146)$$

whereas by using the LSND mass splitting in a 4 flavor scenario the limit is shifted an order of magnitude, i.e.,

$$m_{\nu_4} \geq \sqrt{\Delta m_{\text{LSND}}^2} \gtrsim 0.4 \text{ eV}. \quad (147)$$

For recent surveys see [417, 418, 419]. The search for mass imprints in the endpoint spectrum of tritium β decay combined with experimental constraints from oscillations yield upper bounds on the mass of the heaviest neutrino,

$$m_{\nu_3} \leq \sqrt{m_\beta^2 + \Delta m_{\text{atm}}^2} \lesssim 2.5 \text{ eV}, \quad (148)$$

in a 3 flavor, and

$$m_{\nu_4} \leq \sqrt{m_\beta^2 + \Delta m_{\text{LSND}}^2} \lesssim 3.8 \text{ eV}, \quad (149)$$

in a 4 flavor scenario [420]. Additional information on the neutrino mass scale can be derived through cosmological and astrophysical observations [421]. For instance, analyses of galaxy clustering, including recent CMB measurements and other cosmological constraints, give an upper bound

$$\sum_i m_{\nu_i} < 1.8 - 4.4 \text{ eV} \quad (150)$$

on the sum of the neutrino masses [422, 423, 424, 425, 426, 427].

Big bang cosmology predicts that the Universe is filled with a shallow degenerate Fermi sea of neutrinos [428]. Neutrino decoupling occurred at a temperature of 1.9 K, just one second after the bang. This thermal neutrino background (TNB) has an average number density of

$$\langle n_{\nu_i} \rangle_0 = \langle n_{\bar{\nu}_i} \rangle_0 = \frac{3}{22} \underbrace{\langle n_\gamma \rangle_0}_{\text{CMB}} \simeq 56 \text{ cm}^{-3}, \quad (151)$$

³¹ i, j run over the possible neutrino species.

per neutrino flavor. The dominant interaction mode of extremely high energy neutrinos with the TNB is the exchange of a W^\pm boson in the t -channel ($\nu_i \bar{\nu}_j \rightarrow l_i \bar{l}_j$), or of a Z^0 boson in either the s -channel ($\nu_i \bar{\nu}_j \rightarrow f \bar{f}$) or the t -channel ($\nu_i \bar{\nu}_j \rightarrow \nu_i \bar{\nu}_j$). Here, l denotes a charged lepton, f a charged fermion, and $i \neq j$ for the first reaction [390]. Therefore, one expects neutrinos within a few Z widths of the right energy,

$$E_\nu^{RZ} = \frac{M_Z^2}{2m_{\nu_i}} = 4 \left(\frac{\text{eV}}{m_{\nu_i}} \right) \times 10^{21} \text{ eV}, \quad (152)$$

to annihilate with the TNB into hadrons at the Z -pole with large cross section,

$$\langle \sigma_{\text{ann}} \rangle^Z \equiv \int \frac{ds}{M_Z^2} \sigma_{\text{ann}}(s) = 2\pi \sqrt{2} G_F \sim 40.4 \text{ nb}, \quad (153)$$

producing a “local” flux of nucleons and photons [429, 430].³² Remarkably, the energy of the neutrino annihilating at the peak of the Z -pole has to be well above the GZK limit. At this stage, it is worthwhile to point out that in view of the expected rapid decrease of the ultrahigh energy ν flux with rising energy, the t -channel W - and Z -exchange annihilation processes can be safely neglected. On resonance, the s -channel Z -exchange interactions completely overwhelm them.

The mean energies of the ~ 2 nucleons and ~ 20 γ -rays in each process can be estimated by distributing the resonant energy among the mean multiplicity of 30 secondaries. The proton energy is given by

$$\langle E_p \rangle \sim \frac{M_Z^2}{60 m_{\nu_j}} \sim 1.3 \left(\frac{\text{eV}}{m_{\nu_j}} \right) \times 10^{20} \text{ eV}, \quad (154)$$

whereas the γ -ray energy is given by

$$\langle E_\gamma \rangle \sim \frac{M_Z^2}{120 m_{\nu_j}} \sim 0.7 \left(\frac{\text{eV}}{m_{\nu_j}} \right) \times 10^{20} \text{ eV}. \quad (155)$$

The latter is a factor of 2 smaller to account for the photon origin in two body π^0 decay.

If the neutrino sources are randomly distributed in space, then the total rate of super-GZK events induced by $\nu \bar{\nu}$ annihilation at the Z pole within a distance D of the Earth is [429]

$$F_Z \sim E_\nu^{RZ} F_\nu \langle \sigma_{\text{ann}} \rangle^Z B_h^Z \int d^3x \frac{n_\nu}{4\pi r^2} = E_\nu^{RZ} F_\nu \langle \sigma_{\text{ann}} \rangle^Z B_h^Z \int_0^D n_\nu dr, \quad (156)$$

³² $G_F = 1.16639(1) \times 10^{-5} \text{ GeV}^{-2}$ is the Fermi coupling constant.

where F_ν is the incident neutrino flux evaluated at the resonant energy, $B_h^Z \sim 0.70$ is the hadronic branching fraction of the Z , and n_ν is the column number density of relic neutrinos. In deriving Eq. (156) one assumes that $\langle \sigma_{\text{ann}} \rangle \int_0^D dr n_\nu \ll 1$. The Z -burst rate can be amplified if neutrinos are clustered rather than distributed uniformly throughout the Universe [429, 430]. In such a case the probability of neutrinos to annihilate within the GZK zone is generally on the order of 1%.

An exhaustive analysis of the Z -burst parameter space has recently been reported by Fodor, Katz and Ringwald (FKR) [431, 432]. The analysis includes two possibilities for a diffuse background of protons, as distinct from protons resulting from the Z -burst itself. On the one hand they analyze the case where all events above 4×10^{19} eV consist of protons which are produced within our Galactic halo or at least within the GZK zone. For this case, hereafter referred to as halo background (Halo bk'd), no GZK attenuation is considered. On the other hand, they analyze the situation where CRs are protons which originate from uniformly distributed extragalactic sources, or so-called “extragalactic background” (EG bk'd). In view of the observed distributions of arrival directions, the EG bk'd seems to be phenomenologically more realistic. In such a case, a FKR maximum likelihood fit yields $0.08 \text{ eV} \leq m_{\nu_i} \leq 1.3 \text{ eV}$, while for a Halo bk'd $2.1 \text{ eV} \leq m_{\nu_i} \leq 6.7 \text{ eV}$, both at the 68 % CL.

The FKR analysis seems to be pretty insensitive to the precise values of the cosmological parameters: h , Ω_M , and Ω_Λ , the normalized Hubble expansion rate, and the matter and vacuum energy densities, respectively. The high energy ν -flux is described by

$$F_\nu(E_\nu, z) = F_\nu(E_\nu) (1 + z)^\alpha, \quad (157)$$

where z is the redshift and α characterizes the source evolution. Since neutrinos are produced as secondaries in hadronic astrophysical sources, the flux at zero redshift is expected to fall off like, $F_\nu(E_\nu) \propto E_\nu^{-\gamma}$, with $\gamma \gtrsim 1$. The FKR analysis takes into account two extreme scenarii: (i) strong γ -ray attenuation, where ultrahigh energy photons from the Z -bursts do not contribute to the observed flux [this is certainly the case if the radio background is sufficiently large and/or the EGMF is $\mathcal{O}(\text{nG})$], and (ii) minimal universal radio background with vanishing EGMF.

EGRET [433] measurements of the diffuse γ -background in the energy range between 30 MeV and 100 GeV strongly constrain the source evolution, yielding $\alpha \lesssim 0$ quite independently of different assumptions about the radio background. It should be noted that a correlation between ultrahigh energy CRs and BL Lac objects at redshifts $z > 0.1$ has been claimed [152]. There is evidence that such a sub-class of AGN has zero or negative cosmological evolution.

The required neutrino fluxes for the Z -burst hypothesis are given in Fig. 22, together with existing upper limits and projected sensitivities of present and near future experiments. Power-law extrapolation of the fluxes $F_\nu \propto E^{-\gamma}$ below the resonance energy

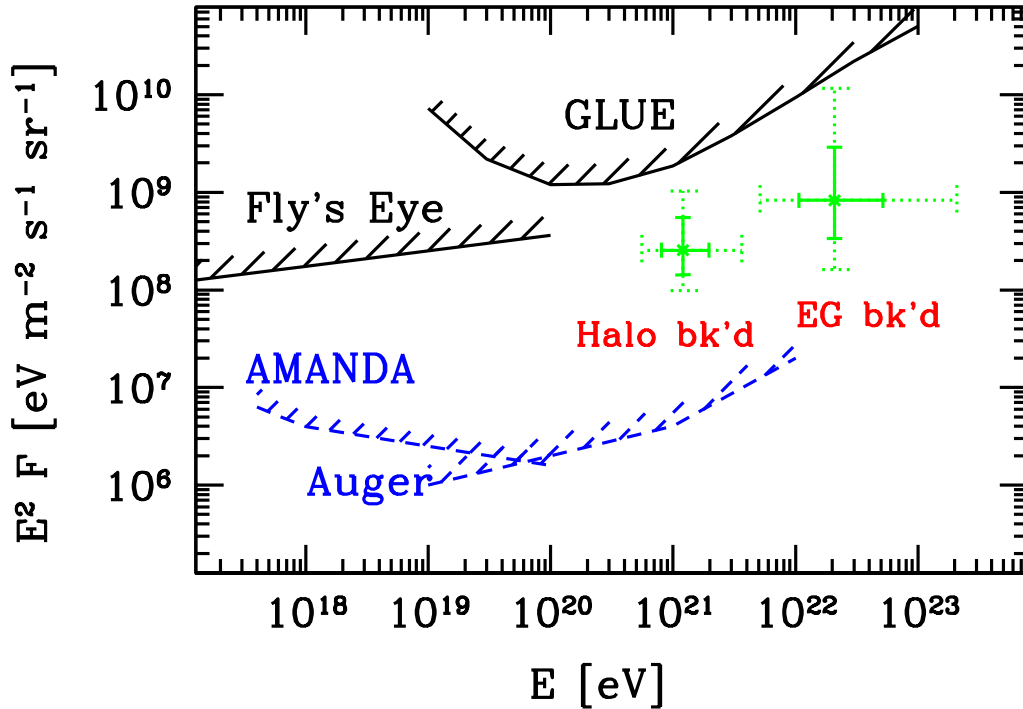


FIG. 22: Neutrino fluxes, $F = \frac{1}{3} \sum_{i=1}^3 (F_{\nu_i} + F_{\bar{\nu}_i})$, required by the Z -burst hypothesis for the case of a halo and an extragalactic background of ordinary cosmic rays, respectively ($\alpha = 0, h = 0.71, \Omega_M = 0.3, \Omega_\Lambda = 0.7, z_{\max} = 2$). Shown, as two crosses, are the necessary fluxes obtained for the case of a strong ultrahigh energy γ attenuation. The horizontal errors indicate the 1σ (solid) and 2σ (dotted) uncertainties of the mass determination and the vertical errors also include the uncertainty of the Hubble expansion rate. Also shown are upper limits from Fly’s Eye [125] on $F_{\nu_e} + F_{\bar{\nu}_e}$ and the Goldstone Lunar Ultrahigh energy neutrino Experiment GLUE [136] on $\sum_{\alpha=e,\mu} (F_{\nu_\alpha} + F_{\bar{\nu}_\alpha})$, as well as projected sensitivities of AMANDA [434] on $F_{\nu_\mu} + F_{\bar{\nu}_\mu}$ and PAO on $F_{\nu_e} + F_{\bar{\nu}_e}$. Published in Ref. [431].

with spectral indices $\gamma \gtrsim 1.5$ are excluded by the Fly’s Eye data. Furthermore, in the Z -burst hypothesis, the flux required for power-law extrapolations with indices $\gamma \gtrsim 1$ to lower energies is larger than the theoretical upper limit from “hidden” hadronic astrophysical sources, $E^2 F_\nu \sim 2 \times 10^7 \text{ eV m}^{-2} \text{ s}^{-1} \text{ sr}^{-1}$ [435]. Hidden hadronic astrophysical sources are those from which only photons and neutrinos can escape. Therefore, one has to invoke sources that have to be opaque to their primary protons, and should emit secondary photons (unavoidably produced together with the neutrinos) only in the sub-MeV region to avoid conflict with the diffuse γ -ray background measured by the EGRET experiment [436, 437].

It is fair to say that nowadays no convincing astrophysical sources are known which

can accelerate protons at least up to 10^{23} eV, have zero or negative cosmological evolution, are opaque to nucleons, and emit photons only in the sub-MeV region.³³ It is still an open question whether such challenging conditions can be realized in Nature. As one can see in Fig 22, the PAO should give a definite answer to this question.

C. SUSY U

Certainly, a novel beyond-SM-model explanation to the high end of the spectrum is to assume that ultrahigh energy CRs are not known particles but a new species of particle, generally referred to as the uhecron, U [440, 441]. The meager information we have about super-GZK particles allows a naïve description of the properties of the U . The muonic content of EASs suggests U should interact strongly. At the same time, if uhecrons are produced at cosmological distances, they must be stable, or at least remarkably long lived, with mean-lifetime

$$\tau \sim 10^6 \left(\frac{m_U}{3\text{GeV}} \right) \left(\frac{d}{\text{Gpc}} \right) \text{ s}, \quad (158)$$

where d is the distance to the source and m_U , the uhecron's mass. In addition, to avoid photopion production on the CMB, $m_U \gtrsim 1.5$ GeV, because the threshold energy for the reaction $U\gamma \rightarrow U\pi$, increases linearly with m_U ,

$$E_{\text{th}} = m_\pi \frac{(m_U + m_\pi/2)}{w}. \quad (159)$$

Moreover, to avoid deflections on EGMFs and the consequent energy loss due to pair production and other mechanisms, the hadron has to be neutral. Note that the latter may not be an essential requirement, depending on the distance to the accelerator.

It has been known since the early days of Supersymmetry (SUSY) that the gluino \tilde{g} , the spin $\frac{1}{2}$ SUSY partner of a gluon, could be the lightest supersymmetric particle (LSP), with the possible exception of the gravitino $g_{3/2}$ [442, 443, 444, 445].³⁴ Therefore, in a SUSY background the plausible candidates satisfying the U requirements are gluino containing hadrons (\tilde{g} -hadrons).³⁵ QCD sum rules suggest that the glueballino

³³ The authors of [438] have pointed out that an extra $U(1)$ boson (the Z') with sufficiently low mass could reduce the extreme proton energies required in the Z -burst hypothesis. Speculations about a Z' of a few GeV have been entertained as one possible explanation of the NuTeV anomaly [438, 439].

³⁴ If the LSP is the gravitino, the gluino decays gravitationally into a gluon and gravitino $\tilde{g} \rightarrow gg_{3/2}$, and its lifetime can be long enough.

³⁵ We note that an alternative proposal (where CRs above the GZK-energy originate from sources at cosmological distances) that relies on a supersymmetric extension of the SM, assumes the existence of a new exotic pseudo-scalar axion-like particle [446].

$\tilde{G} = \tilde{g}g$ is the lightest hadron. In the 1980s, \tilde{G} was suggested as the possible primary particle in attempts to explain the hadronic nature of CRs from Cygnus X-3 [447, 448].

There are, however, arguments against a light quasi-stable gluino [449]. The main problem follows from the fact that along with a neutral hadron \tilde{G} there must exist a charged hadron of the type $\tilde{g}qqq$ having baryon number (gluebarino). The lightest gluebarino must be a hadron ($\tilde{g}uud$) in which the triplet of light quarks has total spin $\frac{1}{2}$ and is in a color octet state. The gluebarino must be stable to the same extent as the gluino, since the lightest two particle state with the same quantum numbers $(\tilde{g}g) + (uud)$ must be heavier than $(\tilde{g}uud)$ by the mass of a constituent gluon (> 0.6 GeV). Now, production of charged gluebarinos in the Earth atmosphere by CRs and their accumulation in the oceans would result in a too high abundance of anomalous heavy isotopes of hydrogen and oxygen in contradiction with observational data [449]. However, it may well be that the lightest baryonic state is the neutral flavor singlet $S^0 = \tilde{g}uds$ [383, 450], due to strong quark attraction in this state. We stress that even in this case conflict with observational data emerges if $\tilde{g}uds$ -gluebarino and proton are bound into anomalous deuterium.

In addition, direct searches for glueballino decays [451, 452, 453] as well as for decays of other unstable \tilde{g} -hadrons [454] have severely eroded the attractiveness of the light gluino scenario. A practically model-independent analysis, which takes into account contributions of the light gluino to the running of α_s and to QCD colour coefficients excludes light gluinos with $m_{\tilde{g}} = 3(5)$ GeV with 93% (91%) CL [455]. By combining these analysis with the determination of QCD colour coefficients from the analysis of multi-jets events [456], the conclusion of [455] becomes much stronger: light gluinos with mass $\lesssim 5$ GeV are excluded with at least 99.89% CL. Recent analyses based on currently available OPAL and CDF data conclude that the range $3 \text{ GeV} \lesssim m_{\tilde{g}} \lesssim 130 - 150 \text{ GeV}$ can be excluded at the 95% CL [457]. For certain choices of the parameters, a window in the intermediate mass region $25 \text{ GeV} \lesssim m_{\tilde{g}} \lesssim 35 \text{ GeV}$ remains open [458, 459]. This leaves two narrow windows for allowed masses of \tilde{g} -hadrons $1.5 \text{ GeV} \lesssim m_{\tilde{g}-h} \lesssim 3 \text{ GeV}$ and $25 \text{ GeV} \lesssim m_{\tilde{g}-h} \lesssim 35 \text{ GeV}$. Gluino-containing hadrons corresponding to the second window would produce EASs very different from those detected by current CR-experiments [384]. However, light \tilde{g} -hadrons corresponding to the first gluino window produce EASs very similar to those initiated by protons. Furthermore, as shown in Fig. 23, light glueballinos, $m_{\tilde{G}} \gtrsim 1.5 \text{ GeV}$, have a spectrum with GZK-cutoff beyond the currently observed energy range [384].

D. Lorentz symmetry violations with anomalous kinematics

At present, there is no reason to anticipate the existence of a universal scale below which our present notion of flat spacetime geometry is not valid. However, local Lorentz

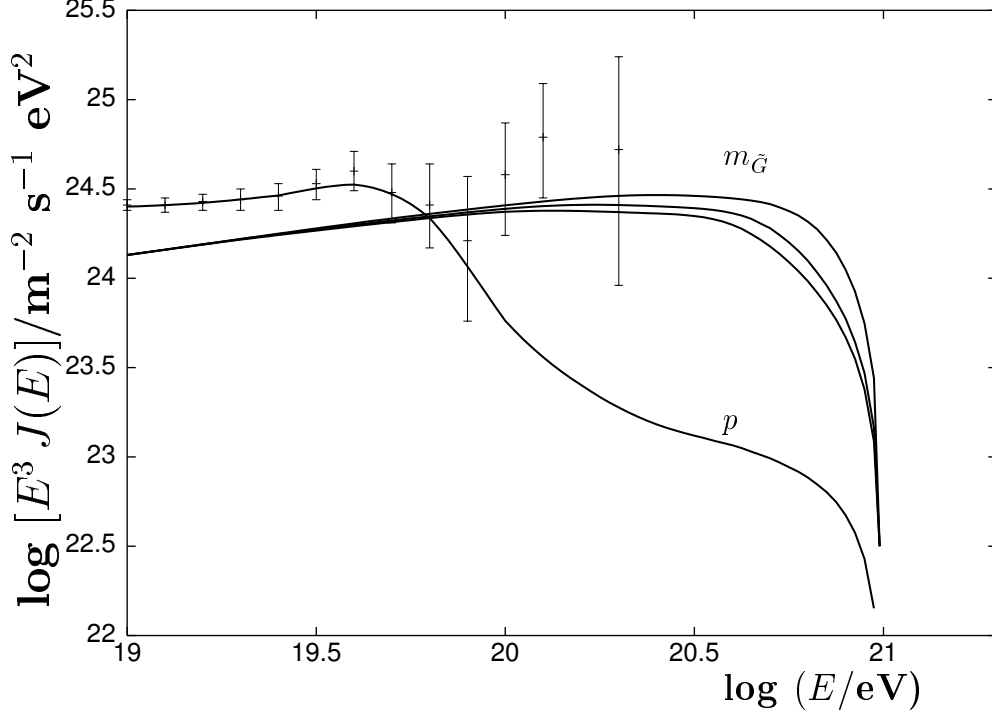


FIG. 23: The three solid curves that accurately fit the observational data from AGASA above 10^{20} eV indicate the diffuse glueballino flux from uniformly distributed sources with injection spectra $dN_0/dE \propto E^{-2.7}$ and intrinsic cutoff $E = 10^{21}$ eV for $m_{\tilde{G}} = 1.5, 2$ and 3 GeV (from below). The proton flux is also shown for comparison. Published in [384].

invariance (LLI) should not be accepted on faith but rather as a plausible hypothesis subject to experimental test. It is possible to introduce the notion of LLI violation either with or without accompanying anomalous kinematics. If no anomalous kinematics is involved, any search for LLI non-conservation effects will require testing length scales below 10^{-16} cm or less [460]. However, introducing anomalous kinematical constraints allows tiny departures from LLI, which would be undetectable at the electroweak scale, to be magnified rapidly with rising energy. LLI-violation with anomalous kinematics could then help to break the GZK barrier [385, 386, 387, 388, 389].

For instance, it was noted by Coleman and Glashow [388] that renormalizable and gauge invariant perturbations to the SM Lagrangian that are rotationally invariant in a preferred frame, but not Lorentz invariant, lead to species-specific maximum attainable velocities c_i for different particles. In such a case, the possible departure from LLI can be phrased in terms of the difference between the particle maximum attainable

velocities

$$\delta_{ij} = c_i - c_j. \quad (160)$$

Within this framework the energy conservation can be expressed by [389]

$$4w \geq \delta_{\Delta p} E + \frac{m_{\Delta}^2 - m_p^2}{E}. \quad (161)$$

If Lorentz symmetry is unbroken, $\delta_{\Delta p} = 0$ and Eq. (161) leads to the conventional threshold for a head-on collision. Otherwise, Eq. (161) is a quadratic form in E with discriminant $4w^2 - (m_{\Delta}^2 - m_p^2)\delta_{\Delta p}$. For

$$\delta_{\Delta p} > \hat{\delta}(w) \equiv \frac{4w^2}{m_{\Delta}^2 - m_p^2} \approx 3.5 \times 10^{-25} \left(\frac{w}{w_0}\right)^2 \quad (162)$$

the discriminant < 0 , and therefore the reaction $p\gamma \rightarrow \Delta \rightarrow p\pi$ is kinematically forbidden for all E . Now, recalling that the relic photons follow a Planck distribution, it is easily seen that for $\delta_{\Delta p}$ comparable to $\hat{\delta}(w_0)$, the GZK effect would be relaxed.

There are no direct experimental constraints on the parameter $\delta_{\Delta p}$. However, if we compare the speed of photons to that of high energy CRs, it is possible to obtain a very stringent bound on violations of LLI. This bound follows from the emission of Čerenkov radiation and consequent loss of energy by charged CRs, a process which is allowed if $c_{\gamma} < c_{\text{CR}}$. Primary protons (electrons) with energies up to 10^{20} eV (1 TeV) have been seen, thus $\delta_{p\gamma} < 3.0 \times 10^{-23}$ [461] ($\delta_{\gamma e} < 1.3 \times 10^{-13}$ [462]). Moreover, if LLI is broken and $c_e > c_{\gamma}$ the threshold energy for pair production is altered, yielding $\delta_{\gamma e} \leq 2m_e^2/E_{\gamma}^2$. Multi-TeV γ -ray observations from Markarian 501 then lead to $\delta_{\gamma e} < 1.3 \times 10^{-15}$ [462]. On the other hand, if $c_{\gamma} > c_e$, the decay of a photon into an electron positron pair is kinematically allowed for photons with energies exceeding $E_{\text{max}} = m_e \sqrt{2/|\delta_{e\gamma}|}$. The decay would take place rapidly, so that photons with energies above E_{max} would not be observable. Detection of primary photons with energies $E_{\gamma} \geq 50$ TeV leads to $\delta_{e\gamma} < 1.3 \times 10^{-15}$ [462]. The failure to detect velocity oscillations of neutrinos translates into $|\delta_{\nu\nu'}| < 2 \times 10^{-21}$, whereas the detection of neutrinos from SN 1987a yields $|\delta_{\nu\gamma}| < 10^{-8}$ [463]. An additional constraint $|\delta_{m\gamma}| < 6 \times 10^{-22}$ results from a Hughes-Drever type experiment [464]. In the latter, the maximum attainable velocity of material matter c_m was taken to be the same for all massive particles. It is interesting to remark that none of these constraints reaches the level of sensitivity to Lorentz violation needed to overcome the GZK paradox. However, the future PAO observations of faraway sources could provide constraints on, or even a measurement of, the violation of Lorentz symmetry, yielding essential insights into the nature of gravity-induced wave dispersion in the vacuum [465, 466, 467, 468, 469, 470].

VII. SPACETIME’S UNSEEN DIMENSIONS

In recent years, it has become evident that a promising route towards reconciling the apparent mismatch of the fundamental scales of particle physics and gravity is to modify the short distance behavior of gravity at scales much larger than the Planck length. Such modification can be most simply achieved by introducing extra dimensions, generally thought to be curled-up, in the sub-millimeter range [471, 472, 473, 474]. Within this framework the fundamental scale of gravity can be lowered all the way to \mathcal{O} (TeV), and the observed Planck scale turns out to be just an effective scale valid for energies below the mass of Kaluza–Klein (KK) excitations.³⁶ Clearly, while the gravitational force has not been directly measured far below the millimeter range [478], SM interactions have been investigated well below this scale. Therefore, if large extra dimensions really exist, one needs some mechanism to prevent SM particles from feeling them. Remarkably, there are several possibilities to confine SM fields to a 4 dimensional subspace (referred to as a brane-world) within the $(4 + n)$ dimensional spacetime [479, 480].

Theories with TeV scale gravity can be classified into two broad categories according to whether they do or do not assume that the full spacetime manifold is of factorized form. In these theories, in addition to the 4 dimensions that we see (with coordinates x^μ) there are n unseen dimensions with coordinates y^m . In the case of non-factorizable geometries the metric takes the form

$$ds^2 = dx^\mu dx_\nu + g_{mn}(y) dy^m dy^n, \quad (163)$$

where the characteristic size of the *large* extra dimensions is of the order of the fundamental Planck length, explaining their invisibility. In the case of *warped* extra dimensions, the scale of the 4-dimensional metric may vary depending on the location in the extra dimension, due to the warp factor $e^{2A(y)}$ that can be thought of as the carrier of a position-dependent redshift. The metric in this case reads,

$$ds^2 = e^{2A(y)} dx^\mu dx_\nu + g_{mn}(y) dy^m dy^n. \quad (164)$$

To illustrate the two cases we treat the following representative examples.

Large extra dimensions: Arkani-Hamed, Dimopoulos, and Dvali (ADD) [471] imagine the spacetime as a direct product of ordinary four-dimensional spacetime and a (flat) spatial n -torus with circumferences $L_i = 2\pi r_i$ ($i = 1, \dots, n$), generally of common linear size $r_i = r_c$. As mentioned above, SM fields cannot propagate freely in the extra

³⁶ Theories with small periodic internal dimensions where the low energy degrees of freedom are restricted to zero modes and separated by a large mass gap from the massive modes were first proposed by Kaluza [475] and Klein [476, 477].

dimensions and remain consistent with observations. This is avoided by trapping the fields to a thin shell of thickness $\delta \sim M_s^{-1}$. Assuming that the higher dimensional theory at short distance is a string theory, one expects that the fundamental string scale M_s and the higher dimensional Planck scale M_* are not too different. The only particles propagating in the (4+n) dimensional bulk are the (4+n) gravitons. Because of the compactification, the extra n components of the graviton momenta are quantized

$$k_i = \frac{2\pi\ell_i}{L_c} = \frac{\ell_i}{r_c}, \quad i = 1, \dots, n. \quad (165)$$

Thus, taking into account the degeneracy on $\ell_i \in \mathbb{Z}$, the graviton looks like a massive KK state with mass

$$m_{\ell_1, \dots, \ell_n} = \left(\sum_{i=1}^n \ell_i^2 \right)^{1/2} r_c^{-1}. \quad (166)$$

It is important to stress that the graviton's self-interactions must conserve both ordinary 4-momenta and KK momentum components, whereas SM fields (that break translational invariance) do not have well defined KK momenta in the bulk for $\ell/r_c \leq M_s$.³⁷ Therefore, interactions of gravitons with SM particles do not conserve KK momentum components. Applying Gauss' law at $r \ll r_c$ and $r \gg r_c$, it is easily seen that the Planck scale of the four dimensional world is related to that of a higher dimensional space-time simply by a volume factor,

$$r_c \sim \left(\frac{M_{\text{Pl}}}{M_*} \right)^{2/n} \frac{1}{M_*} \sim 2.0 \times 10^{-19} \left(\frac{\text{TeV}}{M_*} \right) \left(\frac{M_{\text{Pl}}}{M_*} \right)^{2/n} \text{ cm}, \quad (167)$$

so that M_* can range from $\sim \text{TeV}$ to $M_{\text{Pl}} \sim 10^{19} \text{ GeV}$, for $r_c \lesssim 1 \text{ mm}$ and $n \geq 2$. For $n \leq 6$, the mass splitting,

$$\Delta m \sim \frac{1}{r_c} \sim M_* \left(\frac{M_*}{M_{\text{Pl}}} \right)^{2/n} \sim \left(\frac{M_*}{\text{TeV}} \right)^{n+2/2} 10^{(12n-31)/n} \text{ eV}, \quad (168)$$

is so small that the sum over the tower of KK states can be replaced by a continuous integration. Then the number of modes between $|\ell|$ and $|\ell| + d\ell$ reads,

$$dN = d\ell_1 d\ell_2 \dots d\ell_n = S_{n-1} |\ell|^{n-1} d\ell, \quad (169)$$

where

$$S_{n-1} = \frac{2\pi^{n/2}}{\Gamma(n/2)} \quad (170)$$

³⁷ For $\ell/r_c > M_s$ we would expect higher order quantum gravity and string effects to become important, providing some sort of a natural cut-off in the field theory.

is the surface of a unit-radius sphere in n dimensions. Now using Eqs. (166) and (167), Eq. (169) can be re-written as

$$dN = S_{n-1} \left(\frac{M_{\text{Pl}}}{M_*} \right)^2 \frac{1}{M_*^n} m^{n-1} dm. \quad (171)$$

From the 4-dimensional viewpoint the graviton interaction vertex is suppressed by M_{Pl} . Roughly speaking, $\sigma_m \propto M_{\text{Pl}}^{-2}$. Now, introducing $d\sigma_m/dt$, the differential cross section for producing a single mode of mass m , one can write down the differential cross section for inclusive graviton production

$$\frac{d^2\sigma}{dt dm} = S_{n-1} \left(\frac{M_{\text{Pl}}}{M_*} \right)^2 \frac{1}{M_*^n} m^{n-1} \frac{d\sigma_m}{dt}, \quad (172)$$

or else, the branching ratio for emitting any one of the available gravitons

$$\Gamma_g \sim \frac{s^{n/2}}{M_*^{2+n}}, \quad (173)$$

where $s^{1/2}$ is the c.m. energy available for graviton-KK emission. As one can see by inspection of Eq. (173), the enormous number of accessible KK-states can compensate for the M_{Pl}^2 factor in the scattering amplitude.

Warped extra dimensions: Randall and Sundrum (RS) [474] have proposed a simple and attractive scenario to ameliorate the hierarchy problem in which our Universe plus a hidden brane are embedded in a 5-dimensional bulk with a negative cosmological constant. The set-up is in the shape of a gravitational capacitor: two 3-branes with equal and opposite tensions rigidly reside at S_1/Z_2 orbifold fixed points at the boundaries ($y = 0$ and $y = \pi r_c$) of a slab of anti-de Sitter (AdS) space of radius ℓ . The line element satisfying this Ansatz in horospherical coordinates reads

$$ds^2 = e^{-2|y|/\ell} \eta_{\mu\nu} dx^\mu dx^\nu + dy^2, \quad (174)$$

where $\eta_{\mu\nu}$ is the metric of Minkowski space. Examination of the action in the 4-dimensional effective theory leads to [474]

$$\overline{M}_{\text{Pl}}^2 = M^3 \ell \left(1 - e^{-2\pi r_c/\ell} \right), \quad (175)$$

where \overline{M}_{Pl} is the reduced effective 4-dimensional Planck scale, and M the fundamental scale of gravity. The AdS warp factor is exponential in the y -coordinate, and so the energy scales on the negative tension brane become exponentially redshifted. In other words, a field with the fundamental mass parameter m_0 will appear to have the physical mass $m = e^{-\pi r_c/\ell} m_0$ on the the 3-brane living at $y = \pi r_c$. Therefore, the weak scale is generated from fundamental scales of order M_{Pl} through the

exponential hierarchy, requiring $r_c/\ell \approx 12$. Additionally, in the “single brane” limit ($r_c \rightarrow \infty$) [481], the bulk continuum can be described by a Conformal Field Theory (CFT) [482, 483, 484], reproducing the duals discussed in [485]. For finite but large r_c , deviations from conformality are exponentially damped in the infrared [486, 487]. In the RS model there exists a KK tower of gravitons with essentially electroweak couplings and masses $m_n = \ell^{-1} x_n e^{-\pi r_c/\ell}$, where x_n is the n^{th} root of the Bessel function J_1 [481]. This implies that the tower mass spectrum, $m_n = m_1 x_n/x_1$, is completely determined by the lowest lying excitation. Note that while the zero mode graviton couples with a strength $\overline{M}_{\text{Pl}}^{-1}$, all the remaining states couple as $(\overline{M}_{\text{Pl}} e^{-\pi r_c/\ell})^{-1}$. The phenomenology of this scenario (recall that only gravity spills into the extra dimension) is governed by two parameters: m_1 , and $c = (\ell \overline{M}_{\text{Pl}})^{-1}$ which is expected to be near, though somewhat less than, unity [488]. The analysis [488] of Tevatron data [489, 490, 491, 492, 493, 494] for anomalous Drell-Yan and dijet production as well as the calculation of indirect contributions to electroweak observables [495] yield $m_1 \gtrsim 500$ GeV, whereas AdS/CFT considerations suggest $c \lesssim 0.1$ [496].

Clearly, the ADD and the RS model would have different manifestations in scattering processes. In the case of the product spacetime, each excited state couples with gravitational strength, and the key to observing KK-modes in particle collisions is the large multiplicity of states, due to their fine splittings. However, in the RS geometry, instead of gravitational strength coupling $\sim \text{energy}/M_{\text{Pl}}$, each excited state coupling is of order energy/TeV , and hence each resonance can be individually detected via its decay products. In the first part of this section we discuss how virtual graviton exchange would disturb high energy neutrino interactions [396]. Under some extremely speculative hypotheses this phenomenon may allow neutrinos to interact strongly in the atmosphere [497, 498]. More realistic assumptions would lead to a lower cross section which would predict an increase in the event rate of quasi-horizontal deeply developing showers. In the last part of the section, we discuss the possibility that ultrahigh energy neutrino interactions on the TNB produce gravitons of weak scale mass and coupling, resulting in “gravi-burst” fragmentation jets that can contribute to the super-GZK spectrum in a way that is similar to the Z -burst mechanism [499].

A. Influence of KK-modes on the development of extensive air showers

A novel feature of the contribution of KK graviton exchange to high energy scattering cross sections is the fact that it is projectile independent, and thus the same for scattering of pp , γp , νp , etc. We focus here on νp interactions where the contribution from KK-modes leads to a radical departure from SM particle physics.

A simple Born approximation to the elastic ν -parton cross section [503] (which underlies the total ν -proton cross section) leads, without modification, to $\sigma_{\nu p}^{\text{tot}} \sim s^2$.

Unmodified, this behavior by itself eventually violates unitarity. This may be seen either by examining the partial waves of this amplitude, or by noting the high energy Regge behavior of an amplitude with exchange of the graviton spin-2 Regge pole: with intercept $\alpha(0) = 2$, the elastic cross section

$$\frac{d\sigma_{el}}{dt} \sim \frac{|A_R(s, t)|^2}{s^2} \sim s^{2\alpha(0)-2} \sim s^2, \quad (176)$$

whereas

$$\sigma_{tot} \sim \frac{\text{Im}[A_R(0)]}{s} \sim s^{\alpha(0)-1} \sim s, \quad (177)$$

so that eventually $\sigma_{el} > \sigma_{tot}$. Eikonal unitarization schemes modify these behaviors: in the case of the tree amplitudes [396] the resulting (unitarized) cross section ($n = 2$) $\sigma_{\nu p}^{tot} \sim s$, the all-order loop resummation yields $\sigma_{\nu p}^{tot} \sim s^{2/n}$ [500], whereas for the single Regge pole exchange amplitude, $\sigma_{\nu p}^{tot} \sim \ln^2(s/s_0)$ [501].³⁸

The other relevant parameter which has direct influence on the shower profile is the inelasticity. The KK-modes couple to neutral currents, and thus the scattered neutrino carries away 90% of the incident energy per interaction. Therefore, the cross section has to be at least a few 10^{-26} cm² to be consistent with observed showers which start within the first 50 g/cm² of the atmosphere. Specifically, the survival probability N at atmospheric depth X of a particle a with mean free path

$$\lambda_a = \frac{m_{\text{air}}}{\sigma_{a-\text{air}}}, \quad (178)$$

is given by

$$N(X) = e^{-X/\lambda_a}, \quad (179)$$

where $m_{\text{air}} \sim 2.43 \times 10^{-23}$ g is the mass of an average atom of air, and $\sigma_{a-\text{air}}$ the cross section on air. For a proton energy $\sim 10^{20}$ eV, the mean free path is $\lambda_p \sim 40$ g/cm². Therefore, a proton air shower is initiated at the top of the atmosphere. The key feature in the evolution of the shower is the ratio of decay to interaction of secondary hadrons along their path in the atmosphere. The latter strongly depends both on particle energy and target density. For protons of this energy, $\langle X_{\text{max}} \rangle \sim 800$ g/cm², corresponding to 20 hadronic interaction lengths. The neutrino nucleon cross section estimates discussed above indicate that $\lambda_\nu \gtrsim 10\lambda_p$. Due to the larger mean free path, X_{max} is shifted 360 g/cm² downwards in the atmosphere. Moreover, in a neutral current interaction the neutrino only transfers 10% of its energy to the shower and

³⁸ Note that the KK contribution to the cross section at $s \sim 2 \times 10^4$ TeV² gives $\sigma_{\text{KK}} \lesssim 10^{-34}$ cm², whereas the usual hadronic pp cross section at this energy is $\sigma_{pp} \sim 1.5 \times 10^{-25}$ cm², so the impact on the pp scattering process is almost innocuous [502].

consequently elongates the longitudinal development even further [501, 504]. Events consistent with these features have not been observed. However, the model may still be salvaged if the neutrino-nucleon cross section can be enlarged enough ($\sigma_{\nu N} \gtrsim 20$ mb), then multiple scattering within the nucleus may provide a sufficiently large energy transfer to reproduce the super-GZK events [497, 498].

The question of whether the interaction cross section of neutrinos with matter could reach typical hadronic values at high energies is yet undecided. The Regge picture of graviton exchange is not yet entirely established, the apparently increasing dominance assumed by successive Regge cuts due to multiple Regge pole exchange, as well as the presence of the zero mass graviton can introduce considerable uncertainty in the eventual energy behavior of the cross section [505, 506]. However, it is fair to say that recent calculations for the rate of rise of the cross section in the context of string theory tend not to support hadronic-like cross sections in ν -interactions [507, 508].

Now we turn to the possibility of experimental input into the issue. In the following we discuss a method to test scenarii in which neutrinos are super-GZK primaries which relies directly on EAS observables and is independent of the type of interaction enhancing physics. Any physics beyond the SM that increases the neutrino-nucleon cross section to typical hadronic values at $E_\nu \gtrsim 10^{20}$ eV should also affect standard shower observables at lower energies, where the cross section attains sub-hadronic-sizes. In particular, for $\sigma_{\nu N} \gtrsim 10^{-27}$ cm², one expects neutrinos to trigger moderately penetrating showers, where 1000 g/cm² $\lesssim X_{\max} \lesssim 2500$ g/cm². For the specific case discuss in Ref. [497, 498] the cross section is likely to be sub-hadronic near the energy at which the cosmogenic neutrino flux peaks (see Fig. 12), and so this kind of shower should be copiously produced [504].³⁹ Clearly, the absence of moderately penetrating showers in the CR data sample should be understood as a serious objection to the hypothesis of neutrino progenitors of the super-GZK events. Even though neutrino-nucleon interactions in TeV-gravity models seems insufficient to explain the showers above the GZK-limit, virtual graviton exchanged can still lead to interesting new phenomena which may be observed in upcoming CR and neutrino experiments [510, 511]. Recall that the atmosphere provides a detector medium with a column depth ~ 36000 g/cm² for horizontal arrival directions, and so can probe cross sections in the range $\sim 10^{-29} - 10^{-27}$ cm². Due to the increase column depth, water/ice detectors would probe cross sections in the range $\sim 10^{-31} - 10^{-29}$ cm².

³⁹ There is no significant signal of showers with $X_{\max} \gtrsim 1000$ g/cm² in the Fly's Eye data [509].

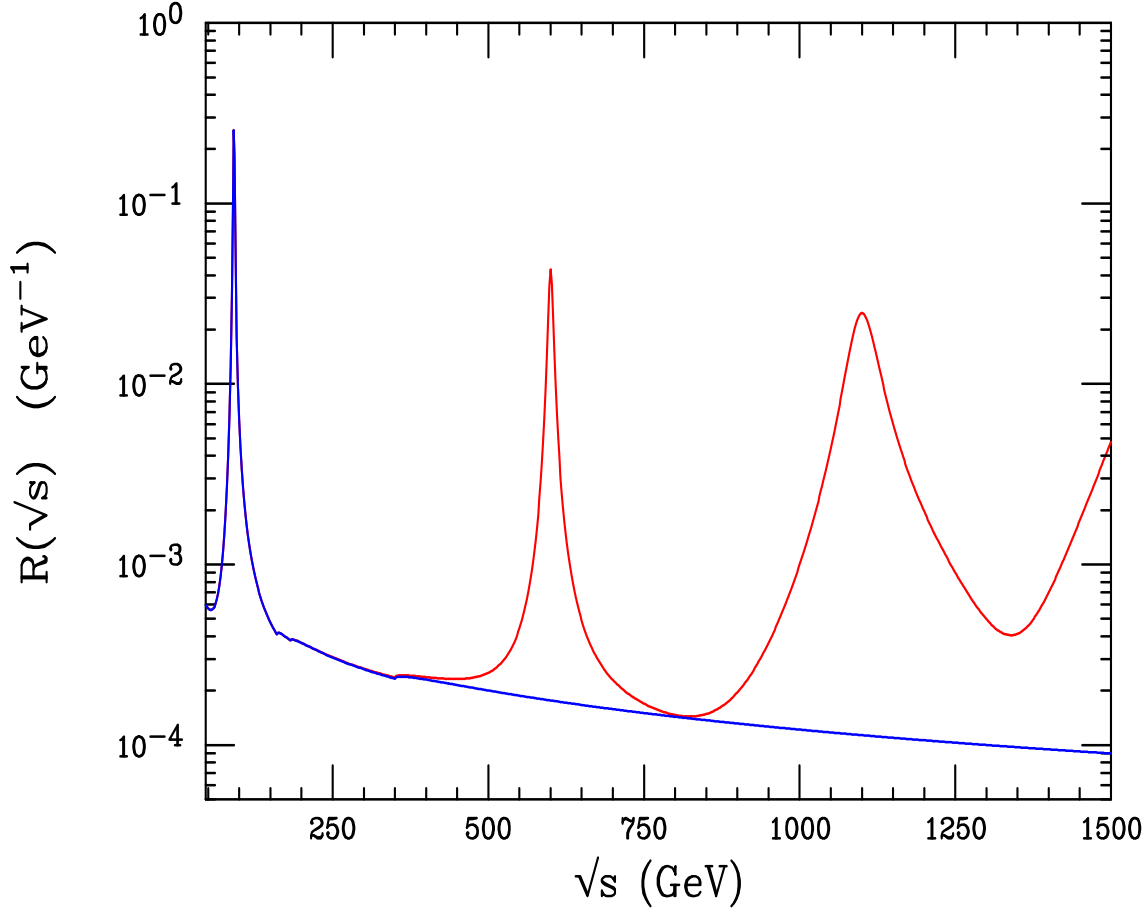


FIG. 24: Energy weighted total cross section for hadron production in units of that for the Z pole in the Weiler Z -burst model for $\gamma = 0$ as a function of c.m. energy. The relatively flat lower curve shows the SM, and the upper curve shows the RS model with $c = 0.1$ and $m_1 = 600$ GeV. Published in Ref. [499].

B. Gravi-burst

The RS [474] model of localized gravity would open up new channels for high energy neutrinos to annihilate with the TNB to produce a single graviton KK state on resonance which subsequently decays hadronically [499]. For neutrino masses $m_{\nu_j} \sim 10^{-2} - 10^1$ eV, and graviton resonance of order a TeV, super-GZK events can be produced. Therefore, if one assumes that the incoming neutrino spectrum extends in energy with a reasonably slow fall-off, the existence of a series of s -channel KK graviton resonances may lighten the requirements on neutrino fluxes given in the Z -burst model shown in Fig. 22.

To estimate the event rate of a $\nu\bar{\nu}$ graviton mediated process, consider a point in

the parameter space allowed by all current constraints: $m_1 = 600$ GeV and $c = 0.1$. For these parameters, Davoudiasl, Hewett, and Rizzo [499] have estimated the cross section for $\nu\bar{\nu}$ annihilation into hadrons. Such a cross section has a number of distinct contributions, because gravitons not only lead to pairs of quarks, and W and Z final states, but also to pairs of gluons and Higgs bosons.⁴⁰ By combining all these individual process cross sections and assuming the neutrino spectrum above the Z pole energy falls like $\sim E_\nu^{-\gamma}$, it is straightforward to compute the full energy dependence of the total $\nu\bar{\nu} \rightarrow$ hadrons cross section, and afterwards the ratio of expected CR rates in units of the Z -pole induced rate given in Eq. (156),

$$R(\sqrt{s}) = \frac{F_{\text{SM+GRAV}}(\sqrt{s})}{F_Z} = \frac{2 \sqrt{s} \sigma_{\text{ann}}^{\text{SM+GRAV}}(s) (M_Z/\sqrt{s})^{2\gamma}}{M_Z^2 \langle \sigma_{\text{ann}} \rangle^Z B_h^Z}. \quad (180)$$

To get an idea of what this ratio looks like, Fig. 24 shows the case of $\gamma = 0$. Integration of R over a range of \sqrt{s} leads to the relative rate of events expected in the RS model to those originating from the Z -burst model. Note that the integral of R under the Z pole gives the value unity as it should to reproduce the Z -burst results. If the ultrahigh energy neutrino spectrum above the Z -pole falls with spectral index $\gamma \sim 0.5$, it is easily seen from Eq. (180) that correction from the first RS excitation to the ν -fluxes required to fit the observed spectrum (see Fig. 22) is $\lesssim 5\%$, quickly falling below 1% for $\gamma \gtrsim 1$.

VIII. EXOTICA

The difficulties so far encountered in modeling the production of ultrahigh energy CRs arise from the need to identify a source capable of launching particles to extreme energy. In contrast to the “bottom-up” acceleration of charged particles, the “top-down” scenario avoids the acceleration problem by assuming that charged and neutral primaries simply arise in the quantum mechanical decay of supermassive elementary X particles. Sources of these exotic particles could be:

- Topological defects (TDs) left over from early Universe phase transitions associated with the spontaneous symmetry breaking that underlies unified models of high energy interactions [512, 513, 514, 515, 516, 517].
- Some long-lived metastable super-heavy ($m_X \gtrsim 10^{12}$ GeV) relic particles produced through vacuum fluctuations during the inflationary stage of the Universe [518, 519, 520, 521].

⁴⁰ For numerical purposes the mass of the Higgs is set to 120 GeV.

Due to their topological stability, the TDs (magnetic monopoles, cosmic strings, domain walls, etc.) can survive forever with X particles ($m_X \sim 10^{16} - 10^{19}$ GeV) trapped inside them. Nevertheless, from time to time, TDs can be destroyed through collapse, annihilation, or other processes, and the energy stored would be released in the form of massive quanta that would typically decay into quarks and leptons. Similarly, super-heavy relics would also have quarks and leptons as the ultimate decay products. The strongly interacting quarks fragment into jets of hadrons resulting in typically $10^4 - 10^5$ mesons and baryons. In this way, very energetic CRs, with energies up to m_X , can be produced directly without any acceleration mechanism. Another exotic explanation of the highest energy CRs postulates that relic TDs themselves constitute the primaries [522, 523]. General features of the exotic scenario have been discussed in several comprehensive reviews [170, 524, 525, 526, 527, 528]. Here we give just a general overview with emphasis on recent developments.

A. Top-down origin

In an epic paper, well ahead of its time, Lemaître [529] introduced what may well be the ultimate top-down model. According to Lemaître the entire material filling the Universe, as well as the Universe’s expansion, originated in the super-radioactive disintegration of a “Primeval Atom”, which progressively decayed into atoms of smaller and smaller atomic weight. The CRs were introduced as the energetic particles emitted in intermediate stages of the decay-chain. As a matter of fact, Lemaître regarded the CRs as vestigial evidence of the primeval fireworks. Of course, we now know that the existence of the CMB precludes the origin of super-GZK CRs in a very early cosmological epoch. However, it is amusing that one of the earliest explanations considered for the CR origin was a top-down mechanism.

Topological defects: A more contemporary top down model proposes the vestiges of phase transitions in the early Universe as responsible for the highest energy CRs. According to current unified models of high energy interactions, the Universe may have experienced several spontaneous symmetry breakings, where some scalar field, generally referred to as the Higgs field, acquired a non-vanishing expectation value in the new vacuum (ground) state. Quanta associated with these fields are typically of the order of the symmetry-breaking scale, which in Grand Unified Theories (GUTs) can be $\sim 10^{16} - 10^{19}$ GeV. During a phase transition, non-causal regions may evolve towards different states, so that in different domain borders the Higgs field may keep a null expectation value. Energy is then stored in a TD whose characteristics depend on the topology of the manifold where the Higgs potential reaches its minimum [530, 531, 532, 533]. The relic defects such as magnetic monopoles [512, 517], cosmic strings [514, 515], superconducting cosmic strings [513], vortons (superconduct-

ing string loops stabilized by the angular momentum of the charge carriers) [534, 535], and cosmic necklaces [536]⁴¹ are all relatively topologically stable, but can release part of their energy (through radiation, annihilation, or collapse) in the form of X particles that typically decay to quarks and leptons. The quarks hadronize producing jets of hadrons containing mainly pions together with a 3% admixture of nucleons. Note that, in contrast to the case of bottom-up acceleration models, top-down models predict a flux above 10^{20} eV which is dominated by gamma rays and neutrinos produced via pion decay. Therefore, the photon/proton ratio can be used as a diagnostic tool in determining the CR origin [538]. In light of the mounting evidence that ultrahigh energy CRs are not gamma rays [40, 41], one may try to force a proton dominance at ultrahigh energies by postulating efficient absorption of the dominant ultrahigh energy photon flux on the universal and/or galactic radio background. However, the neutrino flux accompanying a normalized proton flux is inevitably increased to a level where it should be within reach of operating experiments such as AGASA [539].

Certainly, the precise decay modes of the X particles and the detailed dynamics of the first secondary particles depend on the exact nature of the particles under consideration. However, one expects the bulk flow of outgoing particles to be almost independent of such details. Moreover, the gross features of the hadronic jet systems can be reasonably well described by using Local Parton-Hadron Duality (LPHD) [540, 541]. In this approach, the primary hadron spectrum is taken to be the same, up to an overall normalization constant, as the spectrum of partons in the parton cascade after evolving the latter all the way down to a cutoff transverse momentum $\langle k_{\perp}^2 \rangle_{\text{cutoff}}^{1/2} \sim \text{few hundred MeV}$. A common picture for the parton cascade evolution is provided by the so-called Modified Leading Logarithmic Approximation (MLLA) of QCD [542, 543]. Within this approximation the energy spectrum can be expressed analytically, and simplifies considerably when the QCD scale Λ_{eff} is equal to the transverse momentum cutoff, \tilde{Q}_0 . In such a limiting case the energy distribution of the partons is given by [540, 541, 544]

$$x \frac{dN_{\text{part}}}{dx} = \frac{4C_F}{b} \Gamma(B) \int_{-\pi/2}^{\pi/2} \frac{d\ell}{\pi} e^{-B\alpha} \left[\frac{\cosh \alpha + (2\xi/Y - 1) \sinh \alpha}{(4N_c/b) Y (\alpha/\sinh \alpha)} \right]^{B/2} \times I_B \left\{ \left[\frac{16N_c}{b} Y \frac{\alpha}{\sinh \alpha} [\cosh \alpha + (2\xi/Y - 1) \sinh \alpha] \right]^{1/2} \right\}, \quad (181)$$

where dN_{part} is the number of partons with a fraction $(x, x + dx)$ of the energy E_{jet} of the original jet-initiating quark q , $\xi = \ln(1/x)$, $Y = \ln(E_{\text{jet}}/\Lambda_{\text{eff}})$, and $\alpha = [\tanh^{-1}(1 - 2\xi/Y) + i\ell]$. I_B is the modified Bessel function of order B , where $B = a/b$ with

⁴¹ A cosmic necklace is a possible hybrid TD consisting of a closed loop of cosmic string with monopole “beads” on it [537].

$a = [11N_c/3 + 2n_f/(3N_c^2)]$ and $b = (11N_c - 2n_f)/3$, n_f is the number of flavors of quarks, $N_c = 3$ is the number of colors, and $C_F = (N_c^2 - 1)/2N_c = 4/3$. Now, using LPHD one obtains the fragmentation function due to the hadronization of a quark q ,

$$x \frac{dN_h}{dx} = K(Y) x \frac{dN_{\text{part}}}{dx}, \quad (182)$$

where $x = E_h/E_{\text{jet}}$. The overall normalization constant $K(Y)$, which takes into account the effect of conversion of partons into hadrons, is fixed from the conservation of energy

$$\int_0^1 x \frac{dN_h(Y, x)}{dx} dx = 1. \quad (183)$$

Of course, there is a great uncertainty in the extrapolation of the QCD (MLLA + LPHD) spectra, which has been tested so far only at collider energies, up to super-ultrahigh energies $\gtrsim 10^{23}$ eV. In particular, new processes may alter energy thresholds as well as the content of particles in the jets. For instance, if SUSY turns on at an energy scale M_{SUSY} of \mathcal{O} (TeV), the shower development is expected to tie up not only quarks and gluons but also their supersymmetric partners with equal probability, provided the 4 momentum transfer \tilde{Q} is above the SUSY scale. Once $\tilde{Q} < M_{\text{SUSY}}$, the SUSY particles in the cascade would decouple from the cascade, and eventually decay into the stable LSPs. In such a case, the final state may contain ultrahigh energy LSPs [545], thus modifying the shape of the fragmentation spectrum [546].

It is clear that the wide variety of TDs produce X particles at different rates. However, as noted in [516], the X particle production rate, \dot{n}_X , may be parametrized on dimensional grounds in a very general way,

$$\dot{n}_X(t) = \frac{Q_0}{m_X} \left(\frac{t}{t_0} \right)^{-4+p}, \quad (184)$$

where t is the Hubble time, t_0 denotes the present age of the Universe, and $Q_0 \equiv \dot{n}_X(t_0) m_X$ is the rate of energy injected in the form of X particles of mass m_X per unit volume in the present epoch. In most cases $p = 1$. Exceptions are superconducting string models where $p \leq 0$, or decaying vortons which have $p = 2$. Certainly, the evolutionary properties of the TD system are unknown, and so one is not able to infer the value Q_0 *a priori* in a parameter-free manner. However, if a TD scenario is to explain the origin of ultrahigh energy CRs, Eq. (184) can be normalized to account for the super-GZK events without violating any observational flux measurements or limits at higher or lower energies, as shown in Fig. 25. The top-down neutrino and gamma ray fluxes depend on the energy released integrated over redshift, and thus on the specific TD model. Note that the electromagnetic energy injected into the Universe above the pair production threshold on the CMB is recycled into a generic cascade spectrum below

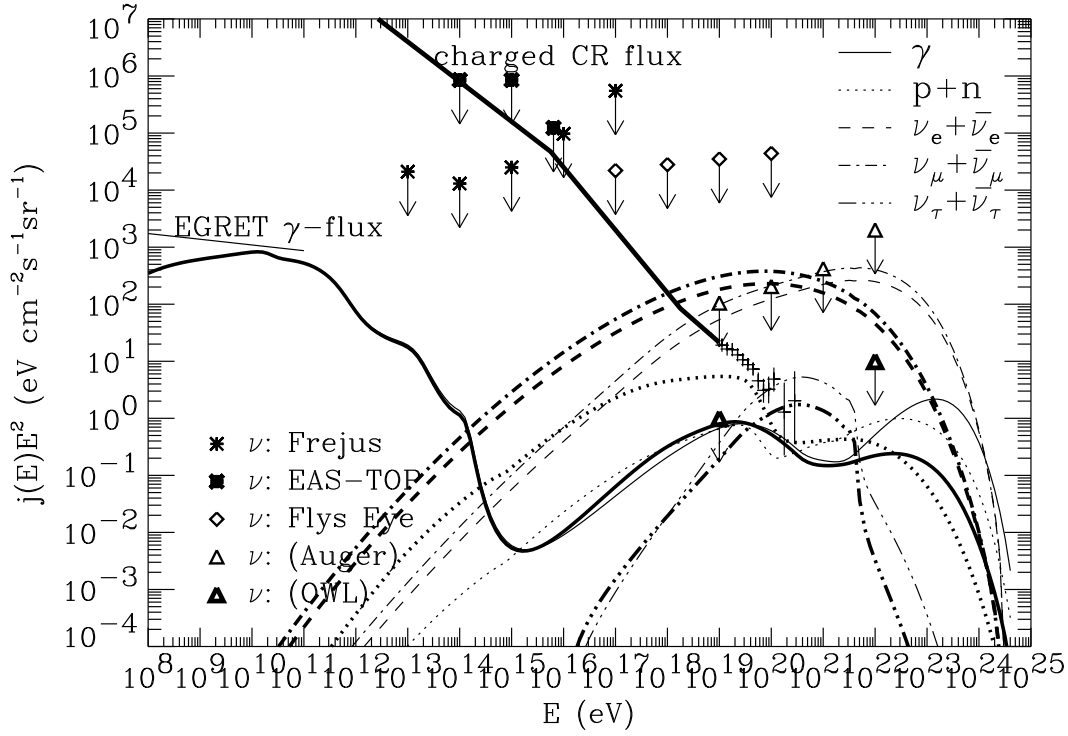


FIG. 25: Energy-weighted spectra of nucleons, γ -rays and neutrinos for the TD model with $m_X = 10^{16}$ GeV, $p = 1$, and decay mode $X \rightarrow q + q$, assuming an EGMF of 10^{-10} G. Thick and thin lines represent the SUSY and no-SUSY fragmentation functions, respectively. The 1 sigma error bar crosses represent combined data from the Haverah Park, Fly’s Eye, and AGASA experiments above 10^{19} eV. Also shown are piecewise power law fits to the observed charged CR flux below 10^{19} eV, the EGRET measurement of the diffuse γ -ray flux between 30 MeV and 100 MeV, experimental neutrino flux limits from Frejus and Fly’s Eye, as well as projected neutrino sensitivities of PAO and NASA’s OWL project. Published in Ref. [547].

this threshold on a time scale short compared with the Hubble time. Therefore, it can have several potential observable effects, such as modified light element abundances due to ^4He photodisintegration, or induce spectral distortions of universal gamma-ray and neutrino backgrounds [548, 549]. In particular, measurements of the diffuse gamma ray background in the 100 MeV region, to which the generic cascade spectrum would contribute directly, limit significantly the parameter space in which TDs can generate the flux of the highest energy CRs [232, 550, 551, 552].

Super-heavy relics: The highest energy CRs may also be produced from the decay of some metastable superheavy relic particle with mass $\gtrsim 10^{12}$ GeV and lifetime exceeding the age of the Universe [518, 519, 520, 521]. Of course, there are no metastable superheavy relics within the SM. However, a number of candidate metastable relics are

predicted in theories beyond the SM [553, 554, 555, 556, 557, 558, 559, 560, 561, 562, 563, 564, 565, 566]. Here, the predicted CR flux is driven by the ratio of the density of the relics to their lifetime. Since the decay should occur within the GZK-sphere, a reasonable parametrization of the decay rate is

$$\dot{n}_X = \frac{n_X}{\tau_X} \quad (185)$$

where τ_X is the relic's lifetime, $n_X = \rho_c \Omega_X h^2 / m_X$, is the relic density, Ω_X is the cosmic average mass density contributed by the superheavy relics in units of the critical density $\rho_c \approx 1.05 \times 10^{-4} h^2 \text{ GeV cm}^{-3}$, and h is the present value of the Hubble constant in units of $100 \text{ km sec}^{-1} \text{ Mpc}^{-1}$. Clearly, neither Ω_X nor τ_X is known with any degree of confidence. Additionally, as in the case of TDs, the details of the CR spectrum depend on the fragmentation function. Several models have been used to approximate the fragmentation in superheavy relic decay, including the HERWIG Monte Carlo program [567], MLLA [568, 569], numerical integration of the Dokshitzer-Gribov-Lipatov-Altarelli-Parisi (DGLAP) equations [570, 571, 572], as well as a combination of MLLA (for small x) and DGLAP (for large x) [573]. In general, these approaches all yield similar results in the region 10^{19} – 10^{20} eV [568]. As an example, Fig. 26 shows the resulting ultrahigh energy CR flux from the decay of relics ($m_X = 5 \times 10^{12}$ GeV) clustered in the halo of our Galaxy (more on this below) obtained by numerical solution of the DGLAP equations, including effects of SUSY [570]. The hard injection spectra in top-down scenarii ($\propto E^{-1}$) have roughly the inverse structure to that of the attenuation length of baryonic CRs and γ -rays. Therefore, over the limited energy range $\sim 10^{19.5}$ – 10^{20} eV, where the attenuation length drops quickly, the attenuated spectra can be easily fitted to the observed spectrum. However, the spectra of such models have entirely the wrong shape below the photopion production threshold, and at $10^{18.7}$ eV, where the flux is well measured, the predicted flux is more than an order of magnitude too small (see Figs. 25 and 26). Thus, to be consistent with observations, top-down models need to be smoothly matched to a bottom-up model which describes the spectrum below the GZK energy [574]. An elegant explanation which can account for all the events with energy $\gtrsim 10^{19.0}$ eV can be concocted by mixing the neutrino fluxes of top-down models with the Z -burst mechanism ($m_{\nu_j} = 0.07$ eV) [575, 576]. This hybrid scenario predicts that most primaries above the ankle should be nucleons up to 10^{20} eV (with a slight accumulation at the GZK energy) and photons at higher energies. In addition, the model predicts a new break in the observed spectrum above 10^{20} eV, reflecting the hard top-down spectra.

Under certain circumstances the superheavy relics could also constitute the dark matter (DM) of the Universe.⁴² Even though the nature of the DM is still unknown,

⁴² Nowadays there is mounting evidence that about 90% of the matter in our Universe may be dark.

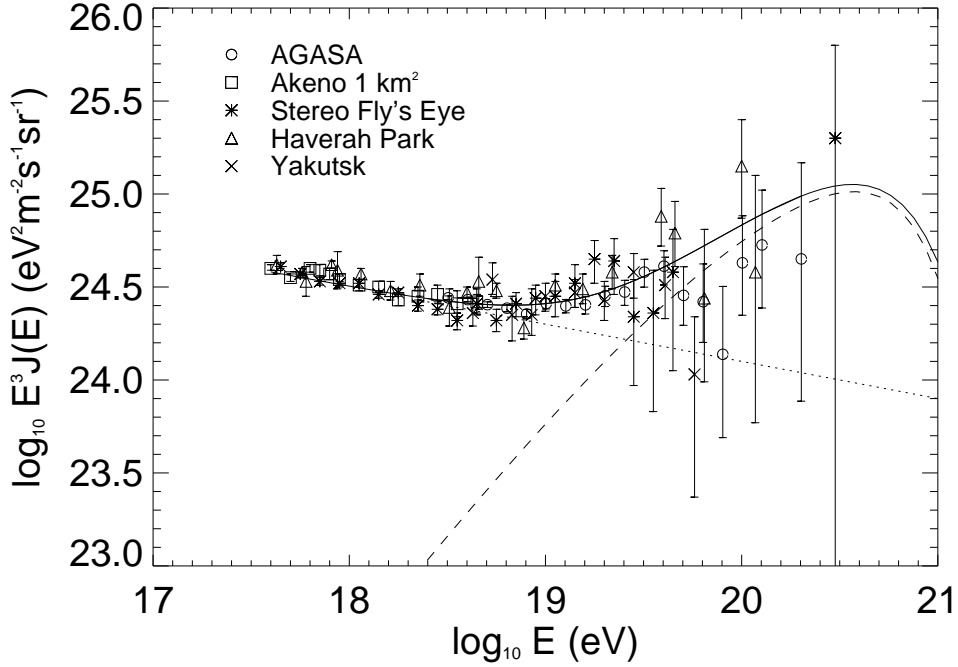


FIG. 26: The best SUSY evolution fit to the CR data with a decaying particle mass of 5×10^{12} GeV (*cf.* Fig. 25). The dotted line indicates the extrapolation of the power law component from lower energies, the dashed line shows the decay spectrum, and the solid line is their sum. It is important to stress that this model would have an anomalous accumulation factor (see Sec.V). Published in [570].

the DM hunt traditionally concentrates on particles with mass of the order of the weak scale and with interaction with ordinary matter on the scale of the weak force. Importantly, big bang nucleosynthesis constraints imply that such weakly interacting massive particles (WIMPs) cannot be baryonic, and must therefore comprise non-SM particles. If the WIMP is a thermal relic, then it was once in local thermodynamic equilibrium in the early Universe, and its present abundance is determined by its self-annihilation cross section. The largest annihilation cross section at early times is expected to be $\propto m_X^{-2}$. This implies that heavy WIMPs would have such a small annihilation cross section that their present abundance would be too large. Therefore, the mass of a thermal WIMP is found to be less than about 500 TeV [584]. Nevertheless, it was recently put forward that DM particles may have never experienced local thermal equilibrium, and so their masses may be as high as 10^{12} – 10^{19} GeV [559, 560, 561, 562,

Current observations supporting the DM hypothesis include gravitational lensing [577, 578], peculiar velocities of large scale structures [579, 580], CMB anisotropy [581, 582], and recession velocities of high redshift supernovae [583].

563, 564, 565]. Such monsters have been christened “wimpzillas” [585]. One of the more promising candidates is the “crypton”, the analog of the hadron in the hidden sector of supersymmetry breaking string theories [560]. Cryptons naturally emerge from the theory with about the right mass, they are cosmologically stable, and their interaction rate is sufficiently weak such that thermal equilibrium with the primordial plasma was never obtained. Furthermore, a sufficient abundance of these particles could have been produced near the end of the inflationary epoch.

If superheavy relics play the role of DM, then irrespective of the abundance Ω_X the ratio of the mass density contribution from X particles to that from DM particles should be roughly the same everywhere in the Universe, because both X and DM particles respond to gravity in the same way. Therefore, since DM particles (by definition) cluster on galactic halos, so will the X particles. This suggests that a clean signature of the superheavy relic X hypothesis is the anisotropy imposed by the asymmetric position of the sun in the Galactic halo [586, 587, 588]. The exact value of this asymmetry is, however, model dependent, because the distribution of dark matter inside the halo is by no means certain. The study in [589], following the *cusped* Navarro-Frenk-White (NFW) DM density distribution [590], gives a substantial anisotropy signal in the arrival direction of ultrahigh energy CRs. Indeed, the analysis seems to indicate that less than 10% of the ultrahigh energy CRs could come from relic particles in the Galactic halo. However, recent observations suggest that the NFW profile, for which the inner regions are dominated by DM, does not give an accurate description of the Galaxy [591]. Specifically, the mass density implied by the luminous disk is already sufficient to account for the rotation curve in the inner Galaxy without any contribution from DM [592]. In addition, the microlensing optical depth to the red clump stars already shows that almost all the density in the inner Galaxy must be in the form of compact objects that yield microlensing, and therefore cannot be DM [593, 594].

Recently, Evans, Ferrer and Sarkar (EFS) [595] have analyzed in detail the dependence of the expected CR anisotropy with the DM density distribution in the Galaxy. They studied 4 typical models of the dark matter halo: *cusped*, *isothermal*, *triaxial*, and *tilted* (see Appendix F). In these models, the amplitude of the anisotropy is controlled by the extent of the halo, whereas the phase is controlled by its shape. The results of EFS, given in Fig. 27, show that the amplitude, which is ~ 0.5 for a *cusped* halo, falls to 0.3 for an *isothermal* halo with realistic core radii. The phase points in the direction of the Galactic center, with deviation of up to 30° when considering *triaxial* and *tilted* haloes. These amplitudes and phases are very similar to those obtained by Medina-Tanco and Watson in a separate analysis [597]. Unfortunately, the current CR data are too sparse above 10^{19} eV to have statistically significant discriminators between any dark halo model density profiles, or to either confirm or refute any correlation with the Galactic halo. Moreover, due to the limited size of the present ultrahigh energy

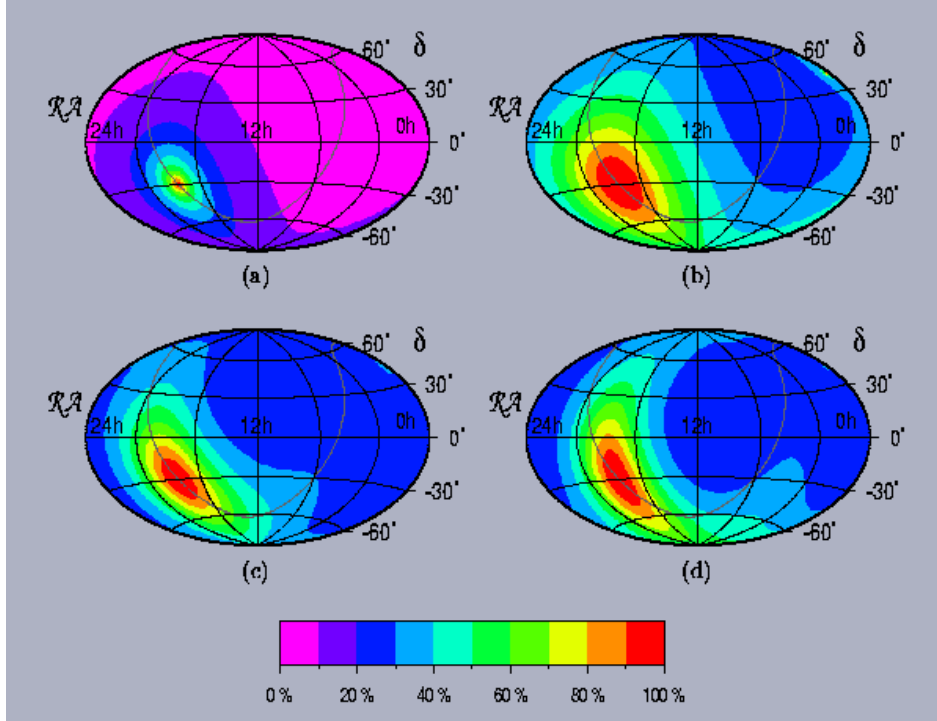


FIG. 27: Contour plots in equatorial coordinates ($\mathcal{R}\mathcal{A}$, δ) of the predicted ultrahigh energy cosmic ray sky for 4 different dark halo models (from left to right, downwards: *cusped*, *isothermal*, *triaxial* and *tilted*). The effect of the halo of M31 is seen in the upper right of each plot: a hotspot at $\mathcal{R}\mathcal{A} \approx 00^{\text{h}} 43^{\text{m}}$, $\delta \approx 41^{\circ}$ (referred to the J2000.0 epoch). Published in [596].

CR sample, nothing can yet be said about the hypothesized existence of an ultrahigh energy CR contribution originating in the dark halo of Andromeda (M31) [595, 597]. Certainly these issues will be resolved by PAO after a few years of operation.

B. Monopoles and other topological defects as primaries

It has long been known that any early Universe phase transition occurring after inflation which leaves an unbroken $U(1)$ symmetry group may produce magnetic monopoles [598, 599]. For instance, minimal $SU(5)$ breaking may lead to “baryonic monopoles” of mass $M \sim T_c/\alpha$, with magnetic charge $U(1)_{\text{EM}}$ and chromomagnetic $SU(3)_C$ [600]. Here α stands for the fine structure constant at symmetry breaking temperature T_c . These monopoles easily pick up energy from the magnetic fields permeating the Universe and can traverse unscathed through the primeval radiation. Thus,

they are likely to generate extensive air showers [522, 601, 602].⁴³ Before proceeding further, it is important to point out that if the monopoles are formed at the usual GUT scale $\sim 10^{15}$ GeV, the energy density overcloses the Universe. Thus, to avoid this effect, the symmetry breaking scale associated with the production of monopoles has to be shifted to lower energies. Remarkably, if the GUT scale is at $\sim 10^9$ GeV, one would end up with an abundance of relativistic monopoles well below the closure limit, and yet potentially able to explain the tail of the CR-spectrum. In addition, for such a critical temperature the observed flux of ultrahigh energy CRs is below the flux allowed by the Parker limit.⁴⁴ Unfortunately, contrary to the observed CR arrival directions, the expected flux of relativistic monopoles would be highly anisotropic, roughly aligned with the magnetic lines near the Earth [605].

In models with large extra dimensions, the low-scale unification enables the production of light-mass monopoles, say $M \sim 100$ TeV. Furthermore, the physical embodiment of these theories would allow a natural generalization of the 't Hooft-Polyakov monopole providing a convenient set of representations for D1-branes ending on D3-branes, and consequently even lighter monopoles [606]. The light-mass monopoles could lose and gain energy as they random-walk towards the Earth. The maximum energy attainable before hitting the atmosphere is roughly 10^{25} eV [607]. Therefore, these “particles” would be ultra-relativistic, and the expected flux would have no imprint of correlation with the local magnetic field. Note, however, that direct searches at accelerators pretty much exclude masses below a few hundreds of GeV, whereas bounds stemming from quantum effects on current observables turn out to be ~ 1 TeV [608]. The value for the lower limit of the mass of the monopole is still under debate [609].

To mimic a shower initiated by a proton the monopole must transfer nearly all of its energy to the atmospheric cascade in a very small distance. The large inertia of a massive monopole makes this impossible if the cross-section is typically strong, say ~ 100 mb. Wick, Kephart, Weiler and Biermann (WKWB) [607] have recently pointed out that this problem can be avoided in models in which the baryonic monopole consists of q -monopoles confined by strings of chromomagnetic flux. To describe the interactions of such a monopole in air, WKWB have developed a model based on the four following axioms: i) before hitting the atmosphere the monopole-nucleus cross section (unstretched state) is roughly hadronic ($\sigma_0 \sim \Lambda_{\text{QCD}}^{-2}$), attaining a geometric growth after the impact; ii) in each interaction almost all of the exchanged energy goes into stretching the chromomagnetic strings of the monopole; iii) the chromomagnetic

⁴³ The idea of monopoles as constituents of primary cosmic radiation is actually quite old, it can be traced back at least as far as 1960 [603].

⁴⁴ This bound requires that there not be so many monopoles around as to effectively “short out” the Galactic magnetic field [604].

strings (of tension $T \sim \Lambda_{\text{QCD}}^{-1}$) can only be broken to create monopole-antimonopole pairs, a process highly suppressed and consequently ignored; iv) the average fraction of energy transferred to the shower in each interaction is soft $\Delta E/E \equiv \eta \approx \Lambda_{\text{QCD}}/M$. Generally speaking, in this set-up the monopole will penetrate into the atmosphere, because the cross section is comparable to that of a high energy proton. However, since the geometrical cross-section grows proportionally with the Lorentz factor Γ , the interaction length after the impact shrinks to a small fraction of the depth of the first interaction. Stated mathematically, the unstretched monopole's string length, $L \sim \Lambda_{\text{QCD}}^{-1}$, increases by $\delta L = \Delta E/T$. Recalling that nearly all of the exchanged energy goes into stretching the color magnetic strings, the fractional increase in the length is $\delta L/L = \Gamma$, yielding $\sigma_1 \sim (1 + \Gamma)/\Lambda_{\text{QCD}}^2$. Now, the total mean free path after the N -th interaction reads,

$$\lambda_N \sim \frac{1}{\sigma_N n_{\text{nuc}}} \sim \frac{\Lambda_{\text{QCD}}^2}{(1 + \sum_{j=1}^N \Gamma_j) n_{\text{nuc}}} \sim \frac{\Lambda_{\text{QCD}}^2}{N \Gamma n_{\text{nuc}}}, \quad (186)$$

where we have assumed a constant density of nucleons ($n_{\text{nuc}} \approx (4/3) \pi A R_0^3$) and we have used the approximation $\Gamma_N \sim (1 - \Lambda_{\text{QCD}}/M)^N \Gamma \sim \Gamma$. Here A stands for the mass number of an atmospheric nucleus, and $R_0 \approx 1.2 - 1.5$ fm. It should also be stressed that for $N = \eta^{-1}$ the approximation has an error bounded by $\lim_{N \rightarrow \infty} (1 - N^{-1})^N = e^{-1}$. For $\eta^{-1} \gg 1$, the total distance traveled between the first interaction and the η^{-1} -th interaction is then

$$\Delta X \sim \frac{\Lambda_{\text{QCD}}^2}{\Gamma n_{\text{nuc}}} \sum_{N=1}^{\eta^{-1}} \frac{1}{N} \sim \frac{\Lambda_{\text{QCD}}^2}{\Gamma n_{\text{nuc}}} \ln \eta^{-1}. \quad (187)$$

Note that the mean free path for all secondary interactions is $\mathcal{O}(1/\Gamma)$ of the first one. Thus, a baryonic monopole encountering the atmosphere will diffuse like a proton, producing a composite heavy-particle-like cascade after the first interaction. A distinctive feature of the monopole shower would be the great number of muons among all the charged particles [610]. Although this feature was observed in a poorly understood super-GZK event [611], it seems unlikely that a complete explanation for the ultrahigh energy CR data sample would be in terms of magnetic monopoles alone. Moreover, any confirmed directional pairing of events would appear difficult to achieve with the monopole hypothesis.

An alternative TD that can be easily accelerated to ultrahigh energies is the vorton [523]. However, the interaction properties of vortons with ordinary matter are completely uncertain, and so no clear predictions can be made.

IX. THE ATMOSPHERE AS A BLACK HOLE FACTORY

In this chapter we shift the focus of our discussion from what CRs tell us about astrophysical phenomena to what they tell us about fundamental interactions. In particular, ultrahigh energy CR neutrinos provide a means to probe the fundamental Planck scale in a regime not currently accessible to man-made accelerators. If Planck scale is of $\mathcal{O}(\text{TeV})$, then cosmic neutrinos could produce microscopic BHs when they interact in the atmosphere. The BHs would decay promptly, initiating deeply developing showers far above the SM rate [612], and with very distinctive characteristics when the BH entropy $\gg 1$ [613]. In the subsequent sections, we discuss first the phenomenology of BH production, and then experimental signatures for BHs created in CR events [253]. For dessert, we examine the parameter space left for p -brane production [614, 615].

A. Black hole production in particle collisions

Black holes (BHs) are among the most fascinating and inaccessible phenomena in nature. It has been known for quite a long time that microscopic BHs can be produced in particle collisions with c.m. energies above the fundamental scale of gravity [616, 617, 618, 619], where they should be well described semi-classically and thermodynamically [620]. In the ordinary 4-dimensional scenario, where the fundamental scale of gravity is $\sim 10^{19}$ GeV, the study of such BHs is hopelessly beyond the realm of experimental particle physics. However, if TeV scale gravity is realized in nature, production of BHs should be observed in particle collisions with $\sqrt{s} \gg 1$ TeV and sufficiently small impact parameter [621, 622, 623, 624, 625].

The ensuing discussion will be framed in the context of large extra dimensions [471], and will be valid at distances that are small compared to the compactification radius r_c . The requirements for validity of the picture in the warped scenario [474, 626] are discussed in Appendix G. For purposes of normalization we use the notation of Ref. [627], where the fundamental mass scale reads

$$M_D = [(2\pi)^n / 8\pi]^{1/(n+2)} M_* , \quad D = 4 + n . \quad (188)$$

The radius of a Schwarzschild BH of mass $M_{\text{BH}} = \sqrt{\hat{s}}$ in $(4 + n)$ dimensions is [628]

$$r_s(M_{\text{BH}}) = \frac{1}{M_D} \left[\frac{M_{\text{BH}}}{M_D} \right]^{\frac{1}{1+n}} \left[\frac{2^n \pi^{(n-3)/2} \Gamma(\frac{n+3}{2})}{n+2} \right]^{\frac{1}{1+n}} . \quad (189)$$

If one envisions a head-on collision involving partons i and j with c.m. energy $\sqrt{\hat{s}} = M_{\text{BH}}$ and impact parameter less than r_s , semiclassical reasoning suggests that a BH

would be formed [629].⁴⁵ The total cross section of the process can be estimated from geometrical arguments [624, 625] and is of order

$$\hat{\sigma} \sim \pi r_s^2. \quad (190)$$

Criticisms [630, 631] of this cross section, which center on the exponential suppression of transitions involving a (few-particle) quantum state to a (many-particle) semiclassical state, have been addressed in [632, 633, 634, 635, 636]. However, it is worthwhile to point out that the heuristic arguments supporting Eq. (190) only determine $\hat{\sigma}$ up to an overall factor of order one [253]. Uncertainties in this factor are due, for instance, to the inclusion of angular momentum when considering BH creation for collisions with non-zero impact parameter.

Note that even though the colliding particles are confined to the brane, if $r_s \ll r_c$ then the BH should be treated as a fully $(4+n)$ dimensional object in an asymptotically Minkowskian spacetime. In addition, for $\sqrt{s} \gg M_D$, BH production should dominate over all other SM processes because of the rapidly increasing cross section $\hat{\sigma} \propto \hat{s}^{1/(n+1)}$. To calculate the total production cross section, we have to take into account that only a fraction of the total c.m. energy in a collision is available to the parton participating. In our discussion of BH production in the atmosphere, we are most interested in collisions of ultrahigh energy neutrinos with the nucleons in the air molecules, where [612]

$$\sigma_{\nu N \rightarrow \text{BH}}(E_\nu) = \sum_i \int_{(M_{\text{BH}}^{\text{min}})^2/s}^1 dx \hat{\sigma}_i(\sqrt{xs}) f_i(x, Q). \quad (191)$$

Here, $s = 2m_N E_\nu$, f_i are parton distribution functions, $M_{\text{BH}}^{\text{min}}$ is the minimum BH mass for which the parton cross section into BHs is applicable, and the sum is carried out over all partons in the nucleon. The momentum transfer Q is set to $\min\{M_{\text{BH}}, 10 \text{ TeV}\}$, where the upper limit comes from the CTEQ5M1 distribution functions [637]. The cross section $\sigma_{\nu N \rightarrow \text{BH}}$ is highly insensitive to the details of this choice [612]. Once produced, the BH will Hawking evaporate with a temperature proportional to the inverse radius

$$T_H = \frac{n+1}{4\pi r_s}. \quad (192)$$

Note that the wavelength $\lambda = 2\pi/T_H$ corresponding to this temperature is larger than the BH size. Hence, to first approximation the BH behaves like a point-radiator with entropy [253]

$$S = \frac{4\pi M_{\text{BH}} r_s}{n+2}. \quad (193)$$

⁴⁵ Here, $\hat{s} \equiv xs$, where x is the parton momentum fraction and s is the square of the c.m. energy.

The BH lifetime estimated from [638]

$$\frac{dE}{dt} \sim A T_H^{4+n} \quad (194)$$

is found to be

$$\tau_{\text{BH}} \sim \frac{1}{M_D} \left(\frac{M_{\text{BH}}}{M_D} \right)^{\frac{3+n}{1+n}}, \quad (195)$$

where A is the horizon area. For $M_{\text{BH}} \gg M_D$, the BH is a well defined resonance and may be thought of as an intermediate state in the s channel. This means that the decay of a BH is only sensitive to the radial coordinate and does not make use of the angular modes available in the bulk. Therefore, BHs decay with equal probability to a particle on the brane and in the bulk [622, 624, 625].⁴⁶ Since there are many more particles on the brane, we expect the BH to decay visibly into SM particles giving rise to events with large multiplicity, $\langle N \rangle \approx M_{\text{BH}}/(2T_H)$, large total transverse energy, and a characteristic ratio of hadronic to leptonic activity of roughly 5:1. As M_{BH} approaches M_D , semiclassical arguments are no longer valid, because the BHs become “stringy” and their properties rather complex.

The magnitude of the entropy determines the validity of the semiclassical approximation. Thermal fluctuations due to particle emission are small when $S \gg 1$ [640], and statistical fluctuations in the microcanonical ensemble are small for $\sqrt{S} \gg 1$ [624]. Searches for BH production at colliders are viable when $x_{\text{min}} \equiv M_{\text{BH}}^{\text{min}}/M_D$ is high enough that the decay branching ratios predicted by the semiclassical picture of BH evaporation are reliable. The QCD background is large, and therefore the extraction of signal from background at hadron colliders depends on knowing the BH decay branching ratios reliably [624, 625, 641, 642, 643, 644, 645, 646, 647, 648, 649, 650, 651]. Therefore, in searches at colliders a cutoff of $x_{\text{min}} = 5.5$ or more may be appropriate. In contrast, the search for deeply penetrating quasi-horizontal showers initiated by BH decay products can afford to be much less concerned with the details of the final state, since the background from hadronic showers is filtered out by the atmosphere. As a result, the signal relies only on the existence of visible decay products, which, in this context, includes all particles other than neutrinos, muons, and gravitons. Indeed, there is very little about the final state, other than its total energy and to some degree its multiplicity and electromagnetic component [613], that we can reasonably expect to observe, since detailed reconstruction of the primary BH decay process is not possible at cosmic ray detectors. With this in mind, one can choose a significantly lower value of $M_{\text{BH}}^{\text{min}}$ than the one needed for collider searches. Although BHs of mass around M_D will be outside the semiclassical regime, it seems quite reasonable to expect that they, or

⁴⁶ One caveat is that BHs may jump off the brane, as suggested in a recent article [639].

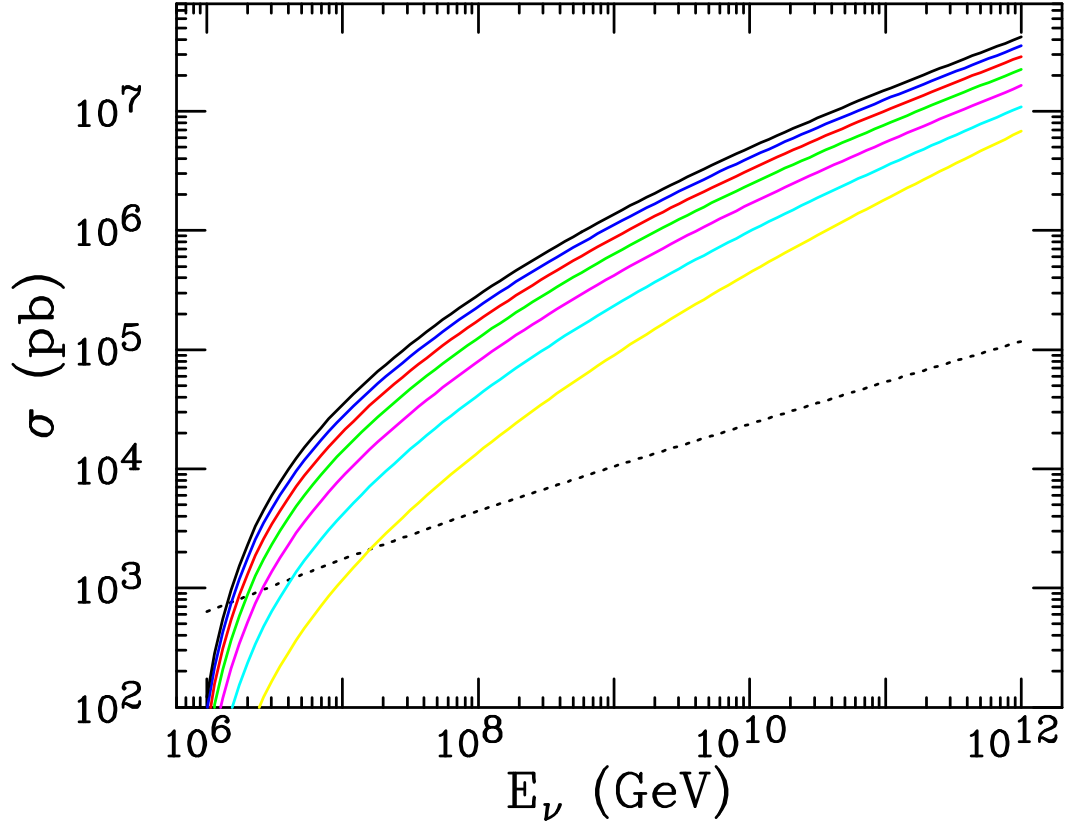


FIG. 28: Cross sections $\sigma_{\nu N \rightarrow \text{BH}}$ for $n = 1, \dots, 7$ (bottom to top) for $M_D = 1 \text{ TeV}$, $x_{\min} = 1$. The SM cross section [124] is indicated with a dotted line. Published in Ref. [253].

their stringy progenitors, will nevertheless decay visibly, whatever stringy or quantum gravitational description applies.

Cross sections for BH production by cosmic neutrinos are given in Fig. 28.⁴⁷ They scale as

$$\sigma_{\nu N \rightarrow \text{BH}} \propto \left[\frac{1}{M_D^2} \right]^{\frac{2+n}{1+n}}. \quad (196)$$

Despite the fact that the BH production cross section reduces the neutrino interaction length to

$$\lambda_\nu = 1.7 \times 10^7 \text{ km w.e.} \left(\frac{\text{pb}}{\sigma} \right), \quad (197)$$

the Earth's atmospheric depth, which is only 0.36 km w.e. even when traversed horizontally, is still smaller than λ_ν . Neutrinos therefore produce BHs uniformly at all

⁴⁷ It should be stressed that the neutrino-gluon scattering may dominate neutrino-nucleon collisions below 10^8 GeV [652].

atmospheric depths.

B. Probes of TeV scale gravity in CR experiments

Given the provocative new features of models with large-compact-dimensions (LCDs), there is a strong motivation for phenomenological studies to assess their experimental viability. The most obvious consequence of the existence of LCDs is the violation of Newton's Gravitational Law at distances of order r_c . Applying Eq. (167) for $n = 1$ one obtains $r_c \sim 10^{13}$ cm, which immediately suggests this case is excluded because Newtonian gravity would be modified at the scale of our solar system. For $n \geq 2$, r_c is sufficiently small so that these scenarii are not yet excluded. For $n = 2$, sub-millimeter tests of the gravitational inverse-square law constrain $M_D > 1.6$ TeV [478]. For $n \geq 3$ LCDs become microscopic and therefore elude the search for deviations in gravitational measurements. In the presence of LCDs, however, the effects of gravity are enhanced at high energies due to the large multiplicity of KK-modes, yielding astrophysical bounds on r_c . For instance, the requirement that the neutrino signal of SN 1987A not be unduly shortened by the emission of KK modes into the bulk leads to $M_D \gtrsim 50$ TeV, for $n = 2$, and $M_D \gtrsim 5$ TeV, for $n = 3$ [653, 654]. These limits could be even more restrictive when taking into account KK graviton decay in typical astrophysical environments, yielding $M_D \gtrsim 600 - 1800$ TeV for $n = 2$ and $M_D \gtrsim 10 - 100$ TeV for $n = 3$ [655, 656, 657, 658].

For $n \geq 4$, only high energy colliders and CR-experiments provide reasonably sensitive probes of LCDs. The effects of direct graviton emission, including production of single photons or Z 's, were sought at LEP [659, 660]. The resulting bounds are fairly model-independent, as the relatively low energies at LEP imply a negligible dependence on any soft-brane damping factor. For $n = 4$ (6), these null results imply $M_D \gtrsim 870$ (610) GeV [661]. The effects of low-scale gravity can also be seen through virtual graviton effects. These are most stringently bounded by the DØ Collaboration, which recently reported [662] the first results for virtual graviton effects at a hadron collider. The data collected at $\sqrt{s} = 1.8$ TeV for dielectron and diphoton production at the Tevatron agree well with the SM predictions and provide restrictive limits for $n \geq 4$. Specifically, if one adopts a Gaussian cutoff on the transverse momentum of the graviton due to brane excitations, $M_D \gtrsim 1$ TeV [253].

Limits on the fundamental Planck scale derived from CR-observations are mainly due to searches for BH production in the atmosphere by ultrahigh energy neutrinos [253, 663, 664]. The number of BHs to be detected by a given CR-experiment is

$$N = \int dE_\nu N_A \frac{d\Phi}{dE_\nu} \sigma_{\nu N \rightarrow \text{BH}}(E_\nu) A(E_\nu) T, \quad (198)$$

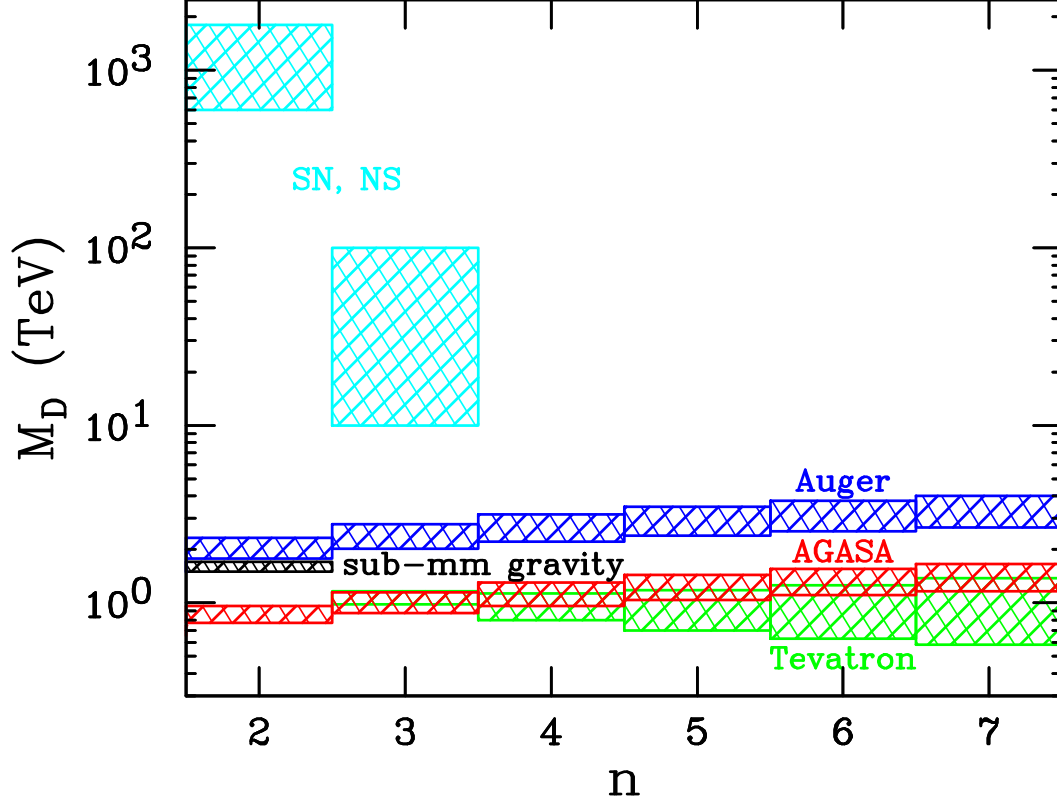


FIG. 29: Bounds on the fundamental Planck scale M_D from tests of Newton’s law on sub-millimeter scales, bounds on supernova cooling and neutron star heating, dielectron and diphoton production at the Tevatron, and non-observation of BH production at AGASA. Future limits from PAO ground array, assuming 5 years of data and no excess above the SM neutrino background, are also shown. The range in Tevatron bounds corresponds to the range of a brane-softening parameter which sets the Gaussian cutoff (see text). The range in cosmic ray bounds is for $x_{\min} = 1 - 3$. Published in Ref. [253].

where $A(E_\nu)$ is the experiment’s acceptance in cm^3 w.e. sr, $N_A = 6.022 \times 10^{23}$ is Avogadro’s number, $d\Phi/dE_\nu$ is the source flux of neutrinos, and T is the running time of the detector. As discussed earlier, for neutrinos with large incident zenith angles the likelihood of interaction is maximized. Observed EASs with $\theta > 70^\circ$ typically must traverse $> 2000 \text{ g/cm}^2$ of atmosphere before interacting. Since the interaction length of the atmosphere for protons is $\sim 45 \text{ g/cm}^2$ one expects the background from hadronic cosmic rays to be eliminated. In 1710.5 days of data collected from December 1995 to November 2000, the AGASA Collaboration found 6 candidate events with $X_{\max} \geq 2500 \text{ g/cm}^2$ [665]. At AGASA, the location of the shower maximum is determined through correlation to two measurable quantities: η , which parameterizes the lateral distribution of charged particles at ground level, and δ , which pa-

parameterizes the curvature of the shower front. The candidate neutrino events must satisfy $X_{\max}^\eta, X_{\max}^\delta \geq 2500 \text{ g/cm}^2$. The expected background from hadronic showers is $1.72^{+0.14+0.65}_{-0.07-0.41}$, where the first uncertainty is from Monte Carlo statistics, and the second is systematic. Of the 6 candidate events, however, 5 have values of X_{\max} that barely exceed 2500 g/cm^2 , and are well within ΔX_{\max} of this value, where ΔX_{\max} is the estimated precision with which X_{\max} can be reconstructed. The AGASA Collaboration thus concludes that there is no significant enhancement of deeply penetrating shower rates given the detector's resolution. The AGASA results imply lower bounds on the scale of low-scale gravity. Of course, the bounds are subject to both small uncertainties inherent in the parton level cross section and uncertainty in the cosmogenic neutrino flux. For the conservative cosmogenic neutrino fluxes given in Fig. 12 the expected rate for deeply penetrating showers at AGASA from SM neutrino interactions is about 0.02 events per year, which is negligible. Given 1 event that unambiguously passes all cuts, and the central value of 1.72 background events, the AGASA results imply an upper bound of 3.5 black hole events at 95% CL [666]. Therefore, the absence of deeply penetrating showers in the AGASA data implies limits on the size of LCDs which are summarized in Fig. 29 [253]. These bounds are conservative. Note that larger cosmogenic neutrino fluxes, as predicted by some models [667], will strengthen them, possibly dramatically. Note also that cosmic neutrino interactions from sub-Planckian extra-dimensional physics can only serve to strengthen these bounds. The absence of a deeply-penetrating signal in the Fly's Eye data also implies lower bounds on M_D . However, these are consistently weaker. The Fly's Eye group searched for deeply developing showers in the sample recorded with the Fly's Eye I during an observation time of $6 \times 10^6 \text{ s}$ [125]. Although they found some events with large incident zenith angle ($\theta > 75^\circ$) [668], the distribution of X_0 , the depth of the first observed interaction, is consistent with $X_0 < 2000 \text{ g/cm}^2$, and there are no events with $X_{\max} \geq 2500 \text{ g/cm}^2$ [125]. This result leads to limits on the size of LCDs. For example, if $n = 6$, $M_D > 900 \text{ GeV}$ [663]. The bounds [126] derived with the combined exposure of the AGASA and Fly's Eye experiments (the latter integrated over all its operating epochs) extend up to 2 TeV for $n = 7$ and $x_{\min} = 1$. Moreover, assuming the conservative value $x_{\min} = 3$, for which the entropy $S > 10$, the bounds derived with the combined exposure, for $n = 5, 6, 7$, are $M_D > 1.26 \text{ TeV}, 1.30 \text{ TeV}, 1.40 \text{ TeV}$, respectively. All of these exceed the Tevatron bounds [662], and represent the best existing limits on the scale of TeV-gravity for $n \geq 5$ extra spatial dimensions.

We now discuss the sensitivity of future CR-experiments. PAO is expected to become fully operational in 2003, and thus would have a running time of roughly 5 years before the LHC begins operation. If no enhancement of quasi-horizontal showers is seen during the pre-LHC epoch, PAO will probe fundamental Planck scales as large as $M_D = 4 \text{ TeV}$ [253, 612, 669]. Moreover, given the prospects for fairly high statis-

tics in the region of high entropy, detailed studies of BH shower profiles [613] are in principle possible. In addition, the projected sensitivity of the OWL satellite project will substantially extend the region of M_D probed in CR-observations before the first collisions at LHC [670]. It should also be stressed that neutrinos that traverse the atmosphere unscathed may produce BHs through interactions in the ice or water. Detailed simulations [671, 672, 673, 674] also find observable BH rates at neutrino telescopes.

In summary, in searches for evidence of TeV scale quantum gravity, CR-experiments are competitive with colliders, and in fact, until the LHC-era, they will provide the most stringent limits.

C. Prospects for distinguishing BH production in neutrino showers

Up to now we have only discussed how to set bounds on physics beyond the SM. An actual discovery of new physics in cosmic rays is a tall order because of large uncertainties associated with the depth of the first interaction in the atmosphere, and experimental challenges of reconstructing cosmic air showers from partial information. However, in the following paragraphs we will discuss an observable which skirts these uncertainties, and may therefore provide a technique for actually discovering BHs in cosmic air showers if TeV-scale quantum gravity exists. If an anomalously large quasi-horizontal shower rate is found, it may be ascribed to either an enhancement on the incoming neutrino flux, or an enhancement in the neutrino-nucleon cross section. However, these two possibilities may be distinguished by separately binning events which arrive at very small angles to the horizontal, the so-called “Earth-skimming” events [127, 128, 129, 130, 131, 132, 133]. An enhanced flux will increase both quasi-horizontal and Earth-skimming event rates, whereas a large BH cross section suppresses the latter, because the hadronic decay products of BH evaporation do not escape the Earth’s crust [612].

Consider a flux of τ -neutrinos in the energy decade 10^{18} to 10^{19} eV. During propagation inside the Earth, a τ -neutrino can produce a tau lepton via a charged current interaction. The interaction length for a neutrino near the Earth’s surface, which is roughly homogeneous with density $\rho_s = 2.15$ g/cm³, is given by

$$\lambda_\nu^{\text{CC}} = [N_A \rho_s \sigma_{\nu N}^{\text{CC}}]^{-1}, \quad (199)$$

where

$$\sigma_{\nu N}^{\text{CC}} = 1.0 \times 10^{-32} \left(\frac{E_\nu}{10^{18} \text{ eV}} \right)^{0.363} \text{ cm}^2 \quad (200)$$

is the charged current cross section accurate to within 10% as given by CTEQ4-DIS parton distribution [124]. Here we neglect neutral current interactions, which at these

energies serve only to reduce the neutrino energy by approximately 20%. Therefore, for $E_\nu \sim 10^{19}$ eV, we have $\lambda_\nu^{\text{CC}} \sim 250$ km. However, if one takes into account the possibility of BH production, the mean free path is reduced to

$$\lambda_\nu^{\text{tot}} = [N_A \rho_s (\sigma_{\nu N}^{\text{CC}} + \sigma_{\nu N \rightarrow \text{BH}})]^{-1} . \quad (201)$$

The energy of the outgoing τ is degraded in Earth by Bremsstrahlung, pair production and deep inelastic scattering, and can be parametrized by

$$\frac{dE_\tau}{dz} = -(\alpha_\tau + \beta_\tau E_\tau) \rho_s , \quad (202)$$

where α_τ is negligible at energies of interest, and $\beta_\tau \approx 0.8 \times 10^{-6}$ cm²/g [675]. The maximal path length for a detectable τ is, then,

$$L^\tau = \frac{1}{\beta_\tau \rho_s} \ln (E_{\text{max}}/E_{\text{min}}) , \quad (203)$$

where $E_{\text{max}} \approx E_\nu$ is the energy at which the tau is created, and E_{min} is the minimal energy at which a τ can be detected. For cosmogenic neutrino fluxes and other reasonable sources, and the acceptances of typical cosmic ray detectors, taus cannot lose much energy and still be detected. For $E_{\text{max}}/E_{\text{min}} = 10$, $L^\tau = 11$ km.

For a given isotropic $\nu_\tau + \bar{\nu}_\tau$ flux, the number of taus that emerge from the Earth with enough energy to be detected is proportional to the ‘‘effective solid angle’’ [132]

$$\Omega_{\text{eff}} \equiv \int d\cos\theta d\phi \cos\theta P(\theta, \phi) , \quad (204)$$

where

$$P(\theta, \phi) = \int_0^\ell \frac{dz}{\lambda_\nu^{\text{CC}}} e^{-z/\lambda_\nu^{\text{tot}}} \Theta [z - (\ell - L^\tau)] \quad (205)$$

is the probability for a neutrino with incident nadir angle θ and azimuthal angle ϕ to emerge as a detectable τ ⁴⁸. Here $\ell = 2R_\oplus \cos\theta$ is the chord length of the intersection of the neutrino’s trajectory with the Earth, where $R_\oplus \approx 6371$ km is the Earth’s radius. Evaluating the integrals, one obtains [133]

$$\Omega_{\text{eff}} = 2\pi \frac{\lambda_\nu^{\text{tot}}}{\lambda_\nu^{\text{CC}}} \left[e^{L^\tau/\lambda_\nu^{\text{tot}}} - 1 \right] \left[\left(\frac{\lambda_\nu^{\text{tot}}}{2R_\oplus} \right)^2 - \left(\frac{\lambda_\nu^{\text{tot}}}{2R_\oplus} + \left(\frac{\lambda_\nu^{\text{tot}}}{2R_\oplus} \right)^2 \right) e^{-2R_\oplus/\lambda_\nu^{\text{tot}}} \right] . \quad (206)$$

⁴⁸ In Eq. (205) we have assumed that BHs produced in the Earth will range out before they can produce a detectable signal.

For $E_\nu \in (10^{18} \text{ eV}, 10^{19} \text{ eV})$, $\lambda_\nu^{\text{tot}} \ll R_\oplus$. Additionally, if the BH cross section is not very large, $\lambda_\nu^{\text{tot}} \gg L^\tau$, and thus Eq. (206) simplifies to

$$\Omega_{\text{eff}} \approx 2\pi \frac{\lambda_\nu^{\text{tot}2} L^\tau}{4R_\oplus^2 \lambda_\nu^{\text{CC}}} . \quad (207)$$

Now, since the τ production is proportional to the incoming neutrino flux Φ^ν , the number of Earth-skimming events detected in 5 years reads

$$N_{\text{ES}} \approx C_{\text{ES}} \frac{\Phi^\nu}{\Phi_0^\nu} \frac{\sigma_{\nu N}^{\text{CC}^2}}{(\sigma_{\nu N}^{\text{CC}} + \sigma_{\nu N \rightarrow \text{BH}})^2} , \quad (208)$$

where C_{ES} is the number of Earth-skimming events expected for the standard cosmogenic flux Φ_0^ν in the absence of BH production. Assuming maximal neutrino mixing and the β_τ value given above, one obtains $C_{\text{ES}} \approx 3.0$ for the PAO ground array [131]. The HiRes fluorescence detectors provide additional sensitivity [132]. In the following discussion we make a conservative assumption of $C_{\text{ES}} = 3.0$ for the SM combined rate over 5 years. The presence of a significant cross section for BH production, as well as their prompt decay and the rapid absorption of the decay products in the Earth, gives rise to a substantial depletion of the ES event rate.

In contrast to Eq. (208), the rate for quasi-horizontal showers follows simply from Eq. (198), and has the form

$$N_{\text{QH}} = C_{\text{QH}} \frac{\Phi^\nu}{\Phi_0^\nu} \frac{\sigma_{\nu N}^{\text{CC}} + \sigma_{\nu N \rightarrow \text{BH}}}{\sigma_{\nu N}^{\text{CC}}} , \quad (209)$$

where $C_{\text{QH}} = 2.5$ for the PAO ground array [105].

Given a flux Φ^ν and BH cross section $\sigma_{\nu N \rightarrow \text{BH}}$, both N_{ES} and N_{QH} are determined. Contours for these two rates are shown in Fig. 30. As can be seen from the figure, it is impossible to differentiate between an enhancement from large BH cross section and large flux, given a quasi-horizontal event rate N_{QH} . However, in the region where significant event rates are expected, the N_{QH} and N_{ES} contours are more or less orthogonal, and thus provide complementary information. With measurements of N_{QH} and N_{ES} , both $\sigma_{\nu N \rightarrow \text{BH}}$ and Φ^ν may be determined independently, and neutrino interactions beyond the SM may be unambiguously identified [253].

As an example, consider the case in which $\sigma_{\nu N \rightarrow \text{BH}}/\sigma_{\nu N}^{\text{CC}} = 3$, and $\Phi^\nu/\Phi_0^\nu = 1$, shown as a dot in Fig. 30. On average, one would then observe a total of $N_{\text{QH}} = 10$ deep quasi-horizontal showers, an excess of 8 above SM expectations. On average, one also expects $N_{\text{ES}} \approx 0.2$ Earth-skimming events. A SM explanation (i.e., $\sigma_{\nu N \rightarrow \text{BH}} = 0$) of the deeply penetrating event rate would require $\Phi^\nu/\Phi_0^\nu = 4$ and predict 12 Earth-skimming events, a possibility that would be clearly excluded at high confidence level. More generally, one might try to salvage a SM explanation by attributing the observed

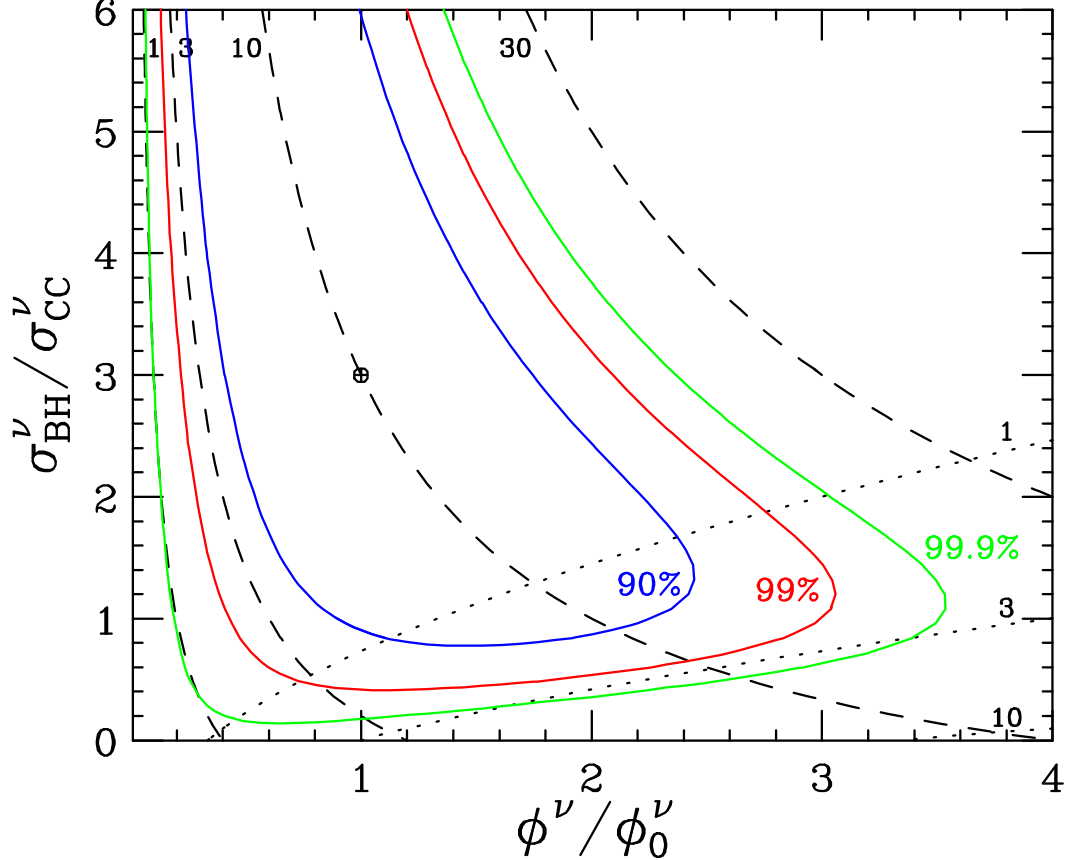


FIG. 30: Contours of constant number of quasi-horizontal showers N_{QH} (dashed) and Earth-skimming neutrino events N_{ES} (dotted) as functions of source flux Φ^ν and BH production cross section $\sigma_{\nu N \rightarrow \text{BH}}$. 5 year running times for PAO and HiRes are assumed. The figure also shows confidence level contours, assuming $\Phi^\nu = \Phi_0^\nu$ and $\sigma_{\nu N \rightarrow \text{BH}} = 3\sigma_{\nu N}^{\text{CC}}$, corresponding to $(N_{\text{QH}}, N_{\text{ES}}) \approx (10, 0.2)$. Published in Ref. [253].

rates to statistical fluctuations in both N_{QH} and N_{ES} . Figure 30 shows contours of constant χ^2 using a maximum likelihood method for Poisson-distributed data [676]. It is easily seen that the possibility of a SM interpretation along the $\sigma_{\nu N \rightarrow \text{BH}} = 0$ axis would be excluded at greater than 99.9% CL for any assumed flux.

BH production will most likely be accompanied by more model-independent sub-Planckian effects. In particular, the virtual exchange of bulk gravitons (KK modes) leads to extra contribution to the neutrino nucleon cross section. As a consequence, the quasi-horizontal event rate will be increased. However, the exchange of spin 2 bulk gravitons has very little effect on the Earth-skimming event rate, because neutrinos suffer very little energy loss during this process [500]. Then one expects KK modes to further enhance the ratio $N_{\text{QH}}/N_{\text{ES}}$, making it still easier to distinguish such effects

from SM expectations.

It is important to stress that during this section we only consider the conservative estimates of the cosmogenic neutrino flux. However, some models predict fluxes far above these conservative values [435].⁴⁹ In such a case the atmosphere would be effectively a BH factory, and 100's of BH events would be observed each year at PAO.

D. p -branes from Heaven

In this penultimate section we come back to a main topic of this review and discuss yet another proposal [677] to sneak away from the GZK cutoff. This recent suggestion is a variant of those discussed in Sec.VI-A where neutrinos interact strongly beyond the GZK-energy. Therefore, the validity of this model is contingent on the observation of moderately penetrating showers.

The basic scaling relation of Eq. (167) is the simplest one possible. Once one envisages the notion of asymmetric compactification radii, a plethora of new phenomena may arise as one can consider the possibility of several compactification scales. Of particular interest here is the next simplest example, where there is a hierarchy of two sets of compactified extra dimensions, with m small dimensions of length $L \lesssim 1 \text{ TeV}^{-1}$, and $n - m$ large extra dimensions of length L' . The relation between M_* and the low energy 4-dimensional Planck mass $M_{\text{Pl}} \simeq 1.2 \times 10^{19} \text{ GeV}$ is [678]

$$M_{\text{Pl}}^2 = M_*^{2+n} L^m L'^{m-m} . \quad (210)$$

For simple toroidal compactifications, $L = 2\pi r_c$, and $L' = 2\pi r'_c$. Scenarios with low values of $n - m$ are already tightly constrained from table-top gravity experiments, as well as from astrophysical and cosmological considerations [478, 653, 654, 655, 656, 657, 658].

In spacetimes with asymmetric compactifications, extended higher dimensional objects wrapped around small extra dimensions, so-called “ p -branes”, can be produced in super-Planckian scattering processes [614, 679, 680]. In general, the formation of higher-dimensional branes dominates the formation of lower-dimensional branes and spherically symmetric BHs (0-branes). The decay of p -branes is not well-understood. One possibility is that they may decay into lower dimensional brane-antibrane pairs, leading to a cascade of branes. In any case, there is no reason to expect them to decay only to invisible particles, and it is reasonable to expect their decays, as with BH decays, to be dominated by visible quanta (those on the brane) that could be detected by cosmic ray observatories [614].

⁴⁹ Clearly, any top-down origin of ultrahigh energy CRs is inconsistent with TeV scale gravity. The arguments in this section then do not apply to neutrino fluxes associated with a top-down origin.

p -brane production is negligible relative to BH production unless the p -brane wraps only Planck-sized dimensions. The enhancement in the p -brane cross section results from wrapping on small dimensions and is a consequence of the dependence of the p -brane radius [614],

$$r_p = \frac{1}{\sqrt{\pi}M_*} \gamma(n, p) \left(\frac{M_p}{M_* V_p} \right)^{\frac{1}{n+1-p}}, \quad (211)$$

solely on the density of the p -brane. Here, $V_p = (L/L_*)^p$ is the volume wrapped by the p -brane in fundamental Planck units,

$$\gamma(n, p) = \left[8 \Gamma \left(\frac{3+n-p}{2} \right) \sqrt{\frac{1+p}{(2+n)(2+n-p)}} \right]^{\frac{1}{1+n-p}}, \quad (212)$$

and L_* is the fundamental Planck length.⁵⁰ p -brane production dominates over BH production only if $L \lesssim L_*$. It is worthwhile to point out that in the string-based low energy Lagrangian, the gauge coupling is inversely proportional to the compactification volume, and a small volume corresponds to strong coupling. In certain explicit models, these small volumes can be removed from the gauge sector via a T -duality transformation [681]. In what follows, we avoid reference to specific models, and for illustrative purposes discuss p -brane production over an inclusive range $0.1 < L/L_* < 10$.

The total cross section for brane production is given by [615]

$$\sigma_{\nu N \rightarrow \text{brane}} = \sum_p \sigma_{\nu N \rightarrow p\text{-brane}}, \quad (213)$$

where

$$\sigma_{\nu N \rightarrow p\text{-brane}} = \sum_i \int_{M_p^{\min 2/s}}^1 dx \hat{\sigma}_i(\sqrt{xs}) f_i(x, Q), \quad (214)$$

is the cross section for p -brane production from neutrino nucleon scattering, $\hat{\sigma}_{ij \rightarrow p\text{-brane}}(\sqrt{\hat{s}}) = \pi r_p^2$, is the parton-parton cross section, the sum is over all partons in the nucleon, the f_i are parton distribution functions, and M_p^{\min} is the minimum mass required for p -brane production which is set equal to M_D .

It was recently proposed [677] that ultrahigh energy neutrinos interacting via p -brane production may trigger vertical EASs. The required cross sections for hadronic-like interactions (~ 100 mb at 10^{20} eV), as given by Eq. (213), are only attained for $n-m = 1, 2$ and M_* of a few TeV, a region of the parameter space excluded by the sub-mm gravity experiments and astrophysical constraints. Therefore, cosmic neutrinos

⁵⁰ Note that for $p = 0$, Eq. (211) reduces to the metric of a $(4+n)$ -dimensional BH and r_p becomes the Schwarzschild radius [628].

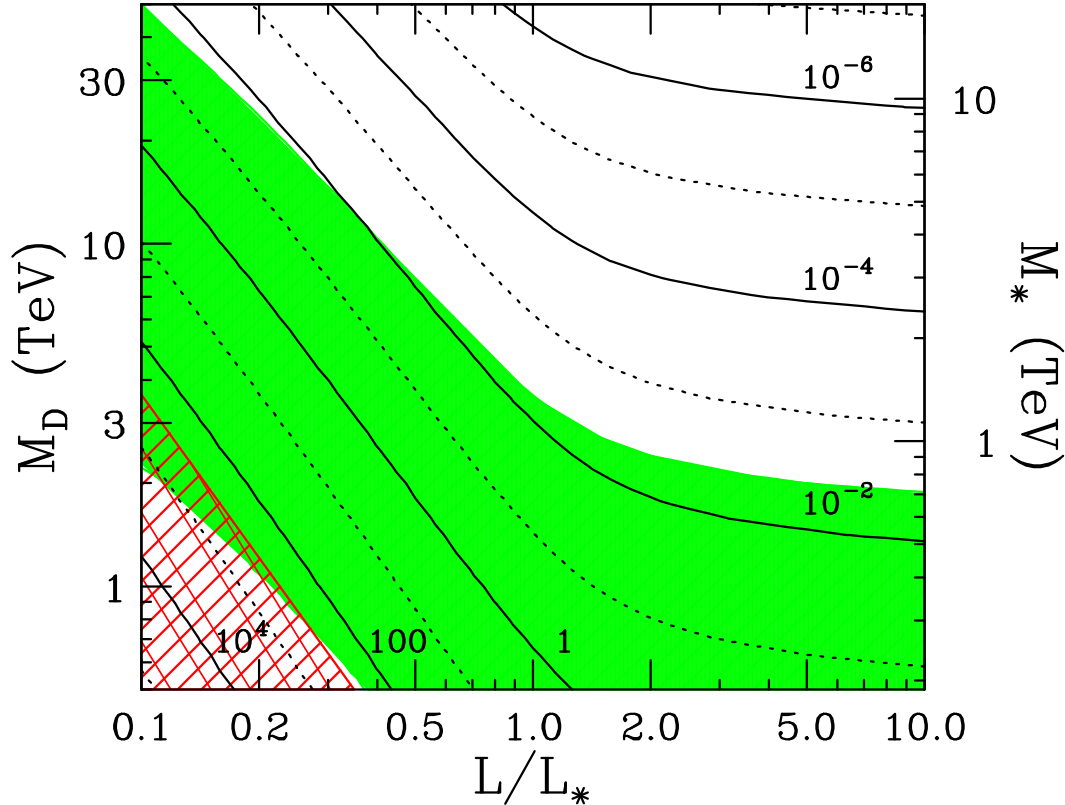


FIG. 31: Contours of $\sigma_{\nu N \rightarrow \text{brane}}^{\text{total}}$ (in mb) at $E_\nu = 10^{11}$ GeV in the $(M_D, L/L_*)$ plane for $(n = 6, m = 5)$. The right vertical axis shows the corresponding values M_* . The shaded region is excluded by the non-observation of deeply penetrating showers at AGASA. The hatched region is excluded by requiring no large corrections to standard model physics at lower energies (see text). Published in Ref. [615].

with interaction strengths enhanced by p -brane production cannot initiate super-GZK showers in factorizable spacetimes. Although no explicit models for warped scenarios are available, in the spirit of [626] one may consider the possibility that Eq. (213) is still valid for $M_* \sim 1$ TeV, and $n - m = 1$. Under these speculative assumptions, hadronic-like neutrino interactions could dominate the scattering to such an extent that the non-observation of deeply developing showers is satisfied because the cross section is *too large* — the showers would develop too high in the atmosphere.

Figure 31 displays contours in the $(M_D, L/L_*)$ plane labeled by the value of the cross section attained at 10^{20} eV (in mb), for $n = 6, m = 5$ (a similar result can be obtained for $n = 7, m = 5$) [615]. The shaded area is excluded by the absence of a significant signal of deeply developing showers reported by the AGASA Collaboration [665]. It is important to stress that the AGASA data serve to restrict the parameter space even in the case where the total cross section at 10^{20} eV is of $\mathcal{O}(100)$ mb, because some among

the tower of p -branes are produced deep in the atmosphere. We note that the upper boundary of this shaded region is in agreement with existing limits [510]. In the lower left of Fig. 31 is an unshaded region with large cross section which ostensibly can evade the AGASA bound because of neutrinos showering high in the atmosphere. However, a new consideration enters in this situation: cross sections which are too large can lead, via a dispersion relation, to large deviations in SM predictions at lower energies [682]. With the cross section behavior given by Eq. (213), it is a straightforward exercise using the result in [682] to show that low energy corrections of $\mathcal{O}(100\%)$ can arise such that

$$\sigma_{\nu N}(10^{20} \text{ eV}) \geq 300 \text{ mb} . \quad (215)$$

In Fig. 31 this region is cross-hatched, to indicate that it is problematic for SM physics at much lower energies ($\sim 100 \text{ GeV}$). As can be seen from Fig. 31, this leaves very little room for explaining the super-GZK events using p -brane physics: part of the potential parameter space is ruled out by AGASA data, most of the rest by requiring small feed-down of these high energy contributions to low energy neutrino physics. Only a tiny window is available in a region where the small extra dimension $L < 0.2L_*$. Furthermore, in this allowed region one has strong coupling effects in the underlying stringy regime.

X. LOOKING FORWARD

It is difficult – and perhaps hazardous – to speculate where CR physics will go in the next ten years. One can never foretell the serendipitous discoveries that will transform our understanding. However, on-going and future experiments will surely provide us with the statistics to begin discriminating among the many promising ideas so far proposed to explain the origin and nature of CRs above the GZK energy limits. The superior angular and energy resolution of the Pierre Auger Observatory will allow the high end of the energy spectrum and the CR arrival directions to be measured with unprecedented precision. These observables provide the most powerful discriminators among candidate sources and primary species.

Distinguishing among CR sources that produce anisotropic distributions is comparatively straightforward. For example, CRs from radio galaxies would appear clustered in the super-Galactic plane, whereas those from super heavy relics are expected to cluster in the halo. It is more challenging to distinguish among the various models that reproduce the observed isotropy below 10^{20} eV . In this case, there are two broad categories: scenarii where isotropy is realized by diffusive CR propagation, and those where the distribution of the sources themselves is isotropic.

First we comment on the case of an isotropic CR distribution resulting from diffusion.

Diffuse propagation of CRs must be associated with relatively nearby sources, and the most likely candidates are characterized by distinctive signatures. Galactic sources, for example, will emit mainly nuclei which will begin to exhibit a correlation with the Galactic plane for energies in excess of 10^{20} eV. If Centaurus A is the culprit, one can expect to observe neutrons above 10^{20} eV which of course would point back to the source. In addition, magnetic fields of $\mathcal{O}(\mu\text{G})$ are required to produce enough diffusion to render an isotropic distribution for the lower energy particles. A third possibility is that CRs coming from M87 are diffused by a Galactic wind, in which case a north-south asymmetry should emerge in the galactic coordinates. Finally, if nearby starburst galaxies are the ultrahigh energy CR generators, one should observe primarily nuclei which, at high energy, are correlated with the sources. In this case, fields of $\mathcal{O}(\text{nG})$ would provide enough diffusion to render the distribution isotropic below about 10^{20} eV.

An isotropic CR distribution could also arise from isotropic sources, such as highly red-shifted AGNs, GRB-fireballs, or decaying TDs. To ascertain whether CRs share a common origin with GRBs, we can make use of the data recorded by the HETE satellite and directly search for correlations between CR and GRB samples. To fill in the picture further, we have to be able to discriminate between the signatures of AGNs and TDs. TD scenarii predict that γ -rays should dominate the super-GZK energy spectrum. In contrast, AGNs could produce GZK-evading messengers like uhecrons or neutrinos that attain hadronic cross sections, both of which would generate typical hadronic EASs. These two types of showers can be distinguished by the rate of vertical compared to inclined showers. Concerning the uhecron option, we note that the allowed parameter space is narrowing and collider experiments will have the final word. Theories which postulate strong neutrino interactions at super-GZK energies also predict that moderately penetrating showers should be produced at lower energies, where the neutrino-nucleon cross section reaches a sub-hadronic size. In TeV scale gravity models the neutrino-nucleon cross section is likely to be sub-hadronic near the energy at which the cosmogenic neutrino flux peaks, and so moderately penetrating showers should be copiously produced. Finally, the Z -burst model eludes a definitive confirmation based on the prediction of the arrival directions, since the distribution will depend on whether relic neutrinos are clustered in the halo or not. However, the sensitivity of the Pierre Auger Observatory will be sufficiently high to test if the neutrino flux is big enough to render the model viable. Interestingly, if the Z -burst model could be verified it would provide experimental evidence for the thermal neutrino background. Moreover, in this case the CR arrival directions would encode some information on the distribution of relic neutrinos in the Universe. Table I summarizes the signatures corresponding to some of the models in the discussion above.

Future CR data will not only provide clues to the origin of the super-GZK events,

TABLE I: Possible signatures for different ultrahigh energy cosmic ray sources.

Source		Signal
M87		Asymmetry in flux with respect to Galactic plane
Pulsars		Arrival directions correlated with Galactic plane
Starbursts		Anisotropy towards sources above 2×10^{20} eV
Cen A		Spike in source-direction due to n -channel
Z-burst		Can only check for required ν flux
Top Down	Superheavy relics	Anisotropy towards Galactic halo
	\longleftrightarrow	Flux dominated by ν 's and γ 's
	Topological defects	Isotropy

but could enhance our understanding of fundamental particle physics. For example, if CR primaries are found to have a significant photon component above 10^{20} eV, this could suggest an exotic ingredient in CRs, such as decay products of TDs, and thus could provide insight into the description of the early Universe as well as particle physics beyond the SM. On the other hand, an absence of ultrahigh energy photons would imply hadronic primaries interacting at c.m. energies well above that achievable at any current or foreseeable collider, thus providing a unique opportunity to evaluate hadronic interaction models at ultrahigh energies. Moreover, a similar technique to that employed in discriminating between photons and hadrons can be applied to search for signatures of extra-dimensions. In this case, comparison of event rates of quasi-horizontal deeply developing showers and Earth-skimming neutrinos will allow better limits to be placed on low scale gravity. An optimist might even imagine the discovery of microscopic BHs, the telltale signature of the Universe's unseen dimensions. The puzzle of ultrahigh energy CRs may even have something to say about issues as fundamental as local Lorentz invariance.

All in all, after 40 years of careful work by many research groups around the world, we are in possession of a tantalizing body of data, more than sufficient to stimulate our curiosity but not yet sufficient to unravel the mystery of the highest energy CRs. The upcoming high quality observations promise to make the next 10 years an extremely exciting time for CR physics.

Note added: After this review was completed, the HiRes Collaboration [683, 684] re-examined their sample and some of the highest energy events were discarded. The small modification induced on the energy spectrum is, however, of little help in attempts to understand the tail of the CR spectrum, leaving the nature and origin of the highest energy events still a mystery. The AGASA Collaboration [685] have also re-evaluated their highest energy events and conclude that there are “surely events above 10^{20} eV

and the energy spectrum extends up to a few times 10^{20} eV.” Certainly, the conclusion of this review remains the same: *more data is needed to understand the shape of the energy spectrum above the GZK-limit*

Acknowledgments

We are most grateful to Haim Goldberg for ongoing collaboration and many illuminating discussions. We also want to thank Jorge Combi, Tere Dova, Luis Epele, Jonathan Feng, Tom McCauley, Santiago Perez Bergliaffa, Gustavo Romero, Sergio Sciutto, Al Shapere, Guenter Sigl, Diego Torres, and Tom Weiler for fruitful collaborations. We also benefited from discussions with Felix Aharonian, Ileana Andruchow, Peter Biermann, Murat Boratav, Analía Cillis, Jim Cronin, Huner Fanchiotti, Carlos García Canal, Diego Harari, Carlos Hojvat, Masha Kirasirova, Johannes Knapp, Jeremy Lloyd-Evans, Jared MacLeod, Gustavo Medina Tanco, Charly Nuñez, Kasper Olsen, John Ralston, Esteban Roulet, Martin Schvellinger, Paul Sommers, Tomasz Taylor, el Tum, and Alan Watson. We acknowledge Rainer Dick, Peter Fisher, Zoltan Fodor, Michal Ostrowski, and Subir Sarkar for valuable comments on the manuscript. We are indebted to several colleagues and collaborators mentioned above as well as Michael Kachelriess, Andreas Ringwald, Tom Rizzo, Simon Swordy, Masahiro Takeda, and the AGASA and Fly’s Eye Collaborations for allowing us to use various figures from their papers in this review. We also wish to thank the American Physical Society for permission to reproduce some of these figures. Special thanks go to Creedence Clearwater Revival for inestimable inspiration. This work has been supported, in part, by the US National Science Foundation (under grant No. PHY-0140407).

APPENDIX A: HADRONIC INTERACTION MODELS IN THE *TERRA INCOGNITA*

The analysis of ultrahigh energy cosmic rays requires the extrapolation of hadronic interaction models more than 2 orders of magnitude in energy beyond the highest accelerator energies ($\sqrt{s} = 1.8$ TeV). Actually, the required extrapolation is much greater than this because the showers involve nuclei as well as single hadrons both as targets and projectiles.

Soft multi-particle production with small transverse momenta with respect to the collision axis is a dominant feature of most events in high energy hadronic collisions. Though strict calculations based on ordinary QCD perturbation theory are not feasible, some phenomenological approaches successfully describe the main properties of soft

diffractive processes (for reviews see Refs. [686, 687]).

The most theoretically advanced type of model (like VENUS [688], QGSJET [689] and DPMJET [690, 691]) is based on Gribov-Regge theory [692, 693]. The interactions are not described by single particle exchange, but by the exchange of highly complicated collective modes known as reggeons. The slow growth of the cross section with \sqrt{s} for many different hadronic reactions measured at colliders can be well described by the form $\sigma_j = Y_j s^{-\eta} + X_j s^\epsilon$, with the universal parameters $\eta \sim 0.47$ and $\epsilon \sim 0.08$ [245]. Here, X_j and Y_j are relative amplitudes differing for each reaction j and they must be determined experimentally. The two terms represent the effect of the exchange of reggeons and pomerons,⁵¹ respectively, between the scattering objects, the latter dominating at high energies. Elastic amplitudes and total cross-sections can be calculated on the basis of multi-pomeron exchange, whereas inelastic reactions are introduced by cut pomerons [688]. The transition from the number of cut pomerons to the secondaries produced is modeled by string theory [694, 695].

On a different track, in *minijet* models (*e.g.* SIBYLL [696]) the rise of the cross section with energy is driven by a growth of the fraction of hard interactions. The probability distribution for obtaining N jet pairs (with $p_T^{\text{jet}} > p_T^{\text{min}}$, where p_T^{min} is a sharp threshold in the transverse momentum below which hard interactions are neglected) in a collision at energy \sqrt{s} , is computed regarding elastic pp or $p\bar{p}$ scattering as a diffractive shadow scattering associated with inelastic processes. The energy of each produced particle is generated using Lund techniques [698]. The algorithms are tuned to reproduce the central and fragmentation region data up to $p\bar{p}$ collider energies, and with no further adjustments they are then extrapolated several orders of magnitude.

The most difficult point in connection with the air shower development is certainly the treatment of nuclear reactions. According to the traditional notion, which treats the projectile simply as a superposition of free nucleons [699], fluctuations in a nucleus initiated shower should be smaller. This notion still stands if one uses the quark-gluon picture of nucleus-nucleus interaction, but the resulting fluctuations in EASs initiated by nuclei become nearly twice as large as semi-superposition model predictions [700]. Such an enhancement is due to the more adequate description of the stochastic behavior of projectile nucleons. Moreover, the different approaches used to model the underlying physics of $p\bar{p}$ collisions show clear differences in multiplicity predictions which increase with rising energy [701, 702, 703, 704]. Therefore, distinguishing between a proton and a nucleus shower is extremely difficult at the highest energies [705]. Recently, a complete analysis on the hadronic core of showers around the knee done by the KASCADE Collaboration [706] provides important information about the quality of

⁵¹ This leading Regge trajectory with vacuum quantum numbers was originally proposed by Chew and Frautschi [697].

the hadronic event generators. The study seems to indicate that QGSJET is the model which best reproduces the spectrum below 5×10^{15} eV. However, above the knee deviations in several observables are seen, suggesting that further investigations (and data) are needed.⁵²

APPENDIX B: REDSHIFTING

There is now a substantial body of observations that support, both directly and indirectly, the idea that our Universe expanded from a super-dense hot phase roughly 13 billion years ago [708]. In particular, in the late 1920's Hubble established that the spectra of galaxies at greater distances are systematically shifted to longer wavelengths. The change in wavelength of a spectral line is expressed as the redshift of the observed feature,

$$1 + z \equiv \frac{\lambda_{\text{observed}}}{\lambda_{\text{emitted}}}. \quad (\text{B1})$$

Interpreting the redshift as a Doppler velocity, for $z \ll 1$, Hubble's relationship can be re-written as $z \sim H_0 d/c$, where H_0 is the expansion rate at the present epoch.

The adiabatic energy losses suffered by cosmic rays due to the expansion of the Universe can be associated with the internal energy loss of a relativistic gas with particle density n and temperature T doing work to expand its volume V ,

$$dU = -P dV, \quad (\text{B2})$$

where $PV = NkT$ or $P = nkT$ (i.e., $nV = N$) is the gas pressure and k is the Boltzmann constant. Now, since the mean energy of each particle is $3kT$, one obtains $dU = nV dE = -nE dV/3$. For a fixed number of particles

$$\left(\frac{dE}{dt}\right)_{\text{adiabatic}} = -\frac{1}{3} \frac{nE}{N} \frac{dV}{dt}, \quad (\text{B3})$$

where dV/dt is the expansion rate of the region with field velocity $\vec{v}(\vec{r})$. The change in the volume $dx dy dz$ moving with the flux is given by,

$$\frac{dV}{dt} = (v_{x+dx} - v_x)dy dz + (v_{y+dy} - v_y)dx dz + (v_{z+dz} - v_z)dx dy, \quad (\text{B4})$$

or, using Taylor's expansion

$$\frac{dV}{dt} = \left(\frac{\partial v_x}{\partial x} + \frac{\partial v_y}{\partial y} + \frac{\partial v_z}{\partial z}\right) dx dy dz = (\nabla \cdot \vec{v})V. \quad (\text{B5})$$

⁵² For a more extensive discussion on hadronic interaction models the reader is referred to [707].

Now, the adiabatic fractional energy loss is obtained by replacing Eq. (B3) into Eq. (B5)

$$\left(\frac{dE}{dt}\right)_{\text{adiabatic}} = -\frac{1}{3}(\nabla \cdot \vec{v}) E. \quad (\text{B6})$$

In standard Friedman-Robertson-Walker cosmology, with vanishing cosmological constant and scale factor R which expands at a velocity v_0 , $v = v_0(r/R)$, and

$$\nabla \cdot \vec{v} = \frac{1}{r^2} \left[\frac{\partial}{\partial r} (r^2 v_r) \right] = 3 \frac{v_0}{R}. \quad (\text{B7})$$

Hence,

$$-\left(\frac{dE}{dt}\right)_{\text{adiabatic}} = \frac{v_0}{R} E = \frac{1}{R} \frac{dR}{dt} E = H_0 E. \quad (\text{B8})$$

APPENDIX C: KINEMATICS OF PHOTOMESON PRODUCTION

The inelasticity K_π depends not only on the outgoing particles but also on the kinematics of the final state. Nevertheless, averaging over final state kinematics leads to a good approximation of K_π . The c.m. system quantities are determined from the relativistic invariance of the square of the total 4-momentum $p_\mu p^\mu$ of the photon-proton system. This invariance leads to the relation.

$$s = (w^{c.m.} + E^{c.m.})^2 = m_p^2 + 2m_p w_r. \quad (\text{C1})$$

The c.m. system energies of the particles are uniquely determined by conservation of energy and momentum. For reactions mediated by resonances one can assume a decay, which in the c.m. frame is symmetric in the forward and backward directions with respect to the collision axis (given by the incoming particles). For instance, we consider single pion production via the reaction $p\gamma \rightarrow \Delta \rightarrow p\pi$. Here,

$$E_\Delta^{c.m.} = \frac{(s + m_\Delta^2 - m_\pi^2)}{2\sqrt{s}}. \quad (\text{C2})$$

Thus, the mean energy of the outgoing proton is

$$\langle E_p^{\text{final c.m.}} \rangle = \frac{(s + m_\Delta^2 - m_\pi^2)}{2\sqrt{s} m_\Delta} \frac{(m_\Delta^2 + m_p^2 - m_\pi^2)}{2 m_\Delta}, \quad (\text{C3})$$

or in the lab frame

$$\langle E_p^{\text{final}} \rangle = \frac{E}{s} \frac{(s - m_\pi^2 + m_\Delta^2)}{2 m_\Delta} \frac{(m_\Delta^2 - m_\pi^2 + m_p^2)}{2 m_\Delta}. \quad (\text{C4})$$

The mean inelasticity $K_\pi = 1 - (\langle E^{\text{final}} \rangle / E)$ of a reaction that provides a proton after n resonance decays can be obtained by straightforward generalization of Eq. (C4), and is given in Eq. (53).

APPENDIX D: IRON PHOTODISINTEGRATION

The photoabsorption cross section roughly obeys the electric dipole sum rule

$$\Sigma_d \equiv \int_0^\infty \sigma(w_r) dw_r = 60 \frac{nZ}{A} \text{ MeV mb}, \quad (\text{D1})$$

where $n = A - Z$ is the number of neutrons.⁵³ These cross sections contain essentially two regimes. At $w_r < 30$ MeV there is the domain of the giant dipole resonance where disintegration proceeds mainly by the emission of one or two nucleons. A Gaussian distribution in this energy range is found to adequately fit the cross section data [255]. At higher energies, the cross section is dominated by multinucleon emission and is approximately flat up to $w_r \sim 150$ MeV. Specifically,

$$\sigma_{Ai} = \frac{\xi_{Ai} \Sigma_d \Theta(w_r - 2) \Theta(30 - w_r) e^{-2(w_r - \epsilon_{0i})^2 / \Delta_i^2}}{W \Delta_i} + \frac{f_i \Sigma_d \Theta(w_r - 30)}{120}, \quad (\text{D2})$$

for $i=1, 2$, and

$$\sigma_{Ai} = \frac{f_i \Sigma_d \Theta(w_r - 30)}{120}, \quad (\text{D3})$$

for $i > 2$ [255]. Here, W is a normalization factor given by

$$W = \left(\frac{\pi}{8}\right)^2 \left[\Phi(\sqrt{2}(30 - \epsilon_{0i})/\Delta_i) + \Phi(\sqrt{2}(\epsilon_{0i} - 2)/\Delta_i) \right],$$

$\Phi(x)$ is the error function, and $\Theta(x)$ the Heaviside step function. The dependence of the width Δ_i , the peak energy ϵ_{0i} , the branching ratio f_i , and the dimensionless integrated cross section ξ_i are given in Ref. [255] for isotopes up to ⁵⁶Fe.

The photon background relevant for nucleus disintegration consists essentially of photons of the 2.7 K CMB. The background of optical radiation turns out to be of no relevance for ultrahigh energy cosmic ray propagation. The infrared background radiation [710]

$$\frac{dn}{dw} = 1.1 \times 10^{-4} \left(\frac{w}{\text{eV}}\right)^{-2.5} \text{ cm}^{-3} \text{ eV}^{-1}, \quad (\text{D4})$$

only leads to sizeable effects far below 10^{20} eV and for time-scales $\mathcal{O}(10^{17}$ s) [711].

By substituting Eqs. (D2) and (D3) into Eq. (61) the photodisintegration rates on the CMB can be expressed as integrals of two basic forms. The first one is

$$I_1 = \frac{\mathcal{A}}{2\Gamma^2 \pi^2 \hbar^3 c^2} \left[\int_{1/\Gamma}^{15/\Gamma} dw (e^{w/kT} - 1)^{-1} \mathcal{J} + \int_{15/\Gamma}^\infty dw (e^{w/kT} - 1)^{-1} \mathcal{J}' \right], \quad (\text{D5})$$

⁵³ Indeed, this integral is experimentally $\sim 20 - 30\%$ larger [709].

TABLE II: Series and functions of Eq. (D9)

\mathcal{A}	$W^{-1}\xi_{Ai}\Sigma_d\Delta_i^{-1}$
\mathcal{S}_1	$\sum_{j=1}^{\infty} kTj^{-1} \exp[\mathcal{B}^2] \{\Phi(\mathcal{B} + 15\sqrt{8}/\Delta_i) - \Phi(\mathcal{B} + \sqrt{8}/\Delta_i)\}$
\mathcal{S}_2	$\sum_{j=1}^{\infty} kTj^{-1} \exp\{-j/\Gamma kT\} [\Phi(\sqrt{2}(2 - \epsilon_{0i})/\Delta_i) - \Phi(\sqrt{2}(30 - \epsilon_{0i})/\Delta_i)]$
\mathcal{S}_3	$\sum_{j=1}^{\infty} \exp[\mathcal{B}^2] \{\Phi(\mathcal{B} + 15\sqrt{8}/\Delta_i) - \Phi(\mathcal{B} + \sqrt{8}/\Delta_i)\}$
\mathcal{S}_4	$\sum_{j=1}^{\infty} \exp\{-15j/\Gamma kT\} [(kT/j)(15/\Gamma)^2 + (kT/j)^2(15/\Gamma) + (kT/j)^3]$
\mathcal{B}	$j\Delta_i/\Gamma kT\sqrt{32} - 2\epsilon_{0i}/\sqrt{2}\Delta_i$
\mathcal{K}	$\sqrt{\frac{\pi}{8}} \epsilon_{0i} \Delta_i \Phi(\sqrt{2}(\epsilon_{0i} - 2)/\Delta_i) + (\Delta_i/2)^2 \exp\{-2(\epsilon_{0i} - 2)^2/\Delta_i^2\}$

where the functions \mathcal{J} and \mathcal{J}' are given by the expressions,

$$\begin{aligned} \mathcal{J} = & \sqrt{\frac{\pi}{8}} \epsilon_{0i} \Delta_i \left[\Phi(\sqrt{2}(2\Gamma w - \epsilon_{0i})/\Delta_i) + \Phi(\sqrt{2}(\epsilon_{0i} - 2)/\Delta_i) \right] \\ & + \left(\frac{\Delta_i}{2} \right)^2 \left\{ e^{-2((\epsilon_{0i}-2)/\Delta_i)^2} - e^{-2((2\Gamma w - \epsilon_{0i})/\Delta_i)^2} \right\}, \end{aligned} \quad (\text{D6})$$

and

$$\begin{aligned} \mathcal{J}' = & \sqrt{\frac{\pi}{8}} \epsilon_{0i} \Delta_i \left[\Phi(\sqrt{2}(30 - \epsilon_{0i})/\Delta_i) + \Phi(\sqrt{2}(\epsilon_{0i} - 2)/\Delta_i) \right] \\ & + \left(\frac{\Delta_i}{2} \right)^2 \left\{ e^{-2((\epsilon_{0i}-2)/\Delta_i)^2} - e^{-2((30-\epsilon_{0i})/\Delta_i)^2} \right\}. \end{aligned} \quad (\text{D7})$$

The second basic integral is of the form

$$I_2 = (\pi^2 \hbar^3 c^2)^{-1} \sigma_{Ai} \left[\int_{15/\Gamma}^{\infty} \frac{w^2 dw}{e^{w/kT} - 1} - \left(\frac{15}{\Gamma} \right)^2 \int_{15/\Gamma}^{\infty} \frac{dw}{e^{w/kT} - 1} \right]. \quad (\text{D8})$$

With this in mind, Eq. (61) can be re-written as [712]

$$\begin{aligned} R_{Ai} = & \frac{1}{\pi^2 \hbar^3 c^2 \Gamma^2} \left\{ \frac{\mathcal{A}}{2} \left(\frac{\pi}{8} \right)^{1/2} \epsilon_{0i} \Delta_i \left[e^{-2\epsilon_{0i}^2/\Delta_i^2} \mathcal{S}_1 + \mathcal{S}_2 \right] - \frac{\mathcal{A}}{2} \mathcal{J}' kT \ln(1 - e^{-15/\Gamma kT}) \right. \\ & - \frac{\mathcal{A}}{8} e^{-2\epsilon_{0i}^2/\Delta_i^2} \left(\frac{\pi}{32} \right)^{1/2} \frac{\Delta_i^3}{\Gamma} \mathcal{S}_3 + \frac{\mathcal{A}}{2} \mathcal{K} kT \left[\ln(1 - e^{-15/\Gamma kT}) - \ln(1 - e^{-1/\Gamma kT}) \right] \\ & \left. + \frac{f_i \Sigma_d}{120} \left[\Gamma^2 \mathcal{S}_4 + 15^2 kT \ln(1 - e^{-15/\Gamma kT}) \right] \right\}, \end{aligned} \quad (\text{D9})$$

with \mathcal{A} , \mathcal{S}_i , and \mathcal{K} as given in Table I.

APPENDIX E: THE NEUTRON CHANNEL

As remarked in Sec.III-B.2, if the radiation energy density of the source is sufficiently high, photopion production leads to copious neutron flux (that can readily escape the system) and associated degradation of the proton spectrum. This occurs only near the maximum proton energy [187]. It is reasonable to assume that the ambient photon density of Cen A is sufficiently high so that near the end of the spectrum the efficiency of neutron production ϵ_n becomes comparable to the proton channel ϵ_p . Because of the leading particle effect, one expects a cutoff in the neutron spectrum at approximately half the maximum injection energy. In what follows, we adopt an energy of 1×10^{20} eV as a lower cutoff on the neutron spectrum, and simplify the discussion by assuming that in the narrow interval $E_{20} \in [1, 2]$ $\epsilon_n \approx \epsilon_p$. The neutron beam observed at Earth is further narrowed because of both decay *en route* and interactions with the CMB. The interaction length is approximately 6 Mpc, so that after 3.4 Mpc, 45% of the neutrons interact. Half go back into neutrons, so this 22% depletion effect falls within errors. However, because of the exponential depletion, about 2% of the neutrons survive the trip at 10^{20} eV, and about 15% at 2×10^{20} eV. Note that the increasing survival of neutrons at energies above 1.5×10^{20} eV has, as a consequence of the Cen A model, that the observed diffuse flux $E^3 J_{\text{obs}}(E)$ should begin to decrease at these energies (unless other factors contribute to an increase).

We may now estimate a signal-to-noise ratio for the detection of neutron CRs in the southern hemisphere. If we assume circular pixel sizes with 2° diameters, the neutron events from Cen A will be collected in a pixel representing a solid angle $\Delta\Omega(\text{CenA}) \simeq 10^{-3}$ sr. For PAO, the event rate of (diffuse) protons coming from the direction of Cen A (say in a 2° angular cone) is found to be [346]

$$\frac{dN_p}{dt} = S \Delta\Omega(\text{CenA}) \int_{E_1}^{E_2} E^3 J_p(E) \frac{dE}{E^3} \lesssim \frac{0.014}{E_{1,20}^2} \text{ events/yr}, \quad (\text{E1})$$

where we have assumed $E^3 J_p(E)$ to be (approximately) constant up to at least $E \approx 3 \times 10^{20}$ eV, in agreement with the observed isotropic flux in this region, $E^3 J_{\text{obs}}(E) = 10^{24.5 \pm 0.2} \text{ eV}^2 \text{ m}^{-2} \text{ s}^{-1} \text{ sr}^{-1}$ [20]. The neutron rate [346]

$$\frac{dN_n}{dt} = \frac{S}{4\pi d^2} \int_{E_1}^{E_2} \frac{dN_0^n}{dEdt} e^{-d/\lambda(E)} = 116 \epsilon_n L_{41} \int_{E_{1,20}}^{E_{2,20}} \frac{dE_{20}}{E_{20}^2} e^{-d/\lambda(E)} \text{ events/yr}, \quad (\text{E2})$$

is potentially measurable. For $E_{20} \in [1, 2]$ one expects

$$\frac{dN_n}{dt} \approx 4 \epsilon_n L_{41} \text{ events/yr} \quad (\text{E3})$$

arriving from the Cen A direction of the sky. With $\epsilon_n L_{41} \approx 1/2$, this gives about 2 direct events per year, against the negligible background of Eq. (E1) [346]. An increase

in the maximum energy attainable at the source will shift the end of the spectrum to higher energy. This will lead to significant enhancement of the neutron flux (at the higher energy) because of a greater survival probability.

APPENDIX F: RECIPES FOR A DARK MATTER HALO

There is a great uncertainty in the structure of the Galaxy's dark matter halo. Strictly speaking, the HI gas rotation of the Galaxy cannot be traced for distances $\gtrsim 20$ kpc, and therefore the best estimates of the total mass ($\sim 2 \times 10^{10} M_\odot$) and the extent of the Galaxy ($\gtrsim 200$ kpc) arise from kinematical analyses of the distant satellite galaxies [713].

Numerical simulations of the structure formation in hierarchical merging cosmologies seem to favor a *cusped* density profile for dark halos [590]

$$n(\vec{r}) \propto \frac{1}{(r + r_\epsilon)(r + r_s)^2}, \quad (\text{F1})$$

where \vec{r} is the position with respect to the Galactic center, $r = |\vec{r}|$ is the spherical polar radius, r_s is the scale radius (which is approximately 10 kpc for the Galaxy), and $r_\epsilon \sim 0.5$ is set by the resolution limit of the simulations. This profile implies that the inner regions are dominated by DM.

An alternative description, in which the luminous matter dominates the central regions and DM the outer parts, assumes the Galaxy's dark halo has an *isothermal* distribution with large core radius ($r_c \sim 10$ kpc) [714]

$$n(\vec{r}) \propto \frac{3r_c^2 + r^2}{(r_c^2 + r^2)^2}. \quad (\text{F2})$$

Actually, the profile of Eq. (F2) is the spherical limit of a more general family of *triaxial* distributions [715] where

$$n(\vec{r}) \propto \frac{Ax^2 + By^2 + CZ^2 + D}{(r_c^2 + x^2 + y^2 p^{-2} + z^2 q^{-2})^2}, \quad (\text{F3})$$

with $\vec{r} = (x, y, z)$, $A = (p^{-2} + q^{-2} - 1)$, $B = p^{-2}(1 - p^{-2} + q^{-2})$, $C = q^{-2}(1 + p^{-2} - q^{-2})$, and $D = r_c^2(1 + p^{-2} + q^{-2})$. Here, p and q are axis ratios of the potential. If $p = 1$, the halo is oblate, whereas if $p = q$, the halo is prolate. In Fig. 27, $p = 0.9$ and $q = 0.75$. This means that the density contours have semi-axes in the ratio $1 : 0.788 : 0.428$, yielding a highly flattened profile with an ellipticity⁵⁴ of roughly E6.

⁵⁴ The ellipticity is $10 \times (1 - b/a)$, where b and a are the projected minor and major axes respectively. A spherical galaxy is E0, whilst the most flattened elliptical galaxies are E7.

It was also pointed out [716] that in some cases the outer parts of the halo may be misaligned with the disk, because of the warping of the neutral gas disk. This effect, which is known to be present in the Galaxy, leads to a new family of *tilted* halos with density

$$n(R', z') \propto \frac{r_c^2(2 + q^{-2}) + q^{-2}R'^2 + z'^2q^{-2}(2 - q^{-2})}{(r_c + R'^2 + z'^2q^{-2})^2}, \quad (\text{F4})$$

where $R'^2 = x'^2 + y'^2$. The coordinates (x', y', z') are related to (x, y, z) by a rotation through an angle θ about the x -axis, on which the Sun lies. The pretext for this transformation is that the Sun lies nearly on the line of nodes of the warp. In Fig. 27, to obtain the main qualitative features of *tilted* haloes, the rotation angle was set to an extreme value: $\theta = 30^\circ$.

APPENDIX G: TUBULAR BLACK HOLES

In what follows, we discuss the domain of the RS [474] parameter space for which a high energy collision, as viewed from the SM brane, can result in the formation of a 5 dimensional flat space BH. Two different kinds of BHs can be produced in super-Planckian particle collisions within the RS setup. On the one hand, there is the AdS/Schwarzschild BH that can propagate freely into the bulk, and in general will fall towards the AdS horizon once produced. On the other hand, there is the tubular pancake shape BH that is bound to the brane [623]. As in the ADD [471] scenario one expects that this type of BH radiates mainly on the brane with interesting phenomenological consequences. To characterize the main features of tubular BHs it is convenient to re-write Eq. (174) by introducing the coordinate $z = \ell e^{y/\ell}$, so that the metric

$$ds^2 = \frac{\ell^2}{z^2} (dz^2 + \eta_{ij} dx^i dx^j) \quad (\text{G1})$$

is manifestly conformally flat [717]. Next, to describe the SM brane, define $w = z - z_c$, where $|w| \in (0, w_c)$, $z_c = \ell e^{r_c/\ell}$, $w_c = \ell (e^{r_c/\ell} - 1)$, and locate the TeV brane at $w = 0$. A calculation of metric perturbations due to a source on the $w = 0$ brane can be made in the flat 5-dimensional space-time approximation, *i.e.*, ignoring the effects of the AdS curvature, if $w \ll z_c$ [718]. This implies that the flat space BH formulae discussed in Sec.IX-A are also valid in the RS scenario if the Schwarzschild radius as measured by an observer in the canonical frame $\ll z_c$. The upper limit on the BH horizon translates into an upper bound on the BH mass

$$\frac{M_{\text{BH}}}{M_D} < 24 c^{-4/3}, \quad (\text{G2})$$

where, $M_D = (4\pi)^{1/3} M \ell / z_c$, and $c \equiv (\ell \overline{M}_{\text{Pl}})^{-1}$ [496]. When the energy exceeds this bound, the behaviour of the cross section may be analyzed within the AdS/CFT dual

picture, and may assume the $\ln^2 E$ behavior conforming to the Froissart bound [719].

- [1] V. F. Hess, Phys. Z. **13**, 1804 (1912).
- [2] P. Auger, R. Maze, T. Grivet-Meyer, Comptes Rendus **206**, 1721 (1938).
- [3] P. Auger, P. Ehrenfest, R. Maze, J. Daudin, Robley, and A. Fréon, Rev. Mod. Phys. **11**, 288 (1939).
- [4] J. Linsley, Phys. Rev. Lett. **10**, 146 (1963).
- [5] K. Suga, H. Sakuyama, S. Kawaguchi and T. Hara, Phys. Rev. Lett. **27**, 1604 (1971).
- [6] H. J. Garmston and A. A. Watson, Nature **237**, 39 (1972).
- [7] M. M. Winn, J. Ulrichs, L. S. Peak, C. B. Mccusker and L. Horton, J. Phys. G **12** (1986) 653.
- [8] M. A. Lawrence, R. J. Reid and A. A. Watson, J. Phys. G **17**, 733 (1991).
- [9] A. V. Glushkov *et al.*, Bull. Acad. Sci. USSR, Phys. Ser. 55 (1991) No. 4 95-97. (Izv. Akad. Nauk SSSR, Fiz. 55 (1991) 717-719).
- [10] D. J. Bird *et al.* [HIRES Collaboration], Phys. Rev. Lett. **71**, 3401 (1993).
- [11] D. J. Bird *et al.* [HIRES Collaboration], Astrophys. J. **424**, 491 (1994).
- [12] D. J. Bird *et al.*, Astrophys. J. **441**, 144 (1995).
- [13] N. Hayashida *et al.*, Phys. Rev. Lett. **73**, 3491 (1994).
- [14] M. Takeda *et al.*, Phys. Rev. Lett. **81**, 1163 (1998) [arXiv:astro-ph/9807193].
- [15] E. E. Antonov *et al.*, JETP Lett. **69**, 650 (1999) [Pisma Zh. Eksp. Teor. Fiz. **69**, 614 (1999)].
- [16] C. C. Jui [High Resolution Fly's Eye Collaboration], in *26th International Cosmic Ray Conference: Invited Rapporteur and Highlight Papers*, edited by B. L. Dingus, D. B. Kieda, and M. H. Salamon, AIP Conf. Proc. No.516 (AIP, Melville, NY, 2000), p.370.
- [17] N. Sakaki *et al.* [AGASA Collaboration], Proc. of 27th ICRC (Hamburg) **1**, 333 (2001).
- [18] J. W. Cronin, T. K. Gaisser, and S. P. Swordy, Sci. Amer. **276**, January 44 (1997).
- [19] G. V. Kulikov and G. B. Khristiansen, J. Exp. Theor. Phys. **8**, 441 (1959) [Zh. Eksp. Teor. Fiz. **35**, 635 (1958)].
- [20] N. Hayashida *et al.*, Astrophys. J. **522**, 225 (1999) [arXiv:astro-ph/0008102].
- [21] G. Cocconi, Astropart. Phys. **4** (1996) 281.
- [22] N. Hayashida *et al.* [AGASA Collaboration], Astropart. Phys. **10**, 303 (1999) [arXiv:astro-ph/9807045].
- [23] M. Teshima *et al.* [AGASA Collaboration] Proc. of 27th ICRC (Hamburg) **1**, 337 (2001).
- [24] P. Sommers, talk presented at the *Pierre Auger Collaboration Meeting*, Malargue, Argentina (2001).
- [25] M. Ave, J. Knapp, J. Lloyd-Evans, M. Marchesini and A. A. Watson, arXiv:astro-ph/0112253.
- [26] M. Nagano and A. A. Watson, Rev. Mod. Phys. **72**, 689 (2000).
- [27] A. A. Watson, arXiv:astro-ph/0112474.
- [28] T. Abu-Zayyad *et al.* [HIRES-MIA Collaboration], Astrophys. J. **557**, 686 (2001)

- [arXiv:astro-ph/0010652].
- [29] J. Szabelski, T. Wibig, and A. W. Wolfendale, *Astropart. Phys.* (to be published).
 - [30] J. Linsley and A. A. Watson, *Phys. Rev. Lett.* **46**, 459 (1981); and references therein.
 - [31] T. K. Gaisser, *Cosmic Rays And Particle Physics*, (Cambridge, UK: Univ. Press, 1990).
 - [32] A. N. Cillis, H. Fanchiotti, C. A. Garcia Canal and S. J. Sciutto, *Phys. Rev. D* **59**, 113012 (1999) [arXiv:astro-ph/9809334].
 - [33] A. Cillis and S. J. Sciutto, *J. Phys. G* **26**, 309 (2000).
 - [34] A. V. Plyasheshnikov and F. A. Aharonian, arXiv:astro-ph/0107592.
 - [35] M. T. Dova, L. N. Epele and A. G. Mariazzi, *Astropart. Phys.* (to be published), arXiv:astro-ph/0110237.
 - [36] R. Walker and A. A. Watson, *J. Phys. G* **8** (1982) 1131.
 - [37] N. Hayashida *et al.* [Akeno Collaboration], *J. Phys. G* **21**, 1101 (1995).
 - [38] T. Wibig and A. W. Wolfendale, *J. Phys. G.* **25** 1099, (1999).
 - [39] T. Abu-Zayyad *et al.* [HIRES Collaboration], *Astropart. Phys.* **16**, 1 (2001) [arXiv:astro-ph/0008206].
 - [40] M. Ave, J. A. Hinton, R. A. Vazquez, A. A. Watson and E. Zas, *Phys. Rev. Lett.* **85**, 2244 (2000) [arXiv:astro-ph/0007386].
 - [41] M. Ave, J. A. Hinton, R. A. Vazquez, A. A. Watson and E. Zas, arXiv:astro-ph/0110613.
 - [42] K. Shinozaki *et al.* [AGASA Collaboration] *Proc. of 27th ICRC (Hamburg)* **1**, 346 (2001).
 - [43] M. Ave, J. A. Hinton, R. A. Vazquez, A. A. Watson and E. Zas, arXiv:astro-ph/0112071.
 - [44] J. Wdowczyk and A. W. Wolfendale, *J. Phys. G* **10** (1984) 1599.
 - [45] J. Szabelski, J. Wdowczyk and A. W. Wolfendale, *J. Phys. G* **12** (1986) 1433.
 - [46] D. J. Bird *et al.* [HIRES Collaboration], arXiv:astro-ph/9806096.
 - [47] J. A. Bellido, R. W. Clay, B. R. Dawson and M. Johnston-Hollitt, *Astropart. Phys.* **15**, 167 (2001) [arXiv:astro-ph/0009039].
 - [48] W. Bednarek, M. Giller and M. Zielinska, arXiv:astro-ph/0205324.
 - [49] T. Stanev, P. L. Biermann, J. Lloyd-Evans, J. P. Rachen and A. Watson, *Phys. Rev. Lett.* **75**, 3056 (1995) [arXiv:astro-ph/9505093].
 - [50] N. Hayashida *et al.*, *Phys. Rev. Lett.* **77**, 1000 (1996).
 - [51] M. M. Winn, J. Ulrichs, L. S. Peak, C. B. Mccusker and L. Horton, *J. Phys. G* **12**, 675 (1986).
 - [52] L. J. Kewley, R. W. Clay and B. R. Dawson, *Astropart. Phys.* **5** (1996) 69.
 - [53] M. Takeda *et al.*, arXiv:astro-ph/9902239.
 - [54] E. Waxman, K. B. Fisher and T. Piran, *Astrophys. J.* **483**, 1 (1997) [arXiv:astro-ph/9604005].
 - [55] H. Goldberg and T. J. Weiler, *Phys. Rev. D* **64**, 056008 (2001) [arXiv:astro-ph/0009378].
 - [56] L. A. Anchordoqui, H. Goldberg, S. Reucroft, G. E. Romero, J. Swain and D. F. Torres, *Mod. Phys. Lett. A* **16**, 2033 (2001) [arXiv:astro-ph/0106501].

- [57] P. G. Tinyakov and I. I. Tkachev, JETP Lett. **74**, 1 (2001) [Pisma Zh. Eksp. Teor. Fiz. **74**, 3 (2001)] [arXiv:astro-ph/0102101].
- [58] Y. Uchihori, M. Nagano, M. Takeda, M. Teshima, J. Lloyd-Evans and A. A. Watson, Astropart. Phys. **13** (2000) 151 [arXiv:astro-ph/9908193].
- [59] R. Clay, B. Dawson, B. Fick, M. Roberts and P. Sommers, GAP Note 2001-047.
- [60] P. Sokolsky, P. Sommers and B. R. Dawson, Phys. Rept. **217** (1992) 225.
- [61] S. Yoshida and H. Dai, J. Phys. G **24**, 905 (1998) [arXiv:astro-ph/9802294].
- [62] A. A. Watson, Phys. Rept. **333**, 309 (2000).
- [63] X. Bertou, M. Boratav and A. Letessier-Selvon, Int. J. Mod. Phys. A **15**, 2181 (2000) [arXiv:astro-ph/0001516].
- [64] S. J. Sciutto, arXiv:astro-ph/9905185.
- [65] J. Linsley, Proc. 13th ICRC (Denver), 3212 (1973).
- [66] M. T. Dova, M. E. Manceñido, A. G. Mariazzi, T. P. McCauley, and A. A. Watson, arXiv:astro-ph/0210464.
- [67] L. A. Anchordoqui, T. P. McCauley, T. Paul, S. Reucroft, J. D. Swain and L. Taylor, Nucl. Phys. Proc. Suppl. **97**, 196 (2001) [arXiv:astro-ph/0006142].
- [68] R. N. Coy, G. Cunningham, C. L. Pryke and A. A. Watson, Astropart. Phys. **6**, 263 (1997).
- [69] S. Yoshida *et al.*, J. Phys. G **20**, 651 (1994).
- [70] N. Inoue [AGASA Collaboration], Proc. of 26th ICRC (Salt Lake City) **1**, 361 (1999).
- [71] G. Matthiae, Proc. of 27th ICRC (Hamburg), 733 (2001).
- [72] Y. Musienko, S. Reucroft, D. Ruuska and J. Swain, Nucl. Instrum. Meth. A **447** (2000) 437.
- [73] D. J. Bird *et al.*, Proc. of 23rd ICRC (Calgary), **2** 450 (1993).
- [74] T. K. Gaisser and A. M. Hillas, Proc. of 15th ICRC (Plovdiv), **8** 353 (1977).
- [75] M. S. Longair, *High-Energy Astrophysics*, (2nd Edition, Cambridge, Uk: Univ. Press, 1992).
- [76] F. Kahn and I. Lerche, Proc. Roy. Soc. **A289**, 206 (1966).
- [77] R. Wilson, Phys. Rev. **108**, 155 (1967).
- [78] J.V. Jelley *et al.*, Nature **205**, 327 (1965).
- [79] K. Green, J. L. Rosner, D. A. Suprun and J. F. Wilkerson, arXiv:astro-ph/0205046.
- [80] H. Falcke and P. Gorham, arXiv:astro-ph/0207226.
- [81] T. Huege and H. Falcke, arXiv:astro-ph/0207647.
- [82] P. M. S. Blackett and A. C. B Lovell, Proc. Roy. Soc. (London) Ser. A **177**, 183 (1940).
- [83] P. W. Gorham, Astropart. Phys. **15**, 177 (2001) [arXiv:hep-ex/0001041].
- [84] P. W. Gorham, AIP Conf. Proc. **579** (2001) 253.
- [85] T. Vinogradova, E. Chapin, P. Gorham and D. Saltzberg, AIP Conf. Proc. **579** (2001) 271.
- [86] J. Linsley, L. Scarsi, and B. Rossi, Phys. Rev. Lett. **6**, 485 (1961).
- [87] J. Linsley and L. Scarsi, Phys. Rev. **128**, 2384 (1962).
- [88] G. Cunningham, J. Lloyd-Evans, A. M. T. Pollock, R. J. O. Reid, and A. A. Watson, Astrophys. J. **236**, L71 (1980).

- [89] D. M. Edge, A. M. Pollock, R. J. Reid, A. A. Watson and J. G. Wilson, *J. Phys. G* **4** (1978) 133.
- [90] G. B. Khristiansen, *Proc. of 19th ICRC (La Jolla)*, **9** 487 (1985).
- [91] A. V. Glushkov, I. T. Makarov, E. S. Nikiforova, M. I. Pravdin and I. E. Sleptsov, *Astropart. Phys.* **4** (1995) 15.
- [92] R. W. Clay, R. Meyhandan, L. Horton, J. Ulrichs, and M. M. Winn, *Astron. Astrophys.* **255**, 167 (1992).
- [93] N. Chiba *et al.*, *Nucl. Instrum. Meth. A* **311**, 338 (1992).
- [94] H. Ohoka, S. Yoshida and M. Takeda [AGASA Collaboration], *Nucl. Instrum. Meth. A* **385**, 268 (1997).
- [95] M. Teshima *et al.* [Akeno Collaboration], *Nucl. Instrum. Meth. A* **247**, 399 (1986).
- [96] H. E. Bergeson *et al.*, *Phys. Rev. Lett.* **39**, 847 (1977).
- [97] R. M. Baltrusaitis *et al.*, *Nucl. Instrum. Meth. A* **240** (1985) 410.
- [98] R. M. Baltrusaitis *et al.*, *Nucl. Instrum. Meth. A* **264** (1988) 87.
- [99] S. C. Corbato *et al.*, *Nucl. Phys. Proc. Suppl.* **28B** (1992) 36.
- [100] A. Borione *et al.*, *Nucl. Instrum. Meth. A* **346**, 329 (1994).
- [101] D. Zavrtnik [AUGER Collaboration], *Nucl. Phys. Proc. Suppl.* **85** (2000) 324.
- [102] J. J. Beatty [AUGER Collaboration], *Int. J. Mod. Phys. A* **16S1C** (2001) 1022.
- [103] I. Allekote *et al.* [AUGER Collaboration], *Proc. of 27th ICRC (Hamburg)*, 370 (2001).
- [104] R. Cester *et al.* [AUGER Collaboration], *Proc. of 27th ICRC (Hamburg)*, 711 (2001).
- [105] K. S. Capelle, J. W. Cronin, G. Parente and E. Zas, *Astropart. Phys.* **8**, 321 (1998) [astro-ph/9801313].
- [106] A. Letessier-Selvon, *AIP Conf. Proc.* **566**, 157 (2000) [arXiv:astro-ph/0009444].
- [107] M. Teshima, *AIP Conf. Proc.* **566**, 184 (2000).
- [108] J. F. Krizmanic, J. F. Ormes and R. E. Streitmatter, *AIP Conf. Proc.* **433**, (1998).
- [109] D. Lamb, R. Chipman, L. Hillman, Y. Takahashi, and J. Dimmock, *AIP Conf. Proc.* **433**, 428 (1998).
- [110] D. Lamb, Internal OWL Technical Note, 1999.
- [111] K. Pitalo, Internal OWL Technical Note, 2000.
- [112] J. F. Krizmanic *et al.* [OWL Collaboration], *Proc. of 27th ICRC (Hamburg)*, 861 (2001).
- [113] O. Catalano, *Nuovo Cim.* **24C** (2001) 445.
- [114] A. Roberts, *Rev. Mod. Phys.* **64** (1992) 259.
- [115] V. A. Balkanov *et al.* [Baikal Collaboration], arXiv:astro-ph/9906255.
- [116] M. Kowalski *et al.* [AMANDA Collaboration], arXiv:hep-ph/0112083.
- [117] E. Aslanides *et al.* [ANTARES Collaboration], arXiv:astro-ph/9907432.
- [118] P. K. Grieder [NESTOR Collaboration], *Nuovo Cim.* **24C** (2001) 771.
- [119] J. Alvarez-Muniz and F. Halzen, *AIP Conf. Proc.* **579**, 305 (2001) [arXiv:astro-ph/0102106].
- [120] M. Aglietta *et al.*, *Nuovo Cim. C* **9** (1986) 262.
- [121] M. Aglietta *et al.*, *Nucl. Instrum. Meth. A* **277** (1989) 23.
- [122] C. Berger *et al.* [FREJUS Collaboration], *Nucl. Instrum. Meth. A* **262**, 463 (1987).
- [123] W. Rhode *et al.* [Frejus Collaboration], *Astropart. Phys.* **4** (1996) 217.

- [124] R. Gandhi, C. Quigg, M. H. Reno and I. Sarcevic, Phys. Rev. D **58**, 093009 (1998) [arXiv:hep-ph/9807264].
- [125] R. M. Baltrusaitis *et al.*, Phys. Rev. D **31**, 2192 (1985).
- [126] L. A. Anchordoqui, J. L. Feng, H. Goldberg and A. D. Shapere, Phys. Rev. D (to be published) [arXiv:hep-ph/0207139].
- [127] G. Domokos and S. Kovesi-Domokos, hep-ph/9801362.
- [128] G. Domokos and S. Kovesi-Domokos, hep-ph/9805221.
- [129] D. Fargion, astro-ph/0002453.
- [130] D. Fargion, astro-ph/0101565.
- [131] X. Bertou, P. Billoir, O. Deligny, C. Lachaud and A. Letessier-Selvon, astro-ph/0104452.
- [132] J. L. Feng, P. Fisher, F. Wilczek and T. M. Yu, Phys. Rev. Lett. **88**, 161102 (2002) [arXiv:hep-ph/0105067].
- [133] A. Kusenko and T. Weiler, Phys. Rev. Lett. **88**, 161101 (2002) [arXiv:hep-ph/0106071].
- [134] I. Kravchenko *et al.* [RICE Collaboration], arXiv:astro-ph/0112372.
- [135] P. W. Gorham, K. M. Liewer and C. J. Naudet, arXiv:astro-ph/9906504.
- [136] P. W. Gorham, K. M. Liewer, C. J. Naudet, D. P. Saltzberg and D. R. Williams, arXiv:astro-ph/0102435.
- [137] F. Halzen and D. Hooper, arXiv:astro-ph/0204527.
- [138] A. M. Hillas, Ann. Rev. Astron. Astrophys. **22**, 425 (1984).
- [139] W. F. G. Swann, Phys. Rev. **43**, 217 (1933).
- [140] E. Fermi, Phys. Rev. **75**, 1169 (1949).
- [141] L. A. Anchordoqui, D. F. Torres, T. P. McCauley, G. E. Romero and F. A. Aharonian, arXiv:hep-ph/0211231.
- [142] R. J. Protheroe, arXiv:astro-ph/9812055.
- [143] R. Blandford and D. Eichler, Phys. Rept. **154**, 1 (1987).
- [144] R. D. Blandford and J. P. Ostriker, Astrophys. J. **221** (1978) L29.
- [145] P. L. Biermann, J. Phys. G **23**, 1 (1997).
- [146] M. Ostrowski, arXiv:astro-ph/0101053.
- [147] P. O. Lagage and C. J. Cesarsky, Astron. Astrophys. **118**, 223 (1983).
- [148] H. J. Voelk and P. L. Biermann, Astrophys. J. Lett. **333**, L65 (1988).
- [149] J. R. Jokipii and G. Morfill, Astrophys. J. **312**, 170 (1987).
- [150] A. Venkatesan, M. C. Miller and A. V. Olinto, Astrophys. J. **484**, 323 (1997) [arXiv:astro-ph/9612210].
- [151] R. J. Protheroe and A. P. Szabo, Phys. Rev. Lett. **69**, 2885 (1992).
- [152] P. G. Tinyakov and I. I. Tkachev, JETP Lett. **74**, 445 (2001) [Pisma Zh. Eksp. Teor. Fiz. **74**, 499 (2001)] [arXiv:astro-ph/0102476].
- [153] D. S. Gorbunov, P. G. Tinyakov, I. I. Tkachev and S. V. Troitsky, arXiv:astro-ph/0204360.
- [154] E. Boldt and P. Ghosh, Mon. Not. Roy. Astron. Soc. **307**, 491 (1999) [arXiv:astro-ph/9902342].
- [155] E. Boldt and M. Loewenstein, Mon. Not. Roy. Astron. Soc. **316**, L29 (2000)

- [arXiv:astro-ph/0006221].
- [156] D. F. Torres, E. Boldt, T. Hamilton and M. Loewenstein, arXiv:astro-ph/0204419.
 - [157] C. A. Norman, D. B. Melrose, and A. Achterberg, *Astrophys. J.* **454**, 60 (1995).
 - [158] H. Kang, J. P. Rachen and P. L. Biermann, *Mon. Not. Roy. Astron. Soc.* **286**, 257 (1997) [arXiv:astro-ph/9608071].
 - [159] F. Miniati, D. Ryu, H. Kang and T. W. Jones, arXiv:astro-ph/9906169.
 - [160] A. Smialkowski, M. Giller, W. Michalak, arXiv:astro-ph/0203337.
 - [161] J. P. Rachen and P. L. Biermann, *Astron. Astrophys.* **272**, 161 (1993) [arXiv:astro-ph/9301010].
 - [162] J. P. Rachen, T. Stanev and P. L. Biermann, *Astron. Astrophys.* **273**, 377 (1993) [arXiv:astro-ph/9302005].
 - [163] L. A. Anchordoqui, G. E. Romero, J. A. Combi and S. E. Perez Bergliaffa, *Mod. Phys. Lett. A* **13**, 3039 (1998).
 - [164] M. Ostrowski, arXiv:astro-ph/9803299.
 - [165] M. Ostrowski, *Mon. Not. Roy. Astron. Soc.* **312**, 579 (2000).
 - [166] C. Litwin and R. Rosner, *Phys. Rev. Lett.* **86**, 4745 (2001) [arXiv:astro-ph/0104090].
 - [167] C. Kouveliotou, *Proc. Natl. Acad. Sci.* **96**, 5351 (1999).
 - [168] C. Kouveliotou *et al.*, *Astrophys. J.* **510**, L115 (1999).
 - [169] C. Kouveliotou *et al.*, *Nature* **393**, 235 (1998).
 - [170] P. Bhattacharjee and G. Sigl, *Phys. Rept.* **327**, 109 (2000) [arXiv:astro-ph/9811011].
 - [171] J. Arons, arXiv:astro-ph/0208444.
 - [172] J. W. Elbert and P. Sommers, *Astrophys. J.* **441**, 151 (1995) [arXiv:astro-ph/9410069].
 - [173] L. A. Anchordoqui, G. E. Romero and J. A. Combi, *Phys. Rev. D* **60**, 103001 (1999) [arXiv:astro-ph/9903145].
 - [174] L. Anchordoqui, H. Goldberg, S. Reucroft and J. Swain, *Phys. Rev. D* **64**, 123004 (2001) [arXiv:hep-ph/0107287].
 - [175] P. Blasi, R. I. Epstein and A. V. Olinto, *Astrophys. J.* **533** (2000) L123 [arXiv:astro-ph/9912240].
 - [176] E. Waxman, *Phys. Rev. Lett.* **75**, 386 (1995) [arXiv:astro-ph/9505082].
 - [177] M. Vietri, *Astrophys. J.* **453**, 883 (1995) [arXiv:astro-ph/9506081].
 - [178] M. Milgrom and V. Usov, *Astropart. Phys.* **4**, 365 (1996) [arXiv:astro-ph/9506099].
 - [179] J. Miralda-Escude and E. Waxman, *Astrophys. J.* **462**, L59 (1996) [arXiv:astro-ph/9601012].
 - [180] J. Madsen and J. M. Larsen, arXiv:astro-ph/0211597.
 - [181] L. Anchordoqui, T. Paul, S. Reucroft and J. Swain, movie-script in preparation.
 - [182] D. F. Torres, G. E. Romero, T. M. Dame, J. A. Combi and Y. M. Butt, arXiv:astro-ph/0209565.
 - [183] F. A. Aharonian, A. A. Belyanin, E. V. Derishev, V. V. Kocharovskiy and V. V. Kocharovskiy, arXiv:astro-ph/0202229.
 - [184] B. L. Fannaroff and J. M. Riley, *Mon. Not. Roy. Astron. Soc.* **167**, 31 (1974).
 - [185] R. D. Blandford and M. J. Rees, *Mon. Not. Roy. Astron. Soc.* **169**, 395 (1974).
 - [186] M. C. Begelman, R. D. Blandford and M. J. Rees, *Rev. Mod. Phys.* **56**, 255 (1984).

- [187] P. L. Biermann and P. A. Strittmatter, *Astrophys. J.* **322** (1987) 643.
- [188] A. N. Kolmogorov, *C. R. Acad. URSS* **30**, 201 (1941).
- [189] L. O. 'C. Drury, *Rep. Prog. Phys.* **46**, 973 (1983).
- [190] K. Mannheim, *Space Sci. Rev.* **75** (1996) 331.
- [191] K. Mannheim, *Science* **279**, 684 (1998) [arXiv:astro-ph/9803241].
- [192] K. Mannheim, *Rev. Mod. Astron.* **12**, 101 (1999) [arXiv:astro-ph/9902185].
- [193] K. Mannheim, *Astron. Astrophys.* **269**, 67 (1993) [arXiv:astro-ph/9302006].
- [194] F. A. Aharonian, *New Astron.* **5** (2000) 377 [arXiv:astro-ph/0003159].
- [195] G. B. Rybicki and A. P. Lightman, *Radiative Processes in Astrophysics* (New York: Wiley-Interscience, 1979).
- [196] T. A. Armstrong *et al.*, *Phys. Rev. D* **5** (1972) 1640.
- [197] L. A. Anchordoqui and H. Goldberg, *Phys. Rev. D* **65**, 021302 (2002) [arXiv:hep-ph/0106217].
- [198] J. T. Stocke, G. H. Rieke, and M. J. Lebofsky, *Nature* **294**, 319 (1981).
- [199] J. R. P. Angel and H. S. Stockman, *Ann. Rev. Astron. Astrophys.* **18**, 321 (1980).
- [200] G. J. Fishman and C. A. Meegan, *An. Rev. Astron. Astrophys.* **33**, 415 (1995).
- [201] B. Link and R. I. Epstein, *Astrophys. J.* **466**, 764 (1996) [arXiv:astro-ph/9601033].
- [202] G. E. Romero, D. F. Torres, I. Andruchow, L. A. Anchordoqui and B. Link, *Mon. Not. Roy. Astron. Soc.* **308**, 799 (1999) [arXiv:astro-ph/9904107].
- [203] C. A. Meegan *et al.*, *Nature* **355**, 143 (1992).
- [204] M. R. Metzger *et al.*, *Nature* **387**, 878 (1997).
- [205] S. R. Kulkarni *et al.*, arXiv:astro-ph/0002168.
- [206] G. Cavallo and M. J. Rees, *Mon. Not. Roy. Astron. Soc.* **183**, 359 (1978).
- [207] B. Paczynski, *Astrophys. J.* **308**, L43 (1986).
- [208] J. Goodman, *Astrophys. J.* **308**, L47 (1986).
- [209] P. Meszaros and M. J. Rees, *Astrophys. J.* **405**, 278 (1993).
- [210] P. Meszaros, P. Laguna, and M. J. Rees, *Astrophys. J.* **415**, 181 (1993).
- [211] T. Piran, *Phys. Rept.* **314** (1999) 575 [arXiv:astro-ph/9810256].
- [212] T. Piran, *Phys. Rept.* **333** (2000) 529 [arXiv:astro-ph/9907392].
- [213] E. Waxman, arXiv:astro-ph/0103186.
- [214] J. Bednarz and M. Ostrowski, *Phys. Rev. Lett.* **80** (1998) 3911 [arXiv:astro-ph/9806181].
- [215] M. Milgrom and V. Usov, *Astrophys. J. Lett.* **449**, L37 (1995) [arXiv:astro-ph/9505009].
- [216] T. Stanev, R. Schaefer and A. Watson, *Astropart. Phys.* **5**, 75 (1996) [arXiv:astro-ph/9601140].
- [217] F. W. Stecker, *Astropart. Phys.* **14** (2000) 207 [arXiv:astro-ph/9911269].
- [218] S. T. Scully and F. W. Stecker, *Astropart. Phys.* **16** (2002) 271 [arXiv:astro-ph/0006112].
- [219] J. N. Bahcall and E. Waxman, arXiv:hep-ph/0206217.
- [220] A. Loeb and E. Waxman, arXiv:astro-ph/0205272.
- [221] G. Sigl, *Lect. Notes Phys.* **576**, 196 (2001).
- [222] A. A. Penzias and R. W. Wilson, *Astrophys. J.* **142** (1965) 419.

- [223] K. Greisen, Phys. Rev. Lett. **16** (1966) 748.
- [224] G. T. Zatsepin and V. A. Kuzmin, JETP Lett. **4**, 78 (1966) [Pisma Zh. Eksp. Teor. Fiz. **4**, 114 (1966)].
- [225] F. W. Stecker, Phys. Rev. Lett. **21**, 1016 (1968).
- [226] C. T. Hill and D. N. Schramm, Phys. Rev. D **31**, 564 (1985).
- [227] V. S. Berezhinsky and S. I. Grigor'eva, Astron. Astrophys. **199**, 1 (1988).
- [228] F. W. Stecker, Nature **342**, 401 (1989).
- [229] F. A. Aharonian, B. L. Kanevsky and V. V. Vardanian, Astrophys. Space. Sci. **167**, 93 (1990).
- [230] S. Yoshida and M. Teshima, Prog. Theor. Phys. **89**, 833 (1993).
- [231] F. A. Aharonian and J. W. Cronin, Phys. Rev. D **50** (1994) 1892.
- [232] R. J. Protheroe and P. A. Johnson, Astropart. Phys. **4**, 253 (1996) [arXiv:astro-ph/9506119].
- [233] L. A. Anchordoqui, M. T. Dova, L. N. Epele and J. D. Swain, Nucl. Phys. Proc. Suppl. **52B**, 249 (1997).
- [234] L. A. Anchordoqui, M. T. Dova, L. N. Epele and J. D. Swain, Phys. Rev. D **55**, 7356 (1997) [arXiv:hep-ph/9704387].
- [235] S. Lee, Phys. Rev. D **58**, 043004 (1998) [arXiv:astro-ph/9604098].
- [236] A. Achterberg, Y. A. Gallant, C. A. Norman and D. B. Melrose, arXiv:astro-ph/9907060.
- [237] T. Stanev, R. Engel, A. Mucke, R. J. Protheroe and J. P. Rachen, Phys. Rev. D **62**, 093005 (2000) [arXiv:astro-ph/0003484].
- [238] Z. Fodor and S. D. Katz, Phys. Rev. D **63**, 023002 (2001) [arXiv:hep-ph/0007158].
- [239] L. A. Anchordoqui and D. F. Torres, Phys. Lett. A **283**, 319 (2001) [arXiv:cond-mat/0009199].
- [240] V. Berezhinsky, A. Z. Gazizov and S. I. Grigorieva, arXiv:hep-ph/0204357.
- [241] V. Berezhinsky, A. Z. Gazizov and S. I. Grigorieva, arXiv:astro-ph/0210095.
- [242] D. E. Groom *et al.* [Particle Data Group Collaboration], Eur. Phys. J. C **15** (2000) 1.
- [243] J. C. Mather *et al.*, Astrophys. J. **354** (1990) L37.
- [244] G. R. Blumenthal, Phys. Rev. D **1** (1970) 1596.
- [245] R. M. Barnett *et al.* [Particle Data Group Collaboration], Phys. Rev. D **54** (1996) 1.
- [246] L. Montanet *et al.* [Particle Data Group Collaboration], Phys. Rev. D **50** (1994) 1173. See p. 1335.
- [247] I. Golyak, Mod. Phys. Lett. A **7** (1992) 2401.
- [248] M. Abramowitz, I. A. Stegun, "Handbook of Mathematical Functions" (Dover, New York, 1970).
- [249] V. S. Berezhinsky and G. T. Zatsepin, Phys. Lett. B **28**, 423 (1969).
- [250] F. W. Stecker, Astrophys. J. **228**, 919 (1979).
- [251] R. J. Protheroe, Nucl. Phys. Proc. Suppl. **77**, 465 (1999).
- [252] R. Engel, D. Seckel and T. Stanev, Phys. Rev. D **64**, 093010 (2001) [arXiv:astro-ph/0101216].
- [253] L. A. Anchordoqui, J. L. Feng, H. Goldberg and A. D. Shapere, Phys. Rev. D **65**,

- 124027 (2002) [arXiv:hep-ph/0112247].
- [254] J. A. Peacock, Mon. Not. Roy. Astron. Soc. **217**, 601 (1985).
 - [255] J. L. Puget, F. W. Stecker and J. H. Bredekamp, Astrophys. J. **205** (1976) 638.
 - [256] M. J. Chodorowski, A. A. Zdziarski, and M. Sikora, Astrophys. J. **400**, 181 (1992).
 - [257] S. Michalowski, D. Andrews, J. Eickmeyer, T. Gentile, N. Mistry, R. Talman and K. Ueno, Phys. Rev. Lett. **39** (1977) 737.
 - [258] F. W. Stecker, Phys. Rev. **180** (1969) 1264.
 - [259] L. A. Anchordoqui, M. T. Dova, L. N. Epele and J. D. Swain, Phys. Rev. D **57**, 7103 (1998) [arXiv:astro-ph/9708082].
 - [260] F. W. Stecker and M. H. Salamon, Astrophys. J. **512**, 521 (1992) [arXiv:astro-ph/9808110].
 - [261] L. A. Anchordoqui, *Ph.D. Thesis* [arXiv:astro-ph/9812445].
 - [262] L. N. Epele and E. Roulet, JHEP **9810**, 009 (1998) [arXiv:astro-ph/9808104].
 - [263] E. M. Burbidge, G. R. Burbidge, W. A. Fowler, and F. Hoyle, Rev. Mod. Phys. **29**, 547 (1957).
 - [264] L. A. Anchordoqui, M. T. Dova, T. P. McCauley, S. Reucroft and J. D. Swain, Phys. Lett. B **482**, 343 (2000) [arXiv:astro-ph/9912081].
 - [265] L. A. Anchordoqui, M. Kirasirova, T. P. McCauley, S. Reucroft and J. D. Swain, Phys. Lett. B **492**, 237 (2000) [arXiv:astro-ph/0007403].
 - [266] L. A. Anchordoqui, M. T. Dova, T. P. McCauley, T. Paul, S. Reucroft and J. D. Swain, Nucl. Phys. Proc. Suppl. **97**, 203 (2001) [arXiv:astro-ph/0006071].
 - [267] N. C. Wickramasinghe, Mon. Not. R. Astr. Soc. **159**, 269 (1972).
 - [268] L. Spitzer Jr., Phys. Rev. **76**, 583 (1949)
 - [269] N. C. Wickramasinghe, Astrophys. Space Sci. **28**, L25 (1974).
 - [270] R. I. Epstein, Mon. Not. R. Astr. Soc. **193**, 723 (1980).
 - [271] V. S. Berezinsky and O. F. Prilutsky, Astrophys. Space Sci. **21**, 475 (1973).
 - [272] V. L. Ginzburg, V. A. Dogiel, V. S. Berezinsky, S. V. Bulanov and V. S. Ptuskin, *Astrophysics Of Cosmic Rays*, (North-Holland, 1990).
 - [273] B. McBreen, S. Plunkett, and C. J. Lambert, Astrophys. Space Sci. **205**, 355 (1993).
 - [274] W. J. Veigele, *Atomic Data Tables* **5**, 51 (1973).
 - [275] J. A. Combi, G. E. Romero, and P. Benaglia, Astrophys. J. **519**, L177 (1999).
 - [276] A. I. Nikishov, Sov. Phys. JETP **14**, 393 (1962) [Zh. Eksp. Teor. Fiz. **41**, 549 (1961)].
 - [277] P. Goldreich and P. Morrison, Sov. Phys. JETP **18**, 239 (1964) [Zh. Eksp. Teor. Fiz. **45**, 344 (1963)].
 - [278] J. V. Jelley, Phys. Rev. Lett. **16**, 479 (1966).
 - [279] R. J. Gould and G. P. Schröder, Phys. Rev. **155**, 1408 (1967).
 - [280] F. W. Stecker, Astrophys. J. **157**, 507 (1969).
 - [281] G. G. Fazio and F. W. Stecker, Nature **226**, 135 (1970).
 - [282] V. Berezinsky, Sov. J. Nucl. Phys. **11**, 222 (1970) [Yad. Fiz. **11**, 399 (1970)].
 - [283] J. D. Bjorken and S. D. Drell, *Relativistic Quantum Mechanics*, (Mc Graw-Hill Book Company, 1964).
 - [284] R. J. Gould and G. P. Schröder, Phys. Rev. **155**, 1404 (1967).

- [285] R. W. Brown, W. F. Hunt, K. O. Mikaelian and I. J. Muzinich, *Phys. Rev. D* **8** (1973) 3083.
- [286] A. J. Turtle, J. F. Pugh, S. Kenderdine, and I. I. K. Pauliny-Toth *Mon. Not. R. Astr. Soc.* **124**, 297 (1962).
- [287] T. A. Clark, L. W. Brown, and J. K. Alexander, *Nature* **228**, 847 (1970).
- [288] R. J. Protheroe and P. L. Biermann, *Astropart. Phys.* **6**, 45 (1996) [Erratum-ibid. **7**, 181 (1996)] [arXiv:astro-ph/9605119].
- [289] J. E. Felten and P. Morrison, *Astrophys. J.* **146**, 686 (1966).
- [290] R. J. Gould, *Astrophys. J.* **230** (1979) 967.
- [291] J. Wdowczyk, W. Tkaczyk, and A. W. Wolfendale, *J. Phys. A* **5**, 1419 (1972).
- [292] O. E. Kalashev, V. A. Kuzmin, D. V. Semikoz and I. I. Tkachev, arXiv:astro-ph/0107130.
- [293] T. Stanev, *Astrophys. J.* **479**, 290 (1997).
- [294] G. A. Medina Tanco, E. M. de Gouveia Dal Pino and J. E. Horvath, arXiv:astro-ph/9707041.
- [295] D. Harari, S. Mollerach and E. Roulet, *JHEP* **08**, 022 (1999) [arXiv:astro-ph/9906309].
- [296] D. Harari, S. Mollerach and E. Roulet, *JHEP* **0002**, 035 (2000) [arXiv:astro-ph/0001084].
- [297] A. A. Lee and R. W. Clay, *J. Phys. G* **21** (1995) 1743.
- [298] D. Harari, S. Mollerach and E. Roulet, arXiv:astro-ph/0205484.
- [299] L. A. Anchordoqui, H. Goldberg and D. F. Torres, arXiv:astro-ph/0209546.
- [300] K.-T. Kim, P. P. Kronberg, G. Giovannini and T. Venturi, *Nature* **341**, 720 (1989).
- [301] T. E. Clarke, P. P. Kronberg and H. Böhringer, *Astrophys. J.* **547**, L111 (2001).
- [302] D. Ryu, H. Kang, and P. L. Biermann, *Astron. Astrophys.* **335**, 19 (1998).
- [303] P. P. Kronberg, *Rept. Prog. Phys.* **57**, 325 (1994).
- [304] J. P. Vallée, *Astrophys. J.* **360**, 1 (1990).
- [305] P. Blasi, S. Burles and A. V. Olinto, *Astrophys. J.* **514**, L79 (1999) [arXiv:astro-ph/9812487].
- [306] E. Waxman and J. Miralda-Escude, *Astrophys. J.* **472**, L89 (1996) [arXiv:astro-ph/9607059].
- [307] J. Wdowczyk and A. W. Wolfendale, *Nature* **281** (1979) 356.
- [308] P. Blasi and A. V. Olinto, *Phys. Rev. D* **59** (1999) 023001 [arXiv:astro-ph/9806264].
- [309] G. Sigl, M. Lemoine and P. Biermann, *Astropart. Phys.* **10**, 141 (1999) [arXiv:astro-ph/9806283].
- [310] G. Medina Tanco, arXiv:astro-ph/9808073.
- [311] M. Lemoine, G. Sigl and P. Biermann, arXiv:astro-ph/9903124.
- [312] G. R. Farrar and T. Piran, *Phys. Rev. Lett.* **84**, 3527 (2000) [arXiv:astro-ph/9906431].
- [313] D. Harari, S. Mollerach, E. Roulet and F. Sanchez, arXiv:astro-ph/0202362.
- [314] J. P. Vallée, *Astron. J.* **99**, 459 (1990).
- [315] R. C. Thomson and A. H. Nelson, *Mon. Not. Roy. Astron. Soc.* **201**, 365 (1982)
- [316] D. G. Wentzel, *Ann. Rev. Astron. Astrophys.* **12**, 71 (1974).
- [317] F. Casse, M. Lemoine and G. Pelletier, *Phys. Rev. D* **65**, 023002 (2002) [arXiv:astro-

- ph/0109223].
- [318] G. F. D. Duff and D. Naylor, *Differential Equations of Applied Mathematics*, (John Wiley & Sons, Inc., New York, 1966).
 - [319] G. R. Farrar and T. Piran, arXiv:astro-ph/0010370.
 - [320] M. Blanton, P. Blasi and A. V. Olinto, *Astropart. Phys.* **15**, 275 (2001) [arXiv:astro-ph/0009466].
 - [321] G. Medina-Tanco, *Astrophys. J.* **510**, L91 (1999) [arXiv:astro-ph/9810366].
 - [322] J. Linsley, *Asrophys. J.* **235**, L167 (1980).
 - [323] L. A. Anchordoqui, *Phys. Rev. D* **61**, 087302 (2000) [arXiv:astro-ph/9911044].
 - [324] V. N. Zirakashvili, D. N. Pochepkin, V. S. Ptuskin and S. I. Rogovaya, *Bull. Russ. Acad. Sci. Phys.* **59** (1995) 668 [*Izv. Ross. Akad. Nauk.* **59N4** (1995) 153].
 - [325] P. Goldreich and W. H. Julian, "Pulsar Electrodynamics," *Astrophys. J.* **157**, 869 (1969).
 - [326] M. A. Ruderman and P. G. Sutherland, *Astrophys. J.* **196**, 51 (1975).
 - [327] J. Arons and E. T. Scharlemann, *Astrophys. J.* **231**, 854 (1979).
 - [328] Y. A. Gallant and J. Arons, *Astrophys. J.* **435**, 230 (1994).
 - [329] M. C. Begelman and Z.-Y. Li, *Astrophys. J.* **426**, 269 (1994).
 - [330] L. Lindblom, B. J. Owen and S. M. Morsink, *Phys. Rev. Lett.* **80**, 4843 (1998) [arXiv:gr-qc/9803053].
 - [331] N. Andersson K. Kokkotas, and B. F. Schutz, *Astrophys. J.* **510**, 846 (1999).
 - [332] L. Rezzolla, F. K. Lamb, and S. L. Shapiro, *Astrophys. J.* **531** L141 (2000) [arXiv:astro-ph/9911188].
 - [333] F. P. Israel, *Astron. Astrophys. Rev.* **8**, 237 (1998).
 - [334] J. O. Burns, E. D. Feigelson, and E. J. Schreier, *Astrophys. J.* **273**, 128 (1983).
 - [335] L. Landau and E. Lifchitz, *Fluid Mechanics* (Pergamon Press, Oxford, 1958).
 - [336] G. E. Romero, S. Perez-Bergliaffa, L. A. Anchordoqui and J. A. Combi, *Grav. Cosmol.* **S5** (1999) 188.
 - [337] G. E. Romero, J. A. Combi, L. A. Anchordoqui and S. E. Perez Bergliaffa, *Astropart. Phys.* **5**, 279 (1996) [arXiv:gr-qc/9511031].
 - [338] N. Junkes, R. F. Haynes, J. I. Harnett, and D. L. Jauncey, *Astron. Astrophys.* **269**, 29 (1993) [Erratum, *ibid* **274**, 1009 (1993)].
 - [339] J. A. Combi and G. E. Romero, *Astron. Astrophys. Suppl.* **121**, 11 (1997).
 - [340] P. Sreekumar, D. L. Bertsch, R. C. Hartman, P. L. Nolan and D. J. Thompson, *Astropart. Phys.* **11** (1999) 221 [arXiv:astro-ph/9901277].
 - [341] J. E. Grindlay *et al.*, *Astrophys. J.* **197**, L9 (1975).
 - [342] H. Steinle, *AIP Conf. Proc.* **587**, 353 (2001) [arXiv:astro-ph/0105482].
 - [343] R. W. Clay, B. R. Dawson and R. Meyhandan, *Astropart. Phys.* **2** (1994) 347.
 - [344] V. L. Ginzburg, S. I. Syrovatsky, *Ann. Rev. Astron. Astrophys.* **3**, 297 (1965).
 - [345] S. Rawlings and R. Saunders, *Nature* **349**, 138 (1991).
 - [346] L. A. Anchordoqui, H. Goldberg and T. J. Weiler, *Phys. Rev. Lett.* **87**, 081101 (2001) [arXiv:astro-ph/0103043].
 - [347] R. L. Kinzer *et al.*, *Astrophys. J.* **449**, 105 (1995).

- [348] H. Steinle *et al.*, *Astron. Astrophys.* **330**, 97 (1998).
- [349] C. Isola, M. Lemoine and G. Sigl, *Phys. Rev. D* **65**, 023004 (2002) [arXiv:astro-ph/0104289].
- [350] C. Isola and G. Sigl, arXiv:astro-ph/0203273.
- [351] R. Blandford, *Lect. Notes Phys.* **530**, 1 (1999).
- [352] V. L. Ginzburg, S. I. Syrovatsky, *The origin of cosmic rays*, (Pergamon Press, Oxford 1964).
- [353] S. Heinz and M. C. Begelman, *Lect. Notes Phys.* **530**, 229 (1999).
- [354] G. V. Bicknell and M. C. Begelman, *Lect. Notes Phys.* **530**, 235 (1999).
- [355] E. J. Ahn, G. Medina-Tanco, P. L. Biermann and T. Stanev, arXiv:astro-ph/9911123.
- [356] P. L. Biermann, E. J. Ahn, G. Medina Tanco and T. Stanev, *Nucl. Phys. Proc. Suppl.* **87** (2000) 417 [arXiv:astro-ph/0008063].
- [357] J. A. Burke, *Mon. Not. Roy. Astron. Soc.* **140**, 241 (1968).
- [358] H. E. Johnson and W. I. Axford, *Astrophys. J.* **165**, 381 (1971).
- [359] W. G. Mathews and J. C. Baker, *Astrophys. J.* **170**, 241 (1971).
- [360] E. N. Parker, *Astrophys. J.* **128**, 664 (1958).
- [361] R. Beck, A. Brandenburg, D. Moss, A. Shukurov, and D. Sokoloff, *Ann. Rev. Astron. Astrophys.* **34**, 155 (1996).
- [362] G. Medina Tanco, private communication.
- [363] P. Billoir and A. Letessier-Selvon, arXiv:astro-ph/0001427.
- [364] P. L. Biermann, E. -J. Ahn, P. P. Kronberg, G. Medina Tanco, and T. Stanev, in *Physics and Astrophysics of Ultra-High-Energy Cosmic Rays*, (Edts. M. Lemoine and G. Sigl, Springer-Verlag, Berlin, 2001).
- [365] M. T. Dova, L. Epele and C. Hojvat, *Proc. of 25th ICRC (South Africa)* **7**, 381 (1997).
- [366] D. Harari, S. Mollerach and E. Roulet, *JHEP* **0010**, 047 (2000) [arXiv:astro-ph/0005483].
- [367] T. Stanev, D. Seckel and R. Engel, arXiv:astro-ph/0108338.
- [368] T. M. Heckman, L. Armus, and G. K. Miley, *Astrophys. J. Suppl.* **74**, 833 (1990).
- [369] G. H. Rieke *et al.*, *Astrophys. J.* **238**, 24 (1980).
- [370] C. W. Engelbracht, M. J. Rieke, G. H. Rieke, D. M. Kelly, and J. M. Achtermann, *Astrophys. J.* **505**, 639 (1998).
- [371] R. de Grijs, R. W. O'Connell and J. S. Gallagher, arXiv:astro-ph/9903188.
- [372] R. de Grijs, R. W. O'Connell and J. S. Gallagher, arXiv:astro-ph/0010046.
- [373] T. A. D. Paglione, A. P. Marscher, J. M. Jackson, and D. L. Bertsch, *Astrophys. J.* **460**, 295 (1996).
- [374] T. J. Davidge and C. J. Pritchett, *Astron. J.* **100**, 102 (1990), and references therein.
- [375] G. Bertone, C. Isola, M. Lemoine and G. Sigl, arXiv:astro-ph/0209192.
- [376] G. R. Farrar and P. L. Biermann, *Phys. Rev. Lett.* **81**, 3579 (1998) [arXiv:astro-ph/9806242].
- [377] C. M. Hoffman, *Phys. Rev. Lett.* **83**, 2471 (1999) [arXiv:astro-ph/9901026].
- [378] G. R. Farrar and P. L. Biermann, *Phys. Rev. Lett.* **83** (1999) 2472 [arXiv:astro-ph/9901315].

- [379] G. Sigl, D. F. Torres, L. A. Anchordoqui and G. E. Romero, Phys. Rev. D **63**, 081302 (2001) [arXiv:astro-ph/0008363].
- [380] A. Virmani, S. Bhattacharya, P. Jain, S. Razzaque, J. P. Ralston and D. W. McKay, arXiv:astro-ph/0010235.
- [381] T. Weiler, Phys. Rev. Lett. **49**, 234 (1982).
- [382] T. Weiler, Astrophys. J. **285**, 495 (1984).
- [383] G. R. Farrar, Phys. Rev. Lett. **76**, 4111 (1996) [arXiv:hep-ph/9603271].
- [384] V. Berezhinsky, M. Kachelriess and S. Ostapchenko, Phys. Rev. D **65**, 083004 (2002) [arXiv:astro-ph/0109026].
- [385] H. Sato and T. Tati, Prog. Theor. Phys. **47**, 1788 (1972).
- [386] D. A. Kirzhnits and V. A. Chechin, Yad. Fiz. **15**, 1051 (1972).
- [387] L. Gonzalez-Mestres, arXiv:physics/9705031.
- [388] S. R. Coleman and S. L. Glashow, arXiv:hep-ph/9808446.
- [389] S. R. Coleman and S. L. Glashow, Phys. Rev. D **59**, 116008 (1999) [arXiv:hep-ph/9812418].
- [390] E. Roulet, Phys. Rev. D **47**, 5247 (1993).
- [391] G. Domokos and S. Nussinov, Phys. Lett. B **187** (1987) 372.
- [392] G. Domokos and S. Kovesi-Domokos, Phys. Rev. D **38**, 2833 (1988).
- [393] J. Bordes, H. M. Chan, J. Faridani, J. Pfaudler and S. T. Tsou, arXiv:hep-ph/9705463.
- [394] J. Bordes, H. M. Chan, J. Faridani, J. Pfaudler and S. T. Tsou, Astropart. Phys. **8**, 135 (1998) [arXiv:astro-ph/9707031].
- [395] G. Domokos and S. Kovesi-Domokos, Phys. Rev. Lett. **82**, 1366 (1999) [hep-ph/9812260].
- [396] S. Nussinov and R. Shrock, Phys. Rev. D **59**, 105002 (1999) [hep-ph/9811323];
- [397] Y. Fukuda *et al.* [Super-Kamiokande Collaboration], Phys. Rev. Lett. **81**, 1562 (1998) [arXiv:hep-ex/9807003].
- [398] Y. Fukuda *et al.* [Super-Kamiokande Collaboration], Phys. Lett. B **433**, 9 (1998) [arXiv:hep-ex/9803006].
- [399] Y. Fukuda *et al.* [Super-Kamiokande Collaboration], Phys. Lett. B **436**, 33 (1998) [arXiv:hep-ex/9805006].
- [400] S. Fukuda *et al.* [Super-Kamiokande Collaboration], Phys. Rev. Lett. **85**, 3999 (2000) [arXiv:hep-ex/0009001].
- [401] M. Ambrosio *et al.* [MACRO Collaboration], Phys. Lett. B **517**, 59 (2001) [arXiv:hep-ex/0106049].
- [402] W. Hampel *et al.* [GALLEX Collaboration], Phys. Lett. B **447**, 127 (1999).
- [403] J. N. Abdurashitov *et al.* [SAGE Collaboration], Phys. Rev. C **60**, 055801 (1999) [arXiv:astro-ph/9907113].
- [404] S. Fukuda *et al.* [SuperKamiokande Collaboration], Phys. Rev. Lett. **86**, 5651 (2001) [arXiv:hep-ex/0103032].
- [405] S. Fukuda *et al.* [Super-Kamiokande Collaboration], Phys. Rev. Lett. **86**, 5656 (2001) [arXiv:hep-ex/0103033].
- [406] M. Altmann *et al.* [GNO Collaboration], Phys. Lett. B **490**, 16 (2000) [arXiv:hep-

- ex/0006034].
- [407] Q. R. Ahmad *et al.* [SNO Collaboration], Phys. Rev. Lett. **87**, 071301 (2001) [arXiv:nucl-ex/0106015].
 - [408] C. Athanassopoulos *et al.* [LSND Collaboration], Phys. Rev. Lett. **75**, 2650 (1995) [arXiv:nucl-ex/9504002].
 - [409] C. Athanassopoulos *et al.* [LSND Collaboration], Phys. Rev. C **54**, 2685 (1996) [arXiv:nucl-ex/9605001].
 - [410] C. Athanassopoulos *et al.* [LSND Collaboration], Phys. Rev. Lett. **77**, 3082 (1996) [arXiv:nucl-ex/9605003].
 - [411] C. Athanassopoulos *et al.* [LSND Collaboration], Phys. Rev. Lett. **81**, 1774 (1998) [arXiv:nucl-ex/9709006].
 - [412] C. Athanassopoulos *et al.* [LSND Collaboration], Phys. Rev. C **58**, 2489 (1998) [arXiv:nucl-ex/9706006].
 - [413] A. Aguilar *et al.* [LSND Collaboration], Phys. Rev. D **64**, 112007 (2001) [arXiv:hep-ex/0104049].
 - [414] K. Eitel [KARMEN Collaboration], Nucl. Phys. Proc. Suppl. **91**, 191 (2000) [arXiv:hep-ex/0008002].
 - [415] M. Apollonio *et al.* [CHOOZ Collaboration], Phys. Lett. B **466**, 415 (1999) [arXiv:hep-ex/9907037].
 - [416] F. Boehm *et al.*, Phys. Rev. Lett. **84**, 3764 (2000) [arXiv:hep-ex/9912050].
 - [417] G. L. Fogli, E. Lisi, D. Montanino and A. Palazzo, Phys. Rev. D **64**, 093007 (2001) [arXiv:hep-ph/0106247].
 - [418] J. N. Bahcall, M. C. Gonzalez-Garcia and C. Pena-Garay, JHEP **0108**, 014 (2001) [arXiv:hep-ph/0106258].
 - [419] M. C. Gonzalez-Garcia and Y. Nir, arXiv:hep-ph/0202058.
 - [420] V. D. Barger, T. J. Weiler and K. Whisnant, Phys. Lett. B **442**, 255 (1998) [arXiv:hep-ph/9808367].
 - [421] A. D. Dolgov, arXiv:hep-ph/0202122.
 - [422] R. A. Croft, W. Hu and R. Dave, Phys. Rev. Lett. **83**, 1092 (1999) [arXiv:astro-ph/9903335].
 - [423] M. Fukugita, G. C. Liu and N. Sugiyama, Phys. Rev. Lett. **84**, 1082 (2000) [arXiv:hep-ph/9908450].
 - [424] E. Gawiser, arXiv:astro-ph/0005475.
 - [425] X. Wang, M. Tegmark, M. Zaldarriaga, arXiv:astro-ph/0105091.
 - [426] S. Hannestad, arXiv:astro-ph/0205223.
 - [427] O. Elgaroy *et al.*, arXiv:astro-ph/0204152.
 - [428] S. Weinberg, Phys. Rev. **128**, 1457 (1962).
 - [429] T. J. Weiler, Astropart. Phys. **11**, 303 (1999) [arXiv:hep-ph/9710431].
 - [430] D. Fargion, B. Mele and A. Salis, Astrophys. J. **517**, 725 (1999) [arXiv:astro-ph/9710029].
 - [431] Z. Fodor, S. D. Katz and A. Ringwald, arXiv:hep-ph/0203198.
 - [432] Z. Fodor, S. D. Katz and A. Ringwald, Phys. Rev. Lett. **88**, 171101 (2002).

- [433] P. Sreekumar *et al.*, “EGRET Observations of the Extragalactic Gamma-Ray Emission,” *Astrophys. J.* **494**, 523 (1998).
- [434] S. Hundertmark *et al.* [AMANDA Collaboration], *Proc. of 27th ICRC (Hamburg)*, 1129 (2001).
- [435] K. Mannheim, R. J. Protheroe and J. P. Rachen, *Phys. Rev. D* **63**, 023003 (2001) [arXiv:astro-ph/9812398].
- [436] A. Ringwald, arXiv:hep-ph/0111112.
- [437] O. E. Kalashev, V. A. Kuzmin, D. V. Semikoz and G. Sigl, arXiv:hep-ph/0112351.
- [438] S. Davidson, S. Forte, P. Gambino, N. Rius and A. Strumia, *JHEP* **0202**, 037 (2002) [arXiv:hep-ph/0112302].
- [439] G. P. Zeller *et al.* [NuTeV Collaboration], *Phys. Rev. Lett.* **88**, 091802 (2002) [arXiv:hep-ex/0110059].
- [440] D. J. Chung, G. R. Farrar and E. W. Kolb, *Phys. Rev. D* **57**, 4606 (1998) [arXiv:astro-ph/9707036].
- [441] I. F. Albuquerque, G. R. Farrar and E. W. Kolb, *Phys. Rev. D* **59**, 015021 (1999) [arXiv:hep-ph/9805288].
- [442] P. Fayet, *Nucl. Phys. B* **90**, 104 (1975).
- [443] G. R. Farrar and P. Fayet, *Phys. Lett. B* **76**, 575 (1978).
- [444] G. R. Farrar and S. Weinberg, *Phys. Rev. D* **27**, 2732 (1983).
- [445] G. R. Farrar, *Phys. Lett. B* **265**, 395 (1991).
- [446] D. S. Gorbunov, G. G. Raffelt and D. V. Semikoz, *Phys. Rev. D* **64**, 096005 (2001) [arXiv:hep-ph/0103175].
- [447] G. Auriemma, L. Maiani and S. Petrarca, *Phys. Lett. B* **164** (1985) 179.
- [448] V. S. Berezinsky and B. L. Ioffe, *Sov. Phys. JETP* **63**, 920 (1986).
- [449] L. B. Okun and M. B. Voloshin, *Sov. J. Nucl. Phys.* **43**, 495 (1986) [*Yad. Fiz.* **43**, 779 (1986)].
- [450] F. Buccella, G. R. Farrar and A. Pugliese, *Phys. Lett. B* **153**, 311 (1985).
- [451] J. Adams *et al.* [KTeV Collaboration], *Phys. Rev. Lett.* **79**, 4083 (1997) [arXiv:hep-ex/9709028].
- [452] V. Fanti *et al.* [NA48 Collaboration], *Phys. Lett. B* **446**, 117 (1999).
- [453] A. Alavi-Harati *et al.* [KTeV Collaboration], *Phys. Rev. Lett.* **83**, 2128 (1999) [arXiv:hep-ex/9903048].
- [454] I. F. Albuquerque *et al.* [E761 Collaboration], *Phys. Rev. Lett.* **78**, 3252 (1997) [arXiv:hep-ex/9604002].
- [455] F. Csikor and Z. Fodor, *Phys. Rev. Lett.* **78**, 4335 (1997) [arXiv:hep-ph/9611320].
- [456] R. Barate *et al.* [ALEPH Collaboration], *Z. Phys. C* **76**, 1 (1997).
- [457] H. Baer, K. Cheung and J. F. Gunion, *Phys. Rev. D* **59**, 075002 (1999) [arXiv:hep-ph/9806361].
- [458] S. Raby and K. Tobe, *Nucl. Phys. B* **539**, 3 (1999) [arXiv:hep-ph/9807281].
- [459] A. Mafi and S. Raby, *Phys. Rev. D* **62**, 035003 (2000) [arXiv:hep-ph/9912436].
- [460] L. Anchordoqui, M. T. Dova, D. Gomez Dumm and P. Lacentre, *Z. Phys. C* **73**, 465 (1997) [arXiv:gr-qc/9512015].

- [461] S. R. Coleman and S. L. Glashow, Phys. Lett. B **405**, 249 (1997) [arXiv:hep-ph/9703240].
- [462] F. W. Stecker and S. L. Glashow, Astropart. Phys. **16**, 97 (2001) [arXiv:astro-ph/0102226].
- [463] L. Stodolsky, Phys. Lett. B **201**, 353 (1988).
- [464] S. K. Lamoreaux, J. P. Jacobs, B. R. Heckel, F. J. Raab and E. N. Fortson, Phys. Rev. Lett. **57**, 3125 (1986).
- [465] G. Amelino-Camelia, J. R. Ellis, N. E. Mavromatos and D. V. Nanopoulos, Int. J. Mod. Phys. A **12**, 607 (1997) [arXiv:hep-th/9605211].
- [466] G. Amelino-Camelia, J. R. Ellis, N. E. Mavromatos, D. V. Nanopoulos and S. Sarkar, Nature **393**, 763 (1998) [arXiv:astro-ph/9712103].
- [467] O. Bertolami and C. S. Carvalho, Phys. Rev. D **61**, 103002 (2000) [arXiv:gr-qc/9912117].
- [468] R. Aloisio, P. Blasi, P. L. Ghia and A. F. Grillo, Phys. Rev. D **62**, 053010 (2000) [arXiv:astro-ph/0001258].
- [469] O. Bertolami, Gen. Rel. Grav. **34**, 707 (2002) [arXiv:astro-ph/0012462].
- [470] R. Aloisio, P. Blasi, A. Galante, P. L. Ghia and A. F. Grillo, arXiv:astro-ph/0205271.
- [471] N. Arkani-Hamed, S. Dimopoulos and G. R. Dvali, Phys. Lett. B **429**, 263 (1998) [hep-ph/9803315].
- [472] I. Antoniadis, N. Arkani-Hamed, S. Dimopoulos and G. R. Dvali, Phys. Lett. B **436**, 257 (1998) [arXiv:hep-ph/9804398].
- [473] N. Arkani-Hamed, S. Dimopoulos and G. R. Dvali, Phys. Rev. D **59**, 086004 (1999) [arXiv:hep-ph/9807344].
- [474] L. Randall and R. Sundrum, Phys. Rev. Lett. **83**, 3370 (1999) [hep-ph/9905221].
- [475] T. Kaluza, Sitzungsber. Preuss. Akad. Wiss. Berlin (Math. Phys.) **K1**, 966 (1921).
- [476] O. Klein, Z. Phys. **37**, 895 (1926) [Surveys High Energ. Phys. **5**, 241 (1926)].
- [477] O. Klein, Nature **118**, 516 (1926).
- [478] C. D. Hoyle, U. Schmidt, B. R. Heckel, E. G. Adelberger, J. H. Gundlach, D. J. Kapner and H. E. Swanson, Phys. Rev. Lett. **86**, 1418 (2001) [hep-ph/0011014].
- [479] G. R. Dvali and M. A. Shifman, Phys. Lett. B **396**, 64 (1997) [Erratum-ibid. B **407**, 452 (1997)] [arXiv:hep-th/9612128].
- [480] B. Bajc and G. Gabadadze, Phys. Lett. B **474**, 282 (2000) [arXiv:hep-th/9912232].
- [481] L. Randall and R. Sundrum, Phys. Rev. Lett. **83**, 4690 (1999) [arXiv:hep-th/9906064].
- [482] S. W. Hawking, T. Hertog and H. S. Reall, Phys. Rev. D **62**, 043501 (2000) [arXiv:hep-th/0003052].
- [483] M. J. Duff and J. T. Liu, Phys. Rev. Lett. **85**, 2052 (2000) [Class. Quant. Grav. **18**, 3207 (2000)] [arXiv:hep-th/0003237].
- [484] L. Anchordoqui, C. Nunez and K. Olsen, JHEP **0010**, 050 (2000) [arXiv:hep-th/0007064].
- [485] J. Maldacena, Adv. Theor. Math. Phys. **2**, 231 (1998) [Int. J. Theor. Phys. **38**, 1113 (1998)] [arXiv:hep-th/9711200].
- [486] R. Rattazzi and A. Zaffaroni, JHEP **0104**, 021 (2001) [arXiv:hep-th/0012248]. See also

- [487] M. Perez-Victoria, JHEP **0105**, 064 (2001) [arXiv:hep-th/0105048].
- [488] H. Davoudiasl, J. L. Hewett and T. G. Rizzo, Phys. Rev. Lett. **84**, 2080 (2000) [arXiv:hep-ph/9909255].
- [489] S. Abachi *et al.* [D0 Collaboration], Phys. Lett. B **385**, 471 (1996).
- [490] S. Abachi *et al.* [D0 Collaboration], Phys. Rev. Lett. **76**, 3271 (1996) [arXiv:hep-ex/9512007].
- [491] B. Abbott *et al.* [D0 Collaboration], Phys. Rev. Lett. **82**, 29 (1999).
- [492] F. Abe *et al.* [CDF Collaboration], Phys. Rev. Lett. **79**, 2192 (1997).
- [493] F. Abe *et al.* [CDF Collaboration], Phys. Rev. Lett. **77**, 5336 (1996) [Erratum-ibid. **78**, 4307 (1996)] [arXiv:hep-ex/9609011].
- [494] F. Abe *et al.* [CDF Collaboration], Phys. Rev. Lett. **74** (1995) 2900.
- [495] H. Davoudiasl, J. L. Hewett and T. G. Rizzo, Phys. Rev. D **63**, 075004 (2001) [arXiv:hep-ph/0006041].
- [496] L. A. Anchordoqui, H. Goldberg and A. D. Shapere, Phys. Rev. D **66**, 024033 (2002) [arXiv:hep-ph/0204228].
- [497] A. Jain, P. Jain, D. W. McKay and J. P. Ralston, arXiv:hep-ph/0011310.
- [498] A. Jain, P. Jain, D. W. McKay and J. P. Ralston, Int. J. Mod. Phys. A **17** (2002) 533.
- [499] H. Davoudiasl, J. L. Hewett and T. G. Rizzo, arXiv:hep-ph/0010066.
- [500] R. Emparan, M. Masip and R. Rattazzi, Phys. Rev. D **65**, 064023 (2002) [arXiv:hep-ph/0109287].
- [501] M. Kachelriess and M. Plumacher, Phys. Rev. D **62**, 103006 (2000) [astro-ph/0005309];
- [502] L. Anchordoqui, H. Goldberg, J. MacLeod, T. McCauley, T. Paul, S. Reucroft and J. Swain, Mod. Phys. Lett. A **16**, 809 (2001) [arXiv:hep-ph/0104114].
- [503] P. Jain, D. W. McKay, S. Panda and J. P. Ralston, Phys. Lett. B **484**, 267 (2000) [hep-ph/0001031].
- [504] L. Anchordoqui, H. Goldberg, T. McCauley, T. Paul, S. Reucroft and J. Swain, Phys. Rev. D **63**, 124009 (2001) [hep-ph/0011097].
- [505] I. J. Muzinich and M. Soldate, Phys. Rev. D **37**, 359 (1988).
- [506] S. Nussinov and R. Shrock, Phys. Rev. D **64**, 047702 (2001) [arXiv:hep-ph/0103043].
- [507] F. Cornet, J. I. Illana and M. Masip, Phys. Rev. Lett. **86**, 4235 (2001) [arXiv:hep-ph/0102065].
- [508] M. Kachelriess and M. Plumacher, arXiv:hep-ph/0109184.
- [509] T. K. Gaisser *et al.* [HIRES Collaboration], Phys. Rev. D **47** (1993) 1919;
- [510] C. Tyler, A. V. Olinto and G. Sigl, Phys. Rev. D **63**, 055001 (2001) [hep-ph/0002257];
- [511] J. Alvarez-Muniz, F. Halzen, T. Han and D. Hooper, Phys. Rev. Lett. **88**, 021301 (2002) [hep-ph/0107057].
- [512] C. T. Hill, Nucl. Phys. B **224**, 469 (1983).
- [513] C. T. Hill, D. N. Schramm and T. P. Walker, Phys. Rev. D **36**, 1007 (1987).
- [514] P. Bhattacharjee, Phys. Rev. D **40**, 3968 (1989).
- [515] P. Bhattacharjee and N. C. Rana, Phys. Lett. B **246**, 365 (1990).
- [516] P. Bhattacharjee, C. T. Hill and D. N. Schramm, Phys. Rev. Lett. **69**, 567 (1992).
- [517] P. Bhattacharjee and G. Sigl, Phys. Rev. D **51**, 4079 (1995) [arXiv:astro-ph/9412053].

- [518] P. Gondolo, G. Gelmini and S. Sarkar, Nucl. Phys. B **392**, 111 (1993) [arXiv:hep-ph/9209236].
- [519] V. Berezhinsky, M. Kachelriess and A. Vilenkin, Phys. Rev. Lett. **79**, 4302 (1997) [arXiv:astro-ph/9708217].
- [520] V. A. Kuzmin and V. A. Rubakov, Phys. Atom. Nucl. **61**, 1028 (1998) [Yad. Fiz. **61**, 1122 (1998)] [arXiv:astro-ph/9709187].
- [521] V. Kuzmin and I. Tkachev, JETP Lett. **68**, 271 (1998) [arXiv:hep-ph/9802304].
- [522] T. W. Kephart and T. J. Weiler, Astropart. Phys. **4**, 271 (1996) [arXiv:astro-ph/9505134].
- [523] S. Bonazzola and P. Peter, Astropart. Phys. **7**, 161 (1997) [arXiv:hep-ph/9701246].
- [524] P. Bhattacharjee, arXiv:astro-ph/9803029.
- [525] V. A. Kuzmin and I. I. Tkachev, Phys. Rept. **320**, 199 (1999) [arXiv:hep-ph/9903542].
- [526] V. Berezhinsky, Nucl. Phys. Proc. Suppl. **81** (2000) 311.
- [527] A. V. Olinto, Phys. Rept. **333**, 329 (2000) [arXiv:astro-ph/0002006].
- [528] P. Bhattacharjee and G. Sigl, Lect. Notes Phys. **576**, 275 (2001).
- [529] A. G. Lemaître, Suppl. Nature **128**, 704 (1931).
- [530] T. W. Kibble, J. Phys. A **9**, 1387 (1976).
- [531] A. Vilenkin, Phys. Rept. **121**, 263 (1985).
- [532] M. B. Hindmarsh and T. W. Kibble, Rept. Prog. Phys. **58**, 477 (1995) [arXiv:hep-ph/9411342].
- [533] R. H. Brandenberger, Int. J. Mod. Phys. A **9**, 2117 (1994) [arXiv:astro-ph/9310041].
- [534] L. Masperi and G. A. Silva, Astropart. Phys. **8**, 173 (1998) [arXiv:astro-ph/9706299].
- [535] L. Masperi and M. Orsaria, Astropart. Phys. **16**, 411 (2002) [arXiv:astro-ph/0005593].
- [536] V. Berezhinsky and A. Vilenkin, Phys. Rev. Lett. **79**, 5202 (1997) [arXiv:astro-ph/9704257].
- [537] M. Hindmarsh and T. W. Kibble, Phys. Rev. Lett. **55**, 2398 (1985).
- [538] F. A. Aharonian, P. Bhattacharjee and D. N. Schramm, Phys. Rev. D **46**, 4188 (1992).
- [539] C. Barbot, M. Drees, F. Halzen and D. Hooper, arXiv:hep-ph/0205230.
- [540] Y. I. Azimov, Y. L. Dokshitzer, V. A. Khoze and S. I. Troian, Z. Phys. C **27**, 65 (1985).
- [541] Y. I. Azimov, Y. L. Dokshitzer, V. A. Khoze and S. I. Troian, Z. Phys. C **31**, 213 (1986).
- [542] A. H. Mueller, Nucl. Phys. B **213**, 85 (1983).
- [543] A. H. Mueller, Nucl. Phys. B **241**, 141 (1984).
- [544] V. A. Khoze and W. Ochs, Int. J. Mod. Phys. A **12**, 2949 (1997) [arXiv:hep-ph/9701421].
- [545] V. Berezhinsky and M. Kachelriess, Phys. Lett. B **422**, 163 (1998) [arXiv:hep-ph/9709485].
- [546] V. Berezhinsky and M. Kachelriess, Phys. Lett. B **434**, 61 (1998) [arXiv:hep-ph/9803500].
- [547] G. Sigl, S. Lee, P. Bhattacharjee and S. Yoshida, Phys. Rev. D **59**, 043504 (1999) [arXiv:hep-ph/9809242].
- [548] G. Sigl, K. Jedamzik, D. N. Schramm and V. S. Berezhinsky, Phys. Rev. D **52**, 6682

- (1995) [arXiv:astro-ph/9503094].
- [549] G. Sigl, S. Lee, D. N. Schramm and P. Coppi, Phys. Lett. B **392**, 129 (1997) [arXiv:astro-ph/9610221].
- [550] G. Sigl, S. Lee and P. Coppi, arXiv:astro-ph/9604093.
- [551] R. J. Protheroe and T. Stanev, Phys. Rev. Lett. **77**, 3708 (1996) [Erratum-ibid. **78**, 3420 (1997)] [arXiv:astro-ph/9605036].
- [552] R. J. Protheroe and P. A. Johnson, Nucl. Phys. Proc. Suppl. **48**, 485 (1996) [arXiv:astro-ph/9605006].
- [553] P. H. Frampton and S. L. Glashow, Phys. Rev. Lett. **44**, 1481 (1980).
- [554] J. R. Ellis, T. K. Gaisser and G. Steigman, Nucl. Phys. B **177**, 427 (1981).
- [555] J. R. Ellis, J. L. Lopez and D. V. Nanopoulos, Phys. Lett. B **247**, 257 (1990).
- [556] J. R. Ellis, G. B. Gelmini, J. L. Lopez, D. V. Nanopoulos and S. Sarkar, Nucl. Phys. B **373**, 399 (1992).
- [557] S. Chang, C. Coriano and A. E. Faraggi, Nucl. Phys. B **477**, 65 (1996) [arXiv:hep-ph/9605325].
- [558] P. H. Frampton, B. Keszthelyi and Y. J. Ng, Int. J. Mod. Phys. D **8**, 117 (1999) [arXiv:astro-ph/9709080].
- [559] D. J. Chung, E. W. Kolb and A. Riotto, Phys. Rev. D **59**, 023501 (1999) [arXiv:hep-ph/9802238].
- [560] K. Benakli, J. R. Ellis and D. V. Nanopoulos, Phys. Rev. D **59**, 047301 (1999) [arXiv:hep-ph/9803333].
- [561] D. J. Chung, E. W. Kolb and A. Riotto, Phys. Rev. Lett. **81**, 4048 (1998) [arXiv:hep-ph/9805473].
- [562] D. J. Chung, E. W. Kolb and A. Riotto, Phys. Rev. D **60**, 063504 (1999) [arXiv:hep-ph/9809453].
- [563] D. J. Chung, P. Crotty, E. W. Kolb and A. Riotto, Phys. Rev. D **64**, 043503 (2001) [arXiv:hep-ph/0104100].
- [564] K. Hamaguchi, Y. Nomura and T. Yanagida, Phys. Rev. D **58**, 103503 (1998) [arXiv:hep-ph/9805346].
- [565] K. Hamaguchi, Y. Nomura and T. Yanagida, Phys. Rev. D **59**, 063507 (1999) [arXiv:hep-ph/9809426].
- [566] K. Hamaguchi, K. I. Izawa, Y. Nomura and T. Yanagida, models in supergravity," Phys. Rev. D **60**, 125009 (1999) [arXiv:hep-ph/9903207].
- [567] M. Birkel and S. Sarkar, Astropart. Phys. **9**, 297 (1998) [arXiv:hep-ph/9804285].
- [568] P. Blasi, R. Dick and E. W. Kolb, Astropart. Phys. **18**, 57 (2002) [arXiv:astro-ph/0105232].
- [569] R. Dick, P. Blasi and E. W. Kolb, arXiv:astro-ph/0205158.
- [570] S. Sarkar and R. Toldra, Nucl. Phys. B **621**, 495 (2002) [arXiv:hep-ph/0108098].
- [571] C. Barbot and M. Drees, Phys. Lett. B **533**, 107 (2002) [arXiv:hep-ph/0202072].
- [572] C. Barbot and M. Drees, arXiv:hep-ph/0211406.
- [573] Z. Fodor and S. D. Katz, Phys. Rev. Lett. **86**, 3224 (2001) [arXiv:hep-ph/0008204].
- [574] G. Sigl, S. Lee, D. N. Schramm and P. Bhattacharjee, Science **270**, 1977 (1995)

- [arXiv:astro-ph/9506118].
- [575] G. Gelmini and A. Kusenko, Phys. Rev. Lett. **84**, 1378 (2000) [arXiv:hep-ph/9908276].
- [576] G. Gelmini and G. Varieschi, arXiv:hep-ph/0201273.
- [577] E. E. Falco, C. S. Kochanek and J. A. Munoz, Astrophys. J. **494**, 47 (1998) [arXiv:astro-ph/9707032].
- [578] A. R. Cooray, J. M. Quashnock and M. C. Miller, Astrophys. J. **511**, 562 (1999) [arXiv:astro-ph/9806080].
- [579] Y. Sigad, A. Eldar, A. Dekel, M. A. Strauss, and A. Yahil, Astrophys. J. **495**, 516 (1998).
- [580] E. Branchini, I. Zehavi, M. Plionis, and A. Dekel, Mon. Not. Roy. Astron. Soc. **313**, 491 (2000).
- [581] S. Dodelson and L. Knox, Phys. Rev. Lett. **84**, 3523 (2000) [arXiv:astro-ph/9909454].
- [582] W. Hu, M. Fukugita, M. Zaldarriaga and M. Tegmark, Astrophys. J. **549**, 669 (2001) [arXiv:astro-ph/0006436].
- [583] S. Perlmutter *et al.* [Supernova Cosmology Project Collaboration], Astrophys. J. **517**, 565 (1999) [arXiv:astro-ph/9812133].
- [584] K. Griest and M. Kamionkowski, Phys. Rev. Lett. **64**, 615 (1990).
- [585] E. W. Kolb, D. J. Chung and A. Riotto, arXiv:hep-ph/9810361.
- [586] S. L. Dubovsky and P. G. Tinyakov, JETP Lett. **68**, 107 (1998) [arXiv:hep-ph/9802382].
- [587] V. Berezhinsky, P. Blasi and A. Vilenkin, Phys. Rev. D **58**, 103515 (1998) [arXiv:astro-ph/9803271].
- [588] V. Berezhinsky and A. A. Mikhailov, Phys. Lett. B **449**, 237 (1999) [arXiv:astro-ph/9810277].
- [589] A. Benson, A. W. Wolfendale and A. Smialkowski, Astropart. Phys. **10** (1999) 313.
- [590] J. F. Navarro, C. S. Frenk and S. D. White, Astrophys. J. **462**, 563 (1996) [arXiv:astro-ph/9508025].
- [591] N. W. Evans, arXiv:astro-ph/0102082.
- [592] P. Englmaier, O. Gerhard, Mon. Not. Roy. Astron. Soc. **304**, 512 (1999).
- [593] J. Binney, arXiv:astro-ph/0004362.
- [594] J. Binney, N. Bissantz, O. Gerhard, Astrophys. J. **537**, L99 (2000).
- [595] N. W. Evans, F. Ferrer and S. Sarkar, Astropart. Phys. **17**, 319 (2002) [arXiv:astro-ph/0103085].
- [596] S. Sarkar, arXiv:hep-ph/0202013.
- [597] G. A. Medina Tanco and A. A. Watson, Astropart. Phys. **12**, 25 (1999) [arXiv:astro-ph/9903182].
- [598] G. 't Hooft, Nucl. Phys. B **79**, 276 (1974).
- [599] A. M. Polyakov, JETP Lett. **20** (1974) 194 [Pisma Zh. Eksp. Teor. Fiz. **20** (1974) 430].
- [600] A. S. Goldhaber, Phys. Rept. **315** (1999) 83 [arXiv:hep-th/9905208].
- [601] T. J. Weiler and T. W. Kephart, Nucl. Phys. Proc. Suppl. **51B**, 218 (1996) [arXiv:astro-ph/9605156].
- [602] J. Swain, L. Anchordoqui, M. T. Dova, T. McCauley, T. Paul and S. Reucroft, AIP Conf. Proc. **566** (2000) 295.

- [603] N. A. Porter, *Nuovo Cim.* **16**, 958 (1960).
- [604] M. S. Turner, E. N. Parker and T. J. Bogdan, *Phys. Rev. D* **26**, 1296 (1982).
- [605] C. O. Escobar and R. A. Vazquez, *Astropart. Phys.* **10**, 197 (1999) [arXiv:astro-ph/9709148].
- [606] E. Roessl and M. Shaposhnikov, arXiv:hep-th/0205320.
- [607] S. D. Wick, T. W. Kephart, T. J. Weiler and P. L. Biermann, arXiv:astro-ph/0001233.
- [608] A. De Rujula, *Nucl. Phys. B* **435**, 257 (1995) [arXiv:hep-th/9405191].
- [609] L. P. Gamborg, G. R. Kalbfleisch and K. A. Milton, *Found. Phys.* **30**, 543 (2000) [arXiv:hep-ph/9906526].
- [610] L. A. Anchordoqui, T. P. McCauley, S. Reucroft and J. Swain, *Phys. Rev. D* **63**, 027303 (2001) [arXiv:hep-ph/0009319].
- [611] N. N. Efimov, N. N. Efremov, A. V. Glushkov, I. T. Makarov, and M. I. Pravdin, in *Astrophysical Aspects of the Most Energetic Cosmic Rays*, (Eds. M. Nagano, F. Takahara, World Scientific 1991), p.434.
- [612] J. L. Feng and A. D. Shapere, *Phys. Rev. Lett.* **88**, 021303 (2001) [hep-ph/0109106].
- [613] L. Anchordoqui and H. Goldberg, *Phys. Rev. D* **65**, 047502 (2002) [hep-ph/0109242].
- [614] E. J. Ahn, M. Cavaglia and A. V. Olinto, arXiv:hep-th/0201042.
- [615] L. A. Anchordoqui, J. L. Feng and H. Goldberg, *Phys. Lett. B* **535**, 302 (2002) [arXiv:hep-ph/0202124].
- [616] D. Amati, M. Ciafaloni and G. Veneziano, *Phys. Lett. B* **197**, 81 (1987);
- [617] D. Amati, M. Ciafaloni and G. Veneziano, *Phys. Lett. B* **289**, 87 (1992).
- [618] G. 't Hooft, *Phys. Lett. B* **198**, 61 (1987);
- [619] G. 't Hooft, *Commun. Math. Phys.* **117**, 685 (1988).
- [620] S. W. Hawking, *Commun. Math. Phys.* **43**, 199 (1975).
- [621] T. Banks and W. Fischler, hep-th/9906038.
- [622] R. Emparan, G. T. Horowitz and R. C. Myers, *Phys. Rev. Lett.* **85**, 499 (2000) [hep-th/0003118].
- [623] S. B. Giddings and E. Katz, hep-th/0009176.
- [624] S. B. Giddings and S. Thomas, hep-ph/0106219.
- [625] S. Dimopoulos and G. Landsberg, *Phys. Rev. Lett.* **87**, 161602 (2001) [hep-ph/0106295].
- [626] S. B. Giddings, S. Kachru and J. Polchinski, arXiv:hep-th/0105097.
- [627] G. F. Giudice, R. Rattazzi and J. D. Wells, *Nucl. Phys. B* **544**, 3 (1999), and revised version [hep-ph/9811291].
- [628] R. C. Myers and M. J. Perry, *Annals Phys.* **172**, 304 (1986).
- [629] K. S. Thorne, In **J R Klauder, Magic Without Magic**, San Francisco 1972, 231-258.
- [630] M. B. Voloshin, *Phys. Lett. B* **518**, 137 (2001) [hep-ph/0107119].
- [631] M. B. Voloshin, *Phys. Lett. B* **524**, 376 (2002) [arXiv:hep-ph/0111099].
- [632] S. Dimopoulos and R. Emparan, hep-ph/0108060.
- [633] S. B. Giddings, hep-ph/0110127.
- [634] D. M. Eardley and S. B. Giddings, gr-qc/0201034.
- [635] S. N. Solodukhin, hep-ph/0201248.
- [636] S. D. Hsu, arXiv:hep-ph/0203154.

- [637] H. L. Lai *et al.* [CTEQ Collaboration], *Eur. Phys. J. C* **12**, 375 (2000) [hep-ph/9903282].
- [638] P. C. Argyres, S. Dimopoulos and J. March-Russell, *Phys. Lett. B* **441**, 96 (1998) [hep-th/9808138].
- [639] V. Frolov and D. Stojkovic, arXiv:hep-th/0206046.
- [640] J. Preskill, P. Schwarz, A. D. Shapere, S. Trivedi and F. Wilczek, *Mod. Phys. Lett. A* **6**, 2353 (1991).
- [641] G. Landsberg, *Phys. Rev. Lett.* **88**, 181801 (2002) [arXiv:hep-ph/0112061].
- [642] G. F. Giudice, R. Rattazzi and J. D. Wells, hep-ph/0112161.
- [643] T. G. Rizzo, *JHEP* **0202**, 011 (2002) [arXiv:hep-ph/0201228].
- [644] S. B. Giddings, arXiv:hep-th/0205027.
- [645] S. B. Giddings, arXiv:hep-th/0205205.
- [646] Y. Uehara, arXiv:hep-ph/0205199.
- [647] R. Rattazzi, arXiv:hep-ph/0205265.
- [648] S. C. Park and H. S. Song, arXiv:hep-ph/0111069.
- [649] A. Chamblin and G. C. Nayak, arXiv:hep-ph/0206060.
- [650] T. Han, G. D. Kribs and B. McElrath, arXiv:hep-ph/0207003.
- [651] L. Anchordoqui and H. Goldberg, arXiv:hep-ph/0209337.
- [652] J. J. Friess, T. Han and D. Hooper, arXiv:hep-ph/0204112.
- [653] S. Cullen and M. Perelstein, *Phys. Rev. Lett.* **83**, 268 (1999) [hep-ph/9903422].
- [654] V. Barger, T. Han, C. Kao and R. J. Zhang, *Phys. Lett. B* **461**, 34 (1999) [hep-ph/9905474].
- [655] C. Hanhart, J. A. Pons, D. R. Phillips and S. Reddy, *Phys. Lett. B* **509**, 1 (2001) [astro-ph/0102063].
- [656] L. J. Hall and D. R. Smith, *Phys. Rev. D* **60**, 085008 (1999) [hep-ph/9904267].
- [657] S. Hannestad and G. Raffelt, *Phys. Rev. Lett.* **87**, 051301 (2001) [hep-ph/0103201].
- [658] S. Hannestad and G. G. Raffelt, hep-ph/0110067.
- [659] M. Acciarri *et al.* [L3 Collaboration], *Phys. Lett. B* **464**, 135 (1999) [hep-ex/9909019].
- [660] M. Acciarri *et al.* [L3 Collaboration], *Phys. Lett. B* **470**, 281 (1999) [hep-ex/9910056].
- [661] C. Pagliarone, hep-ex/0111063.
- [662] B. Abbott *et al.* [D0 Collaboration], *Phys. Rev. Lett.* **86**, 1156 (2001) [hep-ex/0008065].
- [663] A. Ringwald and H. Tu, hep-ph/0111042.
- [664] G. Sigl, arXiv:hep-ph/0207254.
- [665] S. Yoshida *et al.* [AGASA Collaboration], *Proc. of 27th ICRC (Hamburg)* **3**, 1142 (2001).
- [666] G. J. Feldman and R. D. Cousins, *Phys. Rev. D* **57**, 3873 (1998) [physics/9711021].
- [667] O. E. Kalashev, V. A. Kuzmin, D. V. Semikoz and G. Sigl, arXiv:hep-ph/0205050.
- [668] R. Baltrusaitis, R. Cady, G. Cassiday, J. Elbert, P. Gerhardy, E. Loh, Y. Mizumoto, P. Sokolsky and D. Steck, *Astrophys. J.* **281**, L9 (1984).
- [669] L. A. Anchordoqui, J. L. Feng, H. Goldberg, and A. D. Shapere, Auger Internal Note, GAP-2001-053.
- [670] S. I. Dutta, M. H. Reno and I. Sarcevic, arXiv:hep-ph/0204218.
- [671] M. Kowalski, A. Ringwald and H. Tu, hep-ph/0201139.

- [672] J. Alvarez-Muniz, J. L. Feng, F. Halzen, T. Han and D. Hooper, hep-ph/0202081.
- [673] Y. Uehara, arXiv:hep-ph/0110382.
- [674] P. Jain, S. Kar, D. W. McKay, S. Panda and J. P. Ralston, arXiv:hep-ph/0205052.
- [675] S. I. Dutta, M. H. Reno, I. Sarcevic and D. Seckel, hep-ph/0012350.
- [676] F. James and R. Cousins, Eur. Phys. J. C **15**, 195 (2000).
- [677] P. Jain, S. Kar, S. Panda and J. P. Ralston, hep-ph/0201232.
- [678] J. Lykken and S. Nandi, Phys. Lett. B **485**, 224 (2000) [arXiv:hep-ph/9908505].
- [679] K. Cheung, arXiv:hep-ph/0205033.
- [680] E. J. Ahn and M. Cavaglia, arXiv:hep-ph/0205168.
- [681] G. Shiu and S. H. Tye, Phys. Rev. D **58**, 106007 (1998) [hep-th/9805157].
- [682] H. Goldberg and T. J. Weiler, Phys. Rev. D **59** (1999) 113005 [hep-ph/9810533].
- [683] T. Abu-Zayyad *et al.* [High Resolution Fly's Eye Collaboration], arXiv:astro-ph/0208243.
- [684] T. Abu-Zayyad *et al.* [High Resolution Fly's Eye Collaboration], arXiv:astro-ph/0208301.
- [685] M. Takeda *et al.*, arXiv:astro-ph/0209422.
- [686] A. Capella, U. Sukhatme, C. I. Tan and J. Tran Thanh Van, Phys. Rept. **236**, 225 (1994).
- [687] H. J. Drescher, M. Hladik, S. Ostapchenko, T. Pierog and K. Werner, Phys. Rept. **350**, 93 (2001) [arXiv:hep-ph/0007198].
- [688] K. Werner, Phys. Rept. **232**, 87 (1993).
- [689] N. N. Kalmykov, S. S. Ostapchenko and A. I. Pavlov, Bull. Russ. Acad. Sci. Phys. **58** (1994) 1966 [Izv. Ross. Akad. Nauk Ser. Fiz. **58N12** (1994) 21].
- [690] J. Ranft, Phys. Rev. D **51**, 64 (1995).
- [691] S. Roesler, R. Engel and J. Ranft, arXiv:hep-ph/0012252.
- [692] T. Regge, Nuovo Cim. **14**, 951 (1959).
- [693] V. N. Gribov, Sov. Phys. JETP **26**, 414 (1968) [Zh. Eksp. Teor. Fiz. **53**, 654 (1968)].
- [694] B. Andersson, G. Gustafson, G. Ingelman and T. Sjostrand, Phys. Rept. **97**, 31 (1983).
- [695] T. Sjostrand, Int. J. Mod. Phys. A **3**, 751 (1988).
- [696] R. S. Fletcher, T. K. Gaisser, P. Lipari and T. Stanev, Phys. Rev. D **50**, 5710 (1994).
- [697] G. F. Chew and S. C. Frautschi, Phys. Rev. Lett. **7**, 394 (1961).
- [698] H. U. Bengtsson and T. Sjostrand, Comput. Phys. Commun. **46**, 43 (1987).
- [699] J. Engel, T. K. Gaisser, T. Stanev and P. Lipari, Phys. Rev. D **46**, 5013 (1992).
- [700] N. N. Kalmykov and S. S. Ostapchenko, Sov. J. Nucl. Phys. **50** (1989) 315 [Yad. Fiz. **50** (1989) 509].
- [701] J. Knapp, D. Heck, and G. Schatz, Nucl. Phys. B (Proc. Suppl.) **52**, 136 (1997).
- [702] L. A. Anchordoqui, M. T. Dova, L. N. Epele and S. J. Sciutto, Phys. Rev. D **59**, 094003 (1999) [arXiv:hep-ph/9810384].
- [703] J. Ranft, arXiv:hep-ph/0012171.
- [704] J. Alvarez-Muniz, R. Engel, T. K. Gaisser, J. A. Ortiz and T. Stanev, arXiv:astro-ph/0205302.
- [705] L. A. Anchordoqui, M. T. Dova and S. J. Sciutto, Proc. of 26th ICRC (Salt Lake City)

- 1**, 147 (1999). [arXiv:hep-ph/9905248].
- [706] J. R. Horandel *et al.* [KASCADE Collaboration], Nucl. Phys. Proc. Suppl. **75A**, 228 (1999).
- [707] J. Knapp, D. Heck, S. J. Sciutto, M. T. Dova and M. Risse, arXiv:astro-ph/0206414.
- [708] P. J. Peebles, D. N. Schramm, E. L. Turner and R. G. Kron, Nature **352**, 769 (1991).
- [709] E. Hayward, Rev. Mod. Phys. **35**, 324 (1963).
- [710] M. H. Salamon and F. W. Stecker, Astrophys. J. **493**, 547 (1998) [arXiv:astro-ph/9704166].
- [711] L. N. Epele and E. Roulet, Phys. Rev. Lett. **81**, 3295 (1998) [arXiv:astro-ph/9806251].
- [712] L. A. Anchordoqui, M. T. Dova, N. Epele and J. D. Swain, Proc. of 25th ICRC (South Africa) **7**, 353 (1997).
- [713] M. I. Wilkinson and N. W. Evans, Mon. Not. Roy. Astron. Soc. **310** (1999) 645 [arXiv:astro-ph/9906197].
- [714] N. W. Evans, Mon. Not. Roy. Astron. Soc. **260**, 191 (1993).
- [715] N. W. Evans, C. M. Carollo and P. T. de Zeeuw, Mon. Not. Roy. Astron. Soc. **318**, 1131 (2000) [arXiv:astro-ph/0008156].
- [716] J. Binney, Ann. Rev. Astron. Astrophys. **30**, 51 (1992).
- [717] A. Chamblin, S. W. Hawking and H. S. Reall, Phys. Rev. D **61**, 065007 (2000) [arXiv:hep-th/9909205].
- [718] S. B. Giddings, E. Katz and L. Randall, JHEP **0003**, 023 (2000) [arXiv:hep-th/0002091].
- [719] S. B. Giddings, arXiv:hep-th/0203004.